FUNCTIONAL INSIGHTS INTO ONCOGENIC PROTEIN TYROSINE PHOSPHATASES BY MASS SPECTROMETRY

Chad Daniel Walls

Submitted to the faculty of the University Graduate School
in partial fulfillment of the requirements
for the degree
Doctor of Philosophy
in the Department of Biochemistry and Molecular Biology
Indiana University

December 2012

Accepted by the Faculty of Indiana University, in partial
fulfillment of the requirements for the degree of Doctor of Philosophy.

_____

Zhong-Yin Zhang, Ph.D., Chair

_____

Mu Wang, Ph.D.

Doctoral Committee

_____

Clark Wells, Ph.D.

November 9, 2012

_____

Jian-Ting Zhang, Ph.D.

DEDICATION

This work is dedicated to my wife Jennifer who has traveled this journey with me and who has endured countless challenges along the way in support of this most important of sacrifices for the future of our family. Along this path, I realized that my biggest weaknesses were her biggest strengths and without her none of this would have been possible.

This work is dedicated to my son Collin who brought light into our lives in the darkest of times and who will one day look to the triumph of this struggle to bring passion to his own. Son, you have the capacity to do all things. Focus on your life and choose to embrace what is good. Listen and learn and one day you will earn the privilege to teach.

This work is dedicated to my mother-in-law and friend Deborah Collins who lived a beautiful life before succumbing to her struggle with cancer. My memory of Debbie brought such purpose to fulfilling this goal.

This work is dedicated to my family and friends who gave so much support whenever we needed it most.

ACKNOWLEDGEMENTS

I would like to thank Dr. Zhong-Yin Zhang who has devoted a great deal of time and effort into forming me into a critical thinker and practitioner of biochemistry. I appreciate all that Dr. Zhang does so that we can practice our art seemingly free of financial burden. The members of Dr. Zhang's group have helped me a great deal and I wanted to thank all of them for being there when I needed it most.

I would like to thank Dr. Mu Wang who trained me in protein mass spectrometry and who has taught me many valuable lessons over the years in an effort to prepare me for the many challenges that will lie ahead in my career. Dr. Wang has always believed in me and my abilities and through that steadfast support I was able to endure many difficult lessons.

I would like to thank the members of my research committee for providing me with guidance toward problem solving and approaching my research in a critical manner.

I would like to thank Dr. W. Andy Tao and Dr. Anton Iliuk at Purdue University for their steadfast commitment toward helping me find solutions to my challenges with phosphotyrosine-peptide enrichment and protein mass spectrometry. The many years that we struggled together helped me to fully appreciate practical analytical biochemistry.

ABSTRACT

Chad Daniel Walls

FUNCTIONAL INSIGHTS INTO ONCOGENIC PROTEIN TYROSINE PHOSPHATASES BY MASS SPECTROMETRY

Phosphatase of Regenerating Liver 3 (PRL3) is suspected to be a causative factor toward cellular metastasis when overexpressed. To date, the molecular basis for PRL3 function remains an enigma, justifying the use of 'shot-gun'-style phosphoproteomic strategies to define the PRL3-mediated signaling network. On the basis of aberrant Src tyrosine kinase activation following ectopic PRL3 expression, phosphoproteomic data reveal a signal transduction network downstream of a mitogenic and chemotactic PDGF (α and β), Eph (A2, B3, B4), and Integrin (β1 and β5) receptor array known to be utilized by migratory mesenchymal cells during development and acute wound healing in the adult animal. Tyrosine phosphorylation is present on a multitude of signaling effectors responsible for Rho-family GTPase, PI3K-Akt, Jak-STAT3, and Ras-ERK1/2 pathway activation, linking observations made by the field as a whole under Src as a primary signal transducer. Our phosphoproteomic data paint the most comprehensive picture to date of how PRL3 drives pro-metastatic molecular events through Src activation.

The Src-homology 2 (SH2) domain-containing tyrosine phosphatase 2 (SHP2), encoded by the *Ptpn11* gene, is a *bona-fide* proto-oncogene responsible for the activation of the Ras/ERK1/2 pathway following mitogen stimulation. The molecular basis for SHP2 function is pTyr-ligand-mediated alleviation of intramolecular autoinhibition by

the N-terminal SH2 domain (N-SH2 domain) upon the PTP catalytic domain. Pathogenic mutations that reside within the interface region between the N-SH2 and PTP domains are postulated to weaken the autoinhibitory interaction leading to SHP2 catalytic activation in the open conformation. Conversely, a subset of mutations resides within the catalytic active site and cause catalytic impairment. These catalytically impaired SHP2 mutants potentiate the pathogenesis of LEOPARD-syndrome (LS), a neuro-cardio-facial-cutaneous (NCFC) syndrome with very similar clinical presentation to related Noonan syndrome (NS), which is known to be caused by gain-of-function (GOF) SHP2 mutants.

Here we apply hydrogen-deuterium exchange mass spectrometry (H/DX-MS) to provide direct evidence that LS-associated SHP2 mutations which cause catalytic impairment also weaken the autoinhibitory interaction that the N-SH2 domain makes with the PTP domain. Our H/DX-MS study shows that LS-SHP2 mutants possess a biophysical property that is absolutely required for GOF-effects to be realized, *in-vivo*.

Zhong-Yin Zhang, Ph.D., Chair

TABLE OF CONTENTS

LIST OF TABLES

LIST OF FIGURES

ABBREVIATIONS

CRC	Colorectal Carcinoma
CSK	C-terminal Src Kinase
D2O	Deuterium Oxide
DOCK	Dedicator of Cytokinesis
EPHR	Ephrin Receptor
ERK	Extracellular signal-Regulated Kinase
ESI	Electrospray Ionization
FAK	Focal Adhesion Kinase
GOF	Gain of Function
HEK	Human Embryonic Kidney
JAK	Janus Kinase
JNK	c-Jun N-terminal Kinase
LS	LEOPARD Syndrome
LTQ	Linear Trap Quadrupole
MAPK	Mitogen Activated Protein Kinase
MEF	Murine Embryonic Fibroblast
NS	Noonan Syndrome
NWASP	Neural Wiskott Aldrich Syndrome Protein
PAG	Phosphoprotein Associated with Glycosphingolipid Microdomains
PAK	p21 Protein (Cdc42/Rac)-Activated Kinase
PCR	Polymerase Chain Reaction
PDGFR	Platelet-Derived Growth Factor Receptor

PI3K	Phosphatidylinositol 3-Kinase
PIP2	Phosphatidylinositol (4,5)-bisphosphate
PIP3	Phosphatidylinositol (3,4,5)-trisphosphate
PLC	Phospholipase C
PolyMAC	Polymer-based Metal Ion Affinity Capture
PRL	Phosphatase of Regenerating Liver
PTK	Protein Tyrosine Kinase
PTP	Protein Tyrosine Phosphatase
RTK	Receptor Tyrosine Kinase
SHP2	Src homology-2 (SH2) domain-containing tyrosine phosphatase-2
SILAC	Stable Isotope Labeling of Amino acids in Cell culture
STAT	Signal Transducer and Activator of Transcription
WAM	Weighted Average Mass

CHAPTER 1: INTRODUCTION

1.1 Tyrosine Phosphorylation

1.1.1 Tyrosine phosphorylation; a historical perspective

A seminal observation made over 30 years ago by Walter Eckhart, Mary Anne Hutchinson, Bart Sefton, and Tony Hunter during their studies of polyomavirus middle T (PyMT) and *v-Src* associated kinase activities led to the discovery of tyrosine phosphorylation as a new type of protein modification (1-3). At this time, modification of tyrosine by phosphorylation was not only unprecedented, but in the feverish study of the cellular effects of both the polyomavirus tumor (T)-antigens and $pp60^{src}$ (*v-Src*), the transforming gene of the Rous sarcoma virus, gave cancer researchers critical insight that this modification could be intimately linked with cellular transformation. By this time, protein phosphorylation was a well-established principle for reversible regulation of protein activity and it immediately suggested that viral-mediated cellular transformation was governed by phosphotyrosine-modifications to a set of target proteins, thus altering their activity. Seminal studies on protein phosphorylation would give precedent to the importance of tyrosine phosphorylation as a genuine physiological process. Importantly, in conjunction with reports documenting tyrosine phosphorylation being associated with the activities of retroviral oncoproteins like *v-Src* and the Abelson murine leukemia virus protein (*v-Abl*) (4), an additional report surfaced that documented tyrosine phosphorylation being associated with the activity of the cellular epidermal growth factor receptor kinase (EGFR) (5). The critical link that would be established between *v-Src* and *v-Abl* and the EGF receptor gave way to a notion that neoplastic cell transformation by viral protein-tyrosine kinases might involve activation of signaling pathways

stimulated by cellular growth factor receptors. By 1982 the research community knew of three retroviral transforming tyrosine kinases (*v-Src*, *v-Abl*, and *v-Fes*) and three cellular receptor tyrosine kinases (RTKs) (EGFR, insulin receptor-IR, and the platelet-derived growth factor receptor-PDGFR). Ironically, a year later, Sara Courtneidge and Alan Smith revealed that the tyrosine phosphorylation associated with the PyMT was actually due to its association with ($pp60^{sarc}$; c-Src), the cellular homolog of *v-Src* (6). The viral homologs of cellular protein tyrosine kinases, most specifically *v-Src* and its cellular homolog c-Src, would allow cancer researchers of the day to establish a critical link between cellular transformation and aberrant tyrosine phosphorylation. To date, we now understand that the human genome encodes 90 distinct tyrosine kinases and that over half of them have been implicated in the genesis of at least one type of cancer (7).

Ten years after the identification of the first tyrosine kinase, groups headed by Ed Fischer, Nick Tonks, and Jack Dixon, purified/characterized and subsequently cloned the first cystolic protein tyrosine phosphatase (PTP), the human placental phosphatase, PTP1B (8-11). PTP1B and concurrently characterized receptor-linked PTP, CD45 (the leukocyte common antigen) (12), represented prototypes to a new class of phosphohydrolases capable of counteracting the activities of their PTK counterparts. Though at the advent of their discovery PTPs were generally assumed to be 'suppressors' of the oncogenic activities of their PTK counterparts, evidence to date supports PTPs playing specific and active, even dominant, roles in setting the levels of tyrosine phosphorylation in cells and in the regulation of many physiological processes (13-18). In 2004, Andres Alonso and Thomas Mustelin documented the presence of 107 PTPs within the human genome and estimated that only 81 are catalytically active (19), putting

the ratio of active PTKs (85) and active PTPs (81) ~1:1. It is widely appreciated that the reciprocal regulation of tyrosine phosphorylation by the concerted actions of both PTKs and PTPs controls a myriad of processes essential to eukaryotic life. Soon after the discovery and characterization of the first PTPs, critical questions regarding the tight regulation of this post-translational modification and how it is used by the cell to govern biological function would begin to be answered.

By the mid-1990s a resolved picture was emerging about how tyrosine phosphorylation was translated into biological function. Work by Tony Pawson's group in the mid-80s elucidated a domain in the oncogenic *v-Fps/Fes* PTK that was N-terminal to the kinase domain, but modified both kinase activity and substrate recognition and was necessary for cellular transformation (20-21). The domain was given the name Src homology 2 (SH2)-domain as a stretch of ~100 amino acids was shown to be conserved in c-Src and c-Abl and similarly positioned adjacent to the kinase (SH1) domain. This discovery gave way to data in support of a notion that specificity in signaling by tyrosine kinases requires protein-protein interactions that are mediated by a dedicated noncatalytic domain (21-24). By the early 1990s the SH2 domain was shown to specifically associate with phosphotyrosine residues of RTKs and intracellular docking proteins following growth factor stimulation, through experiments involving isolated SH2 domains of aggressively studied signaling effectors of the day including: PLCγ1, RasGAP, and Src (25-30). In fact, effectors such as PLCγ1 and RasGAP were shown to be RTK substrates, giving way to tyrosine phosphorylation being an element of substrate recruitment and signal pathway organization (31-35). Since the discovery of the SH2 domain, a unifying concept of cellular organization has emerged in which modular protein-protein

interactions provide an underlying framework through which signaling pathways/networks are assembled and controlled.

In full circle, it was now clear how the activity of one viral oncoprotein, *v-Src*, could act in a pleiotropic fashion to affect cell shape, adhesion, motility, growth, proliferation, gene expression, metabolism, and survival towards cellular transformation. The answer to the question of why this protein modification must be tightly regulated is precisely that it represents the 'key' that unlocks a cell's response to its environment. The cardinal discovery that *v-Src* and c-Src were tyrosine kinases would lead to a revolution in our understanding of how the regulation of tyrosine phosphorylation governs biological function both in normal and in pathological contexts.

1.1.2 Tyrosine phosphorylation; molecular biochemistry and cellular physiology

Protein tyrosine phosphorylation is now well-recognized to be regulated by the reciprocal enzymatic activities of both protein tyrosine kinases (PTKs) and protein tyrosine phosphatases (PTPs). Opposing the action of the 90 PTKs encoded by the human genome, are 107 PTPs that can remove phosphate from the phosphotyrosyl-residues in proteins (19). As mentioned previously, the ratio of active PTKs (85) and active PTPs (81) is ~1:1, owing to the physiological importance of the reciprocal relationship between these two enzyme families. Despite the large amount of tyrosine kinases encoded by the human genome, tyrosine phosphorylation accounts for <<1% of phosphate esterified to proteins (pSer, pThr, and pTyr) in non-transformed cells, moving closer to ~1% in cells transformed by the *v-Src* oncoprotein (2). The most prominent reasons for the disparity between pSer (~90%), pThr (~10%), and pTyr (<1%) are: unlike pSer/pThr, pTyr rarely plays a structural role in proteins and primarily represents a

regulatory modification, most tyrosine kinases are tightly negatively regulated and only become active under specific conditions, and PTPs have a very high turnover rate and in consequence pTyr-residues have a very short half-life unless protected by binding to src-homology 2 (SH2) or phosphotyrosine-binding (PTB) domains that would protect them from dephosphorylation. Tyrosine phosphorylation is therefore unique with regard to how it is utilized and regulated within the cell.

Of the 90 PTKs, there are 58 RTKs and 32 non-receptor tyrosine kinases with 4 of the RTKs predicted to lack catalytic activity (e.g. ErbB3) (36). In general, PTKs initiate the tyrosine phosphorylation reaction by catalyzing phosphate transfer from the gamma (terminal)-phosphate of ATP to the substrate tyrosine phenolic oxygen. This reaction forms the basis of signal transduction in all metazoans and is regulated to govern all aspects of multicellular life including: cell-cycle control/mitogenesis, cell adhesion, cell migration, metabolism, transcriptional activation, and neural transmission. The first insight into the structural basis of signal transduction by tyrosine phosphorylation came from the study by Hiroshi Ushiro and Stanley Cohen documenting tyrosine phosphorylation by the EGFR following EGF-stimulation of human A431 epidermoid carcinoma cells (5). In short order, the EGFR, IR, and PDGFR would become the cornerstones of a body of research that would demonstrate that RTK signaling is important for the normal cellular response to mitogenic and metabolic hormones, and the pathological activation of such signaling pathways could provoke a cancerous phenotype (37-42). Subsequently, work by Ora Rosen, Tony Pawson, and Joseph Schlessinger would demonstrate that tyrosine kinases become activated by transphosphorylation of their catalytic domains (43-45). On the basis that the RTK was the most abundant

tyrosine phosphorylated protein within growth factor stimulated cells, it was postulated that tyrosine phosphorylation may have unidentified biochemical functions including the ability to recruit target proteins/substrates to the tyrosine kinases. This time in history would set the precedent for the molecular biochemistry and cellular physiology associated with tyrosine phosphorylation.

Receptor tyrosine kinases (RTKs) will be used here as prominent examples highlighting the cellular effects of tyrosine phosphorylation both in normal and in pathological contexts. In non-pathogenic states, tyrosine phosphorylation is initiated by extracellular derived bivalent ligands (growth factors/mitogens) binding to the extracellular regions of inactive monomeric/oligomeric RTKs and inducing/stabilizing intracellular dimeric/oligomeric conformations (hereafter referred to as dimerization) that then activate their tyrosine kinase domains through various mechanisms (46). Each RTK tyrosine kinase domain (TKD) is uniquely *cis*-autoinhibited by a set of specific intramolecular interactions. Release of *cis*-autoinhibition, following ligand-induced receptor dimerization, is the key event that triggers RTK activation. As a prominent example, the insulin receptor (IR) Tyr1162 residue within the activation loop of the TKD physically occludes the active site (*cis*-autoinhibition), thus blocking access of both ATP and protein substrates. When insulin activates the receptor, Tyr1162 in one TKD within the resulting dimer becomes phosphorylated by its partner (along with two additional tyrosine residues; Tyr1152 and 1163) (*trans*-autophosphorylation; autophosphorylation) resulting in the disruption of the *cis*-autoinhibitory interaction made between Tyr1162 and the catalytic active site (47). Upon phosphorylation the activation loop of the TKD is competent to adopt the 'active' conformation seen in all other activated TKDs (48-49).

Collectively, RTKs are relieved of *cis*-autoinhibition by autophosphorylation of tyrosines within the activation loop, the juxtamembrane segment, and/or the C-terminal region. The 'first phase' of receptor autophosphorylation is generally the kinase activation event or the event that generates a maximally efficient catalytic active site for substrate recognition and subsequent phosphate-transfer. The 'second phase' of receptor autophosphorylation generates the phospho-recognition motifs for Src homology-2 (SH2) or phosphotyrosine-binding (PTB) domain-containing cytoplasmic signaling effectors (50-52). These signaling effectors may be either recruited to the multi-phosphorylated RTKs or to multi-phosphorylated docking proteins that physically associate with and become phosphorylated by the RTKs. Additional specificity and complexity is derived from recruited SH2 or PTB domain-containing effectors also containing phospholipid (PH, PX, C1, C2, FYVE) and/or protein·protein (SH3, WW, PDZ) interaction modules. The well-studied lipase, phospholipase C-γ1 (PLCγ1) represents a perfect example illustrating the above point. PLCγ1 contains two SH2 domains, two PH domains, one C2 domain, and one SH3 domain that participate in multivalent signal-dependent targeting of PLCγ to its site of action at the membrane. PLCγ1 uses its SH2 domains to target to activated/tyrosine phosphorylated RTKs/docking proteins; the PH domain to bind membrane phosphoinositides (including the PI 3-kinase product PtdIns(3,4,5)P_3 (PIP_3)); the C2 domain to bind additional membrane phospholipids; and the SH3 domain to associate with signaling complex-recruited Cbl (Casitas B-lineage lymphoma). PLCγ1 is said to permit 'coincidence detection' as it is capable of integrating multiple signal inputs through a combination of recognition modules (53). Figure 1 represents a model illustration of how the multiple domains of signaling effectors recruited to activated

RTKs can coordinate the assembly of multiprotein complexes toward network branching/generation (54). Thus, the tyrosine phosphorylated RTK represents a node within a complex signaling network capable transmitting extracellular signals to a multitude of intracellular signaling effectors designed to integrate multiple signal inputs to drive a diverse array of biological functions. Figure 2 represents a model illustration of the signaling networks activated by the EGFR using the concepts described in Figure 1 (54). The vast majority of this illustration is accurate within the context of many canonical RTK-mediated signaling networks and provides a point of reference for the complexity of signal integration generated following an initial tyrosine phosphorylation event that activates the RTK.

From the above description of the molecular biochemistry and cellular physiology associated with tyrosine phosphorylation, specifically through the RTK as a major conduit of tyrosine phosphorylation, it can be appreciated that aberrant regulation of RTK function results in pathological conditions such as cancer. In fact, it was recognized in the mid-1960s that virally transformed cells rely less on exogenous growth factors for cell proliferation than their normal cell counterparts (55), suggesting that aberrant growth factor signaling might play a key role in cell transformation. Nearly twenty years later it was recognized that the *v-sis* oncogene ($p28^{sis}$) from simian sarcoma virus was actually a virally transduced PDGF gene (PDGF-B ligand) (41-42) capable of promoting cellular transformation by activating the PDGFR in an autocrine fashion. Subsequently, the product of the *v-erbB* oncogene from avian erythroblastosis virus was found to correspond to a truncated and constitutively activated form of EGFR (39). From these insights, came forth data in support of the human gene encoding the EGFR experiencing

aberrant amplification as well as mutation in brain tumors, leading to a proto-oncogenic RTK that was both overexpressed and constitutively active in tumor tissues (56). To date, a large body of evidence implicates deregulated and dysfunctional RTKs in a variety of human diseases. With respect to RTKs, aberrant activation of these kinases in human cancer is well-recognized to be mediated by six principal mechanisms: autocrine activation, chromosomal translocation, RTK overexpression, gain-of-function mutations, loss of suppressor kinase activity, or aberrant PTP activity.

The dynamic regulation of tyrosine phosphorylation within cells represents arguably the most critical biomolecular process that governs multicellular life. Just a single tyrosine phosphorylation event to an RTK can induce the localization and subsequent activation of a myriad of signaling effectors responsible for driving a diverse array of biological functions. This single biomolecular process, when aberrantly regulated, can also represent the causative factor responsible for the death of the entire organism.

1.2 Protein tyrosine phosphatases (PTPs) and disease

1.2.1 Class I cysteine-based PTPs

As described in the previous section, tyrosine phosphorylation represents a governing dynamic of multicellular life. Tyrosine phosphorylation is used as an intra-/inter-cellular communication mechanism to drive complex body formation during development and to maintain tissue/organ homeostasis in the adult organism. At the cellular level, tyrosine phosphorylation drives decisions to proliferate or differentiate, alter adhesion and shape to set tissue barriers or to migrate, and survive or die based upon intra/extra-cellular biochemical cues. In a deregulated, aberrant state, tyrosine

phosphorylation potentiates the pathogenesis of many inherited and acquired human diseases including metabolic abnormalities, immune deficiencies, and cancer.

The human genome encodes 107 protein tyrosine phosphatases (PTPs) (19) that govern the dynamic state of tyrosine phosphorylation within the cell by catalyzing the phosphate hydrolysis reaction on substrate phosphate esters. Of the 107 PTP genes, 11 are catalytically inactive, 2 dephosphorylate mRNA, and 13 dephosphorylate inositol phospholipids. Thus, 81 PTPs are *bona-fide* protein phosphatases capable of dephosphorylating phosphotyrosine. PTPs are classified based upon the amino acid sequences of their catalytic domains. Using this designation, PTPs are grouped into four separate families, each with a range of substrate specificities. Class I cysteine-based PTPs comprise the largest family and contain the 38 well-recognized "classical" PTPs (57), which are strictly tyrosine specific and all have mouse orthologs, and the 65 VH1-like, "dual-specific" protein phosphatases (DSPs), which represents the most diverse group in terms of substrate specificity. Class II PTPs are structurally related to bacterial arsenate reductases, with a single cysteine-based member, the tyrosine-specific low (Mr) enzyme (LMPTP). Class III cysteine-based PTPs are tyrosine/threonine-specific phosphatases, solely represented by the $p80^{Cdc25}$ cell cycle regulators. Conversely, class IV PTPs use a different catalytic mechanism with a key aspartic acid and dependence upon a metal cation. Due to the limited scope of this discussion, only Class I cysteine-based PTPs will be discussed further.

The catalytic domain of Class I "classical" cysteine-based PTPs comprise ~280 residues and are defined by the active site signature motif (HCX_5R), in which the cysteine residue functions as the catalytic nucleophile and is essential for the general

acid-base-dependent phosphate-ester hydrolysis reaction first characterized by Zhong-Yin Zhang and Jack Dixon using the pathogenic PTP of *Yersinia enterocolitica* (YopH) in 1994 (58-59). Of the 38 "classical" PTPs, 21 are designated transmembrane receptor-like PTPs (RPTPs) that regulate tyrosine dephosphorylation through ligand-mediated association to their extracellular regions. The extracellular domains of RPTPs possess molecular features akin to cell-adhesion molecules, thus implicating these PTPs in control of cell·cell and cell·matrix interactions. More than half (12) of the RPTPs have tandem PTP domains in the intracellular segments. While just the membrane proximal catalytic domain is functional, generally both are important for the activity, specificity, and stability of the RPTP as a whole (60-61). The remaining 17 PTPs are non-transmembrane, cytoplasmic enzymes that are characterized by distinct regulatory sequences that surround the catalytic domain. Regulatory domains, such as SH2 domains, act as molecular switches; negatively regulating enzymatic activity in a latent state, while promoting enzymatic activation upon stimulation. SH2 domains target physiological pTyr-motifs and thus control the subcellular distribution of the phosphatase and as a consequence control substrate access/specificity. One of the most prominent examples of a regulatory domain controlling multiple aspects of enzymatic function comes from the proto-oncogenic Src homology-2 (SH2) domain-containing protein tyrosine phosphatase-2 (SHP2). SHP2 possess two tandemly arranged SH2 domains (N-SH2 and C-SH2) N-terminal to its catalytic PTP domain. The N-SH2 domain acts as an elegant molecular switch. In a latent state, the N-SH2 domain inhibits catalytic function by inserting an autoinhibitory loop directly into the active site, thus physically occluding substrate access. Upon stimulation of tyrosine phosphorylation by mitogenic ligands or

through aberrantly activated PTKs, the N-SH2 domain binds resulting phosphotyrosyl-motifs on physiological interacting proteins, which weakens the inhibitory interaction that it makes with the PTP domain, thus activating and directing this PTP to its substrates in one concerted action (62-63). Other regulatory domains/motifs direct cytoplasmic PTPs to their physiological substrates, such as the proline-rich motif (^{335}PPPKPPR) of PTP-PEST (*Ptpn12*) that control access to the SH3 domain of p130^{Cas} (64) and the kinase-interaction motif (KIM) of and STEP (*Ptpn5*) that drives interaction with the MAPKs, ERK1/2 (65).

The 65 VH1-like, "dual-specific" protein phosphatases (DSPs), display the most diversity with regard to substrate specificity within the PTP-superfamily. The DSPs are less well conserved than their "classical" PTP counterparts and display little sequence similarity beyond the cysteine-containing signature motif. They also have smaller catalytic domains than the classical PTPs. Though they share the same catalytic mechanism, the DSP active site can accommodate phosphoserine (pSer), phosphothreonine (pThr), and phosphotyrosine (pTyr). These phosphatases also contain a diverse array of non-catalytic protein·protein/protein·lipid interaction motifs/domains that are known to serve regulatory functions. Mitogen-activated protein kinase phosphatases (MKPs) specifically attenuate the activities of members of the MAPK-family of Ser/Thr-kinases including ERK1/2, JNK1, and p38-MAPK (66-68). Specificity for MAPKs arises through a kinase interaction domain with the consensus sequence (ψψXRRψXXG; where ψ represents a hydrophobic residue and X represents any amino acid) at the N-terminus and an acidic domain at the C-terminus (69-73), flanked by two Cdc25-homology domains (74). Phosphatase and tensin-homolog deleted on

chromosome 10 (PTEN) facilitates membrane association using a C2-phospholipid-binding domain to position its catalytic domain in the vicinity of its phospholipid substrate, phosphoinositide (PtdIns(3,4,5)P_3; PIP_3) (75). PTEN also contains a PDZ protein·protein interaction domain that it uses to facilitate interactions with members of the membrane-associated guanylate kinase family with multiple PDZ domains called MAGI (membrane-associated guanylate kinase inverted), localized to epithelial tight junctions (76-77). The dephosphorylation of PIP_3 by PTEN counteracts the activity of the proto-oncogene PI-3K toward PIP_3-mediated signal transduction including Akt activation (78). Additionally, members of the phosphatase of regenerating liver family (PRLs) contain C-terminal membrane-targeting poly-basic and -CAAX prenylation motifs that are essential to their biological function. Though the substrate(s) of the PRLs remain an enigma, these phosphatases represent *bona-fide* oncogenes within the PTP superfamily (79). Finally, the glucan phosphatase laforin is the only phosphatase documented that possesses a carbohydrate binding domain (CBD) of which it uses to selectively bind glycogen and dephosphorylate glucose (C2/C3) phosphomonoesters (80-81). Figure 3 represents the modular organization of Class I cysteine-based PTPs including the 38 "classical" PTPs and the 65 VH1-like DSPs (82).

1.2.2 PTPs and disease

Our modern understanding of the reciprocal regulation of tyrosine phosphorylation by PTKs and PTPs is heavily curbed toward the activities of PTKs for a variety of reasons. Apart from the fact that a multitude of PTKs were identified and characterized more than 10 years before the discovery of the first PTP, the activities of PTKs are in general 'activating' toward cellular signal transduction and therefore, when

aberrantly regulated, PTKs have the potential to be pathogenic. As it pertains to cancer, we now understand that the human genome encodes 90 distinct tyrosine kinases and that over half of them have been implicated in the genesis of at least one type of cancer (7). In fact, the regulation of protein tyrosine phosphorylation is controlled by the opposing activities of PTKs and PTPs and thus, the aberrant regulation of this modification links both PTKs and PTPs to pathological conditions. At the advent of their discovery, PTPs were not anticipated to be as exciting as their oncogenic PTK counterparts; simply playing 'house-keeping'/'tumor suppressor' roles. Contrary to this assumption, research to date recognizes that PTPs play specific and active, even dominant, roles in setting the levels of tyrosine phosphorylation in cells and in the regulation of many physiological processes (13-18).

Arguably the most prominent example of a "classical" PTP associated with a variety of pathological conditions is the SHP2 tyrosine phosphatase, the proto-oncogenic product of the *Ptpn11* gene. Both biochemical and genetic data support SHP2 inducing the full activation of the Ras/MAPK (ERK1/2; ERK) pathway following mitogenic RTK and cytokine receptor activation through various mechanisms (63). SHP2 localization and activation are regulated by its two tandemly arranged N- and C-SH2 domains. In a latent state, the catalytic PTP domain of SHP2 is physically occluded by the autoinhibitory loop of the N-SH2 domain (62). Following GF-stimulation, SHP2 binds directly to tyrosine phosphorylated motifs present on GF-receptors as well as scaffolding proteins. These binding interactions guide SHP2 subcellular localization to its physiological substrates. Additionally, engagement of the N-SH2 domain to these docking sites is also suggested to diminish its inhibitory interaction with the PTP domain,

leading to SHP2 catalytic activation in the open conformation. A multitude of germ-line as well as somatic mutations are well-recognized to litter the *Ptpn11* gene, leading to SHP2 pathogenic mutant enzymes responsible for the genesis of a pair of 'neuro-cardio-facial-cutaneous' (NFCFC) developmental disorders or 'RASopathies' (e.g. Noonan syndrome (NS) and LEOPARD syndrome (LS) (83-85) as well as a number of hematological malignancies (e.g. juvenile myelomonocytic leukemia and acute myeloid leukemia) (86) and solid tumors (e.g. breast, lung, gastric, and neuroblastoma) (87). Neoplasm- as well as NS-associated SHP2 mutations predominately reside within the N-SH2 domain and induce catalytic activation in the open conformation by strongly disrupting the inhibitory interface created by the N-SH2 and PTP domains in the latent state. The biophysical consequence of this aberrant autoinhibitory relief is the ability to bind pTyr-motifs present on physiological interacting proteins preferentially over the wild-type enzyme and to do so under much less pronounced stimulatory conditions, thus lowering the threshold for and sustaining Ras/ERK pathway activation. Aberrant regulation/activation of the Ras/ERK pathway is a 'hall-mark' of cellular transformation as ERK/MAPK acts as an integration point for multiple biochemical signals, and is involved in a wide variety of cellular processes such as proliferation, differentiation, transcription regulation and development.

The phosphatase of regenerating liver (PRL)-family of phosphatases are becoming respected as *bona-fide* oncogenes within the PTP-family. To date, a putative substrate(s) is not well-recognized for any of the PRLs (1, 2, 3) making efforts at understanding the nature by which they augment tumorigenesis very difficult. Regardless, the PRLs have been implicated as causative factors of tumorigenesis and

metastasis when aberrantly overexpressed. Specifically, PRL3 (*Ptp4a3*) has been shown to be overexpressed in a multitude of advanced neoplasms and metastases originating from physiologically distinct tissues, suggesting a fundamental role for this phosphatase in driving cellular behaviors that are necessary to gain selective advantage toward metastatic dissemination when in excess. At the molecular level, PRL3 is capable of inducing an epithelial-to-mesenchymal transition (EMT) and activate members of the Rho-family GTPases, PI3K-Akt, Ras-ERK, and Src, albeit through a yet enigmatic direct mechanism.

Apart from aberrant activation of proto-oncogenic PTPs, selection against PTP tumor suppressors represents a prominent factor in a multitude of human cancers. PTEN, through dephosphorylation of the 3-position in the sugar head group of inositol phospholipids (e.g. PtdIns(3,4,5)P_3, PIP_3), negatively regulates phosphatidylinositol 3-kinase (PI-3K)-dependent signaling pathways that are associated with cell survival (88). Through its lipid phosphatase activity, PTEN is able to predominately regulate the PI3K/AKT/mTOR pathway responsible for driving survival, proliferation, energy metabolism, and cellular architecture signals. As a consequence, PTEN is the most frequently mutated and deleted tumor suppressor, next to p53, in human cancer. Apart from genetic loss or mutation, PTEN expression and stability are also deregulated in cancer through transcriptional/post-transcriptional (interfering RNA) mechanisms, post-translational modification, and protein·protein interactions (89). Additional PTP tumor suppressors selected against in the pathogenesis of human cancer include: colon cancer-associated receptor/non-receptor ((DEP1; (PTPRJ), PTPρ; (PTPRT), LAR; (PTPRF),

PTPγ; (PTPRG), PTPH1; (PTPN3), PTPBAS; (PTPN13), and PTPD2; (PTPN14)), and PTPκ; (PTPRK) in primary central nervous system lymphomas (82).

Apart from cancer, aberrant regulation of PTPs also plays a fundamental role in other diseases. The lymphoid-specific PTP (Lyp), encoded by the *Ptpn22* gene, is a negative regulator of T and B cell receptor activation. A single nucleotide polymorphism (SNP) in the *Ptpn22* gene generates an R620W mutant Lyp enzyme that has been identified as a putative risk factor in human autoimmunity, including type I diabetes (90), Graves' disease (91), rheumatoid arthritis (92-93), and systemic Lupus erythematosus (94). The R620W mutation has been shown to disrupt an SH3 domain-mediated interaction with the C-terminal Src kinase (Csk), a major negative regulator of the Src tyrosine kinase (90). This mutation has been shown to impart gain-of-function (GOF) properties to Lyp that may cause a pre-disposition to autoimmune disease either by failure to delete autoreactive T cells or due to insufficient activity of regulatory T cells (95).

Finally, the glucan phosphatase Laforin has been postulated to be a glycogen repair enzyme due to its role in dephosphorylating the aberrant C2/C3 phosphomonoesters present in glycogen during glycogen biosynthesis via glycogen synthase (96). Abnormal glycogen phosphorylation is associated with Lafora disease, an autosomal recessive progressive myoclonus epilepsy of which ~50% of patients harbor loss-of-function (LOF) mutations in the *Epm2a* gene that encodes laforin (97-98).

1.3 Research Objectives

The objective of this research is to use mass spectrometry as a tool to provide functional insights into the molecular biochemistry and cellular physiology associated

with two oncogenic PTPs, the phosphatase of regenerating liver 3 (PRL3) and the Src homology-2 (SH2) domain-containing tyrosine phosphatase 2 (SHP2).

1.3.1 Phosphatase of Regenerating Liver 3 (PRL3)

The PRL (Phosphatase of Regenerating Liver) phosphatases represent a unique sub-family of non-classical protein tyrosine phosphatases (PTPs) that are targeted to endomembranes by poly-basic and prenylation motifs at their C-terminus. Available gross-anatomical and biochemical data support these phosphatases being *bona-fide* proto-oncogenes when aberrantly overexpressed, a designation that is rare within the PTP super-family. Unfortunately, since the discovery that PRL1 was an immediate early gene induced during the regeneration period of the rat liver following resection more than two decades ago (99-100), no widely accepted substrate of any of the PRLs (1, 2, or 3) exists to date, making efforts at distilling a concerted mechanism by which these phosphatases potentiate tumorigenesis extremely difficult.

PRL3 represents the 'poster child' of the PRLs due to a large body of research implicating it as a causative factor of metastasis following an initial discovery that its transcript was consistently and massively overexpressed in colorectal carcinoma (CRC) metastases found in the liver, while its expression in non-metastatic primary tumors and normal colorectal epithelium was undetectable (101). In attempts at elucidating the biological function of PRL3, various groups have turned to overexpression studies in a variey of cell culture models. Collectively, data support that the overexpression of PRL3 induces many hallmarks of tumorigenesis in cell culture including: induction of morphological alterations consistent with an epithelial-to-mesenchymal transition (EMT), enhanced proliferative capacity, enhanced migratory/invasive capacity, ability to grow to

heightened densities, and increased capacity to maintain anchorage-independent growth; providing evidence validating the use of this methodology as a plausible avenue towards elucidating the molecular basis for PRL3 function (79). However, data in support of the molecular basis for PRL3 function remains enigmatic and controversial with various proto-oncogenic signaling effectors/modules being implicated in augmenting PRL3-induced tumorigenesis/metastasis including: Integrin receptors, Rho-family GTPases, PI3K-Akt, Ras/ERK, and the Src tyrosine kinase (102-107).

Our group has uncovered that ectopic PRL3 expression in epithelial-HEK293 cells induces the downregulation of Csk (C-terminal Src kinase), a negative regulator of the Src tyrosine kinase, leading to Src-dependent tumorigenic and metastatic bio-functional properties (106). At the molecular level, this aberrant Src activation leads to enhanced 'global' tyrosine phosphorylation including activating phosphotyrosyl-modifications to the extracellular signal-regulated protein kinase 1 and 2 (ERK1/2), signal transducer and activator of transcription 3 (STAT3), and the Crk-associated substrate ($p130^{Cas}$). We postulated that an aberrantly activated Src kinase has the ability to pleiotropically potentiate the many distinct oncogenic bio-functional properties previously mentioned and by following the tyrosine phosphorylation 'profile' we would gain critical insight into the PRL3-mediated signaling network.

Here, we present the application of a novel phosphoproteomic strategy predicated upon a tandem phosphotyrosine-peptide enrichment using 'pan' pTyr-antibody immunoprecipitation and polymer-based metal ion affinity capture (PolyMAC) with titanium (Ti)-functionalized soluble nanopolymers/polyamidoamine-dendrimers (108). We hypothesized that this strategy would allow us the opportunity to define increased

tyrosine phosphorylation initiated from the aberrant activation of an endogenous tyrosine kinase population, amongst an overwhelming population of pSer/pThr-containing and non-phosphorylated proteins. Identification of the complete repertoire of proteins experiencing enhanced levels of tyrosine phosphorylation in the PRL3 expressing cells is postulated to help us paint the most comprehensive picture to date of how PRL3 drives pro-metastatic molecular events through Src activation. The overarching goal of this research is to provide critical insight to future investigations aimed at defining a putative substrate(s) of PRL3 within the context of this network.

1.3.2 Src homology-2 (SH2) domain-containing tyrosine phosphatase 2 (SHP2)

The Src-homology 2 (SH2) domain-containing tyrosine phosphatase 2 (SHP2), encoded by the *Ptpn11* gene, is a *bona-fide* proto-oncogene in the PTP super-family responsible for the full activation of the Ras/extracellular signal-regulated kinase 1/2 (ERK1/2) pathway following mitogenic receptor tyrosine kinase (RTK) and cytokine receptor activation through various mechanisms (63). SHP2 localization and activation are regulated by its two tandemly arranged N- and C-SH2 domains. In a latent state, the catalytic PTP domain of SHP2 is physically occluded by the autoinhibitory loop of the N-SH2 domain (62). Following growth factor (GF)-stimulation, SHP2 binds directly to tyrosine phosphorylated motifs present on GF-receptors as well as scaffolding proteins. These binding interactions guide SHP2 subcellular localization to its physiological substrates. Additionally, engagement of the N-SH2 domain to these docking sites is also suggested to diminish its inhibitory interaction with the PTP domain, leading to SHP2 catalytic activation in the open conformation.

A multitude of germ-line and somatic missense mutations litter the *Ptpn11* gene resulting in aberrantly regulated SHP2 mutant enzymes that potentiate the pathogenesis of the autosomal dominant neuro-cardio-facio-cutaneous (NCFC) developmental disorders, Noonan- and LEOPARD (an acronym for its clinical features of multiple Lentigines, ECG abnormalities, Ocular hypertelorism, Pulmonic stenosis, Abnormal genitalia, Retardation of growth and Deafness)-syndromes (NS and LS) as well as various hematological malignancies and solid tumors (83-84, 86-87). Available biochemical evidence supports NS- and neoplasia-associated SHP2 mutations, which predominately reside within the interface region between the N-SH2 and PTP domains, engendering gain-of-function (GOF) effects through weakening the interaction that these two domains make in the autoinhibited closed state (109-113). On the other hand, LS-associated SHP2 mutations that reside within the catalytic site and induce catalytic impairment create mutant enzymes responsible for the pathogenesis of a syndrome that shares many clinical features with NS, a disease that manifests from the activity of GOF-SHP2 mutants (113-115). How do mutations that provoke opposite effects on SHP2 phosphatase activity cause phenotypically similar disorders? We hypothesized that LS-SHP2 pathogenic mutations, which create catalytically impaired SHP2 mutant enzymes, also perturb the molecular switching mechanism, leading to mutant enzymes with increased propensity to adopt the 'open·active' conformation. As a result, LS-SHP2 mutants bind upstream activators preferentially and stay longer with the scaffolding adaptors thus prolonging specific substrate turnover, which compensate for the reduced phosphatase activity. Thus, catalyically impaired LS-SHP2 mutants may engener GOF phenotypes.

Here we apply hydrogen-deuterium exchange mass spectrometry (H/DX-MS) as a methodology capable of defining how the various SHP2 pathogenic mutations perturb the natural solution-phase dynamic conformational alterations observed to take place in the wild-type enzyme. Our goal is to provide the first direct evidence that LS-associated SHP2 mutations which induce catalytic impairment also weaken the autoinhibitory interaction that the N-SH2 domain makes with the PTP catalytic domain, an absolute requirement for GOF-effects to be realized *in-vivo*. Our H/DX-MS data, in addition to data generated at the structural, biochemical, and cellular levels, will provide critical insight to the relationship that LS-SHP2 mutants have with their GOF NS/neoplasia-mutant counterparts toward engendering pathological GOF-effects, *in-vivo*.

CHAPTER 2: MATERIALS AND METHODS

2.1 Phosphatase of Regenerating Liver 3 (PRL3) drives pro-metastatic molecular events through a Src-dependent aberrant tyrosine phosphoproteome.

2.1.1 Materials

Dulbecco's Modification of Eagles Medium (DMEM) with 4.5g/L glucose, L-glutamine, sodium pyruvate, and penicillin-streptomycin (5,000 I.U/mL penicillin; 5,000 μ/mL streptomycin) were from Mediatech, Inc. (Manassas, VA, USA). Fetal Bovine Serum (FBS) was from Hyclone (Logan, UT, USA). SILAC-DMEM media minus L-Lysine and L-Arginine with 4.5g/L glucose, L-glutamine, and sodium pyruvate was from Thermo-Fisher Scientific (Rockford, IL, USA). Dialyzed Fetal Bovine Serum for SILAC, L-Lysine monohydrochloride, L-Arginine monohydrochloride, L-Lysine ^{13}C hydrochloride, L-Arginine ^{13}C hydrochloride, agarose-conjugated anti-phosphotyrosine monoclonal antibody PT66, Dithiothreitol (DTT), Iodoacetamide, and Trypsin were from Sigma-Aldrich (St. Louis, MO, USA). Anti-phosphotyrosine (PY100), β-Actin, ERK1/2, pERK1/2 (Thr202/Tyr204), STAT3, pSTAT3 (Tyr705), PLCγ1, pPLCγ1 (Tyr783), PDGFRα, and PDGFRβ monoclonal antibodies were from Cell Signaling Technology (Beverly, MA, USA). Protein A/G-Plus agarose was from Santa Cruz Biotechnology (Santa Cruz, CA, USA). Trizol reagent was from Invitrogen (Grand Island, NY, USA). Src inhibitor SU6656 was from Calbiochem/EMD Biosciences (La Jolla, CA, USA).

2.1.2 Cell culture and stable clone selection

HEK293 cells were grown in Dulbecco's modified Eagle's medium (DMEM) supplemented with 10% fetal bovine serum (FBS), penicillin (50 units/mL), and streptomycin (50μg/mL) under a humidified atmosphere containing 5% CO_2. Human

PRL3 was inserted into pCDNA3 (106) and v207 expression vectors (v207 as described in (116)). Transfection and stable clone selection for pCDNA3 as described in (106). HEK293 cells were seeded so that 40-50% confluence would be achieved following an over-night incubation period. v207-PRL3 constructs were transfected into HEK293 cells maintained in antibiotic-free medium using Poly(ethylenimine) (PEI). 24 h after transfection, Puromycin (1μg/mL) was added to the culture medium to initiate stable clone selection. Stable clones were picked after 2 weeks of selection under Puromycin.

2.1.3 mRNA extraction and RT-PCR

mRNA from experimental cell lines was prepared using Trizol reagent. mRNA was treated with DNase and quantified by absorbance at 260 and 280nm following an RNA clean-up using an RNeasy Mini Kit (Qiagen). RT-PCR was performed using the Invitrogen SuperScript one-step RT-PCR kit. Reverse transcription was done at 50 °C for 30min, and cDNA was amplified by PCR for 36 cycles (94 °C, 30s; 55 °C, 30sec; 68 °C, 1min). The sequences of specific primers were as follows: PRL3 sense, 5'-CTTCCTCATCACCCACAACC-3' and PRL3 anti-sense, 5'-GTCTTGTGCG TGTGTGTGGGTC-3'; 18 S ribosome sense, 5'-CGCCGCTAGAGGTGAAATTC-3' and 18 S anti-sense: 5'-TTGGCAAATGCTTTCGCTC-3'. The PCR products were separated by 2% agarose gel and visualized by staining with ethidium bromide.

2.1.4 Immunoblotting and immunoprecipitation

Cells were grown in DMEM supplemented with 10% FBS, penicillin (50 units/mL), and streptomycin (50μg/mL) under a humidified atmosphere containing 5% CO_2 to 70-80% confluency, washed with ice-cold phosphate-buffered saline (PBS), and lysed on ice for 30 min in 500μL-1mL of lysis buffer (100mM Tris-HCl, pH 7.5, 150mM

NaCl, 1% Triton X-100, 5% Glycerol, PhosSTOP phosphatase inhibitor cocktail tablet (Roche), and a Complete EDTA-free protease inhibitor cocktail tablet (Roche)). Cell lysates were cleared by centrifugation at 15,000 rpm for 15 min. Lysate protein concentration was assayed using the BCA protein assay kit (Pierce) (measurements for the standard series and experimental groups were kept under 5% coefficient of variation-CV). For immunoprecipitation, 10µg antibody was added to 1mg protein lysate and incubated at 4 °C for 4h to over-night by end-over-end rotation. 20µL of protein A/G-plus agarose beads was then added and incubated with sample for an additional 2 h at 4 °C using end-over-end rotation. After extensive washing, protein complex was boiled with Laemmli (SDS)-sample buffer, separated by SDS-PAGE, transferred electrophoretically to a nitrocellulose membrane, and immunoblotted with appropriate antibodies followed by incubation with horseradish peroxidase-conjugated secondary antibodies. The blots were developed by the enhanced chemiluminescence technique using the SuperSignal West Pico Chemiluminescent substrate (Pierce). Data shown is a representation of multiple repeat experiments.

2.1.5 Imaging

Stable RFP-PRL3-WT and RFP-vector HEK293 cells were grown to sub-confluence and RFP was visualized by confocal microscopy from live cells. Confocal images were acquired on Zeiss Axio ObserverZ1 as structured light via an Apotome and processed with Axiovision 4.7.

2.1.6 Label-free quantitative mass spectrometry

Stable PRL3-HEK293 cells and their vector control HEK293 cell counterparts were grown to 80% confluency in DMEM supplemented with 10% FBS, penicillin (50

units/mL), and streptomycin (50μg/mL) at 37 °C under a humidified atmosphere containing 5% CO_2. This study was comprised of 2 groups with 7 biological replicates per group allowing for 14 randomized HPLC injections. A detailed account of the label-free LC/MS-based protein quantification method used in this study, including MS-data acquisition and analysis can be viewed in (117-119).

2.1.7 Stable Isotope Labeling of Amino acids in Cell culture (SILAC)-based quantitative mass spectrometry

SILAC (Stable Isotope Labeling of Amino acids in Cell culture) DMEM without L-Lysine or L-Arginine was supplemented with 7.5% dialyzed FBS and 2.5% undialyzed FBS, penicillin (50 units/mL), streptomycin (50μg/mL), and either ($^{12}C_6$ – L-Lysine monohydrochloride; $^{12}C_6$ – L-Arginine monohydrochloride) or ($^{13}C_6$ – L-Lysine monohydrochloride; $^{13}C_6$ – L-Arginine monohydrochloride) to create SILAC-'Light' or SILAC-'Heavy' media, respectively. PRL3-HEK293 and their vector-control HEK293 counterparts were grown in both SILAC-'Heavy' and SILAC-'Light' media, respectively, for a total of 5 passages prior to testing the labeling efficiency of the SILAC-'Heavy' media. Tryptic-peptides from the 'Heavy-labeled' PRL3-HEK293 cell lysate were prepared as documented below in the *Phosphopeptide enrichment using phosphotyrosine-immunoprecipitation and PolyMAC-Ti reagents* section. Data for 2,725 tryptic-peptides were acquired following a single-dimension reverse phase HPLC separation. Of the 2,725 total peptides, 2,613 peptides were completely labeled with $^{13}C_6$-Lysine and/or $^{13}C_6$-Arginine, while just 112 peptides contained no labeled amino acids (96% labeling efficiency). This degree of labeling efficiency was deemed sufficient for quantitative mass spectrometry to be carried out. Quantitative data analysis was

carried out by Proteome Discoverer V1.3. See the *Mass spectrometry (LTQ-Orbitrap) analysis and phosphopeptide data acquisition and analysis* sections for methodology following cell culture.

2.1.8 Phosphopeptide enrichment using phosphotyrosine-immunoprecipitation and PolyMAC-Ti reagents

PRL3-HEK293 and vector-control HEK293 cells were grown in either normal DMEM supplemented with 10% FBS for qualitative analysis or SILAC-'Heavy'/SILAC-'Light' DMEM supplemented with 7.5% dialyzed FBS/2.5% undialyzed FBS for quantitative analysis. Upon reaching 80% confluence cells were lysed in ice cold lysis buffer (100mM Tris-HCl, pH 7.5, 150mM NaCl, 1% Triton X-100, 5% glycerol, PhosSTOP phosphatase inhibitor cocktail (Roche), and Complete EDTA-free protease inhibitor cocktail (Roche)). Lysate protein concentration was quantified using the BCA assay (measurements for the standard series and experimental groups were kept under 5% coefficient of variation-CV). 2.5mg lysate protein/experimental group were used for subsequent steps (at this point if SILAC-based quantitation was performed, the PRL3 and vector-control lysates were consolidated to a single master lysate) (for qualitative assessment lysate protein from both experimental groups was held at an equivalent concentration and total volume). Lysate protein was denatured using 0.1% RapiGest surfactant (Waters) in 50mM trimethylammonium hydrogen carbonate (bicarbonate) (TMAB). Protein disulfides were reduced using 10mM dithiothreitol (DTT) in a 30 min incubation at 50 °C. Reduced sulfhydryls were then alkylated using 20mM iodoacetamide (IAA) in a 1 h incubation at ambient temperature. The pH was adjusted to 8.0 using 1M TMAB prior to the trypsin digestion reaction. Proteins were then subjected

to an over-night (12 h) digestion at 37 °C by the trypsin endoproteinase (Sigma) at a ratio of 1:100 (trypsin:lysate protein). RapiGest was removed by reducing the pH to <3.0 using 1M HCl (final concentration 100-120mM in the sample) and incubating the sample at 37 °C using a water bath for 40 min. The supernatant was transferred to a new non-stick/low-binding OmniSeal tube (Life Science Products, Inc.). The pH was adjusted to 7.5 using 1M Tris and 100µL of the anti-pTyr-antibody PT66-agarose conjugate slurry (Sigma) was added to the sample. Phospho-tyrosyl tryptic peptides were immunoprecipitated using the 'pan' anti-pTyr-PT66 antibody over-night (12 h) at 4 °C by end-over-end rotation. The PT66-agarose beads were extensively washed using ice cold lysis buffer and H_2O. The phosphopeptides were eluted from the PT66-agarose beads using a series of elution steps with 0.1% trifluoroacetic acid (TFA), 0.1% TFA/50% acetonitrile, and 100mM glycine pH 2.5. The consolidated eluent was dried down using vacuum centrifugation. The dried down product was solvated in 150mM HEPES, pH 6.8. A secondary-phosphopeptide enrichment was then performed using a PolyMAC-Ti reagent as per the protocol documented in (108). A complete documentation regarding the above methodology can be viewed in (108).

2.1.9 Mass spectrometry (LTQ-Orbitrap) analysis

Peptide samples were solvated in 8µL of 0.1% formic acid and injected into an Agilent nanoflow 1100 HPLC system. The reverse phase C_{18}-based chromatography was performed using an in-house C_{18}-capillary column packed with 5-µm C_{18} Magic bead resin (Michrom; 75µm inner-diameter and 12-cm bed length) on an 1100 Agilent HPLC system (120). The mobile phase buffer consisted of 0.1% HCOOH in ultrapure water with the eluting buffer of 100% CH_3CN run over a shallow linear gradient over 60 min

with a flow rate of 0.3μL/min. The electrospray ionization emitter tip was generated on the pre-packed column with a laser puller (Model P-2000, Sutter Instrument Co.). The Agilent 1100 HPLC system was coupled on line with a high resolution hybrid linear ion trap orbitrap mass spectrometer (LTQ-Orbitrap XL, Thermo Fisher Scientific). The mass spectrometer was operated in the data-dependent mode in which a full MS scan (from *m/z* 300 to 1700 with a resolution of 30,000 at *m/z* 400) was followed by four MS/MS scans of the most abundant ions meeting a 1000 signal threshold count mark. Ions with a charge state of 1+ were excluded. The mass exclusion time was 180s.

2.1.10 Phosphopeptide data acquisition and analysis

LTQ-Orbitrap raw files were searched directly against a Homo-sapiens database with no redundant entries (67,250 entries; human International Protein Index (IPI) version 3.83) using the SEQUEST and Mascot algorithms as part of Proteome Discoverer software V1.3 (Thermoelectron, San Jose, CA, USA). Peptide mass tolerance was set at 10 ppm, and MS/MS tolerance was set at 0.8 Da. Search criteria included a static modification of cysteine residues of +57.0214 Da, variable modifications of +15.9949 Da to include potential oxidation of methionine residues, and a modification of +79.996 Da on tyrosines for identification of phosphorylation. Searches were performed with full tryptic digestion and allowed a maximum of two missed cleavages on the peptides analyzed from the sequence database. The parameters for FDR were set for 1% for each analysis. Proteome Discoverer software generated a reverse "decoy" database from the chosen database, and any peptides passing the initial filtering parameters that were derived from this decoy database are defined as false positive identifications. The minimum cross-correlation factor (Xcorr) filter was then re-adjusted for each individual

charge state separately in order to optimally meet the predetermined target FDR of 1% based on the number of random false-positive matches from the reversed "decoy" database. Thus, each dataset had its own passing parameters. The Percolator semi-supervised machine learning algorithm, as part of the Proteome Discoverer V1.3 software package, was used to assist in the generation of the 1% FDR threshold (results for each PSM were given as q-values in the data analysis). The most likely phosphorylation site localization from CID mass spectra was determined by PhosphoRS algorithm within the Proteome Discoverer 1.3 software. The number of unique phosphopeptides and nonphosphopeptides identified were then counted and compared. SILAC quantitation was carried out using Proteome Discoverer software V1.3, which uses the MS peak areas of the "light" and "heavy" peptides and reports "light/heavy" (L/H) ratios. The significance threshold for quantitation parameters were determined by Proteome Discoverer V1.3 internal statistical algorithm, resulting in at least 2-fold passing significance ratio for L/H ratio after the removal of outliers. Search criteria included variable modifications of ($^{13}C_6$)-Lys and -Arg residues of +6.02Da. Quantification method was (SILAC 2plex (Arg6, Ly6) (Custom). RT tolerance of isotope pattern multiplets was set to 0.2min.

2.1.11 Ingenuity Pathway Analysis (IPA)

All proteins from the PRL3 and vector-control datasets that possess a tyrosine-phosphorylated peptide(s) and their corresponding SILAC-based quantification values (1% FDR data following Sequest and Mascot searches of the IPI human v3.83 database) were uploaded to Ingenuity Pathway Analysis (IPA) software (Ingenuity Systems, Inc.). A new core analysis was created that included: Ingenuity knowledge base (genes only) reference set, direct and indirect relationships to target proteins, and a filter summary

which included: (species: human, confidence: experimentally observed, data sources: Ingenuity expert findings). The top scoring network (Network 1) and top 10 predicted canonical paths and biofunctions (using a B-H (Benjamini-Hochberg) p-value adjustment) were used to represent the current dataset.

2.2 Functional insights into LEOPARD syndrome-associated SHP2 mutations

2.2.1 Materials

The expression plasmid pET-21a (+) was obtained from Novagen (Milwaukee, WI). The *Escherichia coli* strain BL21 (DE3) pLysS and QuikChange site-directed mutagenesis kit were purchased from Stratagene (La Jolla, CA). Nickel-nitrilotriacetic acid-agarose (Ni-NTA) beads were purchased from Qiagen (Basel, Switzerland). All other reagents were purchased from Fisher (Fair Lawn, NJ). Pepsin endoproteinase was obtained from Sigma. Mass spectrometry grade H_2O and acetonitrile was obtained from Burdick and Jackson. Deuterium oxide (D_2O; 99.9 atom % D) was from Aldrich.

2.2.2 Plasmid construction and mutagenesis

The sequence coding for SHP2 (residues 1-528) were amplified from the full length construct by PCR-based strategy using primers (Table 7). The PCR products were gel purified, digested with Nde I and Xho I restriction enzymes and the resulting fragment was inserted into the pET-21a (+) plasmid with a C-terminus polyhistidine tag, which was previously digested with the same restriction enzymes. The resulting plasmid was designated pET-21a (+)/SHP2 (1-528). All mutants of SHP2 (1-528) were prepared using the QuikChange site-directed mutagenesis kit for generating the single point mutants from the plasmid pET-21a (+)/SHP2 (1-528). All recombinant plasmids

containing wild-type truncations and mutations were verified by DNA sequencing and transformed into *E. coli* strain BL21 (DE3) pLysS competent cells for expression.

2.2.3 Expression and purification of recombinant proteins

SHP2 proteins with C-terminus polyhistidine tag (SHP2 C-6His) were expressed in BL21 (DE3) pLysS cells and grown at 37 °C in Luria broth (LB) containing 100 μg/mL ampicillin for 4 h to an absorbance of 0.6 at 600 nm and then induced for protein production with 0.4 mM IPTG overnight at 22 °C. Cells were harvested by centrifugation (6000 rpm for 15 min at 4 °C), and the cell pellets from 1.5 L LB medium were suspended in 30 mL of ice-cold lysis buffer (5 mM imidazole, 500 mM NaCl, 20 mM Tris-HCl (pH 7.9), 0.05 mg/mL trypsin inhibitor, 5mM β-mercaptoethanol, and 0.1 mM PMSF). The suspensions were passed twice through a French press at 1200 psi, and the cell lysates were centrifuged at 4 °C for 45 min at 15 000 rpm. The supernatants were mixed with 2 mL of Ni-NTA Agarose at 4 °C for 50 min, washed with 100 mL of lysis buffer. After washing with lysis buffer containing 20 mM imidazole, the proteins were eluted with 20 mL lysis buffer containing 200 mM imidazole then dialyzed with buffer (20 mM Tris-HCl, pH 7.8, 150mM NaCl, 1 mM EDTA, 2 mM Dithiothreitol (DTT)) at 4 °C to remove imidazole and then stored at -80 °C until use. Fractions were analyzed by sodium dodecyl sulfate (SDS)-10% polyacrylamide gel electrophoresis (PAGE). (1-528 constructs): WT (37.8mg/mL; 613μM), D61Y (43.1mg/mL; 698μM), E76K (31.8mg/mL; 516μM), Y279C (35.1mg/mL; 570μM), A461T (40.9mg/mL; 663μM), G464A (29.8mg/mL; 483μM), T468M (28.4mg/mL; 460μM), R498L (31.8mg/mL; 516μM), Q506P (28mg/mL; 454μM), Q510E (31.1mg/mL; 504μM), and T507K

(26.1mg/mL; 423μM). Table 7 shows the general purity of all LS-SHP2 mutants by way of a coomassie-stained gel.

2.2.4 Kinetic analysis of SHP2 catalyzed reaction

Initial rate measurements for the enzyme-catalyzed hydrolysis of *p*NPP were conducted at 25°C in a pH 7.0 buffer of 50mM 3,3-dimethylglutarate, containing 1mM DTT and 1mM EDTA, with an ionic strength of 0.15M, adjusted by addition of NaCl. Assay mixtures of 200μl in total volume were set up in a 96-well plate. A substrate concentration range from 0.2~5 K_m was used to determine the k_{cat} and K_m. Reactions were started by the addition of an appropriate amount of wild-type or mutant SHP2. The reaction mixtures were quenched with 50μl of 5M sodium hydroxide, and the absorbance at 405nm was read using a plate reader. The steady state kinetic parameters were determined from a direct fit of the data to the Michaelis-Menten equation using SigmaPlot.

2.2.5 Inhibition of the SHP2 PTP domain by the N-SH2 domain

PTP activity was assayed using *p*-nitrophenyl phosphate (*p*NPP) as a substrate in a pH 7.0 buffer containing 50mM 3,3-dimethylglutarate, 1mM EDTA, 150mM NaCl at 25°C. The assays were performed in 96-well plates with final reaction volume of 0.2mL. The reaction was initiated by the addition of enzyme (catalytic domain of wild-type SHP2 or Y279C) to a reaction mixture containing *p*NPP (2mM for the wild-type or 10mM for Y279C) with various concentrations of the N-SH2 domain. For K_i determination, *p*NPP concentration was varied while the N-SH2 domain was fixed at 3 different concentrations. The reaction rate was measured using a SpectraMax Plus 384

Microplate Spectrophotometer (Molecular Devices). Data fitting was performed using SigmaPlot Kinetics module.

2.2.6 Making the deuterium buffer

Deuterium oxide (^2H_2O; D_2O) (99.99%) (Sigma) was used to make a ^2H_2O-based 20mM Tris·HCl, 50mM NaCl, 2mM DTT, 1mM EDTA buffer stock solution at pD8.0. The D_2O buffer components were weighed as dry material and solvated in pure D_2O (99.99%). To remove residual ^1H_2O contained within the dry buffer materials, the D_2O was evaporated by vacuum centrifugation and the left over dry material was again solvated in pure D_2O (99.99%). This process was repeated two times. The pD was adjusted to 8.0 with very small microliter amounts of 12N HCl so as to not compromise the high purity of the D_2O solution during pD adjustment.

2.2.7 Intact (native) protein preparation and data acquisition

SHP2 (WT or mutant) stock was diluted 30x (1.5μL to 43.5μL) in either the H_2O- or D_2O-based 50mM Tris·HCl, 50mM NaCl, 2mM DTT, 1mM EDTA buffers, pH(D)8.0 (note: Protein stock solutions were held on ice for the entirety of investigation. Prior to dilution, the 1.5μL aliquot was held at ambient temperature for 1min and then introduced into either the H_2O- or D_2O-based buffers held at 37°C by way of a water bath). The deuterium-labeling reactions were 'quenched' using a (1:1 ; v:v) ratio or (45μL) 100mM Sodium phosphate buffer pH2.3 held on ice (note: final pH of the solution after quenching was confirmed to be ~2.3) at various time points from 5sec-1hr. (5s, 10s, 30s, 1m, 10, 30m, 1hr.). The no-label control samples were treated in the same manner as the deuterium-labeled samples except for protein stock dilution was done in a H_2O-based buffer instead of a D_2O-based buffer. (10μg) of intact protein, following the quenching

step, was loaded by a Finnigan Surveyor autosampler onto a Zorbax SB-C8 1.0x50mm 3.5μm column (Agilent). Sample intact protein was washed (85% H_2O/15% ACN/0.1% Formic acid) and then eluted isocratically from the column (65% H_2O/35% ACN/0.1% Formic acid) in 7min. at 150μL/min. (note: full gradient conditions: 0min. (85/15); 0.1min. (65/35); 7min. (65/35); 8min. (40/60); 11min. (40/60); 12min. (85/15); 15min. (85/15)). The eluted sample was electrosprayed into a Finnigan LTQ mass spectrometer at a flow rate of 150μL/min. Data was collected in a 600-1200m/z range. ESI source settings: Spray voltage (4.79kV), Spray current (1.69μA), Sheath gas flow rate (28.01), Aux gas flow rate (0.02), Sweep gas flow rate (0.21), Capillary voltage (26.96V), Capillary temperature (224.93 °C), Tube lens voltage (120.11V).

2.2.8 Peptic peptide preparation and data acquisition

The same procedure was performed for peptide analysis as was performed for intact protein analysis except that the 100mM Sodium phosphate buffer pH2.3 contained solvated Pepsin endoproteinase (Sigma) at a (1:1 ; w:w) ratio with the experimental SHP2 protein (note: (1:1 ; w:w ratio) and a (~1 : 1.75 concentration ratio; SHP2 : Pepsin). Pepsin-mediated digestion was allowed to proceed on ice for 3min. (20μg) of peptic peptides, following the quenching step, were loaded by a Finnigan Surveyor autosampler onto a XBridge C18 2.0x50mm 2.5μm column (Waters). Sample peptic peptides were washed then eluted in 8min. by a shallow gradient (10% ACN/0.1% Formic acid→35% ACN/0.1% Formic acid) at 200μL/min. (note: full gradient conditions: 0min. (98/2), 0.1min. (90/10), 8min. (65/35), 10min. (20/80), 10.1min. (20/80), 12min. (20/80), 12.1min. (98/2), 15min. (98/2)). The eluted sample was electrosprayed into a Finnigan LTQ mass spectrometer at a flow rate of 200μL/min. ESI

source settings: Spray voltage (4.79kV), Spray current (1.69μA), Sheath gas flow rate (28.01), Aux gas flow rate (0.02), Sweep gas flow rate (0.21), Capillary voltage (26.96V), Capillary temperature (224.93 °C), Tube lens voltage (120.11V). Peptide data was acquired first in data-dependent (MS/MS) mode using the following parameters (400-1800m/z range): Isolation width (2.0 m/z), Normalized collision energy (35), Default charge state (+2), Minimum signal threshold counts (500), Activation Q (0.25), Activation time (30ms), Ion time (50ms), $MS \rightarrow MS^2$ on the 5 most intense ions from each parent ion scan. Peptide data was also collected in single MS fashion for weighted average mass (WAM) value generation in an enhanced scan rate setting and in profile mode.

2.2.9 Data analysis and presentation

All no-label and deuterium labeling intact (native)- and peptide-based experiments were done by hand and in triplicate so that comparisons could be made via averages and significance could be established based upon standard deviations per time point. For intact mass analysis, data deconvolution and mass interpretation was performed with aid from ESIprot1.0 software (121). Data presented in the intact protein section is in the format (mutant relative to wild-type) and thus the experimental data points taken per time point for each mutant are deemed significant relative to wild-type based upon a comparison of two means via a paired *t*-test (*p*-value significance marked per time point per criteria documented). Peptide-based data was acquired both in MS scan mode and in $MS \rightarrow MS^2$ (MS/MS) mode per analysis intention. As the SHP2 proteins were purified from *E.coli*, SHP2 peptic peptides were identified based upon a database query of the entire *E.coli* proteome with the SHP2 (WT or mutant; 1-528)

sequence embedded, using the Sequest algorithm as part of the Proteome Discoverer platform (Thermo). For further analysis of purity and confidence in identification, the same query was performed using the entire human proteome. All searches were performed using a decoy database for further aid in confidence in identification (with FDR set at 1-5%). The databases were queried using the general criteria for data coming from an LTQ mass spectrometer: average parent ion ($\leq$ 1.0Da) and daughter ion ($\leq$ 0.8Da) mass tolerance at charge states (+1, +2 and +3). Due to the general promiscuity of pepsin 'no enzyme' was chosen for the database query. High quality parent ion isotopic (no-label) and deuterium-labeling envelopes were acquired in single MS (enhanced) scan mode so that the highest quality spectrums could be used to generated WAM (weighted average mass) measurements following deuterium labeling. Peptides were assigned to representative parent ions in the MS-scan based upon their *m/z*, charge state, and retention time information generated following database query using $MS \rightarrow MS^2$ data. Deuterium incorporation versus time plots were generated based upon plotting average WAM values per time point relative to an average 'zero' point generated from no-label data. Unbiased WAM values were generated with aid from HX-Express software (122). As all proteins were handled in the same manner experimentally, deuterium levels were not corrected for back-exchange and are therefore reported as relative (123). In this work, peptide-based deuterium exchange data is presented in the format (mutant relative to wild-type) and significance in exchange is documented based upon differences in average measurements per time point where an average must be at least (0.4Da) and 2σ (standard deviations) from its counterpart. This significance criteria

must be maintained in at least 2 consecutive time points for the peptide under comparison to be colored based upon the significance legend provided in each figure.

CHAPTER 3: PHOSPHATASE OF REGENERATING LIVER 3 (PRL3) DRIVES PRO-METASTATIC MOLECULAR EVENTS THROUGH A SRC-DEPENDENT ABERRANT TYROSINE PHOSPHOPROTEOME

3.1 Introduction

Protein-tyrosine phosphatases (PTPs) play critical regulatory roles during signal transduction and when deregulated cause aberrant tyrosine phosphorylation that lies at the heart of many human diseases, including cancer (19, 124-125). The PRL (Phosphatase of Regenerating Liver) phosphatases represent a unique sub-family of prenylated PTPs comprised of three members (PRL1, 2, and 3) that share (>75%) of amino acid sequence identity (100, 126-127). A ground-breaking observation that PRL1 was an immediate early gene induced prior to the regeneration period of the rat liver following resection brought attention to the PRL-family as potential proto-oncogenes (99). Over more than two decades, research at the gross anatomical and molecular levels continues to provide evidence that the PRLs may play causative roles in tumorigenic and metastatic processes when aberrantly overexpressed (79).

PRL3 (*Ptp4a3*) was first cast into the spotlight as a potential causative factor of metastasis when its transcript was found to be consistently and massively overexpressed in colorectal carcinoma (CRC) metastases found in the liver, while its expression in non-metastatic primary tumors and normal colorectal epithelium was undetectable (100). Subsequently, PRL3 transcript was found to be elevated in all metastatic lesions derived from CRC, regardless of the site of metastasis (liver, lung, brain, or ovary) (128-129). In addition, PRL3 transcript as well as protein has been found to be overexpressed in a variety of advanced neoplasms or metastases originating from a multitude of

physiologically distinct tissues (79, 130-131), suggesting a fundamental role for this phosphatase in driving cellular behaviors that are necessary to gain selective advantage toward metastatic dissemination when in excess.

To date, biochemical research has focused on overexpression studies in a variety of cell culture models in an effort to decipher the mechanism by which PRL3 drives the acquisition of cellular properties associated with tumorigenesis and metastasis. *In-vivo*, cells stably expressing PRL3 exhibit enhanced motility and invasive activity and are able to induce metastatic tumor formation in mice (132-133), while knockdown of endogenous PRL3 in tumor cells expressing high levels of this phosphatase using small-interfering RNA abrogates cell motility and the ability to metastasize in a mouse model (134-136). Importantly, stable ectopic expression of PRL3 has been shown to induce an epithelial-to-mesenchymal transition (EMT) (102-103, 106, 132-133), an essential process that precedes metastatic dissemination (137). Additionally, stable ectopic expression of PRL3 induces many hallmarks of tumorigenesis that have been shown to be dependent upon its phosphatase activity including: enhanced proliferative capacity, anchorage-independent growth, ability to grow to increased densities, enhanced wound healing capacity, and enhanced migration/invasion potential (79, 130). This data provide evidence validating the use of this methodology as a plausible avenue towards elucidating the molecular basis for PRL3 function. Through a variety of candidate approaches investigators have been successful in documenting molecular evidence supporting the activation of key regulators of transformation and pro-metastatic molecular events following PRL3 expression including: Integrin receptors (104-105, 138), Rho-family GTPases (102), PI3K-Akt (103), Ras-ERK (104, 106), and the Src tyrosine kinase (106-

107). Collectively, these signaling effectors/modules are canonically activated following extracellular ligand-mediated stimulation of tyrosine phosphorylation. How does the overexpression of a phosphatase 'tilt' the natural regulation of tyrosine phosphorylation toward a stimulus that would support the sustained activation of these effectors? Additionally, what transmembrane receptors and molecular adaptors are tyrosine phosphorylated/activated to integrate this pleiotropic response? To date, the molecular basis for PRL3 function remains an enigma, predominately due to a complete lack of knowledge regarding a putative substrate, making efforts at distilling a concerted mechanism that would potentiate metastatic dissemination very difficult.

We have previously documented that stable ectopic expression of PRL3 drives aberrant Src tyrosine kinase activation by downregulating Csk (C-terminal Src kinase), a major negative regulator of Src, in epithelial-HEK293 cells (106). It was shown that this aberrant Src activation leads to enhanced 'global' tyrosine phosphorylation including activating phosphotyrosyl-modifications to the extracellular signal-regulated protein kinase 1 and 2 (ERK1/2), signal transducer and activator of transcription 3 (STAT3), and the Crk-associated substrate ($p130^{Cas}$). We postulated that an aberrantly activated Src kinase has the ability to pleiotropically potentiate the many distinct oncogenic bio-functional properties previously mentioned and by following the tyrosine phosphorylation 'profile' we would gain critical insight into the PRL3-mediated signaling network. Furthermore, we hypothesized that the identities of the complete repertoire of proteins experiencing enhanced levels of tyrosine phosphorylation in the PRL3 expressing cells would help us paint the most comprehensive picture to date of how PRL3 drives pro-metastatic molecular events through Src activation.

Here, we present the application of a novel phosphoproteomic strategy predicated upon a tandem phosphotyrosine-peptide enrichment using 'pan' pTyr-antibody immunoprecipitation and polymer-based metal ion affinity capture (PolyMAC) with titanium (Ti)-functionalized soluble nanopolymers/polyamidoamine-dendrimers (108). Phosphoproteomic data derived from the PRL3 cells provide strong evidence in support of aberrant Src kinase activation and afford insight into the context by which Src drives pro-metastatic molecular events upon PRL3 expression. Interestingly, we have uncovered a rich signal transduction network downstream of a mitogenic and chemotactic PDGF (α and β), Eph (A2, B3, B4) and Integrin (β1 and β5) transmembrane receptor array known to be utilized by migratory mesenchymal cells during development as well as during acute wound healing in the adult animal. Furthermore, tyrosine phosphorylation is present on a multitude of signaling effectors responsible for Rho-family GTPase, PI3K-Akt, Jak-STAT3, and Ras-ERK1/2 pathway activation, linking observations made by the field as a whole under Src as a primary signal transducer. We present the most extensive and comprehensive model to date of how PRL3 potentiates pro-metastatic molecular events through Src activation and provide precedence to future work aimed toward defining a putative substrate(s) within the context of this network.

3.2 Ectopic expression of PRL3 induces enhanced 'global' tyrosine phosphorylation

To begin to investigate the tyrosine phosphoproteome following stable ectopic PRL3 expression, we employed epithelial-human embryonic kidney 293 (HEK293) cells. In addition to the PRL3-WT expressing clone (WT1) used in our previous study (Liang2007), we also generated a second stable PRL3-WT expressing HEK293 cell clone (WT2) with similar morphological and molecular characteristics. Importantly, the second

clone was generated following selection with a different cytotoxic agent and has PRL3 expression being driven from a different promoter to limit the chance of false interpretations being made from a single clonal population. We documented the 3.9-fold overexpression of PRL3 transcript in PRL3-WT1 by quantitative real-time PCR (qRT-PCR) in our previous study (106). Here, we corroborate this data by showing the significantly enhanced PRL3 transcript in the PRL3-WT (1 and 2) and -C104S cells, relative to endogenous levels of PRL3 transcript observed in vector counterparts by RT-PCR using the same reagents/methodology (Figure 4A). Furthermore, using methodology described in this work, HEK293 cells harboring a stably expressed RFP (Red Fluorescent Protein)-tagged PRL3-WT fusion protein were generated to validate the expression and proper localization of PRL3 on endomembranes (Figure 4A). PRL3-WT cells have a 'spindle-like' fibroblast/mesenchymal cell morphology as compared to the 'squamous-like' epithelial morphology of their PRL3-C104S 'phosphatase-dead' and vector counterparts, consistent with an EMT occurring upon PRL3-WT expression in these cells (Figure 4B). PRL3-WT cells have enhanced 'global' tyrosine phosphorylation, a markedly less latent pTyr527-Src population, and constitutively phosphorylated/activated ERK1/2 and STAT3, relative to vector counterparts (Figure 4C). This data validate our previous findings and establish a framework that can be built upon to more extensively define the PRL3-mediated signaling network activated in these cells.

PRL3-WT (WT1) and its vector (Vec1) HEK293 counterpart, used in our previous study, were used to provide material for our phosphoproteomic investigation. The sample handling and analysis flow-chart that was used to acquire both qualitative

and SILAC (stable-isotope labeling of amino acids in cell culture)-based quantitative phosphoproteomic data from these cell lines can be seen in (Figure 5). Qualitative and SILAC-based quantitative data are additive in this work and used to represent the entire PRL3 and vector phosphoproteomic datasets. Briefly, normalized total protein from the two experimental groups was either processed separately (qualitative assessment) or consolidated to one master sample (quantitative assessment). Tyrosine phosphorylated tryptic peptides were enriched using a tandem enrichment strategy based upon a primary 'pan'-pTyr-antibody immunoprecipitation followed by a secondary enrichment using a novel soluble nanopolymer multi-functionalized with Titanium (Ti) (108) and subsequently electrosprayed into an LTQ-Orbitrap mass spectrometer for high resolution/high mass accuracy mass analysis. Quantitative data representing tryptic peptides from the 'house-keeping' genes β-Actin (^{7}SYELPDGQVITIGNER) and β-Tubulin (^{63}AILVDLEPGTMDSVR), show a ~1:1 mixing ratio between the SILAC-'Light' ($^{12}C_6$-Lys/$^{12}C_6$-Arg) and SILAC-'Heavy' ($^{13}C_6$-Lys/$^{13}C_6$-Arg) protein lysates prior to sample processing (Figure 6).

Using this approach, we were able to validate our immunoblot findings that proteins from the PRL3 cells experience enhanced levels of tyrosine phosphorylation by qualitatively identifying 172 phosphotyrosyl-residues on 123 tyrosine phosphorylated proteins from the PRL3 cells and 78 phosphotyrosyl-residues on 61 tyrosine phosphorylated proteins from vector cells with an overlap of 32 phosphotyrosine-containing proteins between the two datasets. Using SILAC, we were able to quantify the relative abundance of 121 of 169 and 66 of 77 phosphotyrosine-peptides observed from the qualitative analysis of phosphoproteins acquired from the PRL3 and vector

cells, respectively. The entire curated phosphoproteomic dataset organized into biofunctional categories can be seen in (Table 1). Out of the 250 total phosphotyrosyl-residues identified in this study 226 (90%) have been previously identified by studies aimed at identifying tyrosine phosphorylation events downstream of tyrosine kinase activation, a strong testament to the quality and credibility of the data presented in this work. Raw mass spectra depicting phosphotyrosine-peptides representing pTyr187 of ERK2 (^{173}VADPDHDHTGFLTEY[PO_3^{2-}]VATR), pTyr705 of STAT3 (^{686}YCRPESQEHPEADPGSAAPY[PO_3^{2-}]LK), and pTyr417 of PAG1 (^{414}ENDY[PO_3^{2-}]ESISDLQQGR) were chosen based upon relevance to Src-mediated signal transduction and validation of data presented in our previous study to represent the general quality of spectra used for SILAC-based quantitative assessment of tyrosine phosphorylation in this study (Figure 7). Additionally, raw mass spectra depicting phosphotyrosine-peptides representing pTyr187 of ERK2 (^{173}VADPDHDHTGFLTEY[PO_3^{2-}]VATR) and pTyr783 of PLCγ1 (^{779}NPGFY[PO_3^{2-}]VEANPMPTFK) were chosen to represent the general quality of spectra used for qualitative assessment of tyrosine phosphorylation in this study (Figure 8).

3.3 Src kinase activation is a prominent consequence of PRL3 expression

A primary observation made from the PRL3 phosphoproteomic dataset is the exclusive or increased presence of phosphopeptides representing 10 putative Src substrates including: pTyr100 (^{92}VFDKDGNGY[PO_3^{2-}]ISAAELR) of calmodulin, pTyr14 (^{6}YVDSEGHLY[PO_3^{2-}]TVPIR) of caveolin-1, pTyr397 (^{386}THAVSVSETDD Y[PO_3^{2-}]AEIIDEEDTYTMPSTR) of focal adhesion kinase (FAK), pTyr44 (^{33}AAVPSGASTGIY[PO_3^{2-}]EALELR) of γ-enolase, pTyr783 (^{775}WDTGENPIY[PO_3^{2-}

]K) of integrin-β1, pTyr774 (^{766}YEMASNPLY[PO_3^{2-}]R) of integrin-β5, pTyr783 (^{779}NPGFY[PO_3^{2-}]VEANPMPTFK) and pTyr1253 (^{1253}Y[PO_3^{2-}]QQPFEDFR) of phospholipase C gamma-1 (PLCγ1), pTyr798 (^{787}VVQEYIDAFSDY[PO_3^{2-}]ANFK) of receptor protein tyrosine phosphatase-alpha (RPTPα), pTyr705 (^{686}YCRPESQEHPEADPGSAAPY[PO_3^{2-}]LK) of signal transducer and activator of transcription-3 (STAT3), and pTyr699 (^{695}AVDGY[PO_3^{2-}]VKPQIK) of STAT5B as assessed through both *phosphosite.org* and manual literature review. Among these, RPTPα is known to be a direct positive regulator of Src-family kinase (SFK) signaling through dephosphorylating the inhibitory phosphotyrosine-residues of these enzymes (139-140). Phosphorylation of Tyr798 has been shown to be SFK-FAK-dependent and be an activating event to this phosphatase attributed to the potentiation of cellular migration (141).

Intriguingly, while analyzing phosphoproteins exclusively present in the vector datasets, we consistently came across Csk-binding protein-phosphoprotein associated with glycosphingolipid microdomains (Cbp-PAG1), a tumor suppressor known to negatively regulate Src activity by both Csk-dependent and -independent mechanisms (142-144). Absence of 6 phosphotyrosyl residues including the pTyr317 Csk binding site of PAG1 provides strong evidence, next to the previously documented downregulation of Csk in our previous study (106), of the endogenous Src population existing in an activated state in the PRL3 cells. Though PAG1 is the most attractive candidate with regard to our current model of Src activation to be a substrate of PRL3, the absence of 6 disparate tyrosine phosphorylation motifs, suggests that this phosphoprotein is most

likely downregulated and not dephosphorylated by a single phosphatase in the PRL3 cells.

To generate a larger scope with regard to the penetrance of Src kinase activity within our PRL3 phosphoproteomic dataset we compared our dataset to extensive phosphoproteomic datasets generated by Rush et al. (145) and Luo et al. (146) while following the global impact of constitutively active SrcY529F overexpression in murine embryonic fibroblasts (MEFs), relative to their parental MEF counterparts. This comparative analysis (Table 2) revealed that our PRL3 dataset has notable overlap with the SrcY529F dataset concerning a variety of phosphoproteins known to regulate cytoskeletal dynamics and mitogenic signal transduction including: PLCγ1 (pTyr771, 783), annexin A2 (pTyr334, 335), ephrin receptor A2 (pTyr594, 772), FAK (pTyr397), neural Wiskott-Aldrich Sydrome protein (N-WASP; pTyr256), talin 1 (pTyr70, 71), and STAT3 (pTyr705). Additionally, a significant overlap exists between phosphoproteins shown to have exclusive or increased presence in the PRL3 dataset and phosphoproteins associated with the parental MEF dataset, providing the first phosphoproteomic evidence in support of fibroblast/mesenchymal-like signal transduction taking place in cells following PRL3 expression (Table 2). Interestingly, the PRL3 phosphoproteomic dataset is largely unique with ~67% of phosphoproteins (74; 101 pTyr-residues) not present in either of the SrcY529F-MEF or parental MEF datasets (Table 2). While an argument could be made regarding a comparative analysis being done using two disparate cell types, this analysis suggests that the phosphoproteomic "finger print" from PRL3-mediated Src activation is distinct from that of constitutive Src activation.

Collectively, these data provide strong evidence in support of the aberrant activation of the Src kinase being a major driving force behind pro-metastatic molecular events observed in the PRL3 cells. Furthermore, data support Src driving a phosphoproteome that is mesenchymal in nature and unique to PRL3 expression.

3.4 Src kinase activates a signal transduction network associated with a mitogenic and chemotactic PDGF, Eph, and Integrin receptor array in PRL3 expressing cells

In our previous study (106), we attributed the significantly increased Src-dependent proliferative and migratory/invasive capacities of PRL3 expressing HEK293 cells to the constitutive activation of key regulators of mitogenic and chemotactic signal transduction including ERK1/2, STAT3, and $p130^{Cas}$. We hypothesized that the identities of the complete repertoire of proteins shown to experience enhanced levels of tyrosine phosphorylation in the PRL3 cells would help us paint the most comprehensive picture to date of how PRL3 drives pro-metastatic molecular events through Src activation.

As a primary method of data analysis we organized the entire phosphoproteomic dataset (Table 1) into biofunctional categories and created a summary of the comparative analysis between the PRL3 and vector datasets (Figure 9A). Data show that while a larger representation of phosphoproteins exists for all biofunctional 'bins' from the PRL3 dataset, a trend known to be associated with aberrant Src kinase activation, the 'Cellular Communication and Signal Transduction' bin encompassing: protein kinases, protein phosphatases, adaptor/scaffolds, G-proteins, and lipases shows the most prominent difference with regard to the number of phosphoproteins between the two datasets. Strikingly, within this group of phosphoproteins, 75% (92 of 123) of the phosphotyrosine-containing proteins identified in the PRL3 cells are unique from those

observed from vector. This observation provides strong evidence that PRL3 expression has significantly altered the regulation of a variety of enzymes responsible for propagating signal transduction through aberrant Src kinase activation. Additionally, we took an unbiased approach towards understanding how our data best fit into canonical signaling networks by employing Ingenuity Pathway Analysis (IPA). We queried the Ingenuity Knowledge Base using proteins from our entire phosphoproteomic dataset including corresponding quantitative information. The top 10 biofunctions and canonical pathways predicted to be significantly represented from our dataset can be seen in (Figure 9B). Biofunctions with (-log(B-H p-values) ~ 7.5) along with a top scoring network from this analysis encompass cellular growth and proliferation, cellular assembly and organization, and cellular movement. These biofunctions are currently accepted in the field as significantly associated with the biology of PRL3 and aid in establishing credibility toward our dataset. IPA also predicted canonical signaling networks from phosphoproteins represented in our dataset that are well known to govern the above processes as well as to be intimately regulated by Src kinase activity including: p21/Cdc42/Rac1-activated kinase (PAK) and Cytokine signaling with (-log(B-H p-values) ~ 15) and Integrin, PDGF, and Ephrin (Eph) receptor signaling with -log(B-H p-values) ~ 12.5). Data analysis by IPA highlights prominent signal transduction experimentally observed to be coordinated downstream of the aforementioned transmembrane receptor classes with consistent representation by FAK-Src, Jak-STAT3/5, N-WASP-Arp2/3, Nck2, PI3K, PLCγ1, Ras-ERK1/2, JNK1, and the Rho-family GTPases, Cdc42 and Rac1. Importantly, the aforementioned transmembrane

receptors and signaling effectors are well recognized regulators of both mitogenic and chemotactic bioprocesses.

Data from a variety of candidate approaches suggest that PRL3 drives the acquisition of cellular properties associated with tumorigenesis and metastasis through the activation of a number of signaling pathways, including the Rho-family of small GTPases, PI3K, ERK1/2, and Src (102-107). Conclusions made from these approaches have naturally been limited in scope towards not only defining how these effectors become activated, but how they can become collectively activated within a PRL3-mediated signaling network. Manual interpretation of our phosphoproteomic dataset, along with aid from IPA, has allowed us to establish a more thorough and comprehensive model of this signaling network. We postulate that the Src kinase activates a signal transduction network associated with a mitogenic and chemotactic PDGF (α and β), Eph (A2, B3, B4), and Integrin (β1 and β5) receptor array in the PRL3 expressing cells. A subset of data selected from the total dataset represented in (Table 1) that provides significant evidence in support of this hypothesis is represented in (Table 3). A graphical model, derived from data in (Table 1), depicting how signal transduction governing mitogenesis, chemotaxis, and survival is propagated in the PRL3 expressing cells is presented in (Figure 10). This figure will be used in the subsequent sections to highlight the molecular relationships that define this signal transduction. Our model is based upon an experimentally derived understanding that the PRL3 expressing cells display significant insensitivity to serum-derived factors, presumably due to an 'oncogenic addiction' to sustained intracellular activation of the aforementioned signaling network

by the Src kinase. In light of this, we provide the most comprehensive model to date of how PRL3 drives pro-metastatic molecular events through aberrant Src activation.

3.5 Src induces the tyrosine phosphorylation of key regulators of cytoskeletal re-organization and Rho-family GTPase activation in PRL3 expressing cells

Enhanced cellular migration and tissue invasion potential are key biofunctional characteristics acquired by disseminating metastatic tumor cells (147). These processes are driven by heterodimeric integrin receptors that translate a mechanical force, through their physical association with components of the extracellular matrix (ECM), to an intracellular response that culminates in the dynamic re-organization and stabilization of actin filaments (148). Tyrosine phosphorylation of integrin receptor complexes is a biomarker of their activation as structural rearrangements of their cytoplasmic domains, following dynamic ECM engagement, stimulates the localization and activation of the FAK·Src kinase signal transducer as a primary step towards the initiation of intracellular 'outside-in' signal propagation from these receptors (149). Phosphoproteomic data provide strong evidence in support of integrin receptor complex activation in our PRL3 expressing cells. Phosphopeptides representing the Src substrates, pTyr783 (^{775}WDTGENPIY[PO_3^{2-}]K) of integrin-β1 and pTyr774 (^{766}YEMASNPLY[PO_3^{2-}]R) of integrin-β5 are shown by SILAC to be exclusively present and up 15-fold in the PRL3 cells, respectively. Phosphopeptides representing pTyr70 (^{67}ALDY[PO_3^{2-}]YMLR) and pTyr71 (^{67}ALDYY[PO_3^{2-}]MLR) of talin-1, a key molecular scaffold and activator of integrin receptors that provides a critical link between these receptors and the actin cytoskeleton (150), are shown to be up 14-fold in the PRL3 cells. Phosphopeptides representing the activating pTyr397 (^{386}THAVSVSETDDY[PO_3^{2-}

]AEIIDEEDTYTMPSTR) modification of FAK as well as pTyr570 (^{570}Y[PO_3^{2-}]MEDSTYYK) are shown to be up 12-fold and exclusively present in the PRL3 cells, respectively. Phosphorylation of FAK on Tyr397 is a biomarker for the establishment of the FAK-Src kinase complex that propagates signal transduction responsible for dynamic disassembly of integrin complexes during productive cellular migration (151). A phosphopeptide representing pTyr798 (^{787}VVQEYIDAFSDY[PO_3^{2-}]ANFK; orthologous to Tyr789 of isoform 2) of RPTPα is shown to be up 2-fold in the PRL3 cells, a modification known to be associated with Src activation and the potentiation of cellular migration downstream of active integrin receptors and the Src-FAK complex.

A major substrate immediately downstream of the FAK-Src complex is the Crk-associated substrate $p130^{Cas}$ (Cas), a hyperphosphorylated molecular scaffold that integrates both integrin- and RTK-mediated signals toward Rho-family GTPase and MAPK activation (152-154). Phosphoproteomic data confirm our previous finding that Cas is hyperphosphorylated in PRL3 expressing cells (106), and provide strong evidence in support of a Rac1-GTPase activation signal known to be coordinated from Cas. The Src-mediated phosphorylation of the substrate domain of Cas promotes the SH2 domain-dependent association of Crk and its constitutively bound effector, dedicator of cytokinesis-180 (DOCK180; DOCK1) Rac1-GEF required for localized Rac activation and lamellipodia extension during cellular migration (154-157). A phosphopeptide representing pTyr522 of DOCK7 (^{511}IDISPAPENPHY[PO_3^{2-}]CLTPELLQVK), a member of the DOCK180-family of Rac1-GEFs expressed at high levels in the brain and heart, is shown to be exclusively present in the PRL3 cells. The presence of a phosphopeptide representing DOCK7 is interesting in light of the fact that PRL3

expression is known to be limited to a few organs, with the brain and heart showing significant PRL3 expression *in-vivo* (79 and our unpublished data). This data provide evidence of a possible PRL3 'mark' on a signaling network otherwise dominated by ubiquitous canonical signaling effectors as it is unique to our phosphoproteomic dataset.

Phosphopeptides representing pTyr246 of Shb (^{240}VTIADDY[PO_3^{2-}]SDPFDAK) and pTyr50 of Nck2 (Grb4) (^{48}TGY[PO_3^{2-}]VPSNYVER) are shown to be exclusively present and up 17-fold in the PRL3 cells. The SH2 and PTB domain-containing adaptor protein Shb is known to bind the SH3 domain of Src via its N-terminal poly-proline motif and become phosphorylated in a Src-dependent manner. Phosphorylated Shb binds FAK via its central PTB domain and induces increased phosphorylation/activation of FAK ultimately leading to increased cell spreading (158). Phosphorylated Shb has also been shown to bind the SH2 domain of Crk (159), providing additional evidence in support of the assembly of a Cas-Crk-DOCK module toward Rac1 activation downstream of the active FAK-Src complex in the PRL3 cells. Nck2, like Shb, is a pleiotropic adaptor protein that plays a major role in driving cytoskeletal re-organization and cell movement following chemotactic-RTK activation. The proto-oncogene Nck2 binds phosphotyrosyl-motifs on stimulated RTKs via its SH2 domain and subsequently recruits proline-rich effector proteins via its SH3 domain to mediate localized interactions between these receptors and regulators of actin cytoskeletal dynamics (160-161). Nck2 is known to be tyrosine phosphorylated following growth factor stimulation and in Src transformed cells (162). This phospho-adaptor protein binds the substrate domain of Cas via its SH2 domain and DOCK180 and the p21/Cdc42/Rac1-activated protein kinase (Pak1) via its 'mid' and 'C-term'-SH3 domains (161, 163), providing further precedent for Cas-

mediated Rac1 activation in the PRL3 cells. Additionally, the ephrin receptor-A2 (EphA2) RTK is phosphorylated exclusively on Tyr588 (^{587}TY[PO_3^{2-}]VDPHTYEDPNQAVLK) and Tyr594 (^{587}TYVDPHTY[PO_3^{2-}]EDPNQAVLK), phosphorylation sites known to coordinate the Nck adaptor proteins as well as Vav2/3 Rac1-GEFs via their SH2 domains (164-165), in the PRL3 cells. Additional phosphopeptides representing pTyr772 (^{763}VLEDDPEATY[PO_3^{2-}]TTSGGKIPIR; up 77-fold) and pTyr960 (^{958}IAY[PO_3^{2-}]SLLGLK) of EphA2 as well as pTyr792 (^{782}FLEDDPSDPTY[PO_3^{2-}]TSSLGGK) of EphB3 and pTyr774 (^{764}FLEENSSDPT Y[PO_3^{2-}]TSSLGGK) of EphB4, are shown to be exclusively present in the PRL3 cells. Phosphorylated B-type Eph-receptors also mediate Nck2 association toward cytoskeletal re-organization associated with ephrinB reverse signaling (163-164). Important to this investigation, EphB-receptors have also been paramount to a discussion about Src (SFKs) in the signaling downstream of Eph-receptors as these cytoplasmic tyrosine kinases are well known to bind these receptors and be a positive regulators of their phosphorylation (164-167).

Finally, evidence suggesting Rac1 activation comes from phosphorylation/activation of the c-Jun N-terminal kinase (JNK1) on Tyr185 (^{175}TAGTSFMMTPY[PO_3^{2-}]VVTR) exclusively in the PRL3 cells. JNK1 activation is well documented downstream of Cas-Crk-mediated Rac1 activation via an Nck-mediated Rac1-Pak1 interaction most notably to prevent anoikis, a major challenge associated with cellular dissemination/metastasis. The JNK1 cascade is also critical to cellular transformation induced by hyperphosphorylated Cas, most notably driven by v-*Src* or v-*Crk* oncogenes (154, 161, 168-170).

Evidence in support of the activation of Cdc42, another member of the Rho-family GTPases which is responsible for filapodia extension during cellular migration, is present in our phosphoproteomic dataset. A phosphopeptide representing pTyr827 (^{827}Y[PO_3^{2-}]ATPQVIQAPGPR) of the Activated Cdc42 Kinase-1 (ACK1) is shown to be up 4-fold by SILAC in the PRL3 cells. ACK1 acts downstream of a multitude of transmembrane receptors following its activation by SFKs (most notably Src) with the predominant role of keeping Cdc42 in an active GTP-bound form (170-172). Furthermore, evidence in support of ACK1 activation and a strong biomarker of dynamic actin-cytoskeletal re-organization comes from the phosphorylation/activation of the putative ACK1 substrate, neural-Wiskott-Aldrich syndrome protein (WASL/N-WASP) on Tyr256 (^{254}VIY[PO_3^{2-}]DFIEK) shown to be up 9-fold in the PRL3 cells. N-WASP is fundamental to filamentous actin growth and stabilization through its association with both the Arp2/3 actin nucleation complex and activated members of the Rho-family GTPases, which provide critical positional information for cellular extensions such as filapodia and lamellipodia (174-175).

Finally, a phosphopeptide representing the putative Src substrate, pTyr100 (^{92}VFDKDGNGY[PO_3^{2-}]ISAAELR) of calmodulin is shown to be exclusively present in the PRL3 cells. Ca^{2+}-bound calmodulin is known to be required for the activation of the myosin light chain kinase (MLCK), a critical component to the MLCK-myosin light chain phosphatase (MLCP) regulatory loop that drives acto-myosin contraction/relaxation cycles underlying cellular migration (176-178).

Collectively, phosphoproteomic data provide strong evidence in support of Src inducing the tyrosine phosphorylation of key regulators of cytoskeletal re-organization

and Rho-family GTPase activation in the PRL3 expressing cells. Data suggest that a prominent signaling network is being coordinated and activated downstream of the integrin-β1 and -β5 fibronectin receptors and the Eph (A2, B3, B4) RTKs. Importantly, Src kinase activity is well-recognized to be critical to the biology downstream of these receptors towards cellular migration/chemotaxis.

3.6 Src induces the tyrosine phosphorylation of key regulators of ERK, PI3K, and STAT activation in PRL3 expressing cells

Migrating mesenchymal cells utilize mitogenic and chemotactic RTKs that are intimately linked through an underlying interconnected signal transduction network to the machinery that drives cellular migration so that efficient cellular migration/chemotaxis can occur. One of the most extensively studied mitogenic and chemotactic RTKs is the platelet-derived growth factor receptor (PDGFR). Canonically, PDGF-ligands are recognized by PDGFR-expressing cells of mesodermal origin that are critical for the normal development of the kidney, brain, cardiovascular and respiratory systems; while being essential to the wound healing response in the adult animal following laceration, myocardial infarction, and ischemic stroke (179-185). The Src kinase has been recognized to be intimately involved in PDGF receptor-mediated signal transduction for more than two decades. Src is known to associate with ligand-activated PDGFβ-receptors via its SH2 domain and subsequently become phosphorylated/activated by receptor-dependent and -independent mechanisms (186-191). Following its activation, Src is also known to phosphorylate the PDGFβ-receptor on Tyr934 and activate the tyrosine kinase c-Abl toward PDGF-mediated mitogenic and chemotactic responses (191-194). Though our phosphoproteomic dataset does not show any evidence of

phosphorylation on Tyr934, a phosphopeptide representing pTyr970 (^{970}Y[PO_3^{2-}]QQVDEEFLR) of the PDGFβ-receptor, a known c-Abl phosphorylation site (195), suggests Src-mediated c-Abl activation towards PDGFRβ-receptor regulation in the PRL3 cells. Furthermore, phosphoproteomic data show that the PDGFα-receptor is phosphorylated on Tyr613 (^{607}VVEGTAY[PO_3^{2-}]GLSR), -720 (^{719}SY[PO_3^{2-}]VILSFENNGDYMDMK), -731 (^{719}SYVILSFENNGDY[PO_3^{2-}]MDMK), -742 (^{736}QADTTQY[PO_3^{2-}]VPMLER), and -988 (^{982}VDSDNAY[PO_3^{2-}]IGVTYK), while the PDGFβ-receptor is phosphorylated on Tyr683 (^{674}GGPIYIITEY[PO_3^{2-}]CR), -692 (^{686}YGDLVDY[PO_3^{2-}]LHR), -857 (^{850}DIMRDSNY[PO_3^{2-}]ISK), and -970 (^{970}Y[PO_3^{2-}]QQVDEEFLR) in the PRL3 cells with no presence of phosphorylation on either of the receptors in vector cells. PDGFα-receptor pTyr720 has been shown to coordinate Grb2, Shb, and Shp2 (196-198), pTyr731 and 742 have been shown to coordinate the p85 regulatory subunit of phosphatidylinositol-3 kinase (PI3K) (199), and pTyr988 has been shown to be an autophosphorylation site and to coordinate phospholipase-C gamma 1 (PLCγ1) (200). Intra-/inter-molecular regulation by the observed PDGFβ-receptor pTyr-residues remain enigmatic to date, with exception to the c-Abl phosphorylation site described earlier.

Surprisingly, the PDGF(α/β)-receptors are unique to the PRL3 phosphoproteomic dataset. Due to the importance of the PDGF-receptors in regulating both mitogenic and chemotactic signal transduction including the prominent role that Src plays in PDGFR-mediated signal transduction, we chose to validate the tyrosine phosphorylation state of these receptors using PDGFα- and β-receptor antibody-specific immunoprecipitation followed by 'pan'-pTyr western blotting (Figure 11A). In validation of our mass

spectrometry-based data, IP-western data show the constitutive tyrosine phosphorylation of both PDGF-α and -β receptors in the PRL3 expressing cells. Surprisingly, while the levels of PDGFα-receptor are equivalent in both the PRL3 and vector cells, the PDGFβ-receptor is selectively expressed and/or stabilized in the PRL3 cells. Furthermore, treatment of these cells with the Src kinase chemical inhibitor (SU6656) at 2.5μM, a concentration shown to be selective for inhibition of Src kinase activity over the kinase activity of the PDGFR (201), revealed that the tyrosine phosphorylation of the α-receptor is independent of Src activity, while the tyrosine phosphorylation of the β-receptor is dependent upon Src activity as measured by this assay. This data is in agreement with previous published results showing only PDGFβ-receptor phosphorylation by the Src kinase. The most likely mechanism responsible for the constitutive phosphorylation of the PDGFα-receptor would be trans-autophosphorylation, due to a heightened sensitivity for serum-derived PDGF ligands driven by the significantly altered signal transduction present in the PRL3 cells, relative to vector counterparts. Data showing the selective expression and/or stabilization of the PDGFβ-receptor in the PRL3 cells is interesting in that signaling from the PDGFβ-receptor has major implications in developmental *neo*-vascularization and in tumor-angiogenesis, processes absolutely required for late stage tumorigenesis and the survival of disseminating metastatic cells (181). Though the mechanism remains enigmatic, PRL3 has been previously implicated in promoting pro-angiogenic events both *in-vitro* and *in-vivo* (128, 202-206). Due to the importance of angiogenesis toward potentiating metastatic dissemination, the direct mechanism by which PRL3 induces the selective expression and/or stabilization of the PDGFβ-receptor is under investigation. Central to PDGF-receptor activation, phosphoproteomic data

provide evidence in support of an extensive signaling network responsible for ERK1/2, PI3K, and STAT3 activation being prominent in the PRL3 expressing cells.

Data corroborating previous immunoblot-derived data showing the constitutive phosphorylation/activation of ERK1/2, are phosphopeptides representing pTyr204 (^{190}IADPEHDHTGFLTEY[PO_3^{2-}]VATR) of ERK1 and pTyr187 (^{173}VADPDHDH TGFLTEY[PO_3^{2-}]VATR) of ERK2 shown by SILAC to be up 4- and 5-fold in the PRL3 cells. ERK1/2 can be activated through both Ras-dependent and -independent mechanisms. Phosphopeptides representing pTyr157 of both the highly transformative N- (^{150}QGVEDAFY[PO_3^{2-}]TLVR) and K- (^{150}QGVDDAFY[PO_3^{2-}]TLVR) Ras family members are shown to be up 22-fold and exclusively present in the PRL3 cells, respectively. Though the physiological relevance of pTyr157 remains unclear, this residue is part of the membrane-binding 'switch' region that is postulated to govern activation state-dependent membrane engagement of this G-protein. Furthermore, mutation of the highly conserved Phe156 residue, immediately adjacent to Tyr157, is shown to significantly increase Ras-GTP levels as well as Ras transforming activity, *in-vivo* (207), suggesting that modification of Tyr157 would engender similar gain-of-function consequences. This data puts N/K-Ras prominently in the discussion regarding Ras-dependent ERK1/2 activation in the PRL3 cells. In addition, exclusive representation of phosphopeptides encompassing pTyr246 (^{240}VTIADDY[PO_3^{2-}]SDPFDAK) of Shb and an activating modification to Tyr542 (^{538}KGHEY[PO_3^{2-}]TNIK) of the proto-oncogenic Shp2 tyrosine phosphatase, provide further evidence in support of a Ras-dependent mechanism of ERK1/2 activation in the PRL3 cells. The pleiotropic adaptor protein Shb described in the previous section to bind the SH3 domain of Src via

its N-terminal poly-proline motif and become phosphorylated in a Src-dependent manner is also known to associate specifically with the PDGFβ-receptor via its SH2 domain (208). Shb is also known to bind Grb2 via an SH3 domain-mediated interaction (209-210), a well-recognized adaptor protein known to localize the Ras-GEF, SOS1, for direct Ras activation. Towards indirect Ras activation, Shp2 attenuates the activities and/or localization of negative regulators of Ras activation by various mechanisms (63). Relevant to a discussion about the role of the PDGF-receptors in mediating ERK1/2 activation, Tyr720 of the PDGFα-receptor, described earlier to be exclusively phosphorylated in the PRL3 cells, has been documented to coordinate Grb2, Shb, and Grb2-bound Shp2 (196-198). Furthermore, the association of both Shb and Shp2 to PDGF-receptor biology was first documented from studies involving the PDGFβ-receptor, with phosphorylation of the latter on Tyr542 linking the β-receptor to Ras activation (208, 211).

Phosphoproteomic data also provide strong evidence in support of Ras-independent ERK1/2 activation most specifically mediated through Raf1 in the PRL3 cells. Phosphopeptides representing pTyr771 (^{764}IGTAEPDY[PO_3^{2-}]GALYEGR), pTyr977 (^{975}ACY[PO_3^{2-}]RDMSSFPETK), and pTyr1253 (^{1253}Y[PO_3^{2-}]QQPFEDFR) of the proto-oncogenic PLCγ1 are shown to be exclusively present, while a phosphopeptide representing pTyr783 (^{779}NPGFY[PO_3^{2-}]VEANPMPTFK) of this enzyme is shown to be up 10-fold by SILAC in the PRL3 cells. While the PDGFα-receptor has been shown to coordinate an SH2 domain-mediated interaction with PLCγ1 via its pTyr988 site following PDGF stimulation, PLCγ1 only attains maximal activation through phosphorylation of its Tyr771, Tyr783, and Tyr1253 sites when in the presence of the

PDGFβ-receptor (200, 212). Through the hydrolysis of $PI(4,5)P_2$ (PIP_2), PLCγ1 drives the activation of 'classic' (c) and 'novel' (n)-type PKC-family members (212-216). c-PKC (α, β, γ)-induced activation of ERK1/2 occurs through the phosphorylation/activation of Raf1 on Ser259 and Ser499 (217-218).

Due to the importance of PLCγ1 in the biology downstream of the PDGF-receptors including the activation of proto-oncogenic PKC enzymes through the hydrolysis of PIP_2, a phosphoinositide that has relevance towards being regulated by PRL3 both *in-vitro* and *in-vivo* (103, 219), we chose to validate our mass spectrometry data with regards to the activation state of this enzyme. Through phospho-specific immunoblotting, we show that PLCγ1 is exclusively phosphorylated on Tyr783, an event essential for lipase activation, in the PRL3 cells (Figure 11B). Additionally, the phosphorylation of Tyr783 is shown to be completely dependent upon Src activity by treatment of the PRL3 cells with the Src kinase inhibitor, SU6656. This data provide insight into a possible mechanism by which PLCγ1 becomes fully activated by Src through the PDGFβ-receptor. Raw mass spectral data showing the extensive coverage of the pTyr783 (^{779}NPGFY[PO_3^{2-}]VEANPMPTFK) phosphopeptide as well as SILAC-data showing the 10-fold increase in abundance of this phosphopeptide in the PRL3 cells relative to its abundance in the vector counterparts, can been seen in (Figure 11C). Additionally, plekstrin-homology (PH) domain-mediated targeting of PLCγ1 to $PI(3,4,5)P_3$ (PIP_3) has been shown to be important for full activation of this enzyme towards its putative substrate, PIP_2 (220-221). Phosphopeptides representing pTyr73 (^{67}GDFPGTY[PO_3^{2-}]VEYIGR), pTyr150 (^{143}GLECSTLY[PO_3^{2-}]R; exclusively present), and pTyr580 (^{578}DQY[PO_3^{2-}]LMWLTQK; up 31-fold) of the p85 regulatory subunit of

PI3K, provide evidence in support of PI3K activation toward PIP_3 production and full PLCγ1 activation in the PRL3 cells. Though the biological function of these pTyr-residues is unknown, p85 has been shown to be phosphorylated in response to a variety of stimuli including being phosphorylated by SFKs, an event that relieves the SH2 domain-mediated inhibitory interaction that p85 makes with the p110 catalytic domain of PI3K in a latent state, leading to PI3K activation (222). As previously mentioned, phosphoproteomic data also support the proper localization of p85 to the phosphorylated Tyr731 and Tyr742 residues of the PDGFα-receptor, an event that would augment PI3K activation via the same mechanism. Phosphoproteomic data in support of PI3K activation corroborates previously published evidence regarding the activation of PI3K, by a yet undefined mechanism, leading to the phosphorylation/activation of Akt on Ser473 following ectopic PRL3 expression (103).

Finally, evidence in support of Ras-independent ERK1/2 activation that is highly relevant with respect to the phosphoproteomic data present in our model is the Pak1 and Src-mediated phosphorylation/activation of Raf1 on Ser338 and Tyr340/341, respectively (223-224).

Signal transducer and activator of transcription (STAT) proteins are latent cytoplasmic transcription factors that transduce signals from the cell membrane to the nucleus upon activation by tyrosine phosphorylation and subsequent dimerization induced by a variety of transmembrane cytokine receptors and RTKs (225-226). Important to this investigation, the Src-dependent activation of STAT3 downstream of PDGF-stimulation and PDGFβ-receptor association is well-recognized (201, 227-229). Following membrane localization, STATs are activated by Src-mediated Jak-dependent/-

independent mechanisms, including the constitutive tyrosine phosphorylation and activation of STAT3 as well as Jak1 in *v-src* transformed cells (226, 230-237). Phosphoproteomic data support the phosphorylation/activation of Jak1 as well as two STAT-family members STAT3 and 5B through phosphopeptides representing pTyr1034 (^{1027}AIETDKEY[PO_3^{2-}]YTVK) of Jak1 as well as pTyr705 (^{686}YCRPESQEH PEADPGSAAPY[PO_3^{2-}]LK) of STAT3 and pTyr699 (^{695}AVDGY[PO_3^{2-}]VKPQIK) of STAT5B shown to be up 6-fold and exclusively present by SILAC in the PRL3 cells, respectively. Constitutive STAT3 activation is associated with various human cancers and commonly suggests poor prognosis as it induces: pro-proliferative, pro-angiogenic, pro-metastatic, pro-inflammatory, and anti-apoptotic effects including being required for oncogenic Src-induced transformation (236-241).

3.7 Discussion/Summary

Despite a large amount of descriptive evidence at the gross-anatomical level implicating PRL3 as a causative factor toward cellular metastasis when overexpressed, mechanistic evidence is lacking at the molecular level in describing a putative signaling network that could be responsible for governing pro-metastatic molecular events downstream of PRL3. Data from the field support the overexpression of PRL3 in a variety of cell culture models inducing the activation of numerous proto-oncogenic signaling effectors/modules including: Integrin receptors, Rho-family GTPases, PI3K-Akt, Ras/ERK, and the Src tyrosine kinase. Collectively, these signaling effectors/modules are canonically activated following extracellular ligand-mediated stimulation of tyrosine phosphorylation. How does the overexpression of a phosphatase 'tilt' the natural regulation of tyrosine phosphorylation toward a stimulus that would

support the sustained activation of these effectors? Additionally, what transmembrane receptors and molecular adaptors are tyrosine phosphorylated/activated to integrate this pleiotropic response?

We expand upon a previously published observation that PRL3 is able to induce the aberrant activation of the Src tyrosine kinase when ectopically expressed in epithelial-derived HEK293 cells (106). In that report we present data in support of a sustained ligand-independent 'global' increase in tyrosine phosphorylation that we postulated would allow us a unique opportunity to extensively define the PRL3-mediated signaling network. We chose to employ a novel phosphoproteomic strategy predicated upon a tandem phosphotyrosine-peptide enrichment using 'pan' pTyr-antibody immunoprecipitation and polymer-based metal ion affinity capture (PolyMAC) with titanium (Ti)-functionalized soluble nanopolymers/polyamidoamine-dendrimers (108). Through phosphotyrosine-peptide enrichment and tandem mass spectrometry we provide strong evidence in support of PRL3 driving aberrant Src kinase activation. In addition to the presence of a multitude of putative Src substrates within the PRL3 phosphoproteomic dataset, a comparative analysis revealed that our PRL3 dataset has notable overlap with SrcY529F-MEF phosphoproteomic datasets generated by Rush (145) and Luo (146) concerning a variety of phosphoproteins known to regulate cytoskeletal dynamics and mitogenic signal transduction. Additionally, significant overlap also exists between phosphoproteins shown to have exclusive or increased presence in the PRL3 dataset and phosphoproteins associated with the parental MEF dataset, providing the first phosphoproteomic evidence in support of fibroblast/mesenchymal-like signal transduction taking place in cells following PRL3 expression. Additional proteomic data

support the mesenchymal state including the exclusive presence of a phosphopeptide representing pTyr117 (^{114}FANY[PO_3^{2-}]IDKVR) of the mesenchymal marker, vimentin as well as an increased abundance of vimentin and related intermediate filament proteins including: peripherin (+3.35-fold), desmin (+2.64-fold), alpha-internexin (+2.64-fold), glial fibrillary acidic protein (+2.64-fold), and vimentin (+2.0-fold) as assessed by a 'label-free' quantitative tandem mass spectrometry approach (117-119), in the PRL3 cells (data not shown). Data show that while Src activity has significant penetrance within the PRL3 phosphoproteomic dataset, the phosphoproteome induced following PRL3 expression is largely unique with ~67% of phosphoproteins (74; 101 pTyr-residues) not present in either of the Src529F-MEF/MEF datasets. One of the most significant 'unique' phosphoproteins within this study is PAG1, a tumor suppressor and Src negative regulator shown to consistently have 6 phosphotyrosyl-residues exclusively present within the vector control datasets. PAG1 represents the most attractive candidate within our model of Src activation to be either a substrate of PRL3 or an immediate indirect target of PRL3 activity. Interestingly, both the phosphorylation state and the expression/stability of PAG1 have been shown to be attenuated in Src-transformed cells as well as in the metastatic progression of colorectal cancer (CRC), a cancer type where aberrant Src activity is prominent and the expression of PRL3 has been shown to be highly correlative with cancer grade and prognosis (79, 144, 242). The magnitude of unique phosphotyrosyl-proteins within the PRL3 dataset suggests that the phosphoproteomic "finger print" from PRL3-mediated Src activation is distinct from that of constitutive Src activation.

Our phosphoproteomic investigation has allowed us to uncover a rich signal transduction network downstream of a mitogenic and chemotactic PDGF (α and β), Eph (A2, B3, B4), and Integrin (β1 and β5) receptor array. Collectively, these receptors are highly significant to the biology of migratory mesenchymal cells during development as well as during acute wound healing in the adult animal (148, 164, 181). Our model is based upon an experimentally-derived hypothesis that these receptors act predominately as signal coordinators rather than signal initiators, augmenting the Src-dependent intracellular activation of critical effectors including: FAK-Src, Rho-family GTPases (i.e. Rac1 and Cdc42), Ras-ERK1/2, JNK1, PLCγ1, PI3K, and Jak-STAT3 proteins toward pro-metastatic bioprocesses.

Surprisingly, we found that the PDGFβ-receptor displays constitutive Src-dependent tyrosine phosphorylation and is selectively expressed and/or stabilized in the PRL3 cells. This data puts the PDGFβ-receptor prominently in a discussion regarding significant molecular responses associated with PRL3 expression for a variety of reasons including: (*i*) signaling from the PDGFβ-receptor has major implications in developmental *neo*-vascularization and in tumor-angiogenesis (181), (*ii*) signaling effectors coordinated by the PDGFα-receptor, such as Shp2 and PLCγ1, only exert their maximum biological effect when a heterodimer is formed with the PDGFβ-receptor (198, 200), and (*iii*) in multiple 'global' phosphoproteomic investigations documenting the phosphoproteomes of mesenchymal-MEF cells stably expressing the constitutively active SrcY529F mutant (145-146), no phosphorylation is observed on either of the PDGF-receptors, suggesting a unique role for these receptors within our model of PRL3-induced aberrant Src activation.

Finally, the constitutive Src-dependent phosphorylation/activation of PLCγ1 at Tyr783 in the PRL3 cells makes this lipase a new and important figure in the discussion regarding significant molecular responses associated with PRL3 expression. Importantly, through the hydrolysis of PIP_2, a phosphoinositide that has relevance towards being regulated by PRL3 both *in-vitro* and *in-vivo* (103, 219), PLCγ1 induces the activation of the proto-oncogenic PKC-family of serine/threonine-kinases that drive pro-tumorigenic and pro-metastatic signals through various signaling effectors including ERK1/2, glycogen synthase kinase-3 beta (Gsk-3β), nuclear factor kappa beta (NFκβ), and P-glycoprotein (216). PKC activity is historically associated with tumor promotion following an initial DNA damaging initiating event, through studies using phorbol 12-myristate 13-acetate (PMA), a DAG mimetic that induces prolonged PKC activation. Our model supports the activation of classical (c)- and novel (n)-type PKC isoenzymes, those that require Ca^{2+} and DAG (classical) or simply DAG (novel) for their activation. In general, sustained activation of c-PKC isoenzymes through the aberrant activity of various oncogenic signaling effectors such as the effectors present in the PRL3 cells leads to increased proliferation, inhibition of apoptosis, invasion, inhibition of cell junctions, and multi-drug resistance.

Our unbiased phosphoproteomic approach has afforded us the ability to document how PRL3-mediated Src kinase activation results in the cumulative activation of effectors shown by the field through a variety of candidate approaches to be associated with the biology of PRL3. The vast majority of publications in the PRL3 field highlight PRL3 transcript as well as protein being overexpressed in a variety of advanced neoplasms or metastases originating from a multitude of physiologically distinct tissues (79, 130-131),

suggesting a fundamental role for this phosphatase in driving cellular behaviors that are necessary to gain selective advantage toward metastatic dissemination when in excess. The PRL3-mediated signaling network documented in this investigation highlights how aberrant Src kinase activation can pleiotropically affect a multitude of disparate cellular behaviors that would be necessary to augment the metastatic dissemination of neoplasms derived from many physiologically distinct tissues. Ongoing efforts are devoted to identifying a putative substrate(s) of PRL3 so that our model can be further refined within the context of this substrate(s).

CHAPTER 4: FUNCTIONAL INSIGHTS INTO LEOPARD SYNDROME-ASSOCIATED SHP2 MUTATIONS

4.1 Introduction

The Src homology-2 (SH2) domain-containing protein tyrosine phosphatase (SHP2), encoded by the *Ptpn11* gene, is a critical signal transducer downstream of growth factor and cytokine receptors (63). Biochemical and genetic evidence have characterized SHP2 as an upstream activator of Ras, a key enzyme in the regulatory network that underlies growth factor/cytokine-induced cell proliferation and survival. Importantly, the phosphatase activity of SHP2 is required for full activation of the Ras-extracellular signal-regulated kinase (ERK1/2) cascade (63). Numerous germ-line as well as somatic mutations have been discovered to arise within the *Ptpn11* gene, leading to aberrant SHP2 mutant enzymes which contribute to the pathogenesis of several human diseases. Mutations that arise within the germ-line *Ptpn11* gene, lead to SHP2 mutant enzymes that drive the pathogenesis of a pair of neuro-cardio-facio-cutaneous (NCFC) sydromes termed Noonan syndrome (NS) and LEOPARD (an acronym for its clinical features of multiple Lentigines, ECG conduction abnormalities, Ocular hypertelorism, Pulmonic stenosis, Abnormal genitalia, Retardation of growth and Deafness) syndrome (LS). NS is a relatively common autosomal dominant disorder that afflicts ~1 in 1000 live births, while LS is a much more rare autosomal dominant disorder that shares many clinical phenotypic features with NS (83-84, 243). In addition to being very difficult to diagnostically distinguish during childhood, NS and LS share many common features in adulthood including: short stature, facial dysmorphism, heart defects and a predisposition to hematological malignancies including juvenile myelomonocytic

leukemia. Additionally, somatic mutations arising within the *Ptpn11* gene, lead to SHP2 mutants that primarily drive the pathogenesis of various leukemias (86, 244-247) as well as solid tumors (87, 248).

SHP2 is a ubiquitously expressed cytoplasmic protein tyrosine phosphatase (PTP) with two tandem SH2 domains positioned at its amino-terminal end (249). The most N-terminal SH2 domain (N-SH2 domain), is currently understood to be critical to both catalytic activation and catalytic inhibition. In a latent state, SHP2 exists in a 'closed' autoinhibited conformation due to the N-SH2 domain physically occluding the active site of the PTP domain (62, 250-252). Upon mitogenic stimulation, SHP2 binds directly to tyrosine-phosphorylated motifs, via its SH2 domains, present in growth factor receptors and associated adaptor/scaffolding proteins. This action concomitantly targets SHP2 to its physiological substrates and allows the active site to become catalytically competent (250-251, 253).

The most extensive assessment of the regulatory interaction that the N-SH2 domain makes with the PTP domain was documented following the analysis of the first crystal-based structure of SHP2 (residues 1-527) lacking the final 66-residues making up the C-terminal end of the PTP domain (62). The SHP2 crystal structure shows the inactive 'closed' form of this enzyme, where the N-SH2 domain makes extensive intramolecular interactions with the PTP domain while physically occluding the active site. A structural comparison of an isolated N-SH2 domain, both in the absence of and in complex with a pTyr-peptide shows that this domain binds pTyr-ligands on the opposite face with respect to the face that binds the PTP domain. Conformational alterations observed upon pTyr-ligand binding reveal that the N-SH2 domain may act as an

allosteric 'switch' and it was postulated that the N-SH2 domain's interaction with the PTP domain in a latent state and its interaction with pTyr-ligands in an active state are mutually exclusive, thus communicating with negative cooperativity (62).

Although SHP2 mutations are associated with a number of developmental and neoplastic disorders, the precise mechanism by which mutations in SHP2 cause disease remains poorly understood. The complete spectrum of NS and neoplasia-associated SHP2 mutations cluster within the interface region created by the N-SH2 and PTP domains. Evidence, generated from both *in-vitro* and *in-vivo* experimentation, reveal that these mutations confer *gain-of-function* (GOF) effects to SHP2, presumably by alleviating the autoinhibitory effect of the N-SH2 domain upon the catalytic active site (109-113). Interestingly, SHP2 mutations associated with NS and various neoplasias are common with regard to the site of mutation, but differ in the amino acid substitution with neoplasia-associated mutations being more activating to SHP2's apparent catalytic function. This evidence suggests that, with regard to SHP2 function, NS and neoplasia are 'spectrum' disorders. Alternatively, LS-associated SHP2 mutations cluster in and around the catalytic active site of the PTP domain and result in mutant enzymes with impaired catalytic abilities, relative to wild-type. It is currently unknown whether LS-associated SHP2 mutations compromise the interaction made between the N-SH2 and PTP domains, a property inherent to GOF mutants. These genetic and biochemical findings generate a conundrum specifically between NS and LS. How do mutations that provoke opposite effects to the catalytic function of SHP2 cause phenotypically similar disorders?

To address this question, we hypothesized that LS-associated SHP2 mutations alter not only SHP2 phosphatase activity but also its molecular switching mechanism to drive disease outcomes. Our results concerning two of the most recurrent LS-associated SHP2 mutants, Y279C and T468M, reveal that although LS-SHP2 mutants are catalytically impaired and adopt a 'closed' conformation, they have an increased propensity for the 'open' conformation. As a result, these LS-SHP2 mutants bind upstream activators preferentially and stay longer with scaffolding adaptors. The ability to loiter for longer periods of time would give these mutants the ability to prolong specific substrate turnover, which would compensate for their reduced phosphatase activity. The ability to outcompete the WT enzyme for phosphotyrosyl-binding motifs due to a compromised ability of the N-SH2 domain to uphold intramolecular autoinhibition, is postulated to be a general property associated with all SHP2 pathogenic mutants and essential for GOF biological effects to be realized, *in-vivo*.

Our data support a notion that the totality of catalytically impaired LS-SHP2 mutants may have the capacity to engender GOF phenotypes, similar to their NS/neoplasm-SHP2 mutant counterparts. Interestingly we also provide evidence that supports LS being a 'spectrum' disorder that, along with NS and various neoplasias, is caused by SHP2 pathogenic mutants with differential capacities for catalysis and intramolecular autoinhibition.

4.2 LS-associated SHP2 mutants are catalytically impaired

As a preface to the work presented in this document, we determined kinetic parameters for the hydrolysis of *para*-nitrophenyl phosphate (*p*NPP) by the full-length (FL, residues 1-528) and catalytic domain (CD, residues 246-547) of wild-type SHP2, the

most representative GOF mutants D61Y and E76K, and two of the most recurrent LS mutants Y279C and T468M. Table 4A shows biochemical data in support of the full-length wild-type SHP2 enzyme being in an autoinhibited closed conformation as the specific activity of the full-length enzyme is just 5% of the isolated catalytic domain. Supporting the expectation that GOF mutants exist in an open, activated state, full-length D61Y and E76K display catalytic parameters that are no different than the isolated wild-type catalytic domain. Conversely, the catalytic parameters for the isolated catalytic domains of the Y279C and T468M LS-SHP2 mutants show that the catalytic activities are 26- and 46-fold lower than that of the wild-type counterpart, providing evidence of their catalytic impairment. Furthermore, the k_{cat} values for the full-length Y279C and T468M enzymes are still 5- and 13-fold lower than those of their corresponding catalytic domains. This data suggest that full-length Y279C and T468M exist in a closed, autoinhibited conformation. A comparison between the k_{cat} values for the FL-enzymes and their CD couterparts reveals that the Y279C and T468M FL-enzymes are 4.2- and 1.6-fold less inhibited than the FL-WT enzyme. Data show that these LS-SHP2 mutants have N-SH2 domains that are less able to uphold intramolecular autoinhibtion, relative to the WT enzyme. In support of these mutants existing in a closed, autoinhibited conformation, full activity is restored to the Y279C enzyme when Glu76 is replaced by a Lys residue, which likely disrupts the autoinhibitory mechanism.

In an additional set of kinetic experiments performed using newly purified constructs, the catalytic parameters for the hydrolysis of *para*-nitrophenyl phosphate (*p*NPP) by the full-length (FL, residues 1-528) and catalytic domain (CD, residues 246-547) of wild-type SHP2, the most representative GOF mutants D61Y and E76K, a

neoplasia-associated catalytic domain-directed mutant T507K, and all seven documented LS-SHP2 mutants (Y279C, A461T, G464A, T468M, R498L, Q506P, and Q510E) were measured. Table 4B shows biochemical data in support of all seven LS-SHP2 mutants having a wide range of impaired catalytic abilities relative to the WT-enzyme. As it pertains to the isolated catalytic domain, all seven LS-SHP2 mutants show catalytic activities that are: 14- (Y279C), 42- (Q506P), 60- (T468M), 211- (G464A), 221- (R498L), 423- (Q510E), and 2180- (A461T) fold lower than WT, suggesting that each mutation uniquely perturbs the catalytic chemistry inherent to the WT-enzyme. Cysteine-dependent phosphatases (CDPs) utilize three structural elements to coordinate the chemistry necessary to efficiently carry out the phosphate monoester hydrolysis reaction, the pTyr-loop (DB-loop), P-loop (MG-loop), and Q-loop (HI-loop). The pTyr-recognition loop is critical to substrate phosphotyrosine docking/positioning with the critical and highly conserved Tyr279 residue setting the depth of the catalytic cleft and its side chain π-π stacks with the benzene ring of pTyr to assist substrate recognition and dephosphorylation (Figure 12), similar to its cognate Tyr46 of PTP1B (254). The P-loop (phosphate-binding loop) contains the active site signature motif (^{458}HCSAGIGR) with the catalytic cysteine (Cys459) responsible for nucleophilic attack of the substrate phosphorus atom to create a covalent phospho-cysteine-intermediate. The Q-loop forms the backside of the active site and coordinates the chemistry of Gln506 (specifically the side chain amide) to position a water molecule for active site regeneration (e.g. nucleophilic attack, following deprotanation by Asp425 of the 'WPD'-(LF)-loop, to hydrolyze the phospho-cysteine-intermediate and recreate the Cys459 nucleophile). All seven LS-SHP2 mutations are directed in and around these structural elements (pTyr-

loop-directed; Y279C) (P-loop-directed; A461T, G464A, T468M) (Q-loop-directed; R498L, Q506P, Q510E) and are postulated to uniquely perturb the coordinate chemistry leading to catalytic inefficiency. Interestingly, when the catalytic activity of each mutant's isolated catalytic domain is compared with the catalytic activity displayed by the corresponding full-length construct a disparity emerges where the two most recurrent LS-SHP2 mutants Y279C and T468M are further inhibited by 14- and 26-fold, respectively, suggesting that full-length Y279C and T468M exist in a closed, autoinhibited conformation, while all of the other catalytically impaired LS-SHP2 mutants are not further inhibited, suggesting that they do not exist in a closed, autoinhibited conformation, relative to their more recurrent counterparts or to the WT-enzyme. A fastidious exception can be made regarding the autoinhibitory competency of the Q506P mutant's N-SH2 domain (k_{cat} (CD/FL) ~3-fold). Biochemical data support a trend in which LS-SHP2 enzymes with the most severe impairment to the catalytic mechanism display the least degree of catalytic autoinhibition. As it pertains to catalytically impaired LS-SHP2 mutants, linking catalytic competency to the autoregulatory 'switching' mechanism would make catalytic activity relevant to a discussion about disease pathogenesis.

4.3 LS-SHP2 mutants exhibit increased propensity for the open conformation

4.3.1 The N-SH2 domain is an inefficient competitive inhibitor to LS-SHP2 mutant catalytic domains

As a preface to the work presented in this document, we determined the first crystal-based structure of a pathogenic SHP2 mutant, the LS-SHP2 Y279C mutant. Though the crystal structure showed the Y279C mutant in a closed, autoinhibited

conformation, similar to the WT-enzyme, analysis of the molecular interactions present within this structure, revealed that the Y279C mutation perturbs both catalytic activity and the ability of the autoinhibitory (D'E)-loop of the N-SH2 domain to effectively interact with and occlude the catalytic active site of the PTP domain (Figure 12). Specifically, Y279C alters the substrate recognition surface constituted by Tyr279, Lys364, and Lys366. Substitution of Tyr279 with Cys abrogates the interaction of the phenol side chain with Asp61 and Tyr62 in the D'E loop of the N-SH2 domain. The substitution also affects the positioning of several nearby residues (Lys364, Lys366, Arg362, and His426) involved in binding the N-SH2 domain. Our kinetic parameters also support this in that the catalytic activity displayed by the wild-type full-length construct is 40-fold less than the wild-type isolated catalytic domain, while the catalytic activity displayed by the Y279C full-length construct is 14-fold less than the Y279C isolated catalytic domain. The full-length constructs (1-528) used in these biochemical experiments encompass both the N-SH2 and C-SH2 domains through the 1-245 range preceding what is used for the catalytic domain (246-547). Corroborating previously published results showing that the N-SH2 domain is predominately responsible for catalytic autoinhibition (62), the Y279C crystal structure reveals, for the first time, that naturally occurring pathogenic mutations target the N-SH2/PTP domain interaction toward alleviating intramolecular autoinhibition. Both structural and biochemical data support the Y279C mutant having an increased propensity for the open conformation when in the context of relevant biological stimulation.

To provide additional evidence in support of a decreased intermolecular interaction between the N-SH2 and PTP domains of SHP2 pathogenic mutants, we

measured the ability of isolated WT N-SH2 domain (4-103) to inhibit the phosphatase activity of each of the LS-SHP2 mutant catalytic domains (224-528). Biochemical data suggest that the E76K N-SH2 domain is incompetent towards inhibiting the catalytic active site of the PTP domain, therefore the isolated E76K N-SH2 domain was used as a positive control for 'no inhibition' against the isolated wild-type PTP domain in these inhibitor experiments. As expected from our current knowledge of the structure and function of the SHP2 enzyme, the isolated N-SH2 domain acts as a competitive inhibitor of the SHP2 catalytic domain-catalyzed *p*NPP hydrolysis (data not shown). Table 5 shows biochemical data in support of the isolated WT N-SH2 domain being a very weak if not completely inefficient competitive inhibitor to each of the LS-SHP2 mutant isolated catalytic domains. It is to note that the A461T mutant remains designated 'Undetermined/No Inhibition'. This designation is due to the fact that because the A461T mutant displays an almost undetectable catalytic signature when *p*NPP is used as a substrate, it makes determining the K_i with a measure of consistency very difficult. Biochemical data show that the wild-type N-SH2 domain inhibits the Y279C catalytic domain with a K_i (11.3 ± 0.3μM) that is 10-fold higher, the G464A catalytic domain with a K_i (74.8 ± 4.3μM) that is 58-fold higher, the T468M catalytic domain with a K_i (2.6 ± 0.1μM) that is 2-fold higher, the Q506P catalytic domain with a K_i (41.9 ± 1.3μM) that is 32-fold higher, and the Q510E catalytic domain with a K_i (128 ± 3.7μM) that is 98-fold higher than the inhibition of the WT catalytic domain K_i (1.3 ± 0.05μM). The R498L catalytic domain shows no inhibition out to 200μM by the WT N-SH2 domain. These observations support the kinetic data presented earlier in that LS-SHP2 mutants have either an increased propensity for the open conformation (e.g. Q510E > G464A > Q506P

> Y279C > T468M; (A461T)) or generally exist in an 'unstimulated' open conformation (e.g. R498L (A461T)) similar to the GOF E76K mutant. The catalytically-competent T507K PTP domain is inhibited ~32-fold less than the WT PTP domain by the WT N-SH2 domain, providing further evidence that Q-loop-directed mutations disrupt the autoregulatory mechanism governing SHP2 function.

4.3.2 The N-SH2/PTP domain interaction is exploited by pathogenic mutations afflicting intact SHP2 enzymes towards alleviation of intramolecular autoinhibition

4.3.2a The LS-associated SHP2-Y279C mutant experiences compromised intramolecular autoinhibition as a consequence of mutation

As a preface to the work presented in this document, we used hydrogen-deuterium exchange mass spectrometry (H/DX-MS) as a tool to directly measure both the tendency of SHP2 pathogenic mutants to adopt an 'open·active' conformation in solution and the location where the pathogenic mutations are most affecting the natural intramolecular interactions present in the WT enzyme toward this open·active state. Data derived from this technique is necessary as to date, our Y279C crystal structure shows no evidence of an open·active conformation and only indirect biochemical evidence supporting pathogenic SHP2 mutants adopting open·active states is available in the field. H/DX-MS is uniquely suited for the task of monitoring the differential solution-phase dynamic conformational alterations inherent to the various SHP2 pathogenic mutants, relative to the WT-enzyme. Briefly, when intact/native SHP2 enzymes are incubated with deuterium oxide (D_2O; ^2H_2O) detectable hydrogen·deuterium exchange (hereafter referred to as hydrogen exchange) will occur at the backbone amide bond with rates proportional to the degree by which each amide hydrogen is exposed to the bulk solvent.

Amide hydrogen atoms that are not protected from the bulk solvent by physical occlusion or intramolecular interaction will be quickly exchanged with deuterium atoms, while those amide hydrogens that experience a degree of protection remain unaffected by hydrogen exchange. Each hydrogen exchange that occurs, accounts for a 1 Da increase in physical mass of the enzyme that can be monitored by mass spectrometry. In experimental H/DX-MS a time course is chosen (e.g. 5s-5h) so that hydrogen exchange over time can be plotted and assessments of the degree by which physical regions of intact proteins are protected from exchange can be made. In comparative analyses, this methodology can provide insight into protein structure and function and reveal enigmatic regulatory mechanisms not readily observed with other techniques. Reviews of H/DX-MS theory and methodology can be found in (123, 255). Documentation of the H/DX-MS methods used in this work can be found in the methods section. Figure 13 is a flow chart of both the native/intact and peptide-based H/DX-MS experimental methodology used in this investigation.

Structural, biochemical, and physiological data put the interdomain region created by the intramolecular interaction made between the N-SH2 domain and the catalytic PTP domain as the most significant location that would experience exposure to the surrounding solvent under stimulatory or mutational circumstances. H/DX-MS has the capacity to monitor the magnitude by which this interdomain region becomes exposed to bulk solvent as a consequence of mutation and was chosen to provide additional support to our initial investigation of the LS-SHP2 Y279C mutant exhibiting increased propensity for the open conformation, while existing in a closed, autoinhibited state. We used peptide-based H/DX-MS to provide direct evidence of both the increased propensity of

the Y279C mutant to adopt an open·active conformation and where the most significant alteration to the tertiary structure is taking place due to mutation. The GOF E76K mutant is used in this investigation as a reference for hydrogen exchange magnitude and location experienced in a 'true' SHP2 open enzyme state. Figure 14 shows that in comparison with the wild-type enzyme, a number of peptides in E76K, located in the interface between the N-SH2 domain and the PTP domain, display significant increase in deuterium incorporation. Within the N-SH2 domain, these peptides reside in the D'E loop and adjacent B, C, D, D', E and F β strands, structural elements known to participate in binding the PTP domain. Within the PTP domain, these peptides represent the catalytic loops at the active site, including the P-loop, the pTyr-recognition loop, loop-βF-loop, and the Q-loop. Given the lack of inhibition of the PTP domain by N-SH2/E76K, the observed increase in deuterium uptake surrounding the N-SH2 and PTP binding site suggests that the binding interface is solvent exposed, providing the first direct evidence that E76K exists in an open·active conformation. Hydrogen exchange data show that Y279C also displays enhanced deuterium uptake in the interface region between the N-SH2/PTP domains, albeit to a lesser degree to the peptides observed in E76K. This result indicates that the Tyr279 to Cys mutation causes dynamic perturbations and increased conformational flexibility to residues in the N-SH2/PTP binding interface and supports our finding that the N-SH2 domain of Y279C has a lower affinity for its PTP domain. Moreover, the result also validates our hypothesis that the Y279C mutant has an increased tendency to adopt the open conformation.

Prior to the initial Y279C H/DX-MS study it was unknown whether LS-associated SHP2 mutants that cause catalytic impairment result in mutant enzymes with

compromised affinity between their N-SH2 and PTP domains, a property inherent to GOF NS/neoplasia-associated SHP2 mutants. The H/DX-MS data provide the first direct evidence that pathogenic SHP2 mutations exploit the autoinhibitory mechanism leading to an increased propensity for SHP2 pathogenic mutants to adopt an open enzyme state. Biochemical data show that the degree by which the catalytic domain is inhibited by the N-SH2 domain varies widely across LS-SHP2 pathogenic mutants, while also showing a trend in which LS-SHP2 enzymes with the most severe impairment to the catalytic mechanism display the least degree of catalytic autoinhibition, thus linking catalytic competency to the autoregulatory 'switching' mechanism. As an extension to the initial Y279C investigation, we were interested in the hydrogen exchange properties of all naturally occurring catalytically impaired LS-SHP2 mutants with a hypothesis that all LS-SHP2 mutations which cause catalytic impairment also alleviate intramolecular autoinhibition. This property could then be regarded as a general trend associated with LS-SHP2 mutants, thus linking them to their GOF NS/neoplasia-SHP2 mutant counterparts through a property that is absolutely required for GOF biological effects to be realized, *in-vivo*.

4.3.2b H/D-exchange within intact/native LS-SHP2 mutant enzymes reveals a disparity between mutants with pTyr-/P-loop-directed mutations and those with 'Q'-loop-directed mutations

We chose to commence our investigation by monitoring differential hydrogen exchange within intact/native SHP2 enzymes to get a general sense of the degree by which each enzyme's PTP domain experiences N-SH2 domain-mediated autoinhibition. While little information can be gained regarding the 'hot-spots' of differential hydrogen

exchange observed between the mutant and WT enzymes, hydrogen exchange at the native protein level can be used in a comparative analysis to assess the overall impact that mutation has upon the inherent dynamic conformational flexibility observed in the WT enzyme. The Y279C study has already provided us with data in support of increased hydrogen exchange occurring within the interface region present between the N-SH2 and PTP domains, thus any increase/decrease in deuterium labeling to SHP2 pathogenic mutants, relative to WT, at the native level can be assumed to be taking place within this region. Complete documentation of the native H/DX-MS methods used in this investigation can be found in the methods section. Briefly, native WT and mutant SHP2 enzymes were exposed to D_2O (^2H_2O) for various periods of time ranging from 5sec to 1h to establish net hydrogen exchange over time that will be used in comparative analyses. Upon quenching the reaction at low pH and at cold temperatures, native enzymes were immediately loaded onto a reverse phase (RP) analytical column, eluted isocratically, and subsequently electrosprayed into a linear ion trap mass spectrometer for mass analysis. Figure 15 shows the general quality of data used in this investigation, including representative raw mass spectra showing hydrogen exchange over time to a native SHP2 enzyme. Following deconvolution of the enzyme's multi-charge (*m/z*) envelope, average total mass was plotted to generate a deuterium incorporation over time plot. We measured hydrogen exchange in all reported native LS-associated SHP2 (1-528) mutant enzymes: Y279C, A461T, G464A, T468M, R498L, Q506P and Q510E. To generate points of reference, we measured hydrogen exchange to native SHP2-WT, GOF Leukemia/NS-associated (-D61Y and -E76K) and solid tumor-associated -T507K mutant enzymes. Both D61Y and E76K mutations are N-SH2 domain-directed and are known

from both *in-vitro* and *in-vivo* experimentation to induce catalytic activation, presumably through compromising the regulatory interaction made between their corresponding N-SH2 and PTP domains. Conversely, the T507K mutation is PTP domain-directed and sits directly between the LS-associated SHP2 mutations Q506P and Q510E on the catalytic structure known as the 'Q'(HI)-loop. Unlike the LS-associated SHP2 mutations, which are also PTP domain-directed, the T507K mutation does not disturb catalytic function (248 as well as our data), making it relevant to a discussion regarding the possibility that PTP domain-directed pathogenic mutations that cause catalytic impairment also cause compromised affinity between the regulatory N-SH2 domain and the catalytic PTP domain. Figure 16 shows a bar-chart representation of the complete H/DX-MS results for all SHP2 enzymes under investigation. Data show that at the native protein level the LS-associated SHP2 mutants: G464A, R498L, Q506P and Q510E take in a significant net positive deuterium over time, while the exchange observed in the remaining mutants: Y279C, A461T and T468M is net zero, relative to the WT enzyme. Corroborating the biochemical data presented in (Table 5) regarding the ability of the isolated WT N-SH2 domain to competitively inhibit each LS-SHP2 mutant PTP domain, hydrogen exchange data reveal a similar trend in that those mutants which experience the largest magnitude of hydrogen exchange are the same mutant PTP domains that are weakly inhibited by the WT N-SH2 domain (H/DX: RL > QP~QE > GA > YC ~TM > AT) (K_i: RL > QE > GA > QP > YC > TM, (AT - undetermined).

In summary, hydrogen exchange data to native SHP2 enzymes reveals: (*i*) like GOF D61Y and E76K mutants, PTP domain-directed, and more specifically 'Q'-(HI) loop-directed mutations (R498L, Q506P, Q510E and T507K) create mutant enzymes that

take in significant net positive amounts of deuterium over-time, relative to WT, (*ii*) with the exception of the G464A mutation which resides within the αG-helix, PTP domain-directed mutations that reside further away from the 'Q'-loop (Y279C; DB-loop) or deeper within the active-site pocket (A461T; MG-loop, T468M; αG-helix) create mutant enzymes that take in net zero amounts of deuterium over-time, relative to WT, and (*iii*) unlike the D61Y and E76K mutants, all of the net positive exchanging mutants with PTP domain-directed mutations take longer times to accumulate net positive deuterium amounts, suggesting that N-SH2 domain-directed mutations cause much more significant alterations to the conformational flexibility of the native SHP2 structure in solution. Interestingly, both biochemical and H/DX data show that the most recurrent LS-SHP2 mutants Y279C and T468M take in the least amount of deuterium over time, suggesting that they experience the most significant intramolecular autoinhibition of all LS-SHP2 mutants. Conversely, data suggest that the catalytic 'Q'-loop could be an 'Achilles' heel' with regard to mutational-disruption of N-SH2 domain-mediated intramolecular autoinhibition. Why is there such a disparity between the LS-SHP2 mutants with regard to catalytic inefficiency and the inherent defect in the capacity for intramolecular autoinhibition by the N-SH2 domain?

4.3.2c H/D-exchange analysis at the peptide-level reveals that the catalytic 'Q'-loop is an 'Achilles' heel' with regard to mutational-disruption of N-SH2 domain-mediated intramolecular autoinhibition

Deuterium exchange to native SHP2 enzymes provides insight into the notion that LS-associated SHP2 mutations that cause catalytic impairment also induce significant alterations to the dynamic conformational flexibility inherent to the native SHP2 structure

in solution. A subset or 'class' of these mutants display conformational flexibilities that are similar in magnitude to those inherent to GOF SHP2 mutants. In light of the intramolecular negative regulatory mechanism associated with SHP2 function described earlier, further insight into the hydrogen exchange properties of these mutants might uncover regions that are predominately exploited by pathogenic mutations in efforts to disturb the N-SH2/PTP domain interaction leading to an increased propensity for the enzyme to become 'opened' in the presence of competing pTyr-ligands, *in-vivo*. Hydrogen exchange at the peptide level will afford a more resolved understanding of this notion and provide more insight into particular regions that experience increased or decreased dynamic conformational flexibility in solution due to mutation, relative to WT.

In order to address the question of whether LS-associated SHP2 mutations cause a weakening of the interaction the N-SH2 domain makes with the PTP domain, leading to an 'open' enzyme state, we chose to monitor hydrogen exchange at the peptide level to get a more resolved understanding of where 'regional' exchange differences occur, relative to WT. We measured the hydrogen exchange properties of the GOF Leukemia/NS-associated SHP2-E76K and -D61Y mutants to establish points-of-reference for known 'open·active' states to be used in comparative analyses with LS-associated SHP2 mutants. Complete documentation of the relevant peptide-based H/DX-MS methods used in this work can be found in the methods section. Briefly, native WT and mutant SHP2 enzymes were exposed to D_2O (^2H_2O) for various periods of time ranging from 5sec to 1h to establish net hydrogen exchange over time that will be used in comparative analyses. Following native enzyme deuterium labeling, peptic peptides were generated at low pH and at cold temperatures using the pepsin endoproteinase during the

reaction quenching step. Peptides were immediately loaded onto a reverse phase (RP) analytical column, chromatographically separated in-time using a steep gradient of acetonitrile, and subsequently electrosprayed into a mass spectrometer for mass analysis. Figure 17 shows the general quality of the peptide data including representative mass spectra of parent ions experiencing deuterium incorporation over time and the unbiased processing steps used to convert the raw spectra into weighted average mass (WAM) values for deuterium incorporation over time plot construction. A total of 46 peptic peptides, across all experimental groups, representing ~95% of the SHP2 (1-528) sequence, were used to generate the data for this analysis. Figure 18 shows a two-dimensional (2-D) plot of the location of all 46 peptic peptides within the primary amino acid sequence of SHP2 (1-528). Corresponding 2º-structures are labeled and color-coded based upon domain arrangement so that each peptide can be associated with a relevant 2º-structure present within the three-dimensional (3-D) enzyme. In this investigation, enzymes are compared based upon significant differences in hydrogen exchange over time to equivalent peptides as documented per figure presented. Table 6 represents a comprehensive 'heat-map' representation of the hydrogen exchange differences observed in all SHP2 pathogenic mutant enzymes under investigation, relative to WT. In this view, hydrogen exchange to peptides derived from the WT enzyme per time is considered 'base-line or zero' (where WT is all 'grey'). Based upon the legend provided, significant differences (both positive and negative) in hydrogen exchange over time to peptides derived from SHP2 mutant enzymes are color-coded based upon magnitude of difference, relative to corresponding WT peptides. A color designation is only provided for mutant peptides that maintain a significant difference over their WT counterpart for at least two

successive time points to limit false positives due to technical variability. Additionally, each (WAM) value presented is an average of a triplicate measurement per time point. A mutant peptide exchange difference that achieves (+0.4-0.7 Da; green) over the corresponding WT peptide is at marginal significance in hydrogen exchange and is regarded as having slight exposure to the bulk solvent. All other values between +0.7 and >2.0 (yellow, orange, and red) are regarded as very significant and are within regions experiencing considerable exposure to the bulk solvent, relative to corresponding WT regions. Figures 19-28 represent the data present in Table 6 as 3-D 'heat-map' plots for all SHP2 pathogenic mutants under investigation. The N-SH2, C-SH2, and PTP domains as well as corresponding 2º-structural elements are labeled in the primary (5s) time point. The catalytic Cys459 is labeled for active site orientation.

SHP2 is understood to exist predominately in two states: a 'closed' inhibited state in which the regulatory N-SH2 domain physically occludes the active site while making extensive intramolecular interactions with the catalytic PTP domain (62, 250-252) and an 'open' active state in which the regulatory N-SH2 domain associates with phosphotyrosyl-ligands (pTyr-ligands), thus freeing the PTP domain's active site from intramolecular autoinhibition (62-63, 250-252). The N-SH2 domain's D'E (auto-inhibition)-loop (^{58}NTGDY^{62}) represents the most significant structure of the intramolecular negative regulatory network present between the N-SH2 and PTP domains, due to its role in occluding the active site of the enzyme and making extensive contacts with residues associated with key mechanistic structures in the 'closed-inhibited' state including: the catalytic cleft proper (MGloop-αG) (S460, A461, I463, G464, R465), substrate coordination loops: 'pTyr'(DB)-loop (Y279, I282) and FH-loop (R362, K364,

K366), 'WPD'(LF)-loop (D425, H426, G427) and the 'Q'(HI)-loop (Q506, T507, Q510). The N-SH2 domain is said to act as an 'allosteric' switch, in that key structures must shift their position to accommodate a pTyr-ligand and in so doing lose complementarity with PTP domain structures to which they were previously bound, a postulation known as 'negative cooperativity' (62). Specifically, the position of the αB-helix and secondary sheet (βD', βE, βF), change with respect to the αA-helix and central sheet (βB, βC, βD) which remain fixed. Significant movement of the βE-EFloop-βF structure, with the EF-loop as a key 'gate-keeper' structure towards pTyr-ligand association, would act to completely displace the D'E-loop from allosteric occlusion of the enzyme's active site.

As the interdomain region present between the N-SH2 and PTP domains is to be solvent exposed following SH2 domain association with pTyr-ligands or by mutational consequence, H/DX-MS represents a relevant technique to monitor this conformational state transition. Here, H/DX-MS data provide the first direct evidence of a common mechanism employed by N-SH2 domain-directed GOF E76K and D61Y mutations to generate an 'open' enzyme state in solution. Due to the sheer magnitude of dynamic conformational alterations caused by the E76K mutation, relative to those caused by the D61Y mutation, we chose to use the hydrogen exchange profiles of the E76K mutant to highlight the common mechanism by which an 'open' enzyme state is achieved. Data presented in (Figure 19) as well as (29A and 29C) show that the net positive hydrogen exchange observed within the native E76K mutant focuses within the interface region formed between the N-SH2 and PTP domains, providing further credibility to the currently accepted regulatory mechanism associated with SHP2 function. Within the PTP domain, the (451-469) peptide representing the catalytic cleft proper (FMloop-βM-

MGloop-αG) as well as the (496-504) and (505-511) peptides representing the catalytically essential 'Q'-loop structure (αH-'Q'(HI)-loop-αI) at the back-side of the active site exchange significantly more hydrogen by early time points, providing evidence that the active site could be constitutively open and free from occlusion by the N-SH2 domain's D'E-loop, relative to WT. The interface region between the N-SH2 and PTP domains goes as far back as the αB helix of the PTP domain, a distance of ~20Å from the 'gate-keeper' D'E-loop of the N-SH2 domain. The (252-261) peptide representing the αB helix exchanges significantly more hydrogen by early time points in E76K, relative to WT. The time and magnitude by which significant exchange is observed within the active site as well as to the distant αB helix provides conclusive evidence that the entire interdomain region is solvent exposed in the E76K mutant, relative to WT. This is further supported by earlier biochemical evidence showing that the Lys76 mutant N-SH2 domain inhibits the WT PTP domain at least 200-fold weaker than the WT N-SH2 domain inhibits the WT PTP domain. In continued support that the N-SH2 domain's D'E-loop is completely displaced from occluding the active site, key mechanistic structures mentioned earlier that make critical intramolecular contacts with the D'E-loop in the 'closed-inhibited' enzyme state, including the substrate coordination loops: 'pTyr'(DB)-loop region represented by the (262-292) peptide and associated (βC-CDloop-βD) region represented by the (304-308 and 315-334) peptides as well as the FH-loop region represented by the (356-374) peptide, also exchange significantly more hydrogen in the E76K mutant, signifying that the intramolecular interactions they make with the D'E-loop are significantly weakened, making their conformations highly dynamic, relative to WT. It is relevant to note that the K_m for substrate has not changed

for the E76K mutant, revealing that the structures that coordinate substrate are conformationally 'sound', but exist in a highly dynamic 'active' state.

In light of the fact that H/DX-MS data show that the native E76K mutant exchanges much more hydrogen by early time points than the native WT enzyme and that this exchange difference has been shown by peptide analysis to be localized largely to the interface region formed between the N-SH2 and PTP domains, it would not be surprising that the E76K N-SH2 domain would exist in an 'open' state in solution, relative to the WT N-SH2 domain. In fact, we believe that our H/DX-MS data show direct evidence of the 'negative cooperativity' postulation towards an 'open' N-SH2 domain state (62, 256), being supported in the E76K mutant. It is important to note that because H/DX-MS monitors backbone amide hydrogen exchange, it is difficult to decipher to what face of the N-SH2 domain exchange differences are actually occurring, relative to WT. Taking into consideration that H/DX-MS data show that backbone amide hydrogen atoms of the PTP domain are completely solvent exposed and assuming that the 'negative cooperativity' postulation is indeed true, differences in exchange to the E76K N-SH2 domain are occurring to both faces and revealing a state that is 'free' from interdomain regulation. Figure 19 as well as (29B and 29C) show that significantly increased hydrogen exchange by the earliest time points, penetrates into structures of the E76K N-SH2 domain consistent with the conformational alterations documented to take place within this domain upon pTyr-ligand association. Specifically, the (44-62) and (63-71) peptides representing the N-SH2 domain's D'E-loop and the secondary sheet structure (βE-EFloop-βF) respectively, exchange significantly more hydrogen by early time points in the E76K mutant, relative to WT. This data provide evidence that the 'gate-keeper'

auto-inhibitory D'E- and pTyr-ligand-binding EF-loops are pulled away from the active site, a key observation previously documented while describing the significant conformational alterations that take place within the N-SH2 domain when it is in a pTyr-ligand-bound 'active' state (62, 256-257). These 'initiating' conformational alterations to an 'open' N-SH2 domain state, allow for further increased exchange to be seen within the (αA-ABloop) region represented by the (19-29) peptide, which leads to the central sheet (βB-BCloop-βC) region, represented by the peptides (30-43) and (44-62). Importantly, these regions, along with the secondary sheet (βE-EFloop-βF) and BG-loop 'gate-keeper' regions form a 'groove' for pTyr-ligand association. Increased exchange observed within the pTyr-ligand 'groove' signifies that this region is in a conformation that resembles an 'open-active' 'pTyr-ligand-bound' state. Additionally, the (30-43) peptide contains the BC-loop structure that represents an apparent regulatory loop whose function is to either block or allows access to the essential Arg32 residue that makes coordinate contact with the pTyr-residue of the bound pTyr-ligand, depending upon the conformational state of the N-SH2 domain. Significantly increased hydrogen exchange to the (βB-BCloop) region shows that it is conformationally more dynamic and provides evidence that the essential Arg32 residue is exposed, a mark that the E76K N-SH2 domain is in an 'open' state, relative to the WT N-SH2 domain. Figure 29D shows the hydrogen exchange 'heat-map' for the E76K N-SH2 domain at the 1 min. time point of deuterium labeling modeled on the (A-state) phosphotyrosyl-peptide-bound N-SH2 domain as documented by (256; PDB: 1AYA). The color-coded 1AYA structure is superimposed upon our WT (3OLR) structure (grey) in order to show that increased hydrogen exchange is occurring to the exact regions that are shown to undergo conformational alterations upon

phosphopeptide-binding, suggesting that the E76K N-SH2 domain is in an 'open·active' conformation in solution due to the magnitude by which interaction with the PTP domain has been compromised because of mutation.

The Glu76 residue resides within the N-SH2 domain's αB-helix, an essential structure located between the critical EF- and BG-loops previously documented to be 'gate-keepers' toward pTyr-ligand association (62). Glu76 predominately associates with Arg265 of the PTP domain's αC-helix through an electrostatic interaction (a water-mediated hydrogen bond). Upon mutation to Lys76, a significant repulsive force between Lys76 and Arg265 causes interdomain instability at the immediate sites of the N-SH2 domain's αB-helix and the PTP domain's αC-helix. Within the N-SH2 domain, this loss of conformational integrity translates immediately to the secondary sheet structure (βE-EFloop-βF) which includes the 'gate-keeper' EF-loop, leading immediately to the autoinhibitory D'E-loop. H/DX-MS elegantly shows the magnitude of conformational disturbance created within the immediate region surrounding the Lys76 mutation. As observed in (Figures 19 and 29), peptides representing the N-SH2 domain's EF-loop (63-71; βE-EFloop-βF) and D'E-loop (44-62; βC-CDloop-βDβD'-D'Eloop) and the PTP domain's αC-helix (262-292; BCloop-αC-CDloop-αD-DBloop-βB) exchange significantly more hydrogen at early time points, relative to WT. These significant conformational alterations transfer immediately to the N-SH2 domain's auto-inhibitory D'E-loop causing it to be significantly displaced from occluding the active site.

This mechanism is common to the D61Y mutant as well, albeit with hydrogen exchange differences occurring with smaller magnitudes and at longer times than those observed between E76K and WT as can be seen in (Table 6). An Asp→Tyr mutation

within the D'E-loop would alter the strength of interactions that Asp61 makes with the FH-loop residues Arg362 and Lys366 and the αG-helix residue Arg465, changing electrostatic interactions to weaker H-bonds. Interestingly, the destabilizing force to the D'E-loop is not as complete as that created by the E76K mutation as observed by the (356-374) peptide, which contains the FH-loop residues Arg362 and Lys366, showing no appreciable difference in exchange, relative to WT. The conformational aberration created by the D61Y mutation is directed more toward the (βE-EFloop-βF) region most likely by significantly disturbing the conformation of the DB-loop and the π-π stacking interaction made by the DB-loop's Tyr279 residue with the D'E-loop's Tyr62 residue. H/DX-MS data show that the D61Y mutation causes immediate conformational disturbance to the final residue (Y62) of the much longer peptide (44-62) shown in E76K to experience significant hydrogen exchange over its entire length. This aberration continues to the (βE-EFloop-βF) region represented by the (63-71) peptide, but to slightly less magnitude in exchange as compared to the corresponding peptide in E76K. Due to the D61Y mutation causing a conformational disturbance to the D'E-loop that is slightly smaller in magnitude than that caused by the E76K mutation, a concomitant smaller degree of exchange to the active site is also observed, relative to E76K. Furthermore, no exchange significance can be observed to the distant αB-helix of the PTP domain, signifying that the entire interdomain region is not completely solvent exposed as it is in the E76K mutant. Additionally, a smaller in magnitude change to the dynamics of other critical regions of the N-SH2 domain associated with pTyr-ligand binding is also observed in the D61Y mutant, signifying that the D61Y N-SH2 domain has not adopted an 'open' state as pronounced as the E76K N-SH2 domain.

Our group has in manuscript a thorough investigation describing the biochemical, biophysical and biological properties of the LS-SHP2-Y279C pathogenic mutant. In this report we proposed a mechanism by which the Y279C mutation causes both compromised catalytic ability as well as a loss of interaction potential between the N-SH2 and PTP domains leading to an N-SH2 domain that is more easily displaced by competing pTyr-ligands, *in-vivo*. We postulated that the observations made in studying the Y279C mutant could be carried over as general phenomenon to all LS-associated SHP2 pathogenic mutants. It is our hypothesis that all seven documented LS-associated SHP2 mutations (Y279C, A461T, G464A, T468M, R498L, Q506P and Q510E) are 'selected-for' in contributing to the pathogenesis of LS due to their ability to concomitantly cause both compromised catalytic ability as well as cause a loss of interaction potential between the N-SH2 and PTP domains leading to an 'open' enzyme state. Additionally, based upon H/DX-MS results generated from exchange to native SHP2 enzymes in solution, it is our hypothesis that the magnitude by which each LS-associated SHP2 mutations causes a loss of interaction potential between the N-SH2 and PTP domains is dependent upon the specific site of the mutation with two specific 'classes' emerging: those mutations that exist shallower into the interdomain region, specifically in and around the catalytic cleft proper (pTyr-/P-loops) (Y279C, A461T, G464A and T468M) and those mutations that exist deeper into the interdomain region, specifically in and around the 'Q'(HI)-loop (R498L, Q506P and Q510E).

To our amazement, H/DX-MS performed at the native level to all LS-SHP2 mutants revealed that there exists class of 'exchangers' that display similar exchange magnitudes in solution to the known GOF 'open-active' SHP2 mutants (E76K and

D61Y) under investigation. Surprisingly, these mutants (R498L, Q506P and Q510E) all harbor mutations that are directed to the mechanistically/catalytically critical 'Q'(HI)-loop region (αH-'Q'(HI)loop-αI). As the catalytically impaired LS-SHP2 mutant R498L represents the most significant hydrogen exchanger with exchange magnitudes similar to the GOF E76K mutant, we chose to use R498L to explain how 'Q'-loop-directed mutations cause both compromised catalytic ability as well as an 'open' enzyme state in solution. We believe our data show that LS-SHP2 mutations that are able to impart significant conformational challenges to both the 'Q'-loop and catalytic cleft proper are able to significantly affect the conformation of the N-SH2 domain's D'E-loop. Alternatively, LS-SHP2 mutations that impart much weaker challenges to these regions are not able to induce a strong conformational disturbance to the D'E-loop resulting in apparent affinities between the N-SH2 and PTP domains that are similar to WT. We have included a solid tumor-associated pathogenic SHP2 mutant (T507K) in this analysis as it is 'Q'-loop-directed, but does not have any effect upon the apparent catalytic function of the enzyme, to corroborate data associated with the 'Q'-loop-directed LS-SHP2 mutants. Our data support the catalytically essential 'Q' (HI)-loop being an 'Achilles' heel' with regard to mutational-disruption of N-SH2 domain-mediated intramolecular autoinhibition.

The Arg498 residue, as part of the PTP domain's αH-helix, inserts itself directly between the PTP domain's 'Q'(HI)-loop and αB-helix and acts to stabilize the conformational positions of these two structures by simultaneously forming multiple interactions including: H-bonds with the main-chain carbonyl oxygen of the 'Q'-loop residues (Gly503, Met504, Val505 and Gln506) and the side-chain primary amines of the

αB-helix residue Gln255 and the αH-helix residue Gln495. Additionally, Arg498 makes a strong electrostatic interaction with Glu257 of the αB-helix. H/DX-MS reveals both the local and far-reaching consequences that mutation to Leu498 imparts upon the conformational dynamics of this enzyme in solution. Though the overall magnitude of hydrogen exchange is similar to the E76K mutant at the native level, exchange at the peptide level reveals that the mechanism by which the R498L mutation affects the N-SH2 domain's D'E-loop is relatively more indirect. Exchange at the native level confirms this, as the major difference between exchange in the E76K mutant and the R498L mutant is at the very early time points, signifying that the perturbation imparted to the D'E-loop by the E76K mutation is more direct than that imparted by the R498L mutation. Figure 25 as well as (29A and 29C) show data depicting how the R498L mutation imparts both local and far-reaching consequences to the catalytic function of the enzyme and to the stability of the N-SH2/PTP domain interaction. In contrast to the mechanism by which E76K alleviates intramolecular autoinhibition explained earlier, the contact lost between Arg498 and the residues of the 'Q'(HI)-loop and αB-helix upon mutation, causes significantly increased conformational dynamics to the (βN-NHloop-αH) region represented by the (486-496) peptide and the (αG-GNloop) region represented by the (470-485) peptide that ultimately lead into and form the αG-helix, where residues of the catalytic signature motif (H<u>C</u>SAG^{463}**IGR**^{465}) reside. Furthermore, the PTP domain-directed dynamic conformational alterations caused by the R498L mutation are larger in magnitude than the same alterations observed while following exchange in the E76K mutant. Specifically, (Figure 29A) shows that peptides representing the catalytic cleft proper (451-469; FMloop-βM-MGloop-αG), 'Q'(HI)-loop (496-504; αH-HIloop) (505-

511; HIloop-αI), substrate-coordination (356-374; βE-EFloop-βF-FHloop) region and associated (315-334; CDloop-βD-DEloop) exchange more hydrogen over time in the R498L mutant than do the corresponding peptides in the E76K mutant. It is interesting to note that between the two substrate coordination loops known to make critical interactions with the D'E-loop, the FH-loop represented by the (356-374) peptide is significantly more dynamic in the R498L mutant, but the DB-loop represented by the (262-292) peptide is significantly more dynamic in the E76K mutant, especially by early time points. It is evident that the repulsive force that the E76K mutation has upon the Arg265 residue of αC-helix, which precedes the DB-loop, creates a very significant destabilizing force to the D'E-loop that translates in magnitude further into the N-SH2 domain. Conversely, the magnitude of conformational instability caused by the distant R498L mutation to the substrate coordination FH-loop, containing the Arg362 and Lys366 residues that make two important electrostatic interactions with the D'E-loop's Asp61 residue, is much more significant as it further translates down through the (βH, βI, βJ) sheet. The conformational alterations mentioned above caused by the R498L mutation have profound consequences on the ability of the N-SH2 domain's D'E-loop to interact and physically occlude the active site, but due to the more indirect route that the R498L mutation takes relative to E76K mutation, the magnitude of exchange differences observed in the N-SH2 domain is smaller in the R498L mutant, relative to the E76K mutant. Figures 25, 29B, and 29C shows that the far-reaching effects of the R498L mutation to the structures of the N-SH2 domain are weaker in magnitude than those caused by the E76K mutation. Specifically, the functionally critical regions of the N-SH2 domain associated with pTyr-ligand association mentioned earlier including: the

(44-62) and (63-71) peptides representing the N-SH2 domain's auto-inhibition (D'E)-loop and the secondary sheet structure (βE-EFloop-βF) as well as the (19-29) peptide representing the (αA-ABloop) region leading to the central sheet (βB-BCloop-βC), represented by the peptide (30-43), show significant hydrogen exchange in the R498L mutant, but the exchange takes longer to be detected and is smaller in magnitude than that observed to all comparative peptides from the E76K mutant. H/DX-MS data at the native and peptide levels reveal that both E76K and R498L exist in an 'open' enzyme state in solution, but achieve this 'open' enzyme state by two distinct mechanisms: E76K influences the conformation of the D'E-loop through perturbing N-SH2 domain structures more directly and strongly, while the R498L mutation influences the D'E-loop more indirectly through perturbing PTP domain structures associated forming the active site, which also explains the compromised catalytic function associated with this mutant. Figure 29D shows the hydrogen exchange 'heat-maps' for the R498L and E76K N-SH2 domains at the 1 min. time point of deuterium labeling modeled on the (A-state) phosphotyrosyl-peptide-bound N-SH2 domain as documented by (256; PDB: 1AYA). The color-coded 1AYA structure is superimposed upon our WT (3OLR) structure (grey) in order to show that increased hydrogen exchange is occurring to the exact regions that are shown to undergo conformational alterations upon phosphopeptide-binding, suggesting that the E76K N-SH2 domain is in an 'open·active' conformation in solution due to the magnitude by which interaction with the PTP domain has been compromised because of mutation.

Similar in mechanism to the conformational perturbations caused by the R498L mutation, the other 'Q'-loop-directed mutations, Q506P and Q510E, also compromise the

interaction made between the D'E-loop and the enzymes active site, but in a more subtle manner. Similar to the R498L mutant, the Q506P mutant experiences significant, albeit smaller in magnitude, exchange to the βN-NHloop-αH (486-496) and the αG-GNloop (470-485) regions. It is to note experimentally that, unlike all other mutants under investigation, both the (496-504) and (505-511) peptides representing the critical 'Q'(HI)-loop region (αH-HIloop-αI) were not identified following database query and were also not identified in the raw mass spectra during manual data processing for the Q506P mutant. It could be reasoned that the Q506P mutation within the (505-511) peptide could lead to a very poor ion signal, but the missing (496-504) peptide signal suggests that the conformation of the 'Q'(HI)-loop (αH-HIloop-αI) region is such that efficient digestion by pepsin is not possible. A profound conformational alteration to the 'Q'(HI)-loop (αH-HIloop-αI) region caused by the Q506P mutation could lead to similar consequences as those observed in the R498L mutant, but hydrogen exchange data reveal that the magnitude of change is not as dramatic in the Q506P mutant, thus leading to more subtle changes to the catalytic cleft proper (451-469; FMloop-βM-MGloop-αG) as well as the substrate-coordination (356-374; βE-EFloop-βF-FHloop) region and associated (315-334; CDloop-βD-DEloop) region. The weaker conformational alterations are further confirmed by much less pronounced exchange penetrating to the N-SH2 domain as compared to that observed in the R498L mutant.

Similar in nature and magnitude to the Q506P mutant, the Q510E mutant experiences increased exchange to the αG-GNloop (470-485) region, but not to the βN-NHloop-αH region (486-496) as observed in R498L and Q506P signifying that the mutational consequences caused by the Glu510 mutation do not go through the βN-

NHloop-αH region, but do significantly affect the conformation of the αG-helix leading to the catalytic cleft proper. This could be explained in that the Gln510 side chain makes a polar interaction with Thr468 residue of the αG-helix, thus stabilizing the conformations of these two structures in the WT enzyme. HDX-MS data within the αG-GNloop (470-485) region suggest that the Q510E mutation, which has the potential to form a stronger H-bond interaction with the Thr468 hydroxyl group, does not adopt a favorable conformation for this interaction to take place possibly because the electronegative acid side chain of Glu510 is present within a hydrophobic pocket created by Trp423 and Val428 of the 'WPD'(LF)-loop, Val505 of the 'Q'(HI)-loop and Ile514 of the αI-helix. Additionally, if the electronegative Glu510 residue did remain in the same relative conformation it would have a repulsive affect upon the N-SH2 domain's D'E-loop residue Asp61. HDX-MS data supports the latter model as the (44-62) peptide representing the D'E-loop exchanges more deuterium and is therefore more conformationally dynamic in the Q510E mutant than the Q506P mutant. This effect is further translated to the N-SH2 domain where slightly more significant penetrance of deuterium to other regions of the N-SH2 domain including peptides representing the βE-EFloop-βF region (63-71) and the βB-BCloop-βC region (30-43) are observed in the Q510E mutant, relative to the Q506P mutant. Biochemical data generated from using the free WT N-SH2 domain as an inhibitor to each LS-associated mutant PTP domain further confirms the magnitude by which the 'Q'-loop-directed LS-SHP2 mutants exist in an 'open' enzyme state in solution. Specifically, the R498L mutant PTP domain is inhibited at least 200-fold weaker than the WT PTP domain, while the Q506P and Q510E mutant

PTP domains are inhibited at least 32- and 98-fold weaker than the WT PTP domain, respectively.

Interestingly, the solid tumor-associated SHP2-T507K mutant shows the least dramatic exchange of all the 'Q'-loop-directed pathogenic mutants. Unlike the exchange observed to take place within the LS-SHP2 'Q'-loop-directed mutants described above, the T507K mutant does not show increased hydrogen exchange to peptides representing the βN-NHloop-αH (486-496) or αG-GNloop (470-485) regions and because of this it is postulated that the T507K mutation does not translate a strong effect through the 'Q'-loop and active site to destabilize the N-SH2 domain's D'E-loop. This is shown by significant exchange occurring within the T507K active site only after much longer times when compared to the other 'Q'-loop-directed mutants. Additionally, no significant exchange penetrates to structures of the N-SH2 domain worth mentioning in the T507K mutant. Different from the other 'Q'-loop-directed mutants, HDX-MS shows that the much weaker conformational disturbances to the 'Q'-loop and catalytic cleft proper, caused by the T507K mutation, do not disrupt catalytic function, suggesting that this is the reason why T507K is not an LS-SHP2 mutation.

The other LS-SHP2 mutant 'class' of exchangers noted earlier (Y279C, A461T, G464A and T468M) are all located very shallow within the interface region created by the N-SH2 and PTP domains with the Y279C mutation located on the surface of the enzyme within the DB-loop; a structure that is not contained within the interdomain region. With the exception of the G464A mutant, the other three mutants show net zero hydrogen exchange at the native protein level, signifying that the conformational perturbations caused by these mutations are relatively minor when compared to WT.

Biochemical data shown earlier support that at least three of the LS-SHP2 mutants within this 'class' exist in an 'open' enzyme state in solution (i.e. have increased propensity for the open conformation). A461T represents the only outlier within this group as it pertains to biochemical data agreeing with the magnitude by which each mutant exchanges net hydrogen. This can be explained as crystallographic assessment of this mutant reveals that a new hydrogen bond has formed between the backbone carbonyl oxygen of the autoinhibition D'E-loop's Asp61 residue and the hydroxyl group of the Thr461 mutation, thus apparently holding the N-SH2 domain's D'E-loop down even tighter than that experienced in the WT enzyme. Additionally, crystallographic assessment shows that the A461T mutation causes both the N-SH2 and C-SH2 domains to shift positions significantly about the PTP domain. These shifted positions reveal that the A461T mutation has caused the PTP domain to be a poor topographical fit with the N-SH2 domain, thus leading to the very weak inhibitory capacity of the WT N-SH2 upon the A461T PTP domain observed during biochemical experiments. HDX-MS data show that the new H-bond formed between Asp61 and Thr461 does indeed hold the D'E-loop down significantly more than that observed in WT as significantly less hydrogen is exchanged within the active site of the A461T mutant, relative to WT. In fact, this is the only mutant that shows this effect in decreased exchange to the active site, relative to WT. As the rate of deuterium penetrance into the active site is slowed due to the 'increased strength' of the D'E-loop 'gate', further exchange significance to the interdomain region can't be appreciated. Though the complete interdomain region experiences no noticeable increase in hydrogen exchange relative to WT, three regions 'outside' the interdomain region that are responsible for substrate coordination as well as

interaction with the autoinhibitory D'E-loop exchange significantly more hydrogen than WT (262-292; BCloop-αC-CDloop-αD-DBloop-βB) (284-303; DBloop-βB-BCloop-βC) (356-374; βE-EFloop-βF-FHloop). Interestingly, these are the same regions shown to be significant to the disruption of intramolecular autoinhibition by the Y279C mutation of the LS-SHP2-Y279C mutant.

Hydrogen exchange at the native level shows that the most significant exchange within this 'class' of exchangers occurs within the G464A mutant. This seems to be due to the G464A mutation disrupting the conformation of the D'E-loop enough to allow for significantly increased exchange by early time points to be seen within the (451-469) peptide representing the catalytic cleft proper (FMloop-βM-MGloop-αG) and the (496-504) peptide representing the 'Q'-loop structure (αH-'Q'(HI)-loop). Significant exchange, but by later time points can be seen within the substrate coordination 'pTyr'(DB)-loop region (262-292) and associated βC-CDloop-βD region (304-308 and 315-334), signifying that the destabilizing effect to the D'E-loop is not as significant as that seen within the E76K, D61Y, R498L, Q506P and Q510E mutants. Interestingly, biochemical data show that the WT N-SH2 domain inhibits the G464A PTP domain almost 2-fold less than it inhibits the Q506P PTP domain. Due to the Q506P mutation being a 'Q'-loop-directed mutation, it would be postulated that the Q506P PTP domain would be less inhibited than the G464A PTP domain by the WT N-SH2 domain. Structurally, replacing a glycine residue with an alanine residue directly before the αG-helix would suggest that the reason for this disparity could be due to the autoinhibitory D'E-loop being a poor topographical fit within the G464A active site. H/DX data reveal that the (177-187) peptide representing the D'E-loop structure experience slightly

negative hydrogen exchange relative to WT, suggesting that in the intact mutant enzyme an aberrant interaction is present with the D'E-loop structure.

As previously reported, the Y279C mutant incorporates significant deuterium into the active site (451-469; FMloop-βM-MGloop-αG) (496-504; αH-HIloop) as well as to the substrate coordination regions (262-292; BCloop-αC-CDloop-αD-DBloop-βB) (284-303; DBloop-βB-BCloop-βC) that lie on the outside of the interdomain region, but by later time points, signifying that the destabilizing effect that the Y279C mutation imparts upon the D'E-loop is relatively weak compared to the 'Q'-loop-directed LS-SHP2 mutants or the G464A mutant from this 'class' of exchangers.

Under the constraints of this methodology only marginal hydrogen exchange difference can be appreciated for the T468M mutant relative to WT. The physical location of the Thr468 residue deep within the αG-helix makes it the most conservative location with respect to a mutation, such as methionine, to significantly perturb any secondary structural element that is critical to maintain the intramolecular autoinhibitory interaction. The only significant interaction that Thr468 makes that could perturb catalytic function and create a marginal negative effect upon the autoinhibitory interaction when mutated to methionine, is a polar interaction with Gln510 of the 'Q'-loop region (HIloop-αI). H/DX data show that a significant difference in hydrogen exchange can be appreciated to the substrate coordinating (356-374; βE-EFloop-βF-FHloop) region, similar to many other SHP2 pathogenic mutants. Biochemical data presented earlier support H/DX-MS data in showing the relatively minor effects the T468M mutation has upon the intramolecular autoinhibitory interaction.

It is worth noting that no exchange penetrance to the structures of the N-SH2 domain can be observed for any mutant within this 'class' of exchangers, due to the much weaker ability of these specific mutations to cause dramatic conformational disturbances to the D'E-loop. This evidence provides further credibility to the importance of the PTP domain's 'Q'-loop region (αH-'Q'(HI)-loop-αI) as a major stabilizing force to the interactions that the PTP domain makes with the N-SH2 domain when the enzyme is in a 'closed-inhibited' state. LS-SHP2 mutations that are directed to the 'Q'-loop region cause major instability to the autoinhibitory D'E-loop that is directed through both the 'Q'(HI)-loop and the αG-helix leading to the catalytic cleft proper. Significant conformational disturbances directed to these regions are postulated to cause both compromised catalytic function as well as a compromised interaction between the N-SH2 and PTP domains leading to mutants that predominately exist in an 'open' state, relative to the WT-enzyme. Though other LS-SHP2 mutations that are not 'Q'-loop-directed perturb catalytic function they predominately exist in a 'closed-inhibited' state, but are able to be more easily 'opened' by competing pTyr-ligands, relative to the WT-enzyme.

4.4 Discussion/Summary

The molecular basis for SHP2 function is pTyr-ligand-induced alleviation of intramolecular autoinhibition of the catalytic active site by the N-SH2 domain following growth factor/cytokine stimulation of transmembrane receptors. In a single action, the N-SH2 domain induces catalytic activation by becoming free of intramolecular autoinhibition, while targeting this enzyme to the location of its putative substrates. Due to this autoregulatory mechanism, the N-SH2 domain is said to be an elegant molecular 'switch'. Consequently, the interaction that the N-SH2 domain makes with the catalytic

PTP domain in a latent state becomes exploited by a multitude of both germ-line and somatic mutations to drive disease pathogenesis. The vast majority of these mutations impair the N-SH2 domain-mediated autoinhibitory mechanism without perturbing catalytic functionality, resulting in SHP2 pathogenic mutant enzymes that are capable of driving gain-of-function (GOF) biological effects *in-vivo*. These GOF SHP2 mutants are known to be responsible for ~50% of documented Noonan syndrome (NS) cases as well as a variety of hematological malignancies and solid tumors. Alternatively, a subset of mutations reside in and around the catalytic active site of the PTP domain and are known to cause catalytic impairment. These catalytically impaired SHP2 mutants drive ~90% of documented LEOPARD syndrome (LS) cases, a rare autosomal dominant disorder that shares many clinical phenotypic features with NS as part of a family of neuro-cardio-facio-cutaneous (NCFC) conditions known as 'RASopathies'. How do mutations which provoke opposite effects on SHP2 phosphatase activity cause phenotypically similar disorders?

Prior to this investigation it was well understood that NS and LS-SHP2 mutants could be distinguished based upon catalytic competency, but what remained an enigma was whether LS-SHP2 mutants possessed incompetent autoinhibitory mechanisms, a general property associated with their GOF mutant counterparts. In fact, a compromised autoinhibitory mechanism is the only biophysical property that creates a GOF SHP2 mutant enzyme as these mutants possess wild-type catalytic domains. Due to the fact that (*i*) LS-SHP2 mutations create catalytically 'impaired' enzymes, not catalytically 'dead' enzymes, (*ii*) no mutation afflicting the catalytic Cys459 residue has been documented to date (a mutation that would create a catalytically 'dead' enzyme), (*iii*) LS as well as NS

are heterozygous at the *Ptpn11* locus and no haploinsufficient alleles have ever been documented (no nonsense mutations observed) in LS patients (83, 258), (*iv*) ubiquitous expression of LS-causing SHP2 alleles (Y279C and T468M) in Drosophila results in GOF phenotypes through increased EGFR-Ras-ERK1/2 signaling (259), which are similar to those of the NS-causing SHP2 mutant transgenic flies (260) (Importantly, the residual phosphatase activity of the LS mutants is required for the GOF developmental effects), (*v*) phosphorylation of MEK1, the upstream kinase of ERK1/2, and basal pERK1/2 levels are increased in induced pluripotent stem cells from LS patients (261), and (*vi*) LS-associated Raf1 GOF alleles have been discovered, providing more direct evidence that enhanced Ras-ERK1/2 signaling might be the cause of LS as well (262), we hypothesized that LS disease pathogenesis is augmented by catalytically impaired LS-SHP2 mutant enzymes capable of engendering GOF phenotypes.

Using hydrogen-deuterium exchange mass spectrometry (H/DX-MS) we set out to provide direct evidence that the complete repertoire of catalytically impaired LS-associated SHP2 mutant enzymes (Y279C, A461T, G464A, T468M, R498L, Q506P, and Q510E) experience incompetent autoinhibitory mechanisms, thus linking these mutants to their GOF SHP2 mutant counterparts through a property that is absolutely required for GOF biological effects to be realized, *in-vivo*. The autoregulatory mechanism that governs SHP2 function relies upon an intramolecular interaction between the N-SH2 domain and the catalytic PTP domain. The interdomain region created by the N-SH2/PTP domain-interaction is well-respected to become exposed to the bulk aqueous environment upon enzymatic activation via competing pTyr-ligands or mutation. This dynamic conformational alteration can be exploited by a technique capable of labeling

the interdomain region upon alleviation of intramolecular autoinhibition. As $^{1}H_2O$ is understood to naturally populate this region during enzymatic activation, $^{2}H_2O$ (D_2O, deuterium oxide) can be effectively utilized as $^{1}H_2O$-surrogate. Natural hydrogen-deuterium exchange within proteins is capable of being 'trapped' at the amide backbone position for mass-spectrometry analysis. In deuterium buffer, amide hydrogen atoms become replaced by deuterium atoms when they are exposed to the bulk solvent and are not engaged in intramolecular interaction(s). Each deuterium atom that becomes 'trapped' accounts for a 1 Da addition to the mass of the protein that can be detected by mass spectrometry. Deuterium labeling (hydrogen exchange) over time can provide a general sense of which regions of proteins are the least protected by physical occlusion or through intramolecular interactions. With regard to the autoregulatory mechanism that governs SHP2 function, H/DX-MS is a technique capable of monitoring the magnitude by which pathogenic mutations induce catalytic activation by afflicting the natural intramolecular interaction that the N-SH2 domain makes with the PTP domain in the WT-enzyme.

As an essential and primary observation, H/DX-MS data show strong evidence in support of pathogenic SHP2 mutations afflicting the natural intramolecular interaction that the N-SH2 domain makes with the PTP domain in the WT-enzyme. As a reference for what hydrogen exchange would 'look like' if a pathogenic mutation was capable of abrogating intramolecular autoinhibition, we used the well-recognized GOF Leukemia/NS-SHP2 mutant, E76K. Through monitoring hydrogen exchange at both the native and 'regional' (peptide) levels, a comparative analysis of data derived from the E76K mutant and WT enzymes corroborated previously published structural,

biochemical, and physiological evidence that the N-SH2 domain is responsible for interacting with the catalytic PTP domain and upholding intramolecular autoinhibition. We set up this study to be a comparative analysis between the WT enzyme and LS-SHP2 pathogenic mutant counterparts. We postulated that if LS-SHP2 mutants are to be compared to their GOF SHP2 mutant counterparts, they should experience significant hydrogen exchange, relative to the WT enzyme, within regions that are in common with the GOF mutants. In addition to the physical location of hydrogen exchange, H/DX-MS methodology provides the added dimensions of magnitude and time. What did we learn about the enigmatic competency of intramolecular autoinhibition associated with the seven naturally occurring catalytically impaired LS-SHP2 mutant enzymes? Our H/DX-MS data provide strong evidence that 5 of the 7 LS-SHP2 mutants (Y279C, G464A, R498L, Q506P, and Q510E) have incompetent autoinhibitory mechanisms as they exchange significantly more hydrogen within the N-SH2/PTP domain interface region, relative to the WT enzyme. Importantly, the peptides that experience significant deuterium incorporation, relative to the WT-enzyme, are the same peptides that experience significant deuterium incorporation in the GOF mutants (E76K and D61Y). Within the detection limits of this technique, an assessment cannot be made regarding the competency of intramolecular autoinhibition associated with the A461T and T468M LS-SHP2 mutants. It is to note, that our investigation of the mechanistic and biological properties associated with the Y279C LS-SHP2 mutant also included the T468M mutant. The T468M mutant was able to loiter for longer periods of time on the multi-tyrosine phosphorylated adaptor protein Gab-1 following EGF stimulation and in turn, induce prolonged activation of the Ras/ERK pathway, relative to the SHP2-WT enzyme (data

not shown). Intriguingly, the marginal incompetency of the T468M mutant's N-SH2 domain to uphold intramolecular autoinhibition, as shown by both biochemical and H/DX-MS data, is sufficient to produce a significant biological effect, relative to the WT enzyme.

If the T468M mutant, which displays poor catalytic competency (~40-fold less than WT) as well as marginal incompetency of its N-SH2 domain to uphold intramolecular autoinhibition, is able to produce a significant GOF biological effect, why does such a disparity exist between all seven LS-SHP2 mutants with regard to the incompetency of their respective N-SH2 domains to uphold intramolecular autoinhibition? In fact, H/DX-MS data reveal that LS-SHP2 mutants with mutations that are pTyr- or P-loop-directed experience significantly less hydrogen exchange within the N-SH2/PTP interdomain region than those mutants with mutations that are 'Q' (HI)-loop directed. The LS-SHP2 R498L mutant experiences the most hydrogen exchange within the N-SH2/PTP interdomain region of all LS-SHP2 mutant enzymes. Surprisingly, the R498L mutant exchanges hydrogen to a similar magnitude as the GOF E76K mutant; a biophysical phenomenon supported by both kinetic- and inhibitor-based biochemical data. H/DX data derived from the R498L, Q506P, and Q510E mutants which possess 'Q' (HI)-loop directed mutations suggest that the catalytic 'Q'-loop is an 'Achilles' heel' with regard to mutational-disruption of N-SH2 domain-mediated intramolecular autoinhibition. It is of relevance to note that 'Q'-loop-directed mutations are not exclusive to the LS-phenotype as various 'Q'-loop-directed mutations have been associated with NS, NS/leukemia (NS/MGCLS, NS/JMML), and leukemia (JMML, ALL, AML, CMML, and MDS) phenotypes including: R498W, R501K, S502(T,P,L),

G503(R,A), M504V, T507K, and Q510K (263). Of these, we have acquired H/DX-MS data for the neoplasia-associated SHP2-T507K mutant and have documented that it, along with its 'Q'-loop-directed LS-mutant counterparts, also experiences significantly impaired N-SH2 domain-mediated intramolecular autoinhibition (Table 6, Figures 16 and 28). There is currently no documented evidence of the catalytic competency or the ability of the N-SH2 domain to uphold intramolecular autoinhibition for any of the previously mentioned mutants, save for the T507K mutant which is known to maintain WT catalytic competency, but have a compromised autoregulatory mechanism (i.e. making T507K a true GOF mutant). Of the three 'Q'-loop-directed mutations associated with LS, the Q506P mutation raises interest in that, apart from its LS-designation, it also has been reported in NS and juvenile myelomonocytic leukemia (JMML) cases (263-264). Apart from its GOF SHP2 mutant counterparts that predominately drive the pathogenesis of NS and various hematological malignancies, including JMML, Q506P is undoubtedly catalytically impaired (e.g. against *p*NPP, Q506P-CD is 42-fold less active than WT-CD, while the Q506P-FL enzyme is 3-fold less active than WT-FL due to a marked inefficiency of its N-SH2 domain to uphold intramolecular autoinhibition). Additionally, Gln (Q)-506 is the residue that coordinates the H_2O molecule that is essential to the final stage of the PTP catalytic mechanism in regenerating the catalytic active site to its original chemical orientation by potentiating the hydrolysis of the phospho-cysteine (thiophosphate) intermediate formed during substrate dephosphorylation. Due to the recurrence of the Q506P mutation in multiple pathogenic conditions that are augmented by both catalytically impaired enzymes (i.e. LS) and GOF enzymes (i.e. NS and various neoplasias), it suggests that, with regard to SHP2 function,

LS, NS, and neoplasia (hematological malignancies and solid tumors) are on a 'spectrum'. Figure 30 represents a hypothetical 'spectrum' of disease states and where the SHP2 pathogenic mutants that have been under investigation by our group would sit on this spectrum based upon their biophysical properties. The order by which these mutants sit on this spectrum is based upon their *in-vitro*-derived k_{cat}/K_m value using *p*NPP as a substrate. k_{cat}/K_m is used in enzyme kinetics to describe an enzyme catalytic efficiency, a property that depends upon, in the case of SHP2, the inherent catalytic competency as well as the ability of the substrate to be hydrolyzed (an action that is physically blocked by the N-SH2 domain's autoinhibition (D'E)-loop, but do to mutation becomes incompetent towards upholding intramolecular autoinhibiton). Q506P sits in the 'grey area' between LS and NS/neoplasia because, apart from its LS-SHP2 mutant counterparts, it retains significant catalytic activity while experiencing significantly impaired N-SH2 domain-mediated intramolecular autoinhibition. Q506P provides evidence that catalytically impaired mutants are capable of giving rise to GOF phenotypes, based upon the extent by which they are catalytically impaired and experience perturbed N-SH2 domain-mediated intramolecular autoinhibition. NS and LS are therefore 'spectrum' diseases potentiated by GOF SHP2 mutants that differ with respect to their inherent catalytic competencies, but are similar with respect to the compromised ability of the N-SH2 domain to uphold intramolecular autoinhibition.

The biochemical and H/DX-MS data presented in this investigation can only go so far in describing the biophysical properties of LS-SHP2 mutants as these experiments are designed to characterize isolated SHP2 enzymes. Due to the fact that LS-SHP2 mutants display a surprisingly wide range of compromised catalytic abilities and

autoregulatory mechanisms, it would be interesting to find out the different 'LS disease states' that each mutant potentiates and be able to trace these phenotypes back to each mutant's inherent biophysical properties. Additionally, we have to keep in mind that LS-SHP2 mutant catalytic PTP domains are variants (mutants) of the WT PTP domain and thus have the potential to have altered substrate specificity. Investigation is underway to understand the nature by which each of the seven documented LS-SHP2 mutants imparts GOF effects towards Ras/ERK signaling.

TABLES

Table 1: Vector·HEK293 Phosphoproteomic Dataset

Protein ID (GI number)	Protein Name (Gene symbol)	pTyr-peptide (q-value; Mascot ion score; Sequest XCorr)	PRL3/Vector Quant. Ratio (q-value; Mascot ion score; Sequest XCorr)	Repro-duced
		Cellular Communication and Signal Transduction		
Adaptor/Scaffold				
NP_066943 (119943106)	Disks Large Homolog 3 (DLG3)	R.RDNEVDGQD**y673**HFVVSR	4.29 (0; 31; 4.0)	No
NP_003740 (38683860)	Insulin Receptor Substrate 2 (IRS2)	R.SSSSNLGADDG**y653**MPMTPGAALAGSGSGS CR (0; 34)	0.015 (0; 65; 4.28)	Yes
		R.SDD**y675**MPMSPASVSAPK (0; 32; 3.52)	0.01 (0; 60; 3.46); Not in PRL3	Yes
		R.SYKAPYTCGGDSDQ**y823**VLMSSPVGR (0; 34; 4.51)	0.01 (0; 41; 3.97); Not in PRL3	Yes
		K.APYTCGGDSDQ**y823**VLMSSPVGR	0.01 (0; 73; 4.51); Not in PRL3	No
NP_006268 (194294521)	Intersectin-2 (ITSN2)	R.EEPEAL**y968**AAVNK (0; 29; 2.87)		No
NP_071919 (38570142)	MAGUK p55 Subfamily Member 5 (MPP5)	R.V**y243**ESIGQYGGETVK	0.01 (0; 33; 3.1); Not in PRL3	No
NP_003944 (4506357)	Myelin Protein Zero-like 1 (MPZL1)	K.SESVV**y263**ADIR (0; 31; 2.13)	0.213 (0; 44; 2.74)	Yes
		K.INKSESVV**y263**ADIR	3.80 (0; 60; 2.93)	No
NP_060910 (63054864)	Phosphoprotein Associated with Glycosphingolipid-Enriched Microdomains 1 (PAG1, CBP)	R.SVDGDQGLGMEGP**y163**EVLK (0; 59; 4.53)	0.01 (0; 59; 4.2); Not in PRL3	Yes
		K.AEFAE**y227**ASVDR (0; 58; 2.28)	0.01 (0; 66; 2.68); Not in PRL3	Yes
		K.SREEDPTLTEEEISAM**y317**SSVNKPGQLVNK	0.01 (0; 88; 4.99); Not in PRL3	No
		K.SGQSLTVPEST**y341**TSIQGDPQR (0; 73; 4.41)	0.01 (0; 81; 4.61); Not in PRL3	Yes
		R.SPSSCNDL**y359**ATVK (0.029; 19; 2.8)	0.01 (0; 64; 3.91); Not in PRL3	Yes
		K.END**y417**ESISDLQQGR (0; 67; 4.0)	0.01 (0; 68; 3.61); Not in PRL3	Yes
NP_003019 (106879210)	SH2 Domain-containing Adaptor Protein B (SHB)	K.VTIADD**y246**SDPFDAK (0; 34; 2.92)	100 (0; 54; 3.59); Not in Vector	Yes
NP_892113 (194239662)	SHC-Transforming Protein 1 (SHC1)	R.ELFDDPS**y427**VNVQNLDK	0.01 (0; 75, 3.82); Not in PRL3	No
Adhesion; Adaptor/Scaffold				
NP_002850 (170932516)	Paxillin (PXN)	R.VGEEEHV**y118**SFPNKQK (0; 34; 2.67)		Yes
NP_006280 (223029410)	Talin-1 (TLN1)	K.TMQFEPSTMV**y26**DACR	0.629 (0; 35; 2.46)	No
Cell Cycle Control Protein/Kinase				
NP_001777 (4502709)	Cyclin-Dependent Kinase 1 (CDK1)	K.IEKIGEGT**y15**GVVYK (0; 32; 3.67)	0.574 (0; 51; 2.83)	Yes
		K.IEKIGEGT**y15**GVVYKGR (0; 32; 4.1)		Yes
		K.IGEGT**y15**GVVYKGR (0; 45; 3.91)	7.30 (0; 60; 3.46)	Yes

		K.IEKIGEGT**y15**GVV**y19**K	0.775 (0.015; 2.31)	No
NP_001789 (16936528)	Cyclin-Dependent Kinase 2 (CDK2)	K.VEKIGEGT**y15**GVVYKAR (0; 53; 4.67)	0.01 (0; 2.72); Not in PRL3	Yes
		K.VEKIGEGT**y15**GVVYK (0; 50; 3.36)	0.443 (0; 70; 3.22)	Yes
		K.IGEGT**y15**GVVYKAR (0; 36; 3.61)	0.01 (0; 51; 3.69); Not in PRL3	Yes
		K.IGEGT**y15**GVVYK (0; 35; 3.17)		Yes
NP_001249 (4557439)	Cyclin-Dependent Kinase 3 (CDK3)	K.VEKIGEGT**y15**GVVYK	0.443 (0; 70; 3.22)	No
NP_004926 (4826675)	Cyclin-Dependent Kinase 5 (CDK5)	K.IGEGT**y15**GTVFK (0.0135; 22; 2.16)	0.331 (0; 26; 1.77)	No
Protein Kinase				
NP_005772 (56549666)	Activated CDC42 Kinase 1 (ACK1; TNK2)	K.**y827**ATPQVIQAPGPR	3.82 (0; 39; 2.59)	No
NP_001387 (18765758)	Dual Specificity Tyrosine-Phosphorylation-Regulated Kinase 1A (DYRK1A)	R.IYQ**y321**IQSR (0; 28; 1.95)	0.290 (0; 39; 2.31)	Yes
NP_002084 (21361340)	Glycogen Synthase Kinase-3 beta (GSK3B)	K.QLVRGEPNVS**y216**ICSR	0.799 (0; 32; 2.62)	Yes
		K.GEPNVS**y216**ICSR (0; 54; 3.0)	0.791 (0; 50; 2.51)	Yes
NP_073577 (164420685)	Homeodomain-Interacting Protein Kinase 2 (HIPK2)	K.AVCST**y361**LQSR (0; 31; 1.39)		Yes
NP_002736 (66932916)	Mitogen-Activated Protein Kinase 1 (MAPK1, ERK2)	R.VADPDHDHTGFLTE**y187**VATR (0; 31; 4.17)	5.32 (0; 54; 4.15)	Yes
NP_002737 (91718899)	Mitogen-Activated Protein Kinase 3 (MAPK3, ERK1)	R.IADPEHDHTGFLTE**y204**VATR (0; 27; 4.34)	3.50 (0; 65; 3.95)	Yes
NP_002960 (48255970)	Mitogen-Activated Protein Kinase 12 (MAPK12, ERK3)	R.QADSEMTG**y185**VVTR (0.012; 34)	0.01 (0; 39; 1.76); Not in PRL3	Yes
NP_001306 (4503069)	Mitogen-Activated Protein Kinase 14 (MAPK14, p38 Alpha)	R.HTDDEMTG**y182**VATR (0; 56; 3.67)	4.37 (0; 64; 3.35)	Yes
NP_003322 (187608615)	Non-Receptor Tyrosine-Protein Kinase TYK2 (TYK2)	R.LLAQAEGEPC**y292**IR (0; 46; 3.96)	0.01 (0; 42; 2.98); Not in PRL3	Yes
NP_003904 (89276756)	Serine/Threonine-Protein Kinase PRP4 Homolog (PRPF4B)	K.LCDFGSASHVADNDITP**y849**LVSR (0; 58; 5.68)	0.543 (0; 60; 4.95)	Yes
NP_005408 (4885609), NP_002028 (4503823), NP_005424 (4885661)	Tyrosine-Protein Kinase Src, Fyn, Yes (SRC, FYN, YES1)	R.LIEDNE**y419,420,426**TAR (0; 45; 2.94)	0.01 (0; 54; 3.20); Not in PRL3	Yes
NP_002028 (4503823), NP_005424 (4885661)	Tyrosine-Protein Kinase Fyn, Yes (FYN, YES1)	R.KLDNGG**y213,222**YITTR (0; 2.4)	100 (0; 34; 2.12); Not in Vector	No
		R.KLDNGGY**y214,223**ITTR (0; 2.4)		No
NP_002341 (4505055)	Tyrosine-Protein Kinase Lyn (LYN)	R.VIEDNE**y397**TAR (0; 33)		No
		R.VENCPDEL**y473**DIMK	0.01 (0; 36; 1.59); Not in PRL3	No
NP_001167638 (293332585)	Tyrosine-Protein Kinase Syk (SYK)	R.QESTVSFNP**y323**EPELAPWAADKGPQR	0.01 (0.012; 2.36); Not in PRL3	No
NP_004422 (32967311)	Ephrin type-A Receptor 2 (EPHA2)	R.VLEDDPEAT**y772**TTSGGK (0; 35; 2.72)		No

NP_005224 (21361241)	Ephrin type-A Receptor 3 (EPHA3)	R.VLEDDPEAA**y779**TTR (0; 44; 3.04)		Yes
NP_004430 (221625401)	Ephrin type-A Receptor 5 (EPHA5)	R.VLEDDPEAA**y833**TTR	0.01 (0; 65; 3.04); Not in PRL3	No
NP_004431 (4758282)	Ephrin type-A Receptor 7 (EPHA7)	R.VIEDDPEAV**y791**TTTGGK (0; 49; 3.54)		No
Protein Phosphatase				
NP_002825 (33356177)	Protein Tyrosine Phosphatase Non-Receptor Type 11 (PTPN11, SHP2)	K.IQNTGD**y62**YDLYGGEK (0; 83; 4.8)	0.01 (0; 78; 3.49); Not in PRL3	Yes
		K.IQNTGDY**y63**DLYGGEK (0; 83)	0.01 (0; 78); Not in PRL3	Yes
NP_002827 (4506303)	Receptor-type Tyrosine-Protein Phosphatase alpha (PTPRA)	K.VVQEYIDAFSD**y798**ANFK	2.03 (0; 100; 4.97)	No
Lipase				
NP_002651 (33598948)	1-Phosphatidylinositol-4,5-bisphosphate Phosphodiesterase Gamma-1 (PLCG1)	K.IGTAEPD**y771**GALYEGR	6.17 (0; 16; 2.70)	No
		R.NPGF**y783**VEANPMPTFK	20 (0; 36; 3.94)	No
		R.**y1253**QQPFEDFR (0; 25)	5.81 (0; 31; 2.18)	Yes
G-Protein: GTPase; GTPase Activating Protein (GAP); Guanine Nucleotide Exchange Factor (GEF); Small GTPase Effector Protein; G-Protein-Coupled Receptor				
NP_071319 (40217831)	G-Protein Coupled Receptor family C group 5 member C (GPRC5C)	K.VPSEGA**y432**DIILPR (0; 58; 3.1)	0.01 (0; 58; 3.04); Not in PRL3	Yes
NP_001028740 (75750480)	Mitochondrial Rho GTPase 1 (RHOT1)	K.SYYAINTVYV**y465**GQEK	0.01 (0; 64; 4.34); Not in PRL3	No
NP_004482 (150417981)	Rho GTPase-Activating Protein 35 (ARHGAP35)	R.NEEENI**y1105**SVPHDSTQGK (0; 50; 4.49)	0.794 (0; 55; 4.24)	Yes
Signaling Other				
NP_001002858 (50845388)	Annexin A2 (ANXA2)	K.LSLEGDHSTPPSA**y42**GSVK (0; 52; 3.66)	0.039 (0; 51; 4.16)	Yes
NP_001171725 (296317244)	Extended Synaptotagamin-1 (ESYT1)	K.HLSP**y832**ATLTVGDSSHK	0.01 (0; 2.13); Not in PRL3	No
NP_002204 (20127446)	Integrin Beta-5 (ITGB5)	R.YEMASNPL**y774**R	14.93 (0; 32; 1.62)	No
NP_006658 (5729875)	Membrane-associated Progesterone Receptor component 1 (PGRMC1)	K.LLKEGEEPTV**y180**SDEEEPKDESAR (0.029; 3.28)		
NP_005018 (4826908)	Phosphatidylinositol 3-Kinase Regulatory Subunit beta (PIK3R2, p85)	R.EYDGL**y464**EEYTR	0.632 (0; 29; 2.78)	No
NP_004595 (20149560)	Syntaxin-4 (STX4)	K.NILSSAD**y251**VER	14.08 (0; 37; 2.54)	No
Energy Metabolism				
Dehydrogenase; Hydratase; Methyltransferase				
NP_001966 (5803011)	Gamma-Enolase (ENO2)	R.AAVPSGASTGI**y44**EALELR	1.18 (0; 66; 3.09)	No

NP_005403 (19923315)	Serine Hydroxymethyltransferase (SHMT2)	R.**y105**YGGAEVVDEIELLCQRR	0.01 (0.025; 2.23); Not in PRL3	No
		R.Y**y106**GGAEVVDEIELLCQRR	0.01 (0.026; 2.2); Not in PRL3	No
		Protein Synthesis, Processing and Protein Fate		
NP_001393 (4503471)	Elongation Factor 1-alpha 1 (EEF1A1)	R.EHALLA**y141**TLGVK	0.626 (0; 23; 2.92)	No
NP_001021 (4506711)	40S Ribosomal Protein S27 (RPS27)	R.LVQSPNS**y31**FMDVK	2.48 (0; 41; 2.84)	No
NP_001035998 (110227619)	MYC-induced Nuclear Antigen 1 (MINA)	K.DFIMHRLPP**y342**SAGDGAELSTPGGK (0; 1.97)		
NP_006214 (38679892)	Peptidyl-Prolyl cis-trans Isomerase NIMA-Interacting 4 (PIN4)	K.FG**y147**HIIMVEGR	16.67 (0.001; 34)	No
		Nucleic Acid Synthesis and Processing		
DNA Binding Protein				
NP_004517 (33356547)	DNA Replication Licensing Factor MCM2 (MCM2)	R.GLL**y137**DSDEEDEERPAR (0; 2.66)		No
Transcription Factor; Transcription Regulatory Protein				
NP_001156752 (253970456)	HIV Tat-Specific Factor 1 (HTATSF1)	K.VFDDESDEKEDEE**y650**ADEK (0; 2.77)		No
NP_644805 (21618340)	Signal Transducer and Activator of Transcription 3 (STAT3)	K.YCRPESQEHPEADPGSAAP**y705**LK (0; 2.24)	5.65 (0.046; 10)	Yes
		Storage and Transport		
NP_000714 (40804468)	Voltage-dependent L-type Calcium Channel Subunit beta-1 (CACNB1)	K.TSMSRGP**y12**PPSQEIPMEVFDPSPQGK**y31**SK (0.037; 1.56)		No
		Cellular Organization		
Structural Protein				
NP_060282 (8923390)	Coiled-Coil-Helix-Coiled-Coil-Helix Domain-containing Protein 3, Mitochondrial (CHCHD3)	R.YSGA**y53**GASVSDEELK	0.01 (0; 39; 2.92); Not in PRL3	No
		Unclassified		
NP_001157787 (256222280)	Ankyrin Repeat Domain-containing Protein 36A (ANKRD36)	K.KKANVNAID**y195**LGR (0.038; 2.3)		No
NP_056526 (163914392)	Glioma Tumor Suppressor Candidate Region Gene 1 (GLTSCR1)	R.LLPYHVYQGALPSPSD**y1130**HK (0; 2.25)		No
NP_004330 (4757886)	Pituitary Tumor-Transforming Gene 1 Protein-Interacting Protein (PTTG1IP)	K.YGLFKEENP**y174**AR	0.01 (0; 37; 2.4); Not in PRL3	No

NP_060844 (40254893)	Transmembrane Protein 106B (TMEM106B)	R.NGDVSQFP**y50**VEFTGR	1.90 (0; 43; 3.19)	No
NP_945352 (259013211)	UPF0574 Protein C9orf169 (C9orf169)	K.NP**y12**AHISIPR	13.89 (0; 16; 2.09)	No

Table 1: PRL3·HEK293 Phosphoproteomic Dataset

Protein ID (GI number)	Protein Name (Gene symbol)	pTyr-peptide (q-value; Mascot ion score; Sequest XCorr)	PRL3/Vector Quant. Ratio (q-value; Mascot ion score; Sequest XCorr)	Repro-duced
		Cellular Communication and Signal Transduction		
Adaptor/Scaffold				
NP_003572 (52630423)	Cytoplasmic Protein NCK2 (NCK2; GRB4)	R.TG**y50**VPSNYVER (0; 32; 1.76)	17.24 (0; 41; 2.34)	Yes
NP_001091894 (148539628)	Disks Large Homolog 1 (DLG1)	K.NTSDFV**y399**LK	100 (0; 1.98); Not in Vector	No
NP_066943 (119943106)	Disks Large Homolog 3 (DLG3)	R.DNEVDGQD**y673**HFVVSR (0; 38; 3.6)		Yes
		R.RDNEVDGQD**y673**HFVVSR	4.29 (0; 31; 2.57)	Yes
NP_004703 (4758528)	Hepatocyte Growth Factor-Regulated Tyrosine Kinase Substrate (HGS)	K.YKVVQDT**y132**QIMK	100 (0; 50; 3.47); Not in Vector	No
NP_060699 (224451116)	MHD Domain-containing Death-inducing Protein (MUDENG)	R.KLISSD**y472**YIWNSKAPAPVT**y485**GSLLL (0.033; 1.9)		No
NP_003944 (4506357)	Myelin Protein Zero-like Protein 1 (MPZL1)	K.SESVV**y263**ADIR	0.343 (0; 58; 2.94)	No
		K.INKSESVV**y263**ADIR (0; 52, 3.57)	3.80 (0; 83; 4.09)	Yes
NP_003932 (51702526)	Neural Wiskott-Aldrich Syndrome Protein (WASL, N-WASP)	K.VI**y256**DFIEK (0; 26; 1.74)	9.17 (0; 27; 2.2)	Yes
NP_060377 (8923579)	Regulator Complex Protein LAMTOR1 (LAMTOR1)	K.ALNGAEPN**y40**HSLPSAR (0; 2.87)		Yes
NP_003019 (106879210)	SH2 Domain-containing Adaptor Protein B (SHB)	K.VTIADD**y246**SDPFDAK (0; 30; 3.34)	100 (0; 54; 3.59); Not in Vector	Yes
Adhesion; Adaptor/Scaffold				
NP_001032409 (116805788)	Cytoplasmic FMR1-Interacting Protein 2 (CYFIP2)	R.AVGPSSTQL**y559**MVR (0; 24; 2.82)		No
NP_060710 (166295173)	Kin of IRRE-like Protein 1 (KIRREL)	K.AI**y572**SSFKDDVDLK (0; 26; 2.97)		No
		K.DPTNG**y605**YNVR (0; 21)		No
		R.CDTIDTREEYEMKDPTNG**y605**YNVR	100 (0; 64; 4.06); Not in Vector	No
		R.EEYEMKDPTNG**y605**YNVR (0; 37; 2.85)		Yes
		R.EEYEMKDPTNGY**y606**NVR (0; 37; 2.91)		Yes
		R.AVL**y622**ADYR	100 (0; 15); Not in Vector	No

		R.LSHSSG**y647**AQLNTYSR (0; 24)		No
		R.LSHSSGYAQLNT**y653**SR (0; 32; 3.28)		No
		R.TP**y721**EAYDPIGK (0; 43; 3.04)	100 (0; 48; 2.73); Not in Vector	Yes
		R.TPYEA**y724**DPIGK (0; 43; 2.48)	100 (0; 40; 2.85); Not in Vector	Yes
NP_062565 (21361831)	Partitioning Defective 3 (PARD3)	R.ERD**y1080**AEIQDFHR	22.22 (0.002; 1.6)	No
NP_003619 (53829374)	Plakophilin- 4 (PKP4)	K.STTN**y1168**VDFYSTK (0; 43)	100 (0; 46; 2.69); Not in Vector	Yes
NP_057358 (20149626)	Pleckstrin Homology Domain-containing Family O Member 1 (PLEKHO1)	R.QTTPHSQ**y404**R (0; 1.46)		
NP_065910 (203098098)	Protein Shroom 3 (SHROOM3)	R.EARASANGQG**y344**DKWSNIPR (0; 2.45)		
NP_002990 (38201675)	Syndecan-4 (SDC4)	K.KAPTNEF**y197**A	100 (0; 26; 1.72); Not in Vector	No
NP_006280 (223029410)	Talin-1 (TLN1)	K.ALD**y70**YMLR (0; 39; 2.66)	13.51 (0; 29; 2.11)	Yes
		K.ALDY**y71**MLR (0; 30; 1.8)	13.51 (0.002; 1.99)	Yes
Cell Cycle Control Protein/Kinase				
NP_001777 (4502709)	Cyclin-Dependent Kinase 1 (CDK1)	K.IEKIGEGT**y15**GVVYK (0; 45; 3.71)	0.574 (0; 70; 3.24)	Yes
		K.IEKIGEGT**y15**GVVYKGR (0; 55; 4.0)	4.78 (0; 1.69)	Yes
		K.IGEGT**y15**GVVYKGR (0; 51; 3.44)	7.30 (0; 55; 3.49)	Yes
		K.IEKIGEGT**y15**GVV**y19**K	0.8 (0.002; 2.20)	No
		K.IGEGTYGVV**y19**K (0.036; 1.96)		No
NP_001789 (16936528)	Cyclin-Dependent Kinase 2 (CDK2)	K.VEKIGEGT**y15**GVVYK	0.443 (0; 67; 2.84)	Yes
		K.IGEGT**y15**GVVYK	1.09 (0; 47; 2.94)	Yes
NP_001249 (4557439)	Cyclin-Dependent Kinase 3 (CDK3)	K.VEKIGEGT**y15**GVVYK (0; 54; 2.18)	0.443 (0; 67; 2.84)	Yes
		K.IGEGT**y15**GVVYK (0; 34; 3.16)	1.09 (0; 47; 2.94)	Yes
		K.IGEGT**y15**GVVYKAK (0; 45; 3.94)	100 (0; 58; 4.18); Not in Vector	Yes
		K.IGEGTYGVV**y19**KAK (0.036; 1.96)		No
NP_004926 (4826675)	Cyclin-Dependent Kinase 5 (CDK5)	K.IGEGT**y15**GTVFK (0; 2.13)	0.331 (0; 42; 2.18)	Yes
NP_006192 (5453860)	Cyclin-Dependent Kinase 16 (CDK16)	K.LGEGT**y176**ATVYK	1.08 (0.002; 1.74)	No
NP_002586 (37595545)	Cyclin-Dependent Kinase 17 (CDK17)	K.LGEGT**y203**ATVYKGR (0; 3.6)		No
		K.LGEGTYATV**y207**K (0; 24)		No
Protein Kinase				
NP_005772 (56549666)	Activated CDC42 Kinase 1 (ACK1; TNK2)	K.**y827**ATPQVIQAPGPR (0; 37; 2.8)	3.82 (0; 33; 3.82)	Yes
NP_001195 (15451916)	Bone Morphogenic Protein Receptor Type-2 (BMPR2)	K.IGPYPD**y546**SSSSYIEDSIHHTDSIVK	100 (0.004; 2.88); Not in Vector	No
NP_001014796 (62420886)	Discoidin Domain-containing Receptor 2 (DDR2)	R.IFPLRPD**y481**QEPSR (0; 28; 2.7)	100 (0; 27; 2.19); Not in Vector	Yes

NP_001387 (18765758)	Dual-Specificity Tyrosine-Phosphorylation-Regulated Kinase 1A (DYRK1A)	R.IYQ**y321**IQSR (0; 27; 2.01)	0.290 (0; 38; 2.40)	Yes
NP_958439 (41327732)	Epidermal Growth Factor Receptor, isoform b (EGFR)	K.TCPAGVMGENNTLVWKYADAGHVCHLCH PNCT**y626**GS (0; 2.9)		No
NP_722560 (24476013)	Focal Adhesion Kinase 1 (PTK2, FAK)	R.THAVSVSETDD**y397**AEIIDEEDTYTMPSTR (0; 34; 3.84)	11.76 (0; 56; 3.42)	Yes
		R.**y570**MEDSTYYK	100 (0; 27; 2.17); Not in Vector	No
NP_002084 (21361340)	Glycogen Synthase Kinase-3 beta (GSK3B)	K.QLVRGEPNVS**y216**ICSR (0; 31; 3.59)	0.799 (0; 45; 3.64)	Yes
		K.GEPNVS**y216**ICSR	0.792 (0; 48; 2.76)	Yes
NP_005725 (114796624)	Homeodomain-Interacting Protein Kinase 3 (HIPK3)	K.TVCST**y359**LQSR (0; 27)		No
NP_002736 (66932916)	Mitogen-Activated Protein Kinase 1 (MAPK1, ERK2)	R.VADPDHDHTGFLTE**y187**VATR (0; 58; 5.68)	5.32 (0; 77; 4.67)	Yes
NP_002737 (91718899)	Mitogen-Activated Protein Kinase 3 (MAPK3, ERK1)	R.IADPEHDHTGFLTE**y204**VATR (0; 53; 4.92)	3.50 (0; 80; 4.96)	Yes
NP_001306 (4503069)	Mitogen-Activated Protein Kinase 14 (MAPK14, p38 Alpha)	R.HTDDEMTG**y182**VATR (0; 60; 3.43)	4.37 (0; 73; 4.19)	Yes
NP_002741 (4506095)	Mitogen-Activated Protein Kinase 8 Isoform JNK1 Alpha 1 (MAPK8, JNK1)	R.TAGTSFMMTP**y185**VVTR (0; 26; 3.25)	100 (0; 43; 3.25); Not in Vector	Yes
NP_004825 (22035602)	Mitogen-Activated Protein Kinase Kinase Kinase Kinase 4 (MAP4K4)	R.SGGSSQV**y1153**FMTLGR (0; 3.44)		Yes
NP_006197 (5453870)	Platelet-Derived Growth Factor Receptor alpha (PDGFRA)	K.VVEGTA**y613**GLSR	100 (0; 25; 1.85); Not in Vector	No
		R.S**y720**VILSFENNGDYMDMK	100 (0; 31; 3.59); Not in Vector	No
		R.SYVILSFENNGD**y731**MDMK	100 (0; 44; 3.88); Not in Vector	No
		K.QADTTQ**y742**VPMLER (0; 52; 3.03)	18.87 (0; 60; 2.98)	Yes
		R.VDSDNA**y988**IGVTYK (0; 37; 2.98)		No
NP_002600 (4505683)	Platelet-Derived Growth Factor Receptor beta (PDGFRB)	K.GGPIYIITE**y683**CR (0; 49; 2.86)	100 (0; 40; 2.97); Not in Vector	Yes
		R.YGDLVD**y692**LHR (0; 27)	5.92 (0; 2.81)	Yes
		R.DIMRDSN**y857**ISK	100 (0; 32; 2.54); Not in Vector	No
		K.**y970**QQVDEEFLR (0; 35; 2.43)		No
NP_079052 (148368962)	Pseudopodium-Enriched Atypical Kinase 1 (PEAK1)	R.**y531**QEVWTSSTSPR (0; 39; 2.37)		Yes
NP_003904 (89276756)	Serine/Threonine-Protein Kinase PRP4 Homolog (PRPF4B)	K.LCDFGSASHVADNDITP**y849**LVSR (0; 54; 5.5)	0.543 (0; 86; 4.93)	Yes
NP_005408 (4885609), NP_002028 (4503823), NP_005424 (4885661)	Tyrosine-Protein Kinase Src, Fyn, Yes (SRC, FYN, YES1)	R.LIEDNE**y419,420,426**TAR (0; 2.36)	0.01 (0; 54; 3.20); Not in PRL3	Yes

NP_002028 (4503823), NP_005424 (4885661)	Tyrosine-Protein Kinase FYN, YES (FYN, YES1)	R.KLDNGG**y213,222**YITTR	100 (0.012; 23; 2.19); Not in Vector	Yes
		K.LDNGG**y213,222**YITTR (0; 27; 2.11)		No
		K.LDNGGY**y214,223**ITTR (0; 27)		
NP_002218 (102469034)	Tyrosine-Protein Kinase JAK1 (JAK1)	K.AIETDKE**y1034**YTVK (0; 29; 3.08)		No
NP_004422 (32967311)	Ephrin type-A Receptor 2 (EPHA2)	K.T**y588**VDPHTYEDPNQAVLK (0; 53; 3.78)	100 (0; 53; 3.43); Not in Vector	Yes
		K.TYVDPHT**y594**EDPNQAVLK (0; 42; 3.92)	100 (0; 66; 4.03); Not in Vector	Yes
		R.VLEDDPEAT**y772**TTSGGKIPIR (0; 55; 3.71)	76.92 (0; 100; 4.44)	Yes
		R.IA**y960**SLLGLK (0.035; 16)		No
NP_004434 (17975768)	Ephrin type-B Receptor 3 (EPHB3)	R.FLEDDPSDPT**y792**TSSLGGK (0; 59; 4.0)		Yes
NP_004435 (32528301)	Ephrin type-B Receptor 4 (EPHB4)	R.FLEENSSDPT**y774**TSSLGGK (0; 82; 4.65)	100 (0; 76; 4.11); Not in Vector	Yes
Protein Phosphatase				
NP_002825 (33356177)	Protein Tyrosine Phosphatase Non-Receptor Type 11 (PTPN11, SHP2)	K.IQNTGD**y62**YDLYGGEK (0; 65; 4.02)		Yes
		K.IQNTGDY**y63**DLYGGEK (0; 65; 3.82)		Yes
		R.**y279**KNILPFDHTR	100 (0; 42; 2.89); Not in Vector	No
		R.KGHE**y542**TNIK	100 (0.013; 32); Not in Vector	No
NP_002827 (4506303)	Receptor-type Tyrosine-Protein Phosphatase alpha (PTPRA)	R.**y271**VNILPYDHSR (0; 43; 2.49)		Yes
		K.VVQEYIDAFSD**y798**ANFK	2.03 (0; 83; 4.46)	No
Lipase				
NP_002651 (33598948)	1-Phosphatidylinositol-4,5-bisphosphate Phosphodiesterase Gamma-1 (PLCG1)	K.IGTAEPD**y771**GALYEGR (0; 37; 2.95)	100 (0; 49; 3.28); Not in Vector	Yes
		R.NPGF**y783**VEANPMPTFK (0; 58; 4.63)	10.42 (0; 100, 3.91)	Yes
		R.AC**y977**RDMSSFPETK	100 (0; 30; 2.67); Not in Vector	No
		K.**y1253**QQPFEDFR (0; 38; 2.01)	100 (0; 40; 2.52); Not in Vector	Yes
NP_001026866 (72534684)	Phospholipase D4 (PLD4)	K.LM**y7**QELK	100 (0.026; 2.33); Not in Vector	No
G-Protein: GTPase; GTPase Activating Protein (GAP); Guanine Nucleotide Exchange Factor (GEF); Small GTPase Effector Protein				
NP_212132 (54112429)	Dedicator of Cytokenisis Protein 7 (DOCK7)	K.IDISPAPENPH**y522**CLTPELLQVK (0; 3.02)	100 (0; 3.08); Not in Vector	Yes
NP_037428 (164519122)	G-protein-Signaling Modulator 2 (GPSM2)	R.AL**y146**NLGNVYHAK (0; 23; 2.84)		Yes
NP_002515 (4893)	GTPase N-Ras (NRAS)	R.QGVEDAF**y157**TLVR (0; 36; 2.34)	21.74 (0; 37; 2.39)	Yes
NP_004976 (15718761)	GTPase K-Ras Isoform B (KRAS)	R.QGVDDAF**y157**TLVR (0; 41; 2.3)	100 (0; 27; 2.48); Not in Vector	Yes

NP_006316 (5453555)	GTP-Binding Nuclear Protein Ran (RAN)	K.NLQ**y146**YDISAK (0.036; 2.15)	100 (0; 38; 2.24); Not in Vector	Yes
		K.NLQY**y147**DISAK	100 (0.002; 2.2); Not in Vector	No
NP_031394 (38201692)	Ras GTPase-Activating Protein 3 (RASA3)	K.SLCPFYGEDF**y66**CEIPR	100 (0; 60; 3.56); Not in Vector	No
NP_004654 (4758984)	Ras-Related Protein Rab-11A (RAB11A)	R.DDE**y8**DYLFK (0; 21; 2.49)		No
NP_112243 (13569962)	Ras-Related Protein Rab-1B (RAB1B)	R.FADDT**y33**TESYISTIGVDFK	100 (0; 26); Not in Vector	No
		R.FADDTYTE**Sy37**ISTIGVDFK	71.43 (0; 106; 4.55)	No
NP_002856 (4506365)	Ras-Related Protein Rab-2A (RAB2A)	A**y3**AYLFK (0; 40)		No
NP_004482 (150417981)	Rho GTPase-Activating Protein 35 (ARHGAP35)	R.NEEENI**y1105**SVPHDSTQGK (0; 28; 3.37)	0.794 (0; 66; 4.34)	Yes
NP_689645 (221307575)	Rho GTPase-Activating protein 42 (ARHGAP42)	K.EPI**y376**TLPAIISK (0.042; 1.81)		No
NP_056342 (167614488)	TBC1 Domain Family Member 10B (TBC1D10B)	R.SCQGM**y577**ETMEQLR	100 (0; 54; 2.77); Not in Vector	No
NP_776257 (27777675)	Vomeronasal type-1 receptor 5 (VN1R5)	R.VHGPLKRLHGD**y241**FIQTIR (0.014; 2.17)		No
Signaling Other				
NP_001633 (4502147)	Amyloid-like Protein 2 (APLP2)	K.MQNHGYENPT**y755**KYLEQMQI	100 (0; 3.41); Not in Vector	No
		K.MQNHGYENPTYK**y757**LEQMQI	100 (0; 3.37); Not in Vector	No
NP_001002858 (50845388)	Annexin A2 (ANXA2)	K.LSLEGDHSTPPSA**y42**GSVK (0; 44; 4.22)		Yes
		R.AEDGSVID**y206**ELIDQDAR (0; 63; 4.27)	9.62 (0; 82; 4.5)	Yes
		K.SL**y334**YYIQQDTK (0; 67; 3.3)	100 (0; 65; 2.43); Not in Vector	Yes
		K.SL**y334**YYIQQDTKGDYQK	100 (0; 65; 4.33); Not in Vector	Yes
		K.SLY**y335**YIQQDTK (0; 32; 3.3)		Yes
		K.SLY**y335**YIQQDTKGDYQK	100 (0; 62; 4.48); Not in Vector	Yes
		K.SLYY**y336**IQQDTK (0; 49; 3.23)		Yes
		K.SLYY**y336**IQQDTKGDYQK	100 (0; 47; 4.36); Not in Vector	Yes
NP_001145 (4502107)	Annexin A5 (ANXA5)	R.LYDA**y94**ELK (0; 25; 2.02)	6.33 (0.001; 32; 1.62)	Yes
NP_005175 (58218968)	Calmodulin (CALM3)	R.VFDKDGNG**y100**ISAAELR (0; 69; 4.3)	100 (0; 98; 4.46); Not in Vector	Yes
NP_001744 (15451856)	Caveolin-1 (CAV1)	K.YVDSEGHL**y14**TVPIR (0; 25; 3.16)		Yes
NP_003807 (4501915)	Disintegrin and Metalloproteinase Domain-Containing Protein 9 (ADAM9)	R.EEMILLAN**y245**LDSSYIMLNIR (0.048; 2.52)		No
NP_002202 (19743813)	Integrin Beta-1 (ITGB1)	K.WDTGENPI**y783**K	100 (0; 37; 2.55); Not in Vector	No
NP_002204 (20127446)	Integrin Beta-5 (ITGB5)	R.YEMASNPL**y774**R (0; 27; 2.0)	14.93 (0; 54; 2.79)	Yes
NP_000518 (4504975)	Low-Density Lipoprotein Receptor (LDLR)	K.NINSINFDNPV**y828**QK (0; 72; 3.42)		No

NP_957718 (41822562)	Neuropilin-2, isoform 1 (NRP2)	R.SCTTLEN**y908**NFELYDGLK	100 (0; 77; 3.82); Not in Vector	No
NP_957719 (41872567)	Neuropilin-2, isoform 5 (NRP2)	K.TSH**y877**TNGAPLAVEPTLTIK	100 (0.012; 1.93); Not in Vector	No
NP_852664 (32455248)	Phosphatidylinositol 3-Kinase Regulatory Subunit alpha (PIK3R1, p85)	R.GDFPGT**y73**VEYIGR (0; 40; 2.26)		No
		R.GLECSTL**y150**R	100 (0.021; 2.13); Not in Vector	No
		R.DQ**y580**LMWLTQK (0; 31; 2.06)	31.25 (0; 56; 3.02)	Yes
NP_005018 (4826908)	Phosphatidylinositol 3-Kinase Regulatory Subunit beta (PIK3R2, p85)	R.EYDGL**y464**EEYTR	0.632 (0; 28; 1.6)	No
NP_115618 (262118282)	Plexin-A1 (PLXNA1)	K.QTSA**y1608**NISNSSTFTK (0; 31)	13.70 (0; 56; 2.36)	Yes
NP_004595 (20149560)	Syntaxin-4 (STX4)	K.NILSSAD**y251**VER (0; 48; 3.37)	14.08 (0; 59; 3.18)	Yes
Energy Metabolism				
Hydrolase; Dehydrogenase; Synthetase				
NP_000687 (115387104)	Aldehyde Dehydrogenase (ALDH9A1)	R.VTIE**y500**YSQLK (0.037; 2.1)		No
NP_061820 (11128019)	Cytochrome C (CYCS)	R.ADLIA**y98**LKK (0.006; 1.64)		No
NP_001966 (5803011)	Gamma-Enolase (ENO2)	R.GNPTVEVDL**y25**TAK (0; 32; 2.53)	100 (0; 57, 3.43); Not in Vector	Yes
		R.AAVPSGASTGI**y44**EALELR	1.18 (0; 67; 4.33)	No
NP_006612 (21361647)	Putative Adenosylhomocysteinase 2 (AHCYL1)	K.**y28**SFMATVTK (0; 33; 2.42)		No
NP_002645 (33286418)	Pyruvate Kinase Isozymes M1/M2 (PKM2)	K.ITLDNA**y148**MEK (0.041; 2.44)		No
NP_036379 (24797148)	Selenide, Water Dikinase 1 (SEPHS1)	K.**y345**GEGHQAWIIGIVEK	100 (0; 79; 4.36); Not in Vector	No
NP_001687 (4502317)	V-type Proton ATPase Subunit E 1 (ATP6V1E1)	R.LKIME**y56**YEK	100 (0; 37; 2.64); Not in Vector	No
		R.LKIMEY**y57**EK	100 (0; 22; 2.37); Not in Vector	No
Protein Synthesis, Processing and Protein Fate				
NP_001190174 (322303127)	40S Ribosomal Protein S10 (RPS10)	R.IAI**y12**ELLFK	9.8 (0; 42; 2.56)	No
NP_001021 (4506711)	40S Ribosomal Protein S27 (RPS27)	R.LVQSPNS**y31**FMDVK (0; 49; 3.45)	3.62 (0; 66; 3.24)	Yes
NP_001393 (4503471)	Elongation Factor 1-alpha 1 (EEF1A1)	R.EHALLA**y141**TLGVK	0.626 (0.001; 23; 1.83)	No
NP_005792 (5032133)	Eukaryotic Translation Initiation Factor 1 (EIF1)	K.GDDLLPAGTED**y30**IHIR (0; 31; 2.45)		No

NP_055093 (31541941)	Heat Shock 70 kDa protein 4L (HSPA4L)	R.QLGQDLLNS**y600**IENEGKMIMQDK (0.019; 2.3)		No
NP_031381 (20149594)	Heat Shock Protein HSP 90-beta (HSP90AB1)	K.SI**y484**YITGESK (0; 14; 1.97)		No
NP_006588 (5729877)	Heat Shock Cognate 71kDa Protein (HSPA8)	R.TTPS**y41**VAFTDTER (0; 31; 2.03)	4.15 (0; 28; 2.10)	Yes
NP_002147 (31542947)	Heat Shock 60kDa protein, mitochondrial (HSPD1)	R.GYISP**y227**FINTSK (0; 2.14)		No
NP_008945 (40806207)	NEDD4-like E3 Ubiquitin Protein Ligase WWP2 (WWP2)	R.INS**y41**VEVAVDGLPSETKK	100 (0.016; 1.98); Not in Vector	No
NP_006214 (38679892)	Peptidyl-Prolyl cis-trans Isomerase NIMA-Interacting 4 (PIN4)	K.FG**y147**HIIMVEGR (0; 37; 2.74)	16.67 (0; 66; 2.19)	Yes
NP_443197 (24308390)	tRNA-Splicing Endonuclease Subunit Sen15 (TSEN15)	K.**y46**LEMMELDIGDATQV**y61**VAFLVYLDLME SK (0.046; 2.82)		No
		Nucleic Acid Synthesis and Processing		
DNA Binding Protein				
NP_000937 (4506051)	Primase, DNA (PRIM1)	K.**y288**GPWLEWEIMLQYCFPR (0; 1.52)		Yes
Ribonucleoprotein				
NP_001524 (52632383)	Heterogeneous Nuclear Ribonucleoprotein L (HNRNPL)	K.NPNGP**y574**PYTLK (0; 2.88)		No
		K.NPNGPYP**y576**TLK (0; 2.76)	100 (0.001; 25; 2.08); Not in Vector	Yes
RNA Binding Protein				
NP_005327 (4885409)	Vigilin (HDLBP)	R.MD**y437**VEINIDHK (0; 19; 2.69)	100 (0; 63; 2.76); Not in Vector	Yes
Transcription Factor; Transcription Regulatory Protein				
NP_005892 (5174511)	Mothers Against Decapentaplegic Homolog 2 (SMAD2)	K.AIENCE**y151**AFNLK (0; 60; 3.1)		Yes
NP_036364 (42734430)	Polymerase I and Transcript Release Factor (PTRF)	K.SFTPDHVV**y308**AR (0; 27; 2.69)		Yes
NP_644805 (21618340)	Signal Transducer and Activator of Transcription 3 (STAT3)	K.YCRPESQEHPEADPGSAAP**y705**LK (0.035; 21)	5.65 (0; 39; 3.37)	Yes
NP_036580 (21618344)	Signal Transducer and Activator of Transcription 5B (STAT5B)	K.AVDG**y699**VKPQIK (0; 22; 1.77)	100 (0; 48; 3.11); Not in Vector	Yes
		Cellular Organization		
Cytoskeletal Protein				
NP_037391 (56549135)	Transgelin-3 (TAGLN3)	K.GASQAGMTG**y192**GMPR	100 (0; 29; 1.75); Not in Vector	No

NP_004990 (92859701)	Unconventional Myosin-VI (MYO6)	K.SVTD**y1147**AQQNPAAQIPAR	100 (0; 62; 2.93); Not in Vector	No
Structural Protein				
NP_115584 (14149904)	Anthrax Toxin Receptor 1 (ANTXR1)	R.VKMPEQE**y425**EFPEPR	100 (0; 31; 3.24); Not in Vector	No
NP_003371 (62414289)	Vimentin (VIM)	R.FAN**y117**IDKVR (0; 27; 2.5)	100 (0; 25; 2.11); Not in Vector	Yes
		Storage and Transport		
NP_116035 (53988385)	Protein Tweety Homolog 2 (TTYH2)	R.**y494**ENVPLIGR (0.008; 23)		
NP_005689 (16445419)	Secretory Carrier-associated Membrane Protein 3 (SCAMP3)	K.N**y83**GSYSTQASAAAATAELLK	100 (0; 31; 2.51); Not in Vector	No
		K.NYGS**y86**STQASAAAATAELLK	100 (0; 110; 4.98); Not in Vector	No
NP_061849 (21361602)	Sodium-Coupled Neutral Amino Acid Transporter 2 (SLC38A2)	K.SH**y41**ADVDPENQNFLLESNLGK (0; 69; 5.91)	100 (0; 70; 4.87); Not in Vector	Yes
		K.SH**y41**ADVDPENQNFLLESNLGKK	100 (0; 76; 4.67); Not in Vector	No
		R.FSISPDEDSSS**y20**SSNSDFN**y28**SYPTK (0; 3.07)		No
NP_005406 (31543630)	Sodium-Dependent Phosphate Transporter 1 (SLC20A1)	K.DSGL**y388**KELLHK	100 (0; 2.22); Not in Vector	No
NP_001244109 (380503859)	Sodium-Dependent Phosphate Transporter 2 (SLC20A2)	K.DSGL**y354**KDLLHK	100 (0.005; 23; 2.18); Not in Vector	No
NP_001121620 (189458819)	Transferrin Receptor Protein 1 (TFRC)	R.SAFSNLFGGEPLS**y20**TR (0; 57; 4.64)	12.05 (0; 72; 4.27)	Yes
		Unclassified		
NP_001478 (315113895)	Biogenesis of Lysosome-related Organelles Complex 1 Subunit 1 (BLOC1S1)	R.TIATALE**y142**VYKGQLQSAPS	100 (0; 3.22); Not in Vector	No
		R.TIATALEYV**y144**KGQLQSAPS	100 (0; 52); Not in Vector	No
NP_569057 (18641360)	Collectin-12 (COLEC12)	MKDDFAEEEEVQSFG**y16**K	100 (0; 77, 4.43); Not in Vector	No
		MKDDFAEEEEVQSFG**y16**KR (0; 38; 4.63)	100 (0; 54); Not in Vector	Yes
NP_786883 (50233787)	Protein NUT (C15orf55)	K.DDCGLQLRVSEDTCPLNVHS**y928**DPQGEGR VDPDLSKPK (0; 2.72)		No
NP_056151 (103471993)	Palmitoyltransferase ZDHHC17 (ZDHHC17)	K.G**y286**DNPSFLR (0; 33; 2.22)		No
NP_055952 (154146218)	Protein EFR3 Homolog A (EFR3A)	K.LTF**y43**AVSAPEK (0; 26; 2.09)		No
NP_065191 (110225358)	Tetratricopeptide Repeat Protein 7A (TTC7A)	R.DAISMYARAGIDDMSMENKPL**y160**QMR (0; 1.96)		No
NP_060844 (40254893)	Transmembrane Protein 106B (TMEM106B)	R.NGDVSQFP**y50**VEFTGR (0; 58; 4.31)	1.90 (0; 57; 3.66)	Yes
NP_064584 (9910278)	Keratinocyte-associated Transmembrane Protein 2 (C5orf15)	K.TVE**y243**HRLDQNVNEAMPSLK	100 (0; 44; 3.43); Not in Vector	No

NP_945352 (259013211)	UPF0574 Protein C9orf169 (C9orf169)	K.NP**y12**AHISIPR (0; 35; 2.58)	13.89 (0; 30; 2.55)	Yes
NP_001171953 (297206817)	Probable Palmitoyltransferase ZDHHC8 (ZDHHC8)	R.ADEDEDKEDDFRAPL**y91**K (0.042; 1.98)		No
NP_075560 (190885491)	Zinc finger SWIM Domain-containing Protein 4 (ZSWIM4)	R.LEEETLTL**y438**PDSGPEKRK (0.047; 2.66)		No

Table 1: Phosphoproteomic study dataset. The entire curated phosphoproteomic dataset generated from phosphotyrosyl-proteins harvested from stable ectopic PRL3 expressing- and vector control-HEK293 cell clones. Statistics for phosphopeptide identification are provided in the format (q-value; Mascot ion score; Sequest XCorr) for both qualitative (pTyr-peptide column) and SILAC-based quantitative data. Quantitation ratio is in the format (PRL3 vs. vector; PRL3/Vector). pTyr-residue number designation is based upon documented (NP and GI numbers). Unless otherwise specified the phosphoprotein documented is the primary isoform (1 or A) as the phosphopeptide(s) identified are redundant amongst the isoforms.

Table 2: PRL3 phosphoproteomic data in common with Src-Y529F (MEF) data by Rush (145) and Luo (146)

Protein ID (GI number)	Protein Name (Gene symbol)	pTyr-peptide (q-value; Mascot ion score; Sequest XCorr)	PRL3/Vector Quant. Ratio (q-value; Mascot ion score; Sequest XCorr)	Repro-duced
		Cellular Communication and Signal Transduction		
NP_002651 (33598948)	1-Phosphatidylinositol-4,5-bisphosphate Phosphodiesterase Gamma-1 (PLCG1)	K.IGTAEPD**y771**GALYEGR (0; 37; 2.95)	100 (0; 49; 3.28); Not in Vector	Yes
		R.NPGF**y783**VEANPMPTFK (0; 58; 4.63)	10.42 (0; 100, 3.91)	Yes
NP_001002858 (50845388)	Annexin A2 (ANXA2)	K.SL**y334**YYIQQDTK (0; 67; 3.3)	100 (0; 65; 2.43); Not in Vector	Yes
		K.SL**y334**YYIQQDTKGDYQK	100 (0; 65; 4.33); Not in Vector	Yes
		K.SLY**y335**YIQQDTK (0; 32; 3.3)		Yes
		K.SLY**y335**YIQQDTKGDYQK	100 (0; 62; 4.48); Not in Vector	Yes
NP_001744 (15451856)	Caveolin-1 (CAV1)	K.YVDSEGHL**y14**TVPIR (0; 25; 3.16)		Yes
NP_004422 (32967311)	Ephrin-type A Receptor 2 (EPHA2)	K.TYVDPHT**y594**EDPNQAVLK (0; 42; 3.92)	100 (0; 66; 4.03); Not in Vector	Yes
		R.VLEDDPEAT**y772**TTSGGKIPIR (0; 55; 3.71)	76.92 (0; 100; 4.44)	Yes
NP_722560 (24476013)	Focal Adhesion Kinase 1 (PTK2, FAK)	R.THAVSVSETDD**y397**AEIIDEEDTYTMPSTR (0; 34; 3.84)	11.76 (0; 56; 3.42)	Yes
NP_006316 (5453555)	GTP-Binding Nuclear Protein Ran (RAN)	K.NLQ**y146**YDISAK (0.036; 2.15)	100 (0; 38; 2.24); Not in Vector	Yes
		K.NLQY**y147**DISAK	100 (0.002; 2.2); Not in Vector	No
NP_060710 (166295173)	Kin of IRRE-like Protein 1 (KIRREL)	K.DPTNG**y605**YNVR (0; 21)		No
		R.CDTIDTREEYEMKDPTNG**y605**YNVR	100 (0; 64; 4.06); Not in Vector	No
		R.EEYEMKDPTNG**y605**YNVR (0; 37; 2.85)		Yes
		R.TP**y721**EAYDPIGK (0; 43; 3.04)	100 (0; 48; 2.73); Not in Vector	Yes
		R.TPYEA**y724**DPIGK (0; 43; 2.48)	100 (0; 40; 2.85); Not in Vector	Yes
NP_003932 (51702526)	Neural Wiskott-Aldrich Syndrome Protein (WASL; N-WASP)	K.VI**y256**DFIEK (0; 26; 1.74)	9.17 (0; 27; 2.2)	Yes
NP_002990 (38201675)	Syndecan-4 (SDC4)	K.KAPTNEF**y197**A	100 (0; 26; 1.72); Not in Vector	No
NP_006280 (223029410)	Talin-1 (TLN1)	K.ALD**y70**YMLR (0; 39; 2.66)	13.51 (0; 29; 2.11)	Yes
		K.ALDY**y71**MLR (0; 30; 1.8)	13.51 (0.002; 1.99)	Yes
		Energy Metabolism		
NP_001966 (5803011)	Gamma-Enolase (ENO2)	R.GNPTVEVDL**y25**TAK (0; 32; 2.53)	100 (0; 57, 3.43); Not in Vector	Yes
NP_002645 (33286418)	Pyruvate Kinase Isozymes M1/M2 (PKM2)	K.ITLDNA**y148**MEK (0.041; 2.44)		No
		Protein Synthesis, Processing and Fate		

NP_001190174 (322303127)	40S Ribosomal Protein S10 (RPS10)	R.IAI**y12**ELLFK	9.8 (0; 42; 2.56)	No
NP_031381 (20149594)	Heat shock protein HSP 90-beta (HSP90AB1)	K.SI**y484**YITGESK (0; 14; 1.97)		No
		Nucleic Acid Synthesis and Processing		
NP_036364 (42734430)	Polymerase I and Transcript Release Factor (PTRF)	K.SFTPDHVV**y308**AR (0; 27; 2.69)		Yes
NP_644805 (21618340)	Signal Transducer and Activator of Transcription 3 (STAT3)	K.YCRPESQEHPEADPGSAAP**y705**LK (0.035; 21)	5.65 (0; 39; 3.37)	Yes

Table 2: Unique phosphoproteomic data to the PRL3 dataset in comparison to Src-Y529F (MEF) data

Protein ID (GI number)	Protein Name (Gene symbol) # - Common w/ Non-transformed MEF	pTyr-peptide (q-value; Mascot ion score; Sequest XCorr); # - Common with Non-transformed MEF	PRL3/Vector Quant. Ratio (q-value; Mascot ion score; Sequest XCorr)	Repro-duced
		Cellular Communication and Signal Transduction		
NP_003572 (52630423)	Cytoplasmic Protein NCK2 (NCK2; GRB4)	R.TG**y50**VPSNYVER (0; 32; 1.76)	17.24 (0; 41; 2.34)	Yes
NP_001091894 (148539628)	Disks Large Homolog 1 (DLG1)	K.NTSDFV**y399**LK	100 (0; 1.98); Not in Vector	No
NP_066943 (119943106)	#Disks Large Homolog 3 (DLG3)	#R.DNEVDGQD**y673**HFVVSR (0; 38; 3.6)		Yes
		#R.RDNEVDGQD**y673**HFVVSR	4.29 (0; 31; 2.57)	Yes
NP_004703 (4758528)	Hepatocyte Growth Factor-Regulated Tyrosine Kinase Substrate (HGS)	K.YKVVQDT**y132**QIMK	100 (0; 50; 3.47); Not in Vector	No
NP_060699 (224451116)	MHD Domain-containing Death-inducing Protein (MUDENG)	R.KLISSD**y472**YIWNSKAPAPVT**y485**GSLLL (0.033; 1.9)		No
NP_060377 (8923579)	Regulator Complex Protein LAMTOR1 (LAMTOR1)	K.ALNGAEPN**y40**HSLPSAR (0; 2.87)		Yes
NP_003019 (106879210)	#SH2 Domain-containing Adaptor Protein B (SHB)	#K.VTIADD**y246**SDPFDAK (0; 30; 3.34)	100 (0; 54; 3.59); Not in Vector	Yes
NP_001032409 (116805788)	Cytoplasmic FMR1-Interacting Protein 2 (CYFIP2)	R.AVGPSSTQL**y559**MVR (0; 24; 2.82)		No
NP_060710 (166295173)	#Kin of IRRE-like Protein 1 (KIRREL)	#K.AI**y572**SSFKDDVDLK (0; 26; 2.97)		No
		#R.AVL**y622**ADYR	100 (0; 15); Not in Vector	No
		R.LSHSSG**y647**AQLNTYSR (0; 24)		No
		R.LSHSSGYAQLNT**y653**SR (0; 32; 3.28)		No
NP_062565 (21361831)	#Partitioning Defective 3 (PARD3)	#R.ERD**y1080**AEIQDFHR	22.22 (0.002; 1.6)	No

NP_003619 (53829374)	Plakophilin- 4 (PKP4)	K.STTN**y1168**VDFYSTK (0; 43)	100 (0; 46; 2.69); Not in Vector	Yes
NP_057358 (20149626)	Pleckstrin Homology Domain-containing Family O Member 1 (PLEKHO1)	R.QTTPHSQ**y404**R (0; 1.46)		
NP_065910 (203098098)	Protein Shroom 3 (SHROOM3)	R.EARASANGQG**y344**DKWSNIPR (0; 2.45)		
NP_005772 (56549666)	#Activated CDC42 Kinase 1 (ACK1; TNK2)	#K.**y827**ATPQVIQAPGPR (0; 37; 2.8)	3.82 (0; 33; 3.82)	Yes
NP_001195 (15451916)	Bone Morphogenic Protein Receptor Type-2 (BMPR2)	K.IGPYPD**y546**SSSSYIEDSIHHTDSIVK	100 (0.004; 2.88); Not in Vector	No
NP_001014796 (62420886)	#Discoidin Domain-containing Receptor 2 (DDR2)	#R.IFPLRPD**y481**QEPSR (0; 28; 2.7)	100 (0; 27; 2.19); Not in Vector	Yes
NP_958439 (41327732)	Epidermal Growth Factor Receptor, *isoform b* (EGFR)	K.TCPAGVMGENNTLVWKYADAGHVCHLCHPN CT**y626**GS (0; 2.9)		No
NP_722560 (24476013)	Focal Adhesion Kinase 1 (PTK2, FAK)	R.**y570**MEDSTYYK	100 (0; 27; 2.17); Not in Vector	No
NP_005725 (114796624)	#Homeodomain-Interacting Protein Kinase 3 (HIPK3)	#K.TVCST**y359**LQSR (0; 27)		No
NP_002736 (66932916)	#Mitogen-Activated Protein Kinase 1 (MAPK1, ERK2)	#R.VADPDHDHTGFLTE**y187**VATR (0; 58; 5.68)	5.32 (0; 77; 4.67)	Yes
NP_002737 (91718899)	#Mitogen-Activated Protein Kinase 3 (MAPK3, ERK1)	#R.IADPEHDHTGFLTE**y204**VATR (0; 53; 4.92)	3.50 (0; 80; 4.96)	Yes
NP_001306 (4503069)	#Mitogen-Activated Protein Kinase 14 (MAPK14, p38 Alpha)	#R.HTDDEMTG**y182**VATR (0; 60; 3.43)	4.37 (0; 73; 4.19)	Yes
NP_002741 (4506095)	#Mitogen-Activated Protein Kinase 8 Isoform JNK1 Alpha 1 (MAPK8, JNK1)	#R.TAGTSFMMTP**y185**VVTR (0; 26; 3.25)	100 (0; 43; 3.25); Not in Vector	Yes
NP_004825 (22035602)	Mitogen-Activated Protein Kinase Kinase Kinase Kinase 4 (MAP4K4)	R.SGGSSQV**y1153**FMTLGR (0; 3.44)		Yes
NP_006197 (5453870)	Platelet-Derived Growth Factor Receptor alpha (PDGFRA)	K.VVEGTA**y613**GLSR	100 (0; 25; 1.85); Not in Vector	No
		R.S**y720**VILSFENNGDYMDMK	100 (0; 31; 3.59); Not in Vector	No
		R.SYVILSFENNGD**y731**MDMK	100 (0; 44; 3.88); Not in Vector	No
		K.QADTTQ**y742**VPMLER (0; 52; 3.03)	18.87 (0; 60; 2.98)	Yes
		R.VDSDNA**y988**IGVTYK (0; 37; 2.98)		No
NP_002600 (4505683)	Platelet-Derived Growth Factor Receptor beta (PDGFRB)	K.GGPIYIITE**y683**CR (0; 49; 2.86)	100 (0; 40; 2.97); Not in Vector	Yes
		R.YGDLVD**y692**LHR (0; 27)	5.92 (0; 2.81)	Yes
		R.DIMRDSN**y857**ISK	100 (0; 32; 2.54); Not in Vector	No
		K.**y970**QQVDEEFLR (0; 35; 2.43)		No
NP_079052 (148368962)	Pseudopodium-Enriched Atypical Kinase 1 (PEAK1)	R.**y531**QEVWTSSTSPR (0; 39; 2.37)		Yes
NP_002028 (4503823), NP_005424 (4885661)	#Tyrosine-Protein Kinase FYN, YES (FYN, YES1)	#R.KLDNGG**y213,222**YITTR	100 (0.012; 23; 2.19); Not in Vector	Yes
		#K.LDNGG**y213,222**YITTR (0; 27; 2.11)		No
		K.LDNGGY**y214,223**ITTR (0; 27)		

NP_002218 (102469034)	#Tyrosine-Protein Kinase JAK1 (JAK1)	#K.AIETDKE**y1034**YTVK (0; 29; 3.08)		No
NP_004422 (32967311)	#Ephrin type-A Receptor 2 (EPHA2)	#K.T**y588**VDPHTYEDPNQAVLK (0; 53; 3.78)	100 (0; 53; 3.43); Not in Vector	Yes
		R.IA**y960**SLLGLK (0.035; 16)		No
NP_004434 (17975768)	#Ephrin type-B Receptor 3 (EPHB3)	#R.FLEDDPSDPT**y792**TSSLGGK (0; 59; 4.0)		Yes
NP_004435 (32528301)	#Ephrin type-B Receptor 4 (EPHB4)	#R.FLEENSSDPT**y774**TSSLGGK (0; 82; 4.65)	100 (0; 76; 4.11); Not in Vector	Yes
NP_002825 (33356177)	Protein Tyrosine Phosphatase Non-Receptor Type 11 (PTPN11, SHP2)	R.**y279**KNILPFDHTR	100 (0; 42; 2.89); Not in Vector	No
		R.KGHE**y542**TNIK	100 (0.013; 32); Not in Vector	No
NP_002827 (4506303)	#Receptor-type Tyrosine-Protein Phosphatase alpha (PTPRA)	R.**y271**VNILPYDHSR (0; 43; 2.49)		Yes
		#K.VVQEYIDAFSD**y798**ANFK	2.03 (0; 83; 4.46)	No
NP_002651 (33598948)	1-Phosphatidylinositol-4,5-bisphosphate Phosphodiesterase Gamma-1 (PLCG1)	R.AC**y977**RDMSSFPETK	100 (0; 30; 2.67); Not in Vector	No
		K.**y1253**QQPFEDFR (0; 38; 2.01)	100 (0; 40; 2.52); Not in Vector	Yes
NP_001026866 (72534684)	Phospholipase D4 (PLD4)	K.LM**y7**QELK	100 (0.026; 2.33); Not in Vector	No
NP_212132 (54112429)	Dedicator of Cytokenisis Protein 7 (DOCK7)	K.IDISPAPENPH**y522**CLTPELLQVK (0; 3.02)	100 (0; 3.08); Not in Vector	Yes
NP_037428 (164519122)	G-protein-Signaling Modulator 2 (GPSM2)	R.AL**y146**NLGNVYHAK (0; 23; 2.84)		Yes
NP_002515 (4893)	GTPase N-Ras (NRAS)	R.QGVEDAF**y157**TLVR (0; 36; 2.34)	21.74 (0; 37; 2.39)	Yes
NP_004976 (15718761)	GTPase K-Ras Isoform B (KRAS)	R.QGVDDAF**y157**TLVR (0; 41; 2.3)	100 (0; 27; 2.48); Not in Vector	Yes
NP_031394 (38201692)	Ras GTPase-Activating Protein 3 (RASA3)	K.SLCPFYGEDF**y66**CEIPR	100 (0; 60; 3.56); Not in Vector	No
NP_004654 (4758984)	Ras-Related Protein Rab-11A (RAB11A)	R.DDE**y8**DYLFK (0; 21; 2.49)		No
NP_112243 (13569962)	Ras-Related Protein Rab-1B (RAB1B)	R.FADDTYTES**y37**ISTIGVDFK	71.43 (0; 106; 4.55)	No
		R.FADDT**y33**TESYISTIGVDFK	100 (0; 26); Not in Vector	No
NP_002856 (4506365)	Ras-Related Protein Rab-2A (RAB2A)	A**y3**AYLFK (0; 40)		No
NP_689645 (221307575)	Rho GTPase-Activating protein 42 (ARHGAP42)	K.EPI**y376**TLPAIISK (0.042; 1.81)		No
NP_056342 (167614488)	TBC1 Domain Family Member 10B (TBC1D10B)	R.SCQGM**y577**ETMEQLR	100 (0; 54; 2.77); Not in Vector	No
NP_776257 (27777675)	Vomeronasal type-1 receptor 5 (VN1R5)	R.VHGPLKRLHGD**y241**FIQTIR (0.014; 2.17)		No
NP_001633 (4502147)	Amyloid-like Protein 2 (APLP2)	K.MQNHGYENPT**y755**KYLEQMQI	100 (0; 3.41); Not in Vector	No
		K.MQNHGYENPTYK**y757**LEQMQI	100 (0; 3.37); Not in Vector	No
NP_001002858 (50845388)	Annexin A2 (ANXA2)	R.AEDGSVID**y206**ELIDQDAR (0; 63; 4.27)	9.62 (0; 82; 4.5)	Yes
		K.SLYY**y336**IQQDTK (0; 49; 3.23)		Yes

		K.SLYY**y336**IQQDTKGDYQK	100 (0; 47; 4.36); Not in Vector	Yes
NP_001145 (4502107)	Annexin A5 (ANXA5)	R.LYDA**y94**ELK (0; 25; 2.02)	6.33 (0.001; 32; 1.62)	Yes
NP_005175 (58218968)	#Calmodulin (CALM3)	#R.VFDKDGNG**y100**ISAAELR (0; 69; 4.3)	100 (0; 98; 4.46); Not in Vector	Yes
NP_003807 (4501915)	Disintegrin and Metalloproteinase Domain-Containing Protein 9 (ADAM9)	R.EEMILLAN**y245**LDSSYIMLNIR (0.048; 2.52)		No
NP_002202 (19743813)	#Integrin Beta-1 (ITGB1)	#K.WDTGENPI**y783**K	100 (0; 37; 2.55); Not in Vector	No
NP_002204 (20127446)	Integrin Beta-5 (ITGB5)	R.YEMASNPL**y774**R (0; 27; 2.0)	14.93 (0; 54; 2.79)	Yes
NP_000518 (4504975)	#Low-Density Lipoprotein Receptor (LDLR)	#K.NINSINFDNPV**y828**QK (0; 72; 3.42)		No
NP_957718 (41822562)	Neuropilin-2, *isoform 1* (NRP2)	R.SCTTLEN**y908**NFELYDGLK	100 (0; 77; 3.82); Not in Vector	No
NP_957719 (41872567)	Neuropilin-2, *isoform 5* (NRP2)	K.TSH**y877**TNGAPLAVEPTLTIK	100 (0.012; 1.93); Not in Vector	No
NP_852664 (32455248)	#Phosphatidylinositol 3-Kinase Regulatory Subunit alpha (PIK3R1, p85)	R.GDFPGT**y73**VEYIGR (0; 40; 2.26)		No
		R.GLECSTL**y150**R	100 (0.021; 2.13); Not in Vector	No
		#R.DQ**y580**LMWLTQK (0; 31; 2.06)	31.25 (0; 56; 3.02)	Yes
NP_115618 (262118282)	Plexin-A1 (PLXNA1)	K.QTSA**y1608**NISNSSTFTK (0; 31)	13.70 (0; 56; 2.36)	Yes
NP_004595 (20149560)	Syntaxin-4 (STX4)	K.NILSSAD**y251**VER (0; 48; 3.37)	14.08 (0; 59; 3.18)	Yes
		Energy Metabolism		
NP_000687 (115387104)	Aldehyde Dehydrogenase (ALDH9A1)	R.VTIE**y500**YSQLK (0.037; 2.1)		No
NP_061820 (11128019)	Cytochrome C (CYCS)	R.ADLIA**y98**LKK (0.006; 1.64)		No
NP_006612 (21361647)	Putative Adenosylhomocysteinase 2 (AHCYL1)	K.**y28**SFMATVTK (0; 33; 2.42)		No
NP_036379 (24797148)	Selenide, Water Dikinase 1 (SEPHS1)	K.**y345**GEGHQAWIIGIVEK	100 (0; 79; 4.36); Not in Vector	No
NP_001687 (4502317)	V-type Proton ATPase Subunit E 1 (ATP6V1E1)	R.LKIME**y56**YEK	100 (0; 37; 2.64); Not in Vector	No
		R.LKIMEY**y57**EK	100 (0; 22; 2.37); Not in Vector	No
		Protein Synthesis, Processing and Protein Fate		
NP_001021 (4506711)	40S Ribosomal Protein S27 (RPS27)	R.LVQSPNS**y31**FMDVK (0; 49; 3.45)	3.62 (0; 66; 3.24)	Yes
NP_005792 (5032133)	Eukaryotic Translation Initiation Factor 1 (EIF1)	K.GDDLLPAGTED**y30**IHIR (0; 31; 2.45)		No
NP_055093 (31541941)	Heat Shock 70 kDa protein 4L (HSPA4L)	R.QLGQDLLNS**y600**IENEGKMIMQDK (0.019; 2.3)		No
NP_006588 (5729877)	Heat Shock Cognate 71kDa Protein (HSPA8)	R.TTPS**y41**VAFTDTER (0; 31; 2.03)	4.15 (0; 28; 2.10)	Yes

NP_002147 (31542947)	Heat Shock 60kDa protein, mitochondrial (HSPD1)	R.GYISP**y227**FINTSK (0; 2.14)		No
NP_008945 (40806207)	NEDD4-like E3 Ubiquitin Protein Ligase WWP2 (WWP2)	R.INS**y41**VEVAVDGLPSETKK	100 (0.016; 1.98); Not in Vector	No
NP_006214 (38679892)	Peptidyl-Prolyl cis-trans Isomerase NIMA-Interacting 4 (PIN4)	K.FG**y147**HIIMVEGR (0; 37; 2.74)	16.67 (0; 66; 2.19)	Yes
NP_443197 (24308390)	tRNA-Splicing Endonuclease Subunit Sen15 (TSEN15)	K.**y46**LEMMELDIGDATQV**y61**VAFLVYLDLMESK (0.046; 2.82)		No
		Nucleic Acid Synthesis and Processing		
NP_000937 (4506051)	Primase, DNA (PRIM1)	K.**y288**GPWLEWEIMLQYCFPR (0; 1.52)		Yes
NP_001524 (52632383)	Heterogeneous Nuclear Ribonucleoprotein L (HNRNPL)	K.NPNGP**y574**PYTLK (0; 2.88)		No
		K.NPNGPYP**y576**TLK (0; 2.76)	100 (0.001; 25; 2.08); Not in Vector	Yes
NP_005327 (4885409)	Vigilin (HDLBP)	R.MD**y437**VEINIDHK (0; 19; 2.69)	100 (0; 63; 2.76); Not in Vector	Yes
NP_005892 (5174511)	Mothers Against Decapentaplegic Homolog 2 (SMAD2)	K.AIENCE**y151**AFNLK (0; 60; 3.1)		Yes
NP_036580 (21618344)	#Signal Transducer and Activator of Transcription 5B (STAT5B)	#K.AVDG**y699**VKPQIK (0; 22; 1.77)	100 (0; 48; 3.11); Not in Vector	Yes
		Cellular Organization		
NP_037391 (56549135)	Transgelin-3 (TAGLN3)	K.GASQAGMTG**y192**GMPR	100 (0; 29; 1.75); Not in Vector	No
NP_004990 (92859701)	Unconventional Myosin-VI (MYO6)	K.SVTD**y1147**AQQNPAAQIPAR	100 (0; 62; 2.93); Not in Vector	No
NP_115584 (14149904)	Anthrax Toxin Receptor 1 (ANTXR1)	R.VKMPEQE**y425**EFPEPR	100 (0; 31; 3.24); Not in Vector	No
NP_003371 (62414289)	#Vimentin (VIM)	#R.FAN**y117**IDKVR (0; 27; 2.5)	100 (0; 25; 2.11); Not in Vector	Yes
		Storage and Transport		
NP_116035 (53988385)	Protein Tweety Homolog 2 (TTYH2)	R.**y494**ENVPLIGR (0.008; 23)		
NP_005689 (16445419)	Secretory Carrier-associated Membrane Protein 3 (SCAMP3)	K.N**y83**GSYSTQASAAAATAELLK	100 (0; 31; 2.51); Not in Vector	No
		K.NYGS**y86**STQASAAAATAELLK	100 (0; 110; 4.98); Not in Vector	No
NP_061849 (21361602)	#Sodium-Coupled Neutral Amino Acid Transporter 2 (SLC38A2)	R.FSISPDEDSSS**y20**SSNSDFN**y28**SYPTK (0; 3.07)		No
		#K.SH**y41**ADVDPENQNFLLESNLGK (0; 69; 5.91)	100 (0; 70; 4.87); Not in Vector	Yes
		#K.SH**y41**ADVDPENQNFLLESNLGKK	100 (0; 76; 4.67); Not in Vector	No
NP_005406 (31543630)	Sodium-Dependent Phosphate Transporter 1 (SLC20A1)	K.DSGL**y388**KELLHK	100 (0; 2.22); Not in Vector	No
NP_001244109 (380503859)	Sodium-Dependent Phosphate Transporter 2 (SLC20A2)	K.DSGL**y354**KDLLHK	100 (0.005; 23; 2.18); Not in Vector	No

NP_001121620 (189458819)	#Transferrin Receptor Protein 1 (TFRC)	#R.SAFSNLFGGEPLS**y20**TR (0; 57; 4.64)	12.05 (0; 72; 4.27)	Yes
		Unclassified		
NP_001478 (315113895)	Biogenesis of Lysosome-related Organelles Complex 1 Subunit 1 (BLOC1S1)	R.TIATALE**y142**VYKGQLQSAPS	100 (0; 3.22); Not in Vector	No
		R.TIATALEYV**y144**KGQLQSAPS	100 (0; 52); Not in Vector	No
NP_569057 (18641360)	Collectin-12 (COLEC12)	MKDDFAEEEEVQSFG**y16**K	100 (0; 77, 4.43); Not in Vector	No
		MKDDFAEEEEVQSFG**y16**KR (0; 38; 4.63)	100 (0; 54); Not in Vector	Yes
NP_786883 (50233787)	Protein NUT (C15orf55)	K.DDCGLQLRVSEDTCPLNVHS**y928**DPQGEGRVD PDLSKPK (0; 2.72)		No
NP_056151 (103471993)	Palmitoyltransferase ZDHHC17 (ZDHHC17)	K.G**y286**DNPSFLR (0; 33; 2.22)		No
NP_055952 (154146218)	Protein EFR3 Homolog A (EFR3A)	K.LTF**y43**AVSAPEK (0; 26; 2.09)		No
NP_065191 (110225358)	Tetratricopeptide Repeat Protein 7A (TTC7A)	R.DAISMYARAGIDDMSMENKPL**y160**QMR (0; 1.96)		No
NP_060844 (40254893)	Transmembrane Protein 106B (TMEM106B)	R.NGDVSQFP**y50**VEFTGR (0; 58; 4.31)	1.90 (0; 57; 3.66)	Yes
NP_064584 (9910278)	Keratinocyte-associated Transmembrane Protein 2 (C5orf15)	K.TVE**y243**HRLDQNVNEAMPSLK	100 (0; 44; 3.43); Not in Vector	No
NP_945352 (259013211)	UPF0574 Protein C9orf169 (C9orf169)	K.NP**y12**AHISIPR (0; 35; 2.58)	13.89 (0; 30; 2.55)	Yes
NP_001171953 (297206817)	Probable Palmitoyltransferase ZDHHC8 (ZDHHC8)	R.ADEDEDKEDDFRAPL**y91**K (0.042; 1.98)		No
NP_075560 (190885491)	Zinc finger SWIM Domain-containing Protein 4 (ZSWIM4)	R.LEEETLTL**y438**PDSGPEKRK (0.047; 2.66)		No

Table 2: Comparative analysis with phosphoproteomic datasets generated from SrcY529F-expressing MEFs. A comparative analysis to phosphoproteomic datasets generated from SrcY529F-expressing MEFs and parental MEF control counterparts by Rush (145) and Luo (146). The PRL3 phosphoproteomic dataset has notable overlap with the SrcY529F dataset concerning regulators of cytoskeletal dynamics and mitogenic signal transduction. Phosphoproteomic data also has significant overlap with parental MEF data, providing the first phosphoproteomic evidence in support of fibroblast/mesenchymal-like signal transduction taking place in cells following PRL3 expression. The PRL3 phosphoproteomic dataset is largely unique (~67%) when compared with these SrcY529F- and MEF-cell datasets. (#)-represents phosphoproteins/pTyr-residues that are in common with phosphoproteomic data from the non-transformed-MEF dataset. Statistics for phosphopeptide identification are provided in the format (q-value; Mascot ion score; Sequest XCorr) for both qualitative (pTyr-peptide column) and SILAC-based quantitative data. Quantitation ratio is in the format (PRL3 vs. Vector; PRL/Vector). pTyr-residue number designation is based upon documented (NP and GI numbers). Unless otherwise specified the phosphoprotein documented is the primary isoform (1 or A) as the phosphopeptide(s) identified are redundant amongst the isoforms.

Table 3: Select phosphoproteomic data supporting a pro-metastatic molecular signature in the PRL3-expressing HEK293 cells

Protein ID (GI number)	Protein Name (Gene symbol)	pTyr-peptide (q-value; Mascot ion score; Sequest XCorr)	PRL3/Vector Quant. Ratio (q-value; Mascot ion score; Sequest XCorr)	Reprod -uced
		Cellular Communication and Signal Transduction		
Adaptor/Scaffold				
NP_003572 (52630423)	Cytoplasmic Protein NCK2 (NCK2, GRB4)	R.TG**y50**VPSNYVER (0; 32; 1.76)	17.24 (0; 41; 2.34)	Yes
NP_001091894 (148539628)	Disks Large Homolog 1 (DLG1)	K.NTSDFV**y399**LK	100 (0; 1.98); Not in Vector	No
NP_066943 (119943106)	Disks Large Homolog 3 (DLG3)	R.DNEVDGQD**y673**HFVVSR (0; 38; 3.6)		Yes
		R.RDNEVDGQD**y673**HFVVSR	4.29 (0; 31; 2.57)	Yes
NP_003932 (51702526)	Neural Wiskott-Aldrich Syndrome Protein (WASL, N-WASP)	K.VI**y256**DFIEK (0; 26; 1.74)	9.17 (0; 27; 2.2)	Yes
NP_060910 (63054864)	Phosphoprotein Associated with Glycosphingolipid-Enriched Microdomains 1 (PAG1, CBP)	R.SVDGDQGLGMEGP**y163**EVLK (0; 59; 4.53)	0.01 (0; 59; 4.2); Not in PRL3	Yes
		K.AEFAE**y227**ASVDR (0; 58; 2.28)	0.01 (0; 66; 2.68); Not in PRL3	Yes
		K.SREEDPTLTEEEISAM**y317**SSVNKPGQL VNK	0.01 (0; 88; 4.99); Not in PRL3	No
		K.SGQSLTVPEST**y341**TSIQGDPQR (0; 73; 4.41)	0.01 (0; 81; 4.61); Not in PRL3	Yes
		R.SPSSCNDL**y359**ATVK (0.029; 19; 2.8)	0.01 (0; 64; 3.91); Not in PRL3	Yes
		K.END**y417**ESISDLQQGR (0; 67; 4.0)	0.01 (0; 68; 3.61); Not in PRL3	Yes
NP_003019 (106879210)	SH2 Domain-containing Adaptor Protein B (SHB)	K.VTIADD**y246**SDPFDAK (0; 34; 2.92)	100 (0; 54; 3.59); Not in Vector	Yes
NP_892113 (194239662)	SHC-Transforming Protein 1 (SHC1)	R.ELFDDPS**y427**VNVQNLDK	0.01 (0; 75, 3.82); Not in PRL3	No
Adhesion; Adaptor/Scaffold				
NP_062565 (21361831)	Partitioning Defective 3 (PARD3)	R.ERD**y1080**AEIQDFHR	22.22 (0.002; 1.6)	No
NP_006280 (223029410)	Talin-1 (TLN1)	K.ALD**y70**YMLR (0; 39; 2.66)	13.51 (0; 29; 2.11)	Yes
		K.ALDY**y71**MLR (0; 30; 1.8)	13.51 (0.002; 1.99)	Yes
Protein Kinase				
NP_005772 (56549666)	Activated CDC42 Kinase 1 (ACK1, TNK2)	K.**y827**ATPQVIQAPGPR (0; 37; 2.8)	3.82 (0; 33; 3.82)	Yes
NP_722560 (24476013)	Focal Adhesion Kinase 1 (PTK2, FAK)	R.THAVSVSETDD**y397**AEIIDEEDTYTMPS TR (0; 34; 3.84)	11.76 (0; 56; 3.42)	Yes
		R.**y570**MEDSTYYK	100 (0; 27; 2.17); Not in Vector	No
NP_002736 (66932916)	Mitogen-Activated Protein Kinase 1 (MAPK1, ERK2)	R.VADPDHDHTGFLTE**y187**VATR (0; 58; 5.68)	5.32 (0; 77; 4.67)	Yes
NP_002737 (91718899)	Mitogen-Activated Protein Kinase 3 (MAPK3, ERK1)	R.IADPEHDHTGFLTE**y204**VATR (0; 53; 4.92)	3.50 (0; 80; 4.96)	Yes
NP_001306 (4503069)	Mitogen-Activated Protein Kinase 14 (MAPK14, p38 Alpha)	R.HTDDEMTG**y182**VATR (0; 60; 3.43)	4.37 (0; 73; 4.19)	Yes

NP_002741 (4506095)	Mitogen-Activated Protein Kinase 8 Isoform JNK1 Alpha 1 (MAPK8, JNK1)	R.TAGTSFMMTP**y185**VVTR (0; 26; 3.25)	100 (0; 43; 3.25); Not in Vector	Yes
NP_006197 (5453870)	Platelet-Derived Growth Factor Receptor alpha (PDGFRA)	K.VVEGTA**y613**GLSR	100 (0; 25; 1.85); Not in Vector	No
		R.S**y720**VILSFENNGDYMDMK	100 (0; 31; 3.59); Not in Vector	No
		R.SYVILSFENNGD**y731**MDMK	100 (0; 44; 3.88); Not in Vector	No
		K.QADTTQ**y742**VPMLER (0; 52; 3.03)	18.87 (0; 60; 2.98)	Yes
		R.VDSDNA**y988**IGVTYK (0; 37; 2.98)		No
NP_002600 (4505683)	Platelet-Derived Growth Factor Receptor beta (PDGFRB)	K.GGPIYIITE**y683**CR (0; 49; 2.86)	100 (0; 40; 2.97); Not in Vector	Yes
		R.YGDLVD**y692**LHR (0; 27)	5.92 (0; 2.81)	Yes
		R.DIMRDSN**y857**ISK	100 (0; 32; 2.54); Not in Vector	No
		K.**y970**QQVDEEFLR (0; 35; 2.43)		No
NP_002218 (102469034)	Tyrosine-Protein Kinase JAK1 (JAK1)	K.AIETDKE**y1034**YTVK (0; 29; 3.08)		No
NP_004422 (32967311)	Ephrin-type A Receptor 2 (EPHA2)	K.T**y588**VDPHTYEDPNQAVLK (0; 53; 3.78)	100 (0; 53; 3.43); Not in Vector	Yes
		K.TYVDPHT**y594**EDPNQAVLK (0; 42; 3.92)	100 (0; 66; 4.03); Not in Vector	Yes
		R.VLEDDPEAT**y772**TTSGGKIPIR (0; 55; 3.71)	76.92 (0; 100; 4.44)	Yes
		R.IA**y960**SLLGLK (0.035; 16)		No
NP_004434 (17975768)	Ephrin type-B Receptor 3 (EPHB3)	R.FLEDDPSDPT**y792**TSSLGGK (0; 59; 4.0)		Yes
NP_004435 (32528301)	Ephrin type-B Receptor 4 (EPHB4)	R.FLEENSSDPT**y774**TSSLGGK (0; 82; 4.65)	100 (0; 76; 4.11); Not in Vector	Yes
Protein Phosphatase				
NP_002825 (33356177)	Protein Tyrosine Phosphatase Non-Receptor Type 11 (PTPN11, SHP2)	K.IQNTGD**y62**YDLYGGEK (0; 83; 4.8)	0.01 (0; 78; 3.49); Not in PRL3	Yes
		K.IQNTGDY**y63**DLYGGEK (0; 83)	0.01 (0; 78); Not in PRL3	Yes
		R.**y279**KNILPFDHTR	100 (0; 42; 2.89); Not in Vector	No
		R.KGHE**y542**TNIK	100 (0.013; 32); Not in Vector	No
NP_002827 (4506303)	Receptor-type Tyrosine-Protein Phosphatase alpha (PTPRA)	R.**y271**VNILPYDHSR (0; 43; 2.49)		Yes
		K.VVQEYIDAFSD**y798**ANFK	2.03 (0; 83; 4.46)	No
Lipase				
NP_002651 (33598948)	1-Phosphatidylinositol-4,5-bisphosphate Phosphodiesterase Gamma-1 (PLCG1)	K.IGTAEPD**y771**GALYEGR (0; 37; 2.95)	100 (0; 49; 3.28); Not in Vector	Yes
		R.NPGF**y783**VEANPMPTFK (0; 58; 4.63)	10.42 (0; 100, 3.91)	Yes
		R.AC**y977**RDMSSFPETK	100 (0; 30; 2.67); Not in Vector	No
		K.**y1253**QQPFEDFR (0; 38; 2.01)	100 (0; 40; 2.52); Not in Vector	Yes
G-Protein: GTPase; GTPase Activating Protein (GAP); Guanine Nucleotide Exchange Factor (GEF); Small GTPase Effector Protein				
NP_212132 (54112429)	Dedicator of Cytokenisis Protein 7 (DOCK7)	K.IDISPAPENPH**y522**CLTPELLQVK (0; 3.02)	100 (0; 3.08); Not in Vector	Yes

NP_002515 (4893)	GTPase N-Ras (NRAS)	R.QGVEDAF**y157**TLVR (0; 36; 2.34)	21.74 (0; 37; 2.39)	Yes
NP_004976 (15718761)	GTPase K-Ras Isoform B (KRAS)	R.QGVDDAF**y157**TLVR (0; 41; 2.3)	100 (0; 27; 2.48); Not in Vector	Yes
Signaling Other				
NP_005175 (58218968)	Calmodulin (CALM3)	R.VFDKDGNG**y100**ISAAELR (0; 69; 4.3)	100 (0; 98; 4.46); Not in Vector	Yes
NP_001744 (15451856)	Caveolin-1 (CAV1)	K.YVDSEGHL**y14**TVPIR (0; 25; 3.16)		Yes
NP_002202 (19743813)	Integrin Beta-1 (ITGB1)	K.WDTGENPI**y783**K	100 (0; 37; 2.55); Not in Vector	No
NP_002204 (20127446)	Integrin Beta-5 (ITGB5)	R.YEMASNPL**y774**R (0; 27; 2.0)	14.93 (0; 54; 2.79)	Yes
NP_000518 (4504975)	Low-Density Lipoprotein Receptor (LDLR)	K.NINSINFDNPV**y828**QK (0; 72; 3.42)		No
NP_852664 (32455248)	Phosphatidylinositol 3-Kinase Regulatory Subunit alpha (PIK3R1, p85)	R.GDFPGT**y73**VEYIGR (0; 40; 2.26)		No
		R.GLECSTL**y150**R	100 (0.021; 2.13); Not in Vector	No
		R.DQ**y580**LMWLTQK (0; 31; 2.06)	31.25 (0; 56; 3.02)	Yes
NP_004595 (20149560)	Syntaxin-4 (STX4)	K.NILSSAD**y251**VER (0; 48; 3.37)	14.08 (0; 59; 3.18)	Yes
Nucleic Acid Synthesis and Processing				
Transcription Factor; Transcription Regulatory Protein				
NP_644805 (21618340)	Signal Transducer and Activator of Transcription 3 (STAT3)	K.YCRPESQEHPEADPGSAAP**y705**LK (0.035; 21)	5.65 (0; 39; 3.37)	Yes
NP_036580 (21618344)	Signal Transducer and Activator of Transcription 5B (STAT5B)	K.AVDG**y699**VKPQIK (0; 22; 1.77)	100 (0; 48; 3.11); Not in Vector	Yes
Storage and Transport				
NP_061849 (21361602)	Sodium-Coupled Neutral Amino Acid Transporter 2 (SLC38A2)	R.FSISPDEDSSSy20SSNSDFN**y28**SYPTK (0; 3.07)		No
		K.SH**y41**ADVDPENQNFLLESNLGK (0; 69; 5.91)	100 (0; 70; 4.87); Not in Vector	Yes
		K.SH**y41**ADVDPENQNFLLESNLGKK	100 (0; 76; 4.67); Not in Vector	No
NP_005406 (31543630)	Sodium-Dependent Phosphate Transporter 1 (SLC20A1)	K.DSGL**y388**KELLHK	100 (0; 2.22); Not in Vector	No
NP_001244109 (380503859)	Sodium-Dependent Phosphate Transporter 2 (SLC20A2)	K.DSGL**y354**KDLLHK	100 (0.005; 23; 2.18); Not in Vector	No
NP_001121620 (189458819)	Transferrin Receptor Protein 1 (TFRC)	R.SAFSNLFGGEPLS**y20**TR (0; 57; 4.64)	12.05 (0; 72; 4.27)	Yes

Table 3: Select phosphoproteomic data supporting a pro-metastatic molecular signature in the PRL3-expressing HEK293 cells. Select data taken from the entire curated phosphoproteomic dataset (Table 1) providing evidence in support of signal transduction responsible for driving pro-metastatic molecular events following ectopic PRL3 expression. A graphical model representing this data is presented in Figure 10. pTyr-residue number designation is based upon documented (NP and GI numbers) from the primary isoform (1 or A).

Table 4A: Kinetic parameters of wild-type and SHP2 pathogenic mutants with *p* NPP as a substrate

Enzyme	k_{cat} (s^{-1})	K_m (mM)
WT/CD	**6.4** ± 0.4	**3.0** ± 0.30
WT/FL	**0.31** ± 0.02	**2.7** ± 0.20
E76K/FL	**6.8** ± 0.30	**3.4** ± 0.20
D61Y/FL	**6.0** ± 0.50	**2.7** ± 0.10
Y279C/CD	**0.25** ± 0.05	**11.3** ± 0.50
Y279C/FL	**0.052** ± 0.003	**7.6** ± 0.40
E76K/Y279C/FL	**0.34** ± 0.04	**8.4** ± 0.60
T468M/CD	**0.14** ± 0.002	**2.4** ± 0.10
T468M/FL	**0.011** ± 0.001	**2.1** ± 0.20

Table 4B: Kinetic parameters of wild-type and SHP2 pathogenic mutants with *p* NPP as a substrate (all LS-SHP2 mutants)

Enzyme	k_{cat} (s^{-1})	K_m (mM)
WT/CD	**5.45** ± 0.08	**3.34** ± 0.13
WT/FL	**0.136** ± 0.003	**3.63** ± 0.21
Y279C/CD	**0.391** ± 0.005	**11.59** ± 0.43
Y279C/FL	**0.0275** ± 0.0003	**7.28** ± 0.36
A461T/CD	**0.0025** ± 0.0001	**3.04** ± 0.19
A461T/FL	**0.00230** ± 0.00001	**2.20** ± 0.04
G464A/CD	**0.0258** ± 0.0003	**3.43** ± 0.13
G464A/FL	**0.0184** ± 0.0002	**2.57** ± 0.08
T468M/CD	**0.0921** ± 0.0018	**2.66** ± 0.16
T468M/FL	**0.00359** ± 0.00006	**3.17** ± 0.15
R498L/CD	**0.0247** ± 0.0003	**9.22** ± 0.12
R498L/FL	**0.0390** ± 0.0003	**5.95** ± 0.12
Q506P/CD	**0.130** ± 0.001	**4.37** ± 0.12
Q506P/FL	**0.046** ± 0.001	**2.49** ± 0.18
Q510E/CD	**0.0129** ± 0.0002	**6.29** ± 0.28
Q510E/FL	**0.0170** ± 0.0003	**2.8** ± 0.16
T507K/FL	**0.230** ± 0.002	**1.66** ± 0.05
D61Y/FL	**6.0** ± 0.50	**2.7** ± 0.10
E76K/FL	**6.8** ± 0.30	**3.4** ± 0.20

Table 4: Kinetic parameters (k_{cat} and K_m) of wild-type and SHP2 pathogenic mutants with *p*NPP as a substrate. Full-length (FL, residues 1-528) and catalytic domain (CD, 246-547) were used to determine kinetic parameters (k_{cat} and K_m) for the hydrolysis of *para*-nitrophenyl phosphate (*p*NPP). Rate measurements were conducted at 25ºC in a pH 7.0 buffer containing 50mM 3.3-dimethylglutarate, 150mM NaCl, 1mM DTT, and 1mM EDTA. **(A)** LS-SHP2 mutants Y279C and T468M are catalytically impaired, but the additional (1-245) residues, encompassing both of the N-SH2 and C-SH2 domains are less able to inhibit *p*NPP hydrolysis than this corresponding region in the wild-type enzyme, suggesting an increase propensity for LS-SHP2 mutants to adopt an open·active conformation. **(B)** Kinetic analysis of all seven LS-SHP2 mutants. LS-SHP2 mutants show a wide range of catalytic impairment, relative to the wild-type enzyme, but a disparity emerges where the most recurrent LS-SHP2 mutants Y279C and T468M are further inhibited by the (1-245) residue range, while the other catalytically impaired mutants are not further inhibited by this residue range. Data suggests that while the Y279C and T468M mutants may predominately exist in a closed, autoinhibited conformation, the other mutants do not experience this degree of intramolecular autoinhibition.

Table 5: Inhibitor contstants for isolated N-SH2 domains against isolated PTP domains of wild-type and SHP2 pathogenic mutants

N-SH2 domain (4-103)	PTP domain (224-528)	K_i (μM)
WT	**WT**	**1.3** ± 0.05
WT	**Y279C**	**11.3** ± 0.3
WT	**A461T**	**Undetermined/No Inhibition**
WT	**G464A**	**74.8** ± 4.3
WT	**T468M**	**2.6** ± 0.1
WT	**R498L**	**No Inhibition**
WT	**Q506P**	**41.9** ±1.3
WT	**Q510E**	**128** ± 3.7
WT	**T507K**	**46.3** ± 1.9
E76K	**WT**	**No Inhibition**

Table 5: Inhibitor constants (K_i) for the isolated wild-type N-SH2 domain against isolated LS-SHP2 mutant PTP domains. Using pNPP as a substrate, rate measurements were conducted at 25ºC in a pH 7.0 buffer containing 50mM 3.3-dimethylglutarate, 150mM NaCl, 1mM DTT, and 1mM EDTA. For K_i determination, *p*NPP concentration was varied while the N-SH2 domain was fixed at 3 different concentrations. Data show that the isolated N-SH2 domain (4-103) is a competitive inhibitor to the isolated catalytic PTP domain (224-528). The wild-type N-SH2 domain is a weak if not completely inefficient competitive inhibitor of the LS-SHP2 mutant PTP domains, providing evidence in support of LS-SHP2 mutations disrupting the inherent intramolecular interactions made between the N-SH2 and PTP domains in the wild-type enzyme. A wide range of inhibition values exist across the mutants suggesting that each mutation has a unique ability to disturb the various intramolecular interactions that are made between these two domains. The E76K N-SH2 domain was used as a positive control for 'No Inhibition' against the WT-PTP domain. Catalytically-competent T507K was used to show that pathogenic SHP2 mutations that are Q-loop-directed disrupt the autoregulatory mechanism governing SHP2 function.

Table 6

Differences in Hydrogen Exchange to all SHP2 Pathogenic Mutants Relative to Wild-Type

Heat map color code (values in daltons) (1.0-2.0) (0.7-1.0) (0.4-0.7) No Significance 0.4-0.7 0.7-1.0 1.0-2.0 >2.0

Residue range color code (by domain) N-SH2 C-SH2 PTP

** (46) peptic peptides covering ~95% of the SHP2 sequence (1-528) were analyzed per experimental group in quadruplicate measurements per time point (0, 10s, 30s, 1m, 10m, 30m, 60m)

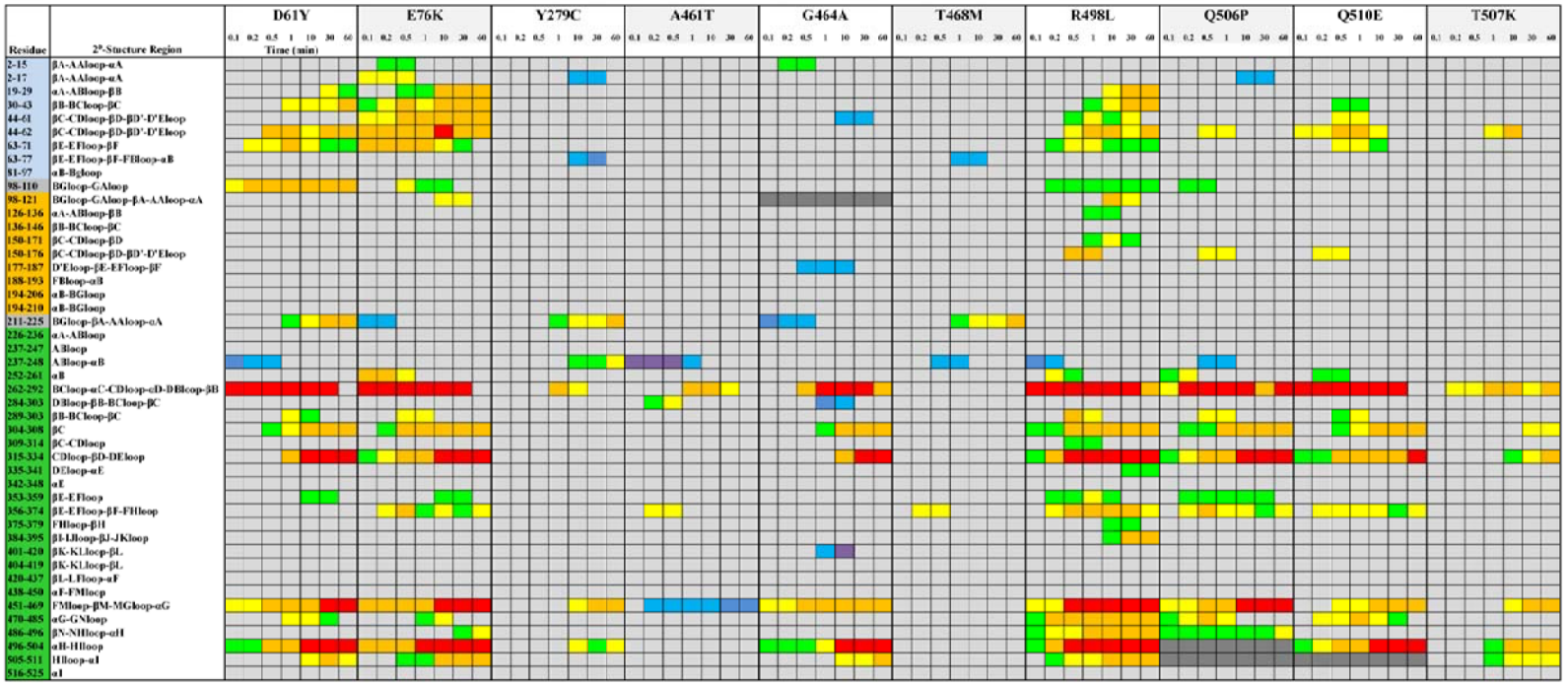

Table 6: 'Heat Map' of hydrogen exchange differences over time to SHP2 pathogenic mutants relative to wild-type (WT). (46) peptic peptide respresenting ~95% of the SHP2 (1-528) sequence are organized according to domain location (N-SH2; blue, C-SH2; orange, PTP; green). Deuterium exchange differences over time are depicted as a 'heat map' for all SHP2 pathogenic mutants under investigation relative to wild-type (WT) according to the legend presented at the top of the table. Positive deuterium exchange relative to WT (which can be considered 'all grey') is represented in the legend as colors according to the magnitude of difference (in Daltons) attained at a specific time point relative to the WT enzyme with (0.4-0.7; green, 0.7-1.0; yellow, 1.0-2.0; orange, and >2.0; red). Negative deuterium exchange relative to WT is represented as ((0.4-0.7); light blue, (0.7-1.0); dark blue, and (1.0-2.0); purple).

A

Name	Sequence (5'→3')	Description
SHP2 1 Nde1 Forward	CAAGCATATGACATCGCGGAGATGGTTTCACCCA	Construction of pET-21a(+)-SHP2(1-528)
SHP2 528 Xho1 Reverse	CGGGCTCGAGCCTGCGCTGTAGTGTTTCAATATA	Construction of pET-21a(+)-SHP2(1-528)
SHP2 Y279C Forward	CAAAAACAAAAATAGATGTAAAAACATCCTGCCC	Site-directed mutagenesis for Y279C
SHP2 Y279C Reverse	GGGCAGGATGTTTTTACATCTATTTTTGTTTTTG	Site-directed mutagenesis for Y279C
SHP2 A461T Forward	GTGCACTGCAGTACTGGAATTGGCC	Site-directed mutagenesis for A461T
SHP2 A461T Reverse	GGCCAATTCCAGTACTGCAGTGCAC	Site-directed mutagenesis for A461T
SHP2 G464A Forward	AGTGCTGGAATTGCCCGGACAGGGACGTT	Site-directed mutagenesis for G464A
SHP2 G464A Reverse	AACGTCCCTGTCCGGGCAATTCCAGCACT	Site-directed mutagenesis for G464A
SHP2 T468M Forward	GGCCGGACAGGGATGTTCATTGTGATTG	Site-directed mutagenesis for T468M
SHP2 T468M Reverse	ATCACAATGAACATCCCTGTCCGGC	Site-directed mutagenesis for T468M
SHP2 R498L Forward	CATCCAGATGGTGCTGTCTCAGAGGTCAG	Site-directed mutagenesis for R498L
SHP2 R498L Reverse	CTGACCTCTGAGACAGCACCATCTGGATG	Site-directed mutagenesis for R498L
SHP2 Q506P Forward	GGTCAGGGATGGTCCCGACAGAAGCACAGT	Site-directed mutagenesis for Q506P
SHP2 Q506P Reverse	GTACTGTGCTTCTGTCGGGACCATCCCTGACC	Site-directed mutagenesis for Q506P
SHP2 Q510E Forward	GTCCAGACAGAAGCAGAGTACCGATTTATC	Site-directed mutagenesis for Q510E
SHP2 Q510E Reverse	GATAAATCGGTACTCTGCTTCTGTCTGGAC	Site-directed mutagenesis for Q510E

B

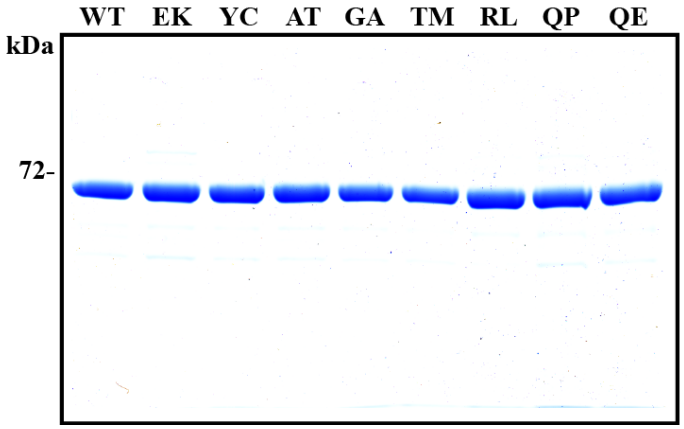

Table 7: Primers used for LS-SHP2 pathogenic mutant generation and sample of purified LS-SHP2 mutant (1-528) constructs. (A) Primers used during site-directed mutagenesis and PCR to generate the seven LS-associated SHP2 mutants used in this investigation. PCR products were gel purified, digested with NdeI and XhoI and inserted into the pET-21a(+) plasmid with C-terminal polyhistidine-tag. Additional information is available in the methods section. **(B)** Coomassie-stained gel showing the relative purity of LS-SHP2 mutant (1-528) constructs (Y279C, A461T, G464A, T468M, R498L, Q506P, and Q510E) following a double purification strategy using Ni-NTA agarose followed by gel-filtration chromatography. Purity of the SHP2 mutant enzymes, along with their WT and E76K mutant counterparts is >95%. Additional information is available in the methods section.

FIGURES

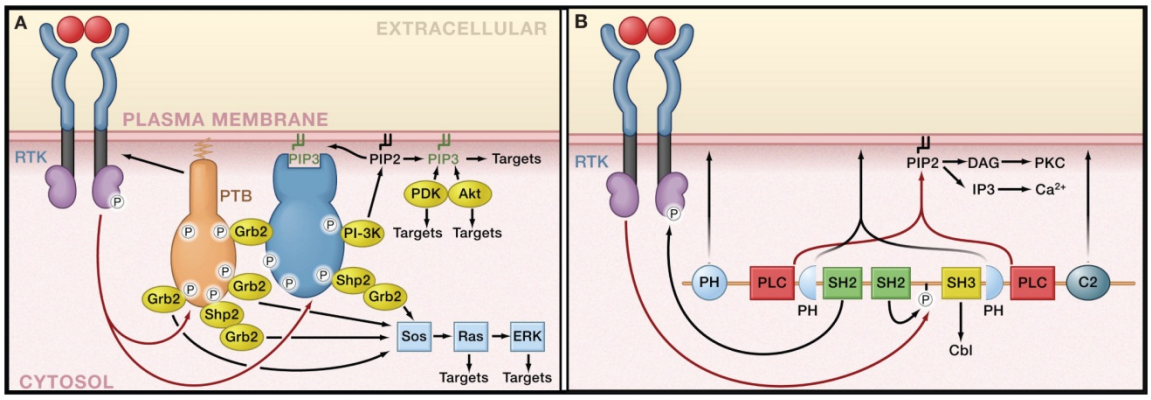

Figure 1: Network branching and coincidence detection in RTK signaling. (A) Organizing multiprotein complexes into a functional branched network following ligand-mediated receptor tyrosine kinase phosphorylation/activation. The docking protein FGF receptor substrate-2 (FRS2α) is recruited to activated fibroblast growth factor (FGF) or nerve growth factor (NGF) receptors via its phosphotyrosine-binding domain (PTB), and subsequently becomes phosphorylated on tyrosine residues by these receptors. The phosphotyrosyl-residues become docking sites for multiple Grb2 and Shp2 molecules, which bring a second docking protein, Gab1, into the complex. Gab1 is tyrosine phosphorylated and recruits additional signaling proteins, including phosphoinositide 3-kinase (PI-3K). PI-3K initiates a positive feedback loop in which PtdIns(3,4,5)P_3(PIP_3), generated by PI-3K, recruits more Gab1, leading to further PI-3K activation. **(B)** Phospholipase C-γ (PLCγ) represents a coincidence detector in that its multiple domains cooperate to integrate multiple signals at the plasma membrane. The N-terminal SH2 domain targets this lipase to phosphorylated/activated receptor tyrosine kinases (RTKs), while the C2 and PH domains cooperate with the SH2 domain to target this enzyme to the plasma membrane. One or both of the PH domains may also specifically recognize products of RTK-activated PI-3K. RTK-mediated tyrosine phosphorylation of PLCγ leads to intramolecular binding of the C-terminal SH2 domain to phosphotyrosine 783. This stimulates enzymatic activity of PLCγ, leading to hydrolysis of PtdIns(4,5)P_2 (PIP_2), and consequently leads to the formation of Ins(1,4,5)P_3 (IP_3) and diacylglycerol (DAG).

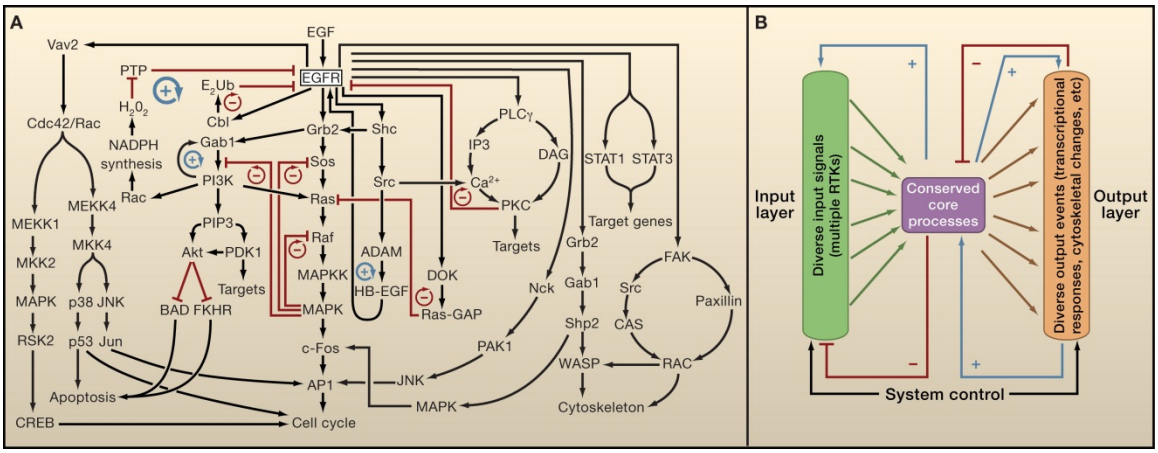

Figure 2: Intracellular signaling networks activated by EGFR. (A) Following EGF-mediated activation of the EGF-receptor (EGFR), a multitude of diverse signals are integrated within a single network. Within the integrated network, distinct pathways are brought together to contextually regulate the entire network. Through a combination of stimulatory (black arrows) or inhibitory (red lines) signals, several key positive feedback loops (blue circular arrows) and negative feedback loops (red circular arrows) emerge in the network and exert significant influence on its behavior. **(B)** A conceptual representation of a "bow tie" or "hourglass" network, as described by Kitano (2004). Diverse input signals converge upon a conserved set of core processes that contextually drive the activation/inhibition of a large array of output events including transcriptional and cytoskeletal responses. Like the EGFR-mediated signaling network to the left, the conserved core of processes regulates the input signals through both feed-forward and feed-back signals. The output layer also regulates the conserved core through both feed-forward and feed-back signals. System control exists at every layer so that the network as a whole can be properly regulated in a context-dependent manner.

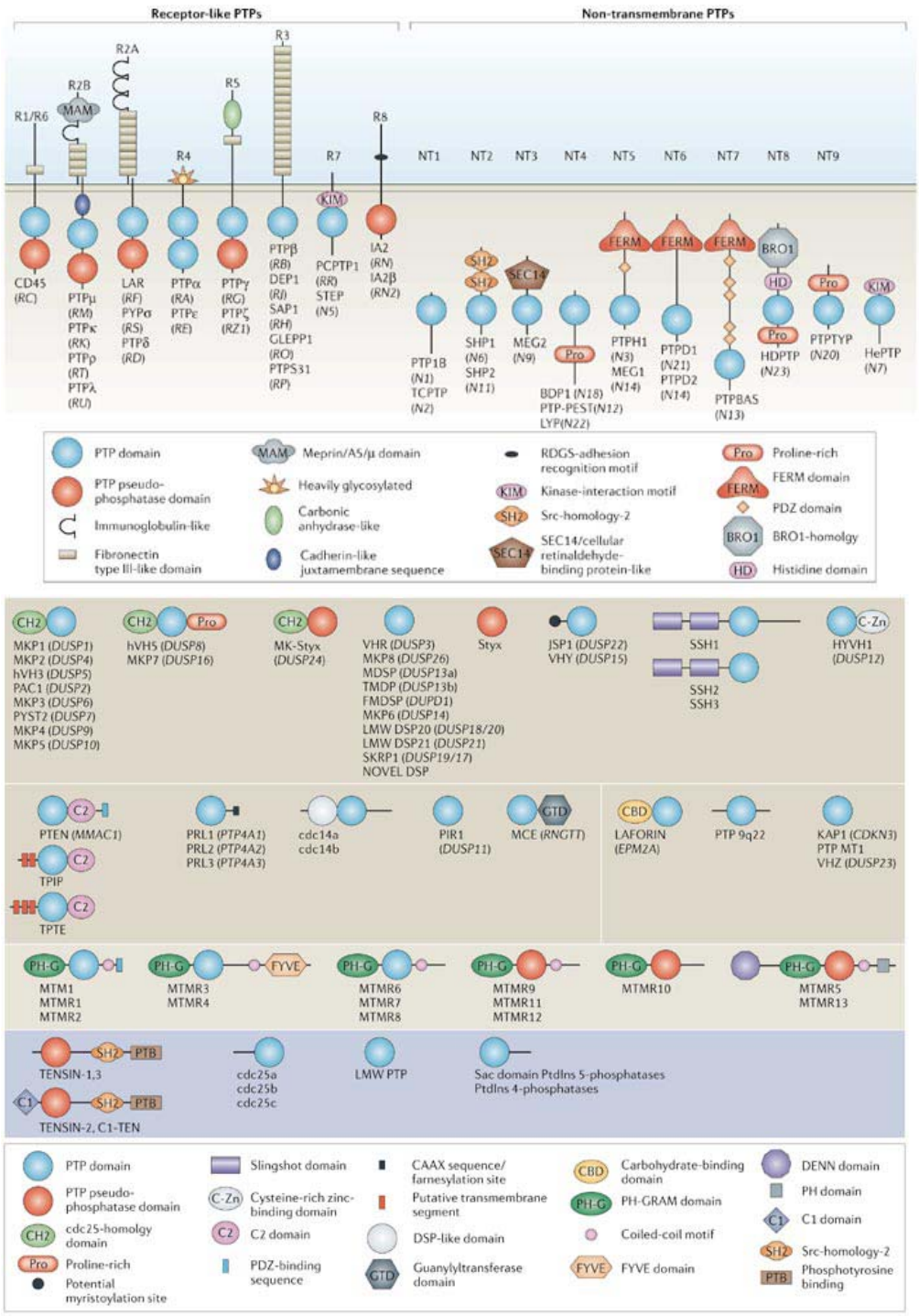

Figure 3: Class I cysteine-based protein tyrosine phosphatases (PTPs). The class I cysteine-based protein tyrosine phosphatases (PTPs), defined by the active site signature motif (HCX_5R), comprise the 38 "classical" PTPs (21 receptor-like and 17 non-receptor; non-transmembrane (NT)) and the 65 VH1-like dual-specificity phosphatases (DSPs). The DSPs are more structurally diverse than the classical PTPs and possess a small conserved catalytic domain.

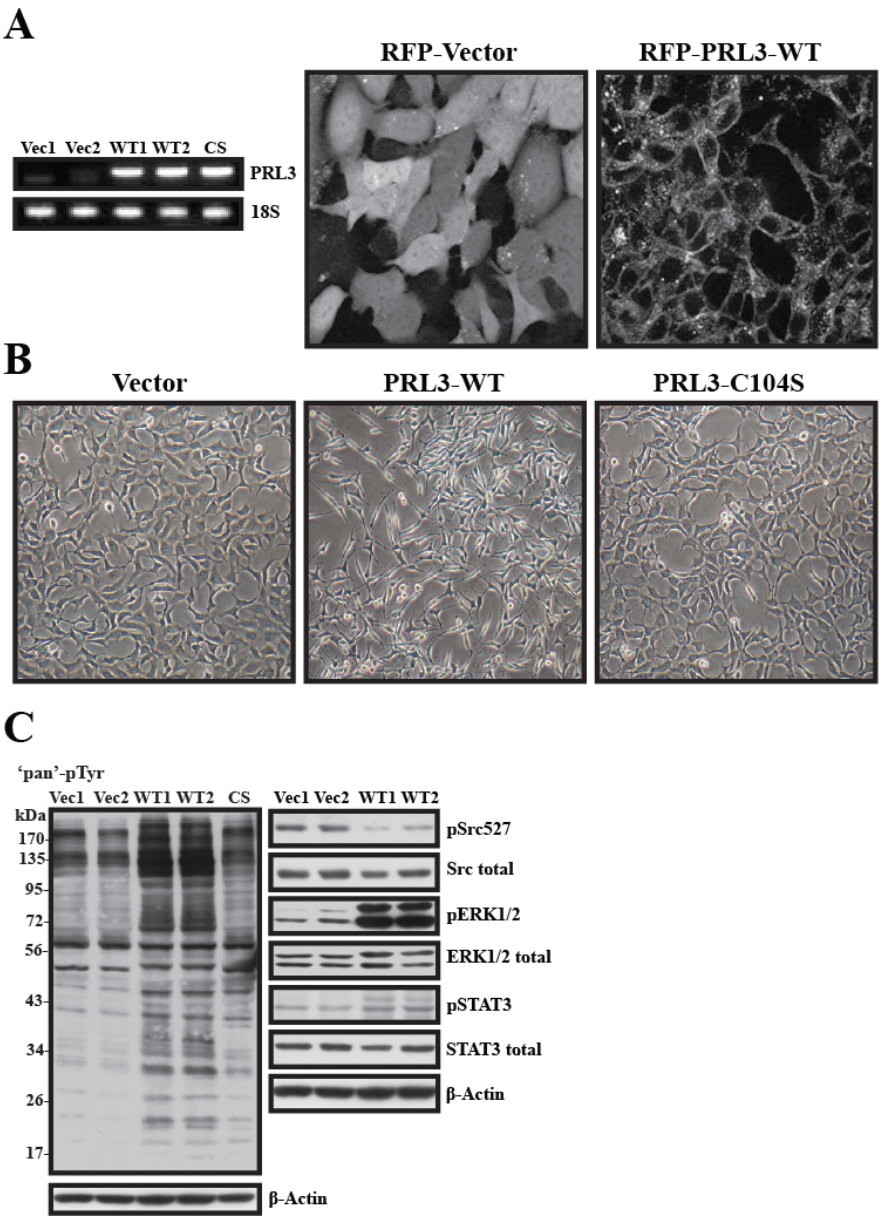

Figure 4: **Ectopic PRL3 expression induces aberrant regulation of tyrosine phosphorylation.** **(A)** PRL3 transcript is significantly enhanced in the PRL3-WT and -C104S expressing HEK293 clones, relative to endogenous levels of PRL3 transcript in vector counterparts as observed through RT-PCR using PRL3-specific oligonucleotides. 18S-rRNA used as control. RFP (red fluorescent protein)-tagged PRL3-WT protein is localized on endomembranes following stable ectopic expression in HEK293 cells as assessed by confocal microscopy. **(B)** PRL3-WT cells have an unmistakable 'spindle-like' fibroblast/mesenchymal morphology as compared to their 'squamous' epithelial PRL3-C104S and vector counterparts. **(C)** PRL3-WT clones have enhanced 'global' tyrosine phosphorylation ('pan' pTyr-α), a markedly less latent pTyr527-Src population, and constitutively phosphorylated/activated ERK1/2 (pThr202/pTyr204-α) and STAT3 (pTyr705-α), relative to vector counterparts as measured by phospho-specific immunoblotting.

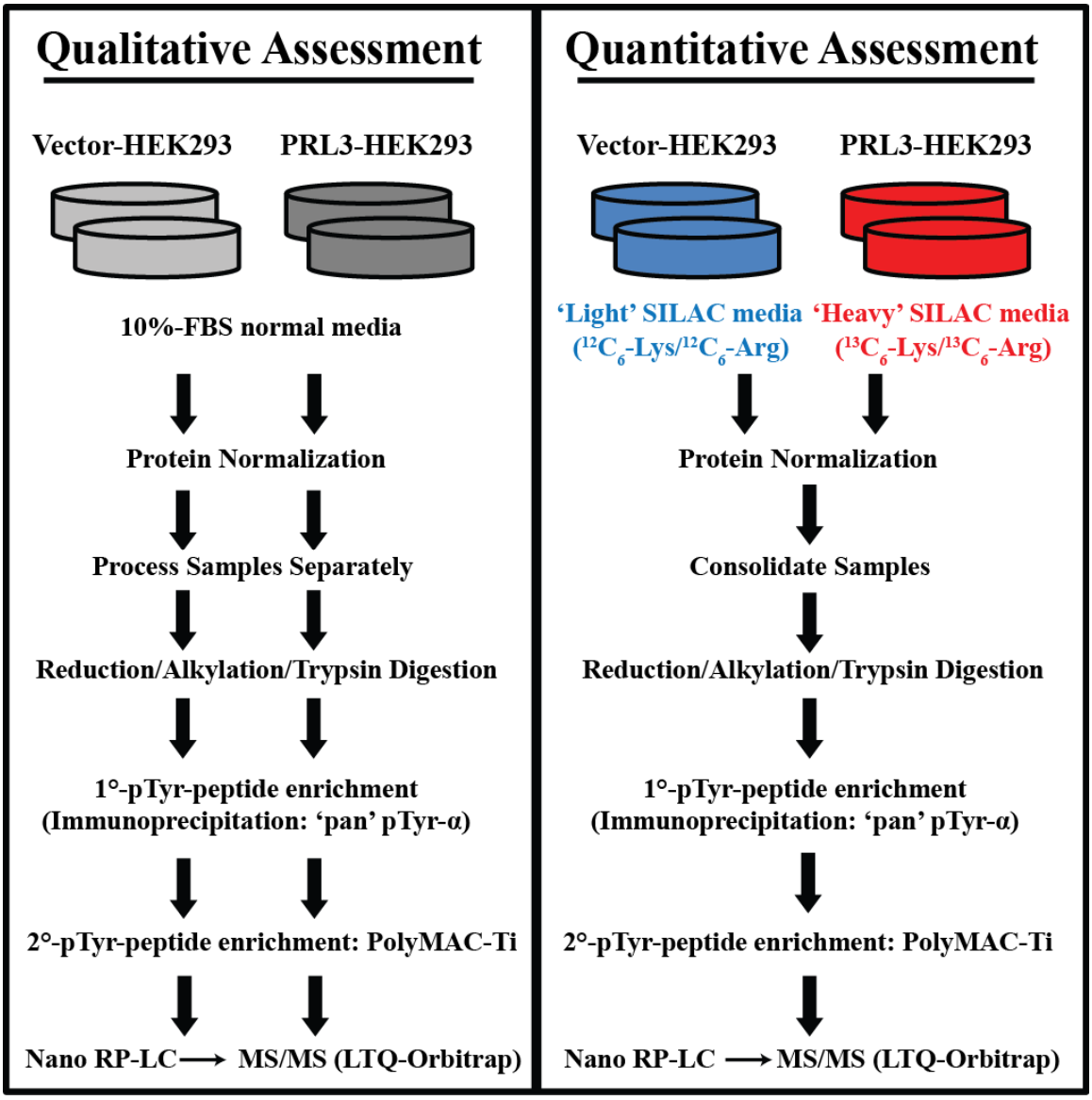

Figure 5: Phosphoproteomic methodology. Data acquisition and analysis flow-chart describing the sample preparation and analysis methodology for both qualitative and SILAC (stable isotope labeling of amino acids in cell culture)-based quantitative assessment of tyrosine phosphorylation.

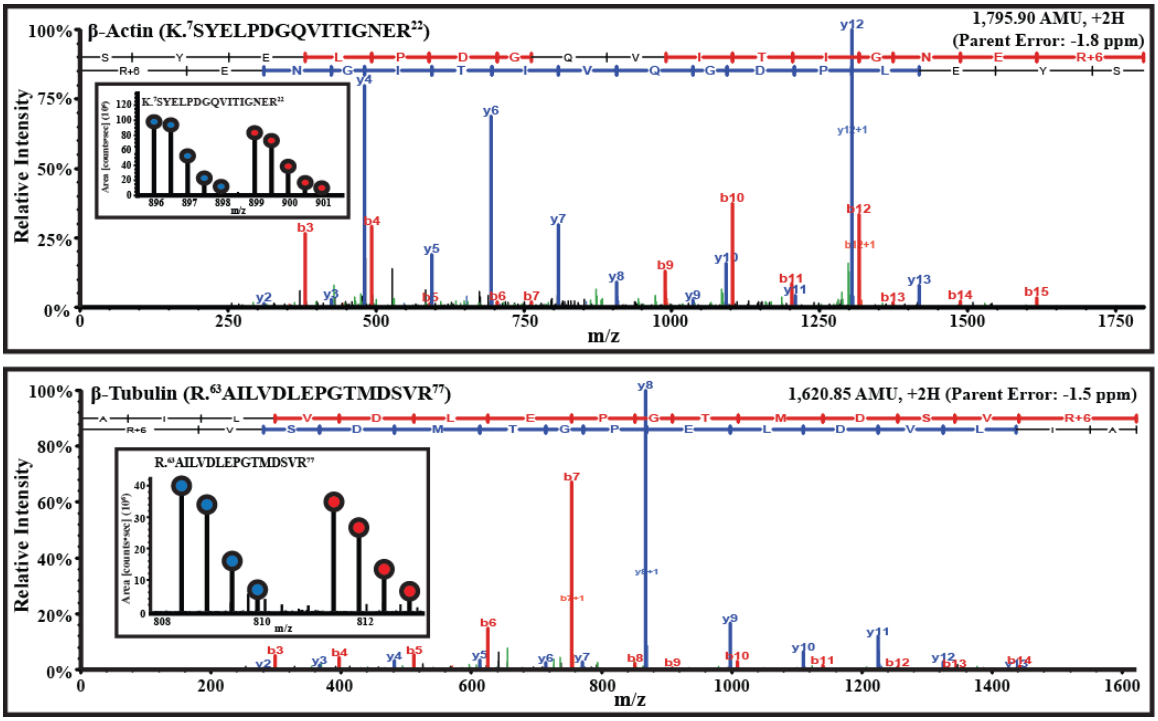

Figure 6: Proteins from the ectopic PRL3 expressing cells are effectively labeled with SILAC-'Heavy' Lys- and Arg-amino acids. Data validation and spectral quality for the 'house-keeping' genes β-Actin (K.[7]SYELPDGQVITIGNER) and β-Tubulin (R.[63]AILVDLEP GTMDSVR) showing a ~1:1 mixing ratio between SILAC-'Light' (vector) and SILAC-'Heavy' (PRL-3) protein lysates prior to sample preparation (a measure of the labeling efficiency of the SILAC-'Heavy' label): Raw fragmentation 'sequencing' spectrums including parent ion abundances (SILAC-based quantitative spectra; SILAC-'Light' (vector; blue points); SILAC-'Heavy' (PRL-3; red points)). b-ion series is colored in 'red' and y-ion series in 'blue'.

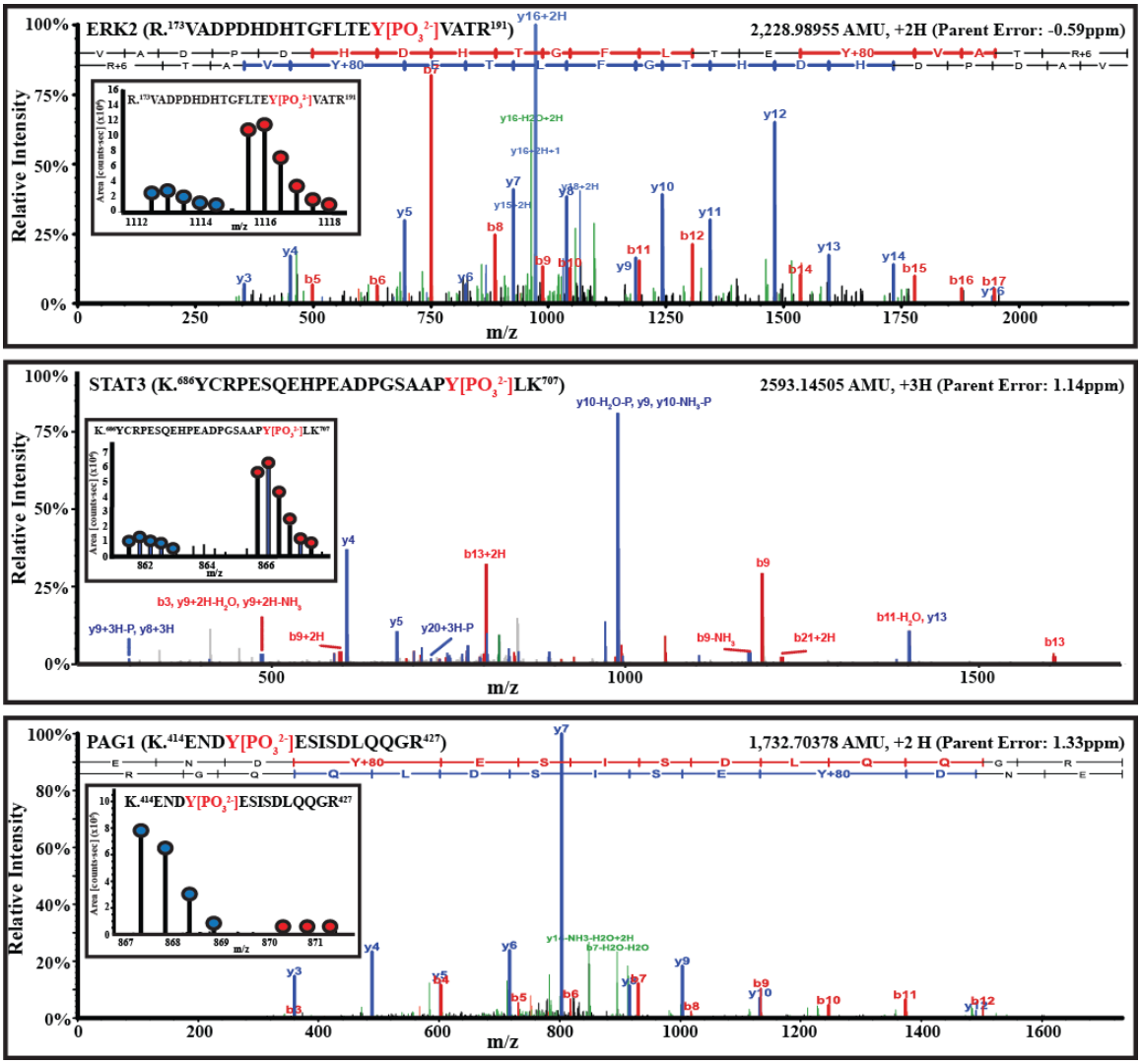

Figure 7: Quality of mass spectra used for SILAC-based quantitative assessment of tyrosine phosphorylation. Representative mass spectra for pTyr187 of ERK2 (^{173}VADPDHDHTGFLTEY[PO_3^{2-}]VATR), pTyr705 of STAT3 (^{686}YCRPESQEHPEAD PGSAAPY[PO_3^{2-}]LK), and pTyr417 of PAG1 (^{414}ENDY[PO_3^{2-}]ESISDLQQGR) showing the quality of mass spectra used for SILAC-based quantitative assessment of tyrosine phosphorylation. Raw fragmentation 'sequencing' spectra including parent ion abundances (SILAC-based quantitative spectra: SILAC-'Light' (vector; blue points); SILAC-'Heavy' (PRL-3; red points)). b-ion series is colored in 'red' and y-ion series in 'blue'.

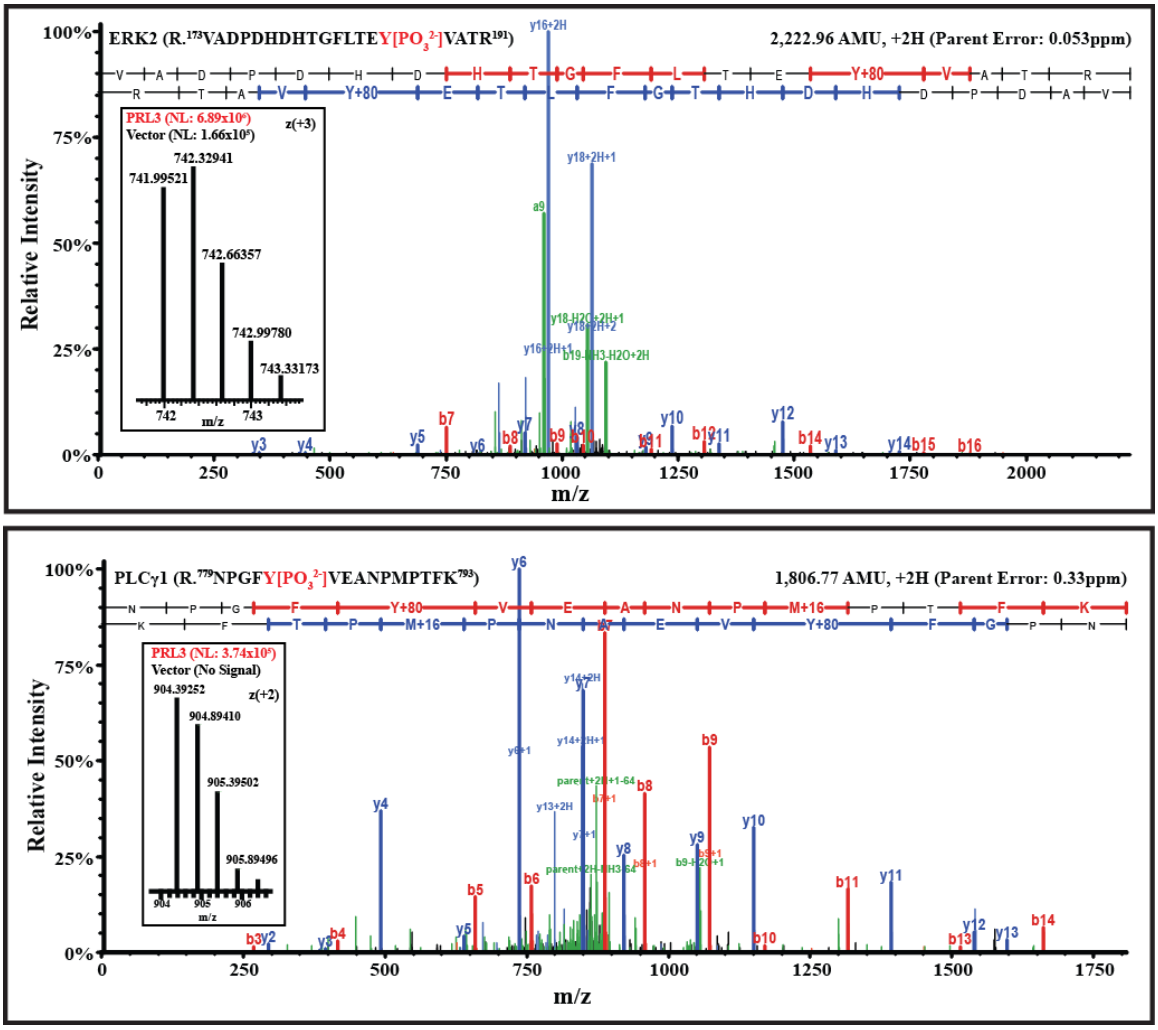

Figure 8: Quality of mass spectra used for qualitative assessment of tyrosine phosphorylation. Representative mass spectra for pTyr187 of ERK2 (^{173}VADPDHDH TGFLTEY[PO_3^{2-}]VATR) and pTyr783 of PLCγ1 (^{779}NPGFY[PO_3^{2-}]VEANPMPTFK) showing the quality of mass spectra used for qualitative assessment of tyrosine phosphorylation. Raw fragmentation 'sequencing' spectra including parent ion abundances (represented as normalization level (NL)). Parent ion relative abundance for both phosphopeptides is in general agreement with what is observed from SILAC-based quantitative data. b-ion series is colored in 'red' and y-ion series in 'blue'.

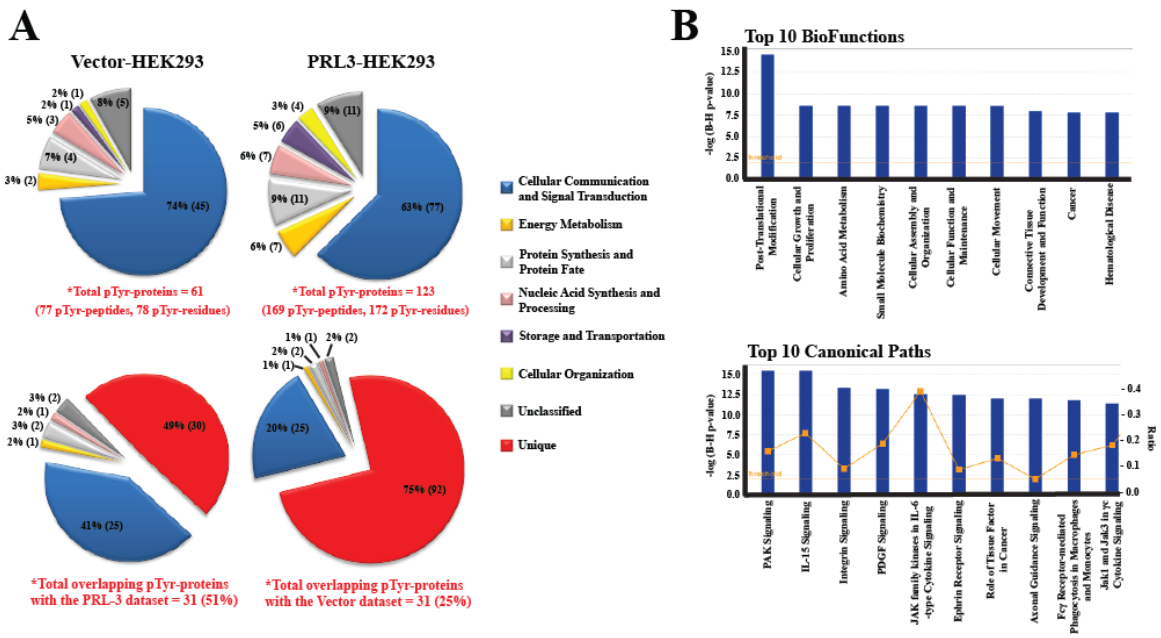

Figure 9: Ectopic PRL3 expression induces aberrant activation of mitogenic and chemotactic signal transduction. (A) Phosphoproteomic study summary in pie-chart format (sub-categories comprising each biofunctional bin can be seen in the entire curated dataset represented in Table 1). 75% of phosphoproteins are unique to the PRL3 expressing cells and concentrate within 'Cellular Communication and Signal Transduction'. **(B)** Ingenuity Pathway Analysis (IPA) results showing the Top 10 biofunctions and canonical pathways predicted from the phosphoproteomic dataset. Data significance is represented using a B-H (Benjamini-Hochberg) p-value adjustment to the false-discovery-rate (FDR; q-value). Phosphoproteomic data provide evidence in support of mitogenic and chemotactic signal transduction being prominently affected following ectopic PRL3 expression including significant representation of networks associated with p21/Cdc42/Rac1-activated kinase (PAK) and cytokine, integrin, PDGF, and Ephrin (Eph) receptor signaling.

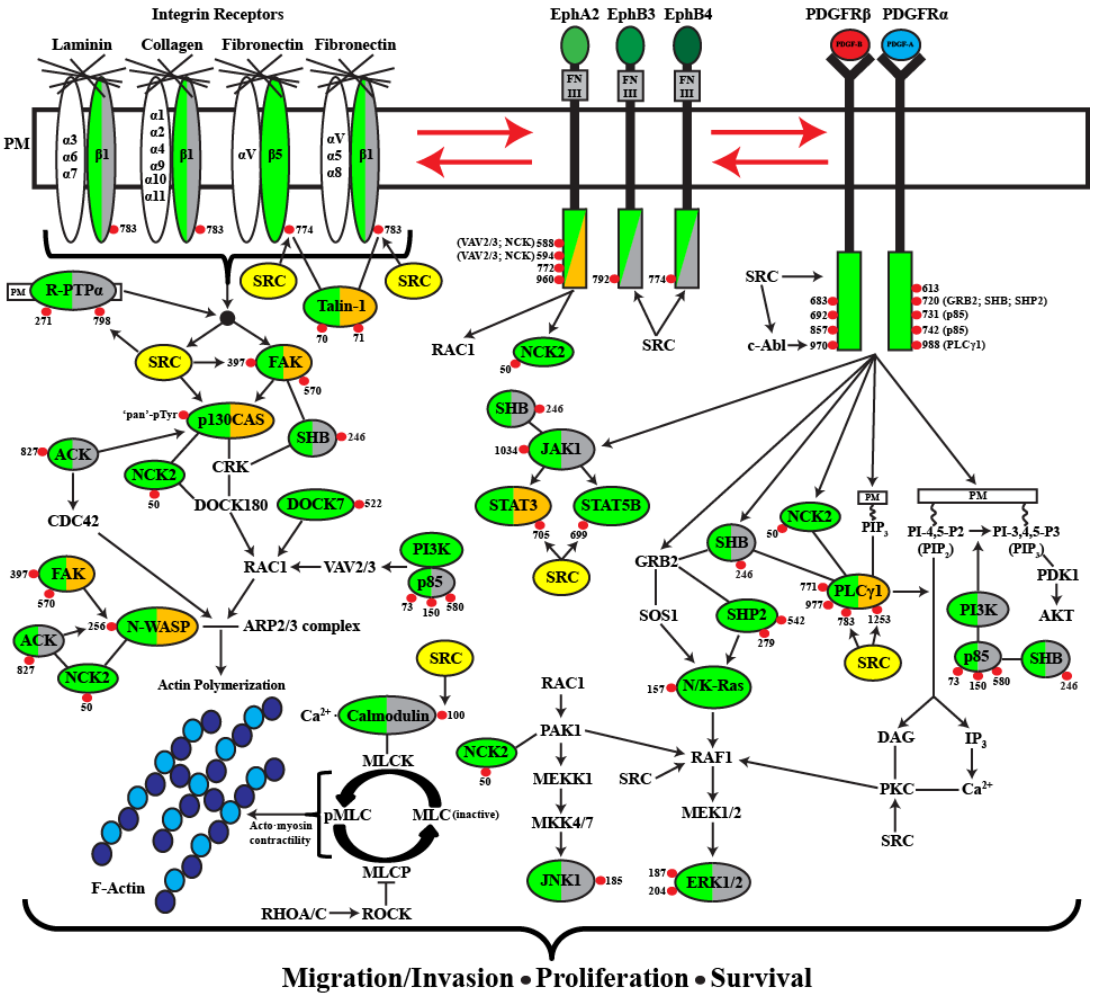

Figure 10: PRL3 potentiates pro-metastatic molecular events downstream of an aberrantly activated Src tyrosine kinase. Graphical model depicting phosphoproteomic data present within the PRL3 dataset that supports how PRL3 potentiates pro-metastatic molecular events through an aberrantly activated Src tyrosine kinase. Src kinase activates a signal transduction network associated with a mitogenic and chemotactic PDGF (α and β), Eph (A2, B3, B4), and Integrin (β1 and β5) receptor array in the PRL3 expressing cells. Proteins highlighted within green ovals represent phosphoproteins (red circles pTyr-residues) shown by both qualitative and SILAC-based quantitative mass analysis to be either upregulated or exclusively present within the PRL3 dataset. As compared to phosphoproteomic datasets by Rush (X) and Luo (X), while following the global impact of constitutively active SrcY529F overexpression in murine embryonic fibroblasts (MEFs), relative to their parental MEF counterparts, PRL3 cells display a notable oncogenic Src signature as well as significant fibroblast/mesenchymal-like signal transduction. Ovals are color-coded based upon this comparative analysis (completely green; unique to the PRL3 dataset, half-green/half-orange; in common with Src529F-MEF dataset, and half-green/half-grey; in common with MEF-control dataset). Non-highlighted proteins represent members of canonical signal transduction pathways assumed to be activated based upon data present within the PRL3 phosphoproteomic dataset. pTyr-residue number designation is based upon documented (NP and GI numbers) in Table 1.

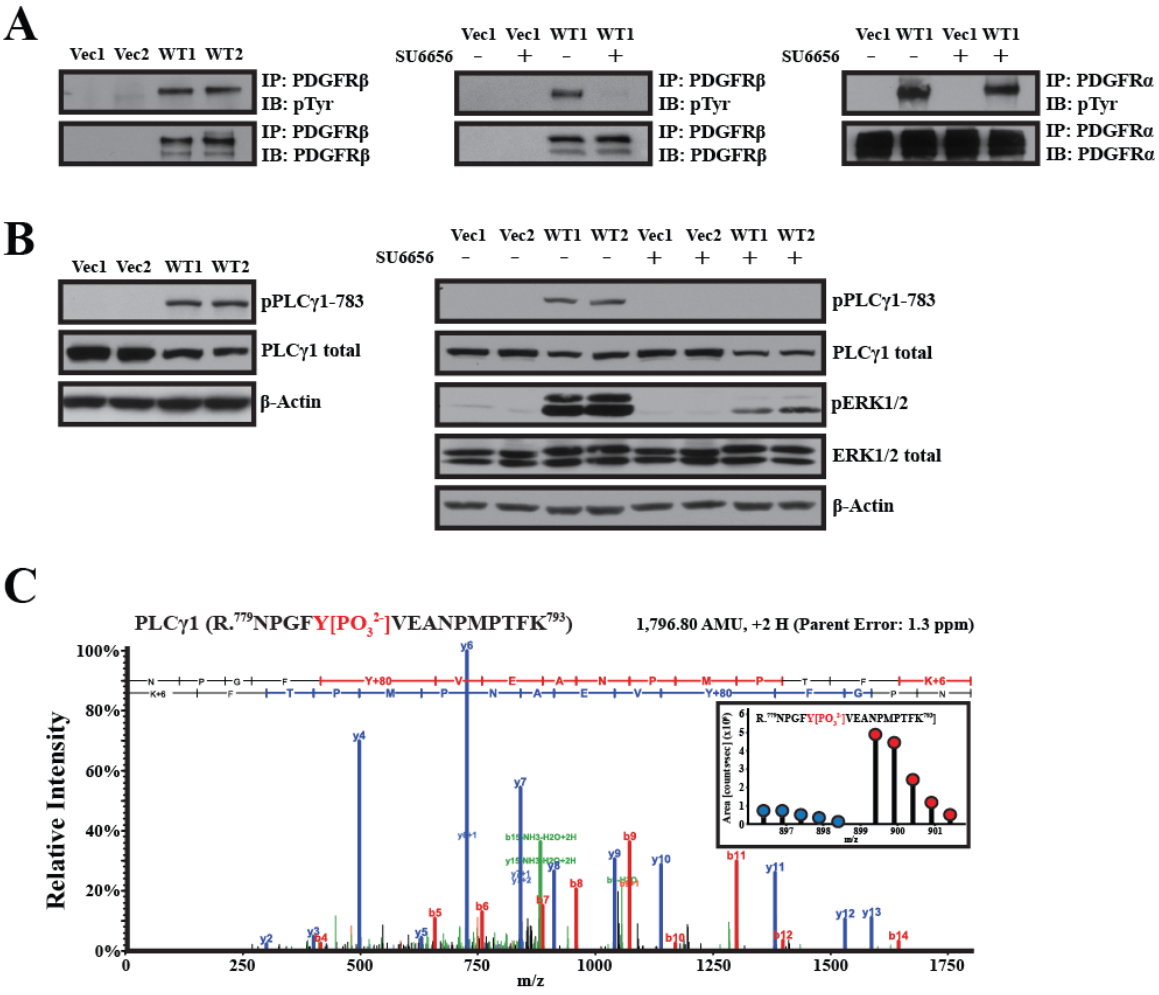

Figure 11: Ectopic PRL3 expression induces selective expression and/or stabilization of the PDGFβ-receptor and Src-dependent constitutive tyrosine phosphorylation of the PDGFβ-receptor and PLCγ1. (A) The PDGFβ-receptor is selectively expressed and/or stabilized and is constitutively phosphorylated in the PRL3 cells as assessed by PDGFRβ antibody-specific immunoprecipitation (IP) followed by 'pan'-pTyr immunoblotting. PDGFRβ phosphorylation is dependent upon the activity of the Src kinase as assessed by the use of the Src kinase chemical inhibitor (SU6656) at 2.5μM. **(B)** Phospholipase-C gamma 1 (PLCγ1) is constitutively phosphorylated in the PRL3 cells as assessed by phosphotyrosine-specific immunoblotting against pTyr-783. Phosphorylation of PLCγ1 on Tyr-783 is dependent upon the activity of the Src kinase. The attenuation of ERK1/2 phosphorylation using SU6656 is used as a positive control for SU6656-mediated Src kinase inhibition based upon our previous published results. **(C)** Data validation and spectral quality for pTyr783-PLCγ1 (^{779}NPGFY[PO_3^{2-}]VEANPMPTFK): Raw fragmentation 'sequencing' spectra including parent ion abundances (SILAC-based quantitative spectra: SILAC-'Light' (vector; blue points); SILAC-'Heavy' (PRL-3; red points)). b-ion series is colored in 'red' and y-ion series in 'blue'.

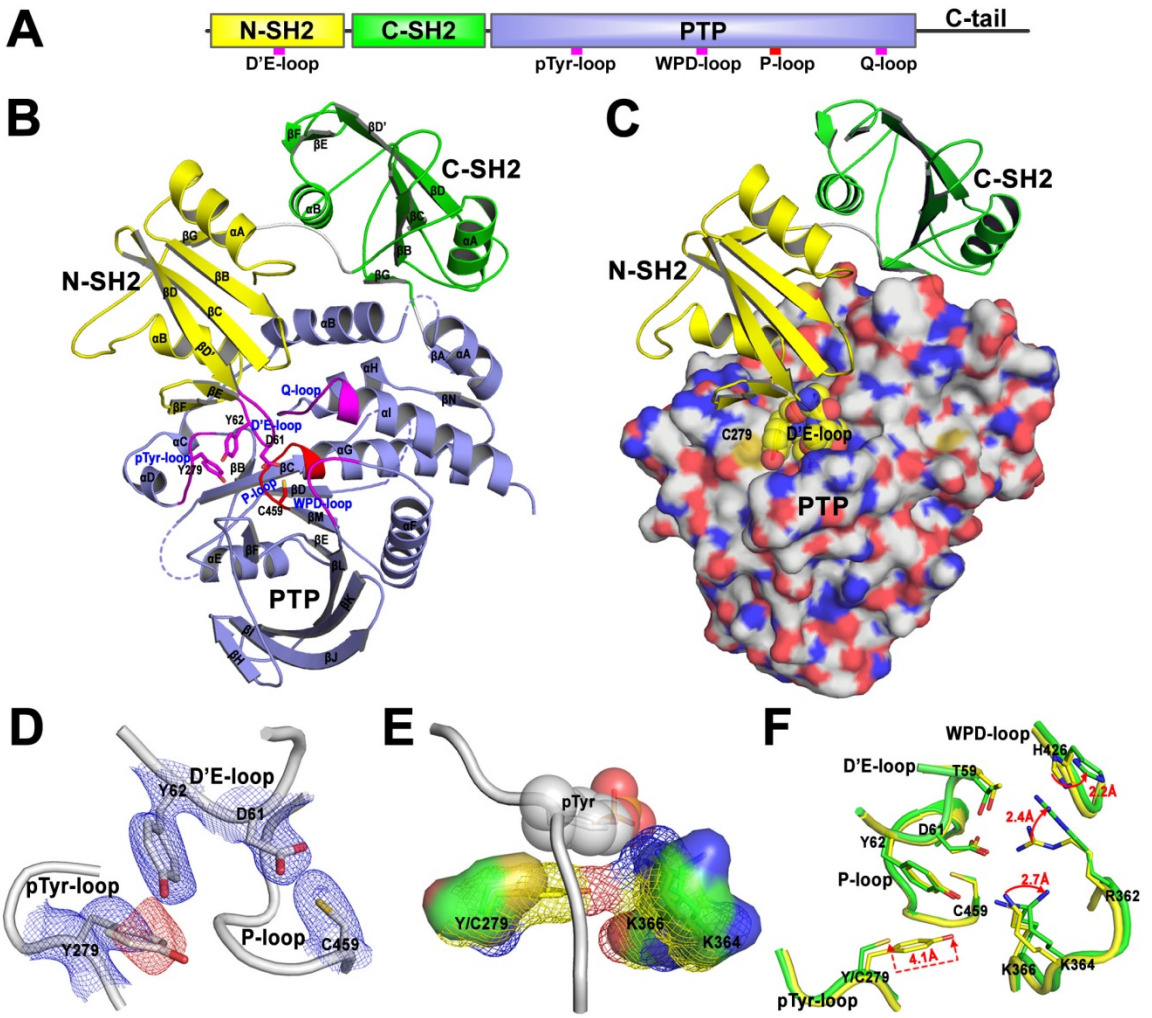

Figure 12: The crystal structures of the wild-type SHP2 and Y279C mutant. (A) Schematic diagram of SHP2. **(B)** The overall structure of the wild-type SHP2. N-SH2, C-SH2 and PTP domain are respectively colored in yellow, green and light-blue. The catalytic P-loop is highlighted in red and the other four important loops are highlighted in magenta. The dash lines represent three undetermined disordered loop in the crystal structures. **(C)** SHP2 Y279C mutant still poses the "closed" conformation with the D'E-loop (spheres) blocking the active site. **(D)** 2Fo-Fc map (contoured at -3σ, red) around Y279 show the mutation of Y279C. These density maps were calculated after the refinement of wild-type structure using the diffraction data of Y279C mutant. **(E)** Y279C mutation alters the substrate recognition surface constituted by Y279, K364 and K366, which is represented in mesh and solid surface respectively in wild-type and Y279C mutant. The bound pTyr (shown in spheres) was modeled by superimposing the SHP1-phosphopeptide complex (PDB#: 1FPR) onto the wild-type SHP2 structure. **(F)** Y279C mutation decreases the interactions of N-SH2 with PTP domain. Residues resulting in the decreased interactions are shown in stick (yellow for wild-type SHP2) and green for Y279C mutant).

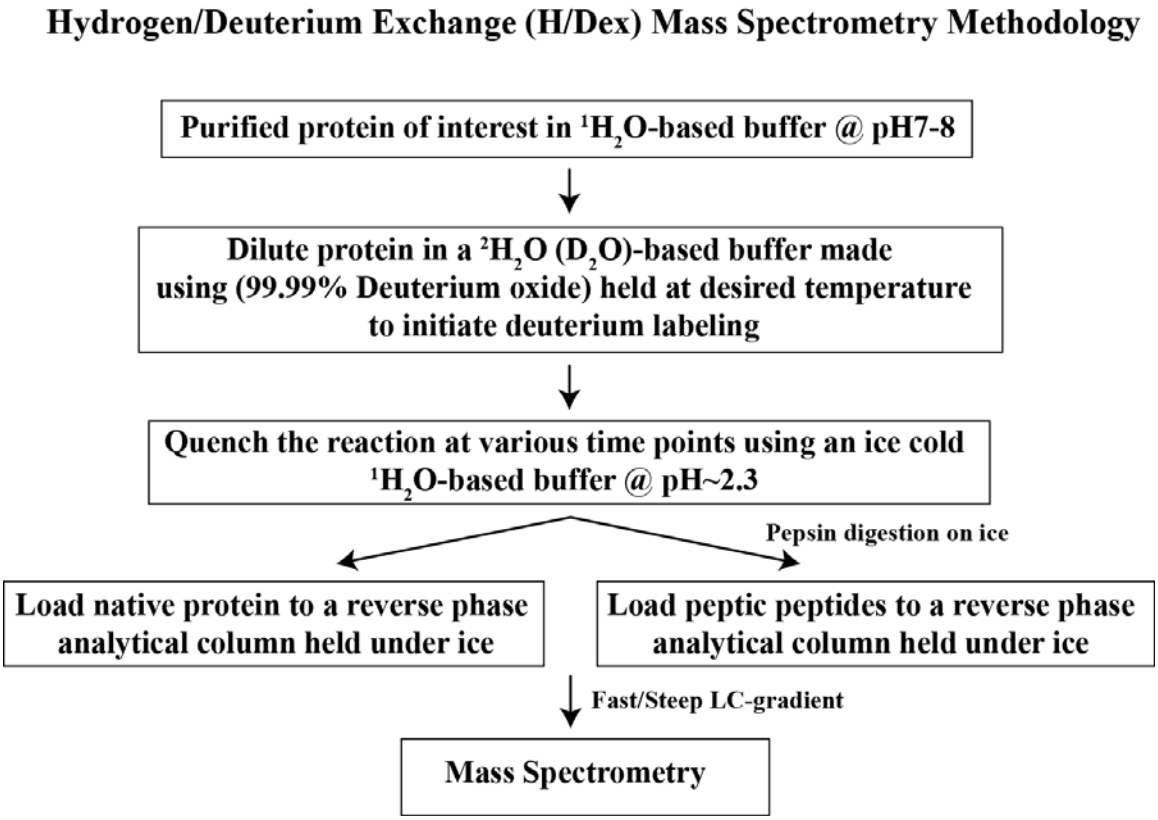

Figure 13: Hydrogen/Deuterium exchange mass spectrometry (H/DX-MS) methodology flow-chart. Purified SHP2 (1-528) mutant and wild-type constructs are incubated in deuterium oxide (D_2O; ^2H_2O) for various times over a 1hr. period, whereby the deuterium labeling reaction is quenched using a low pH buffer. Labeled native/intact proteins are either directly analyzed by mass spectrometry or subjected to a pepsin-mediated digestion to generate peptic peptides that are then analyzed by mass spectrometry. Mass analysis is carried out as protein/peptides leave reverse-phase (RP) liquid chromatography by electrospray.

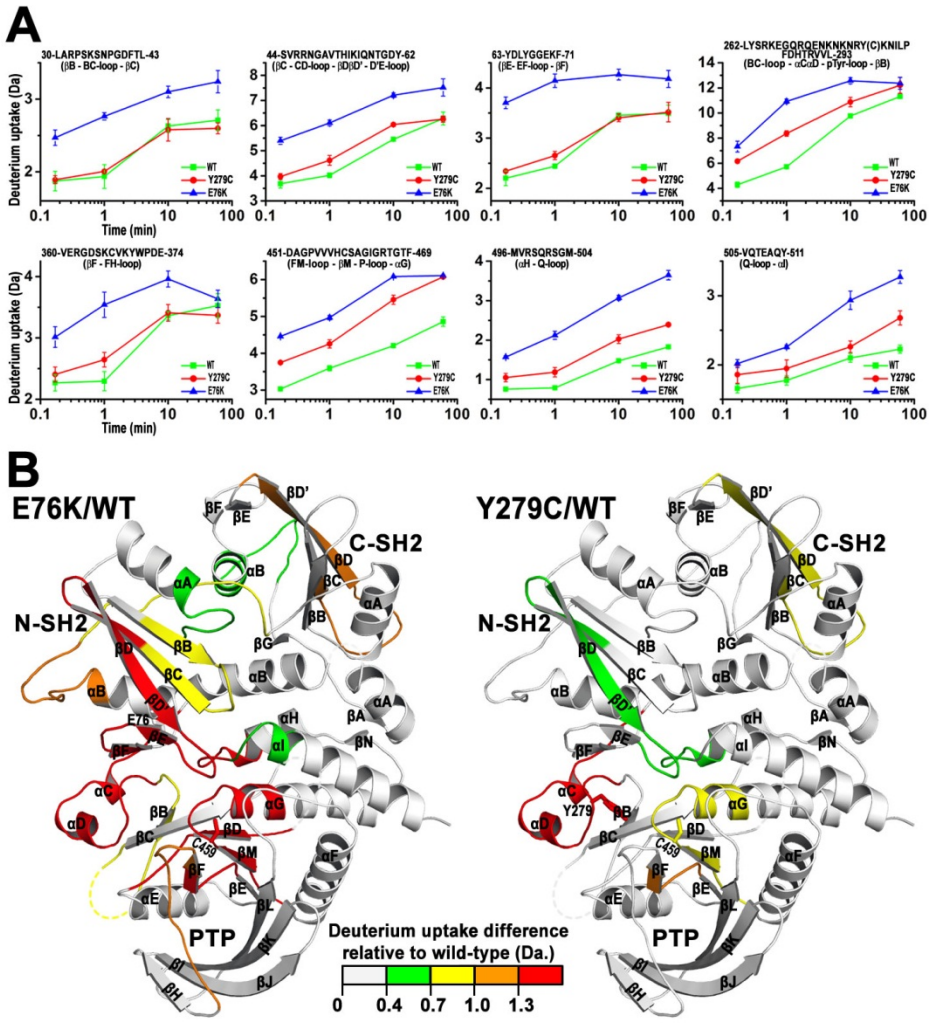

Figure 14: SHP2 mutants E76K and Y279C show increased conformational dynamic flexibility in solution within the interface region between the N-SH2 and PTP domains relative to the wild-type (WT) enzyme as assessed by hydrogen-deuterium exchange mass spectrometry (H/DX-MS). (A) Representative comparative deuterium exchange plots for peptides within the E76K and Y279C N-SH2/PTP domain interface regions that attain significant exchange relative to WT. Secondary-structure elements are documented so that they can be located in (B). **(B)** 'Heat map' showing significantly increased deuterium exchange for both the E76K and Y279C mutants relative to the WT enzyme at the 1 min time point of deuterium labeling modeled on the WT structure crystal (3OLR). WT as all grey and mutants color coded based upon increased exchange relative to WT as described in the legend. Peptides are colored when they attain exchange significance at two consecutive time points and at least 2σ (st.dev.) relative to WT values. The catalytic cysteine (Cys459) is labeled for active site orientation.

Native Deuterium Exchange Data Acquisition/Analysis

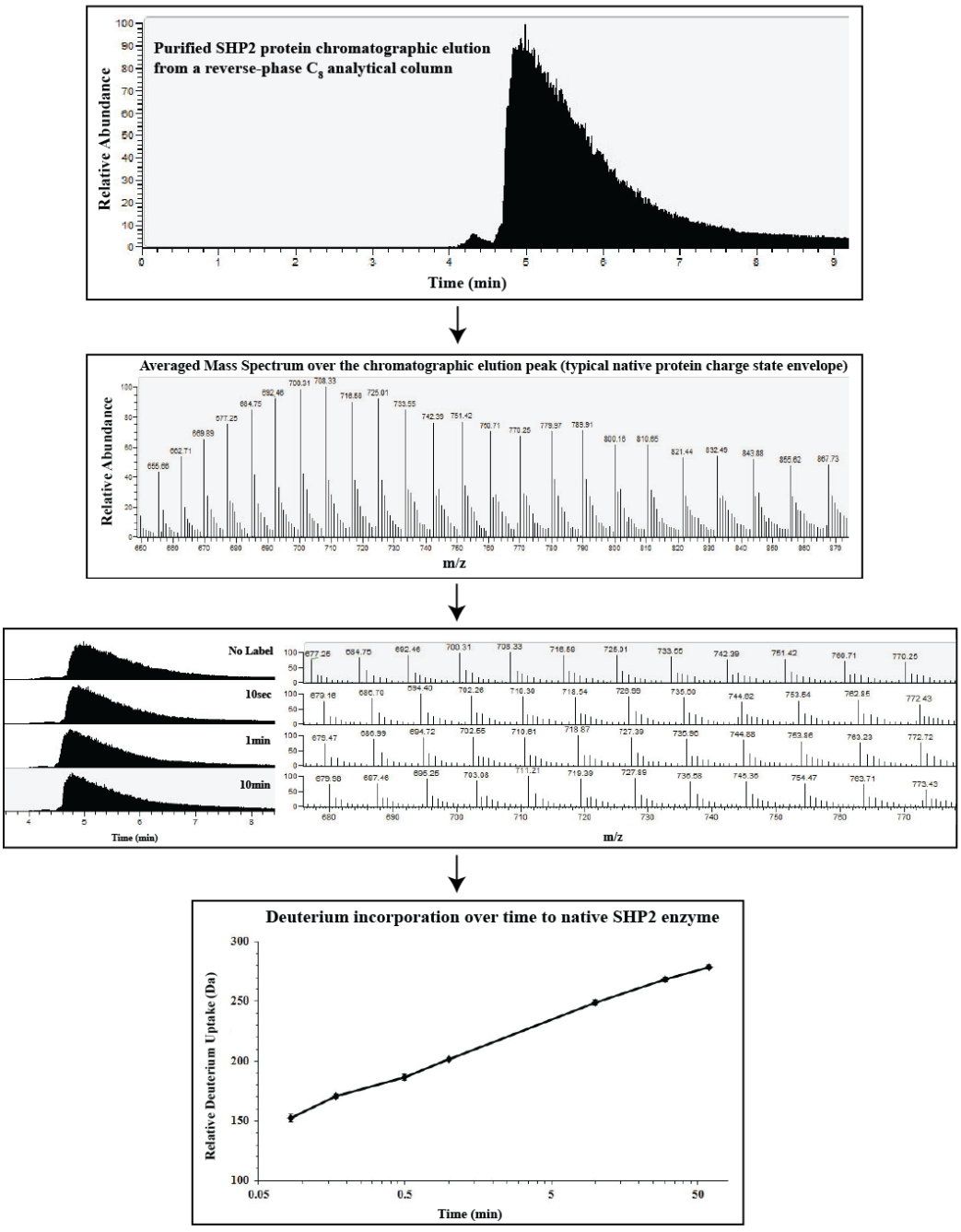

Figure 15: Native/Intact H/DX-MS data acquisition and analysis. Quality of native/intact protein mass spectra used in this analysis. The first panel represents the chromatography associated with the elution of the intact protein from the reverse-phase (RP) analytical column. Panels 2 and 3 represent the intact mass charge envelope for a purified SHP2 protein and the mass-to-charge (m/z) ratios of the monoisotopic peaks as they change over time relative to the degree by which deuterium labeling occurs. Panel 4 represents a general deuterium incorporation over time plot following spectral deconvolution to acquire true mass from the convoluted raw mass spectrum.

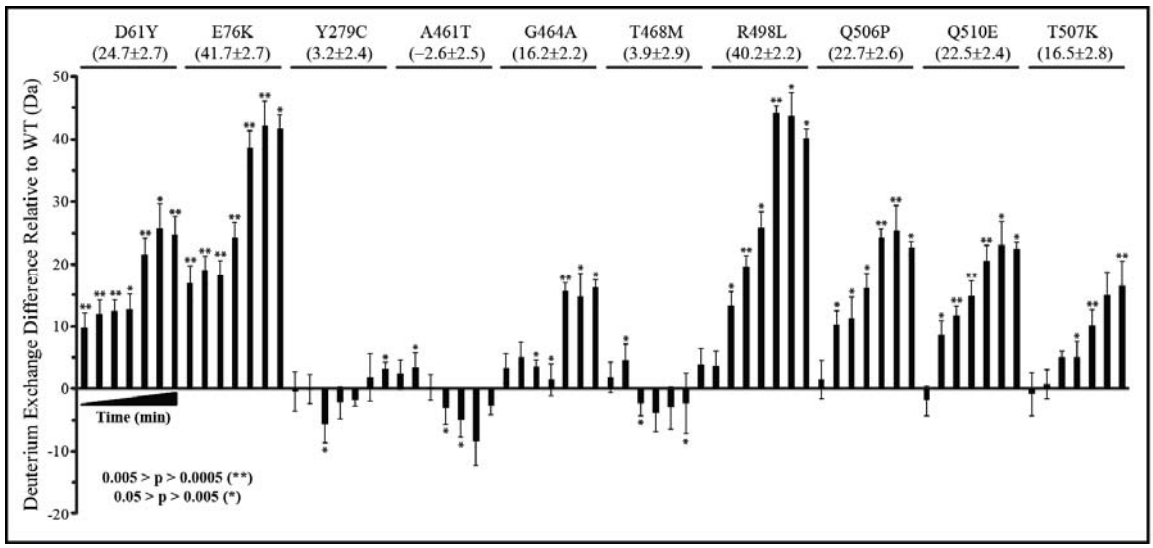

Figure 16: H/D-exchange to native/intact SHP2 (1-528) enzymes. Hydrogen exchange was measured from 5s-1h (5s, 10s, 30s, 1m, 10m, 30m, 1h) and plotted in bar-chart format with error bars representing measurement standard deviation (triplicate measurement per time point). Measurement significance is provided as p-values generated from a comparison of two means via a paired *t*-test. Relative to WT, gain-of-function (GOF) SHP2-D61Y and E76K show significant hydrogen exchange by the earliest time point that extends through the entire measurement period, suggesting that these mutants experience very minor N-SH2 domain-mediated autoinhibition. Conversely, a disparity exists in the magnitude of hydrogen exchange experienced by the LS-SHP2 mutants, relative to WT. Mutants with pTyr-/P-loop-directed mutations (e.g. Y279C, A461T, G464A, and T468M) experience markedly less hydrogen exchange than those mutants with 'Q' (HI)-loop-directed mutations (e.g. R498L, Q506P, and Q510E). Hydrogen exchange observed within the non-LS-SHP2 mutant (T507K) with a Q-loop-directed mutation, further justifies the importance of the catalytic Q-loop structure as a major element responsible for upholding N-SH2 domain-mediated intramolecular autoinhibition in a latent state.

Peptide Deuterium Exchange Data Acquisition/Analysis

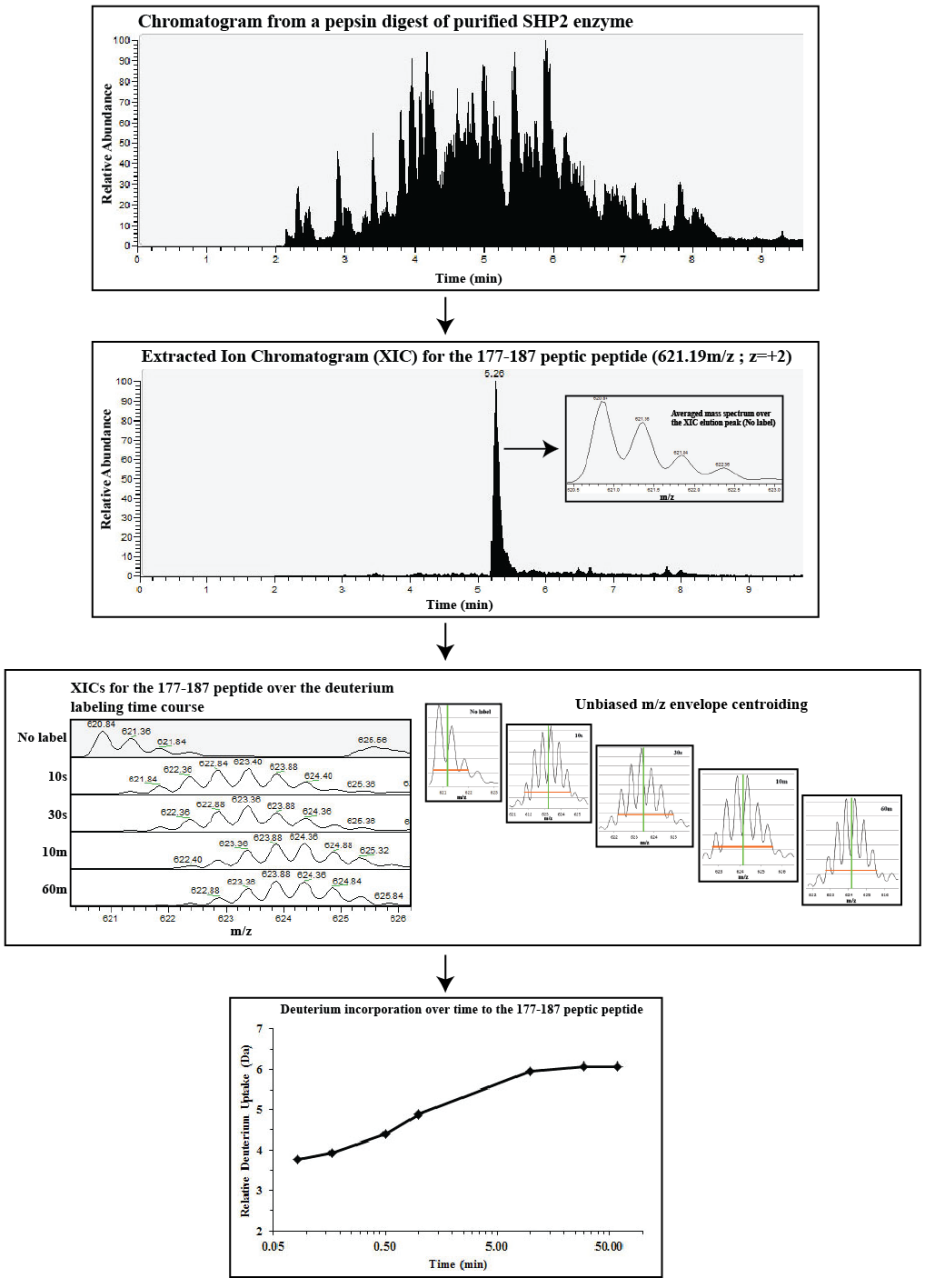

Figure 17: Peptide H/DX-MS data acquisition and analysis. Quality of peptic peptide mass spectra used in this analysis. The first panel represents the chromatography associated with the elution of peptic peptides from the reverse-phase (RP) analytical column. Panels 2 and 3 represent the parent ion isotopic distribution of a single peptide as it increases in mass over time according to the extent of deuterium labeling Unbiased peak envelope centroiding to get weighted average mass (WAM) values is done by HX-Express (Weiss2006). Panel 4 represents a general deuterium incorporation over time plot following WAM value interpretation by HX-Express.

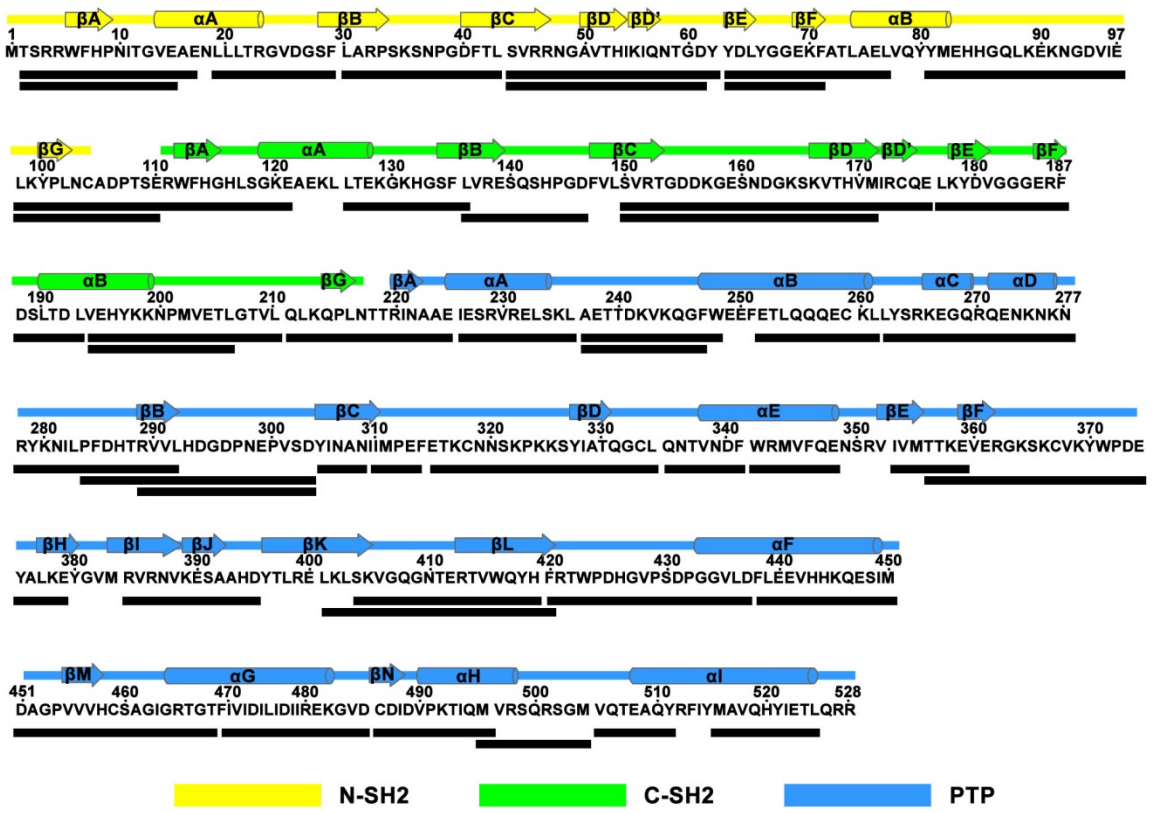

Figure 18: Peptide H/DX-MS 2-D sequence coverage map. Linear primary amino acid sequence for SHP2 wild-type (WT) (1-528) with corresponding 2º-structures labeled. Domain arrangement is color-coded (N-SH2, yellow), (C-SH2, green), and (PTP, blue). The 46 peptic peptides used in the H/DX-MS analysis encompass ~95% of the (1-528) amino acid sequence. Peptides are represented in this figure under the primary amino acid sequence as black bars.

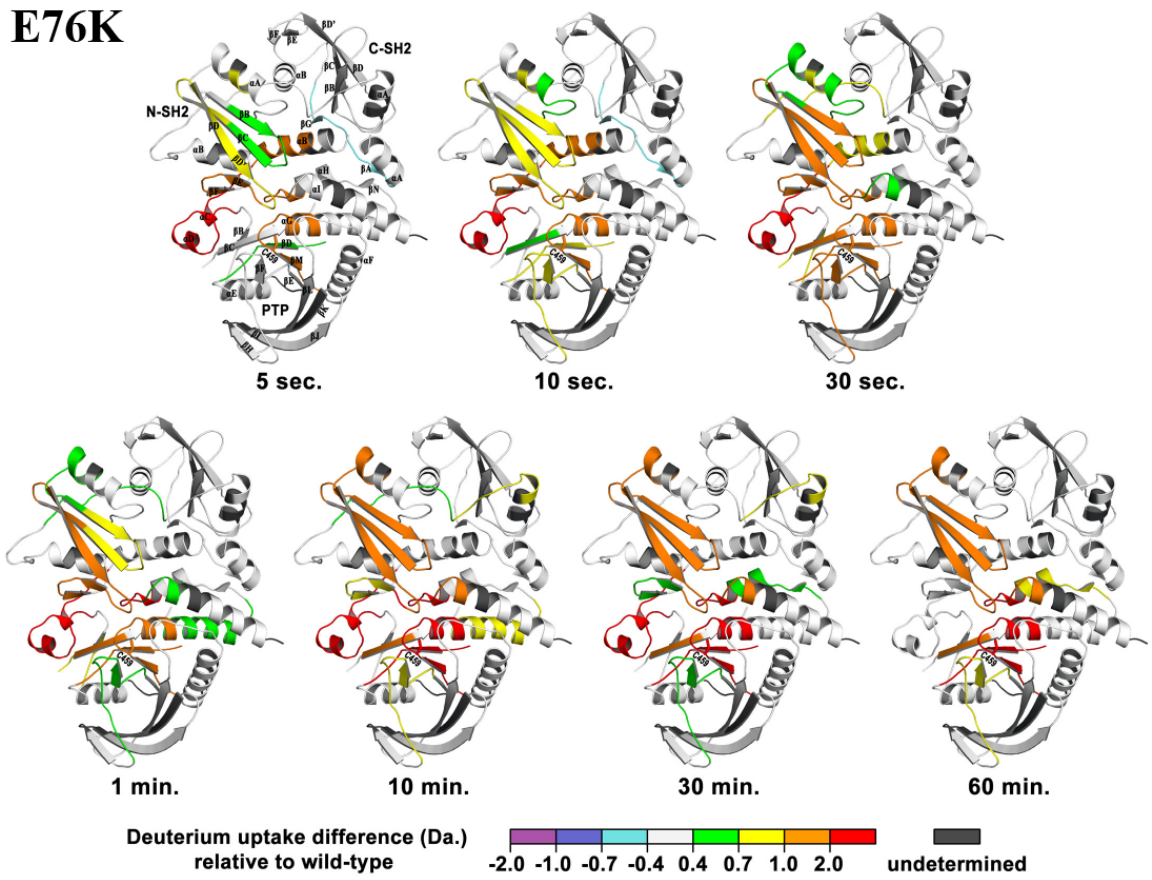

Figure 19: Differential H/DX experienced by the GOF SHP2-E76K pathogenic mutant. Differential hydrogen exchange experienced by the gain-of-function (GOF) SHP2-E76K pathogenic mutant enzyme, relative to the wild-type (WT) enzyme. Differential exchange data is modeled on the WT structure crystal (3OLR). WT as all grey and mutants color coded based upon increased exchange relative to WT as described in the legend. Peptides are colored when they attain exchange significance at two consecutive time points and at least 2σ (st.dev.) relative to WT values. The N-SH2, C-SH2, and PTP domains as well as corresponding 2º-structural elements are labeled in the primary (5s) time point. The catalytic cysteine (Cys459) is labeled for active site orientation.

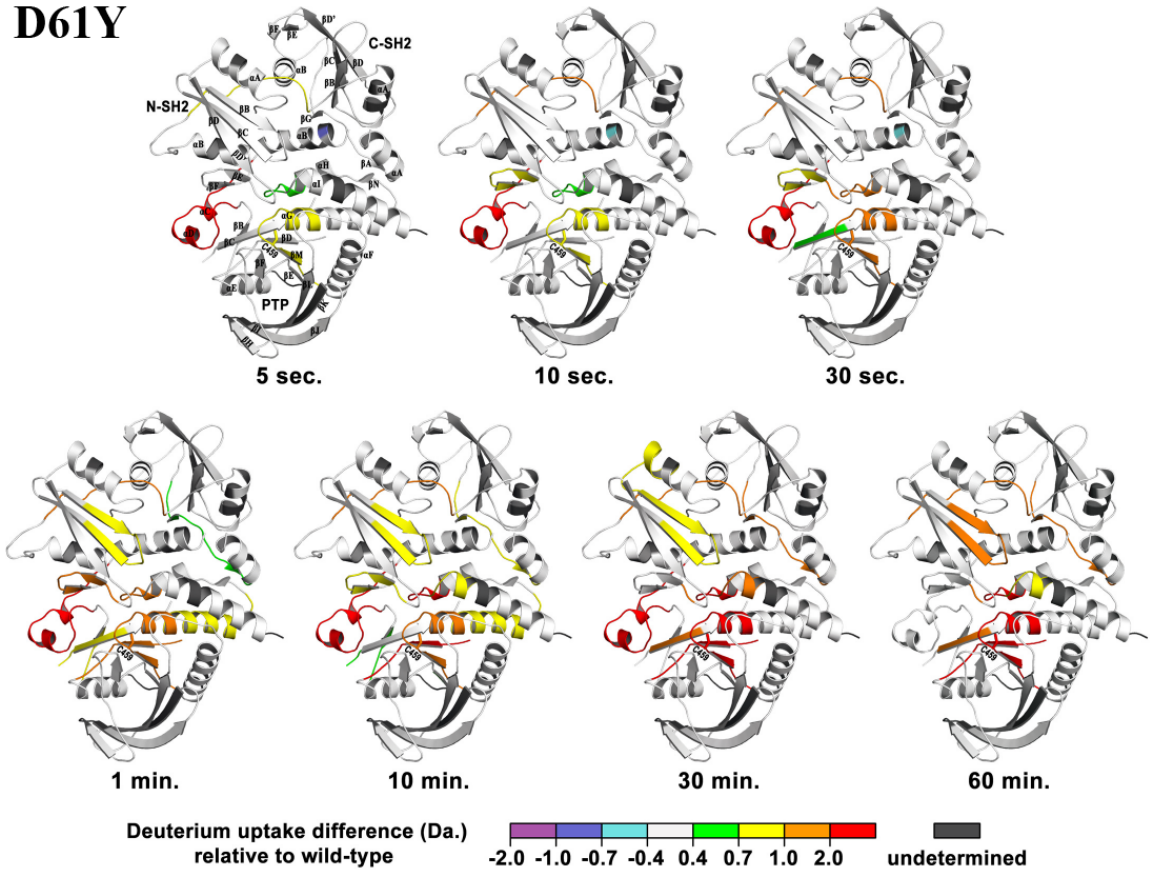

Figure 20: Differential H/DX experienced by the GOF SHP2-D61Y pathogenic mutant. Differential hydrogen exchange experienced by the gain-of-function (GOF) SHP2-D61Y pathogenic mutant enzyme, relative to the wild-type (WT) enzyme. Differential exchange data is modeled on the WT structure crystal (3OLR). WT as all grey and mutants color coded based upon increased exchange relative to WT as described in the legend. Peptides are colored when they attain exchange significance at two consecutive time points and at least 2σ (st.dev.) relative to WT values. The N-SH2, C-SH2, and PTP domains as well as corresponding 2º-structural elements are labeled in the primary (5s) time point. The catalytic cysteine (Cys459) is labeled for active site orientation.

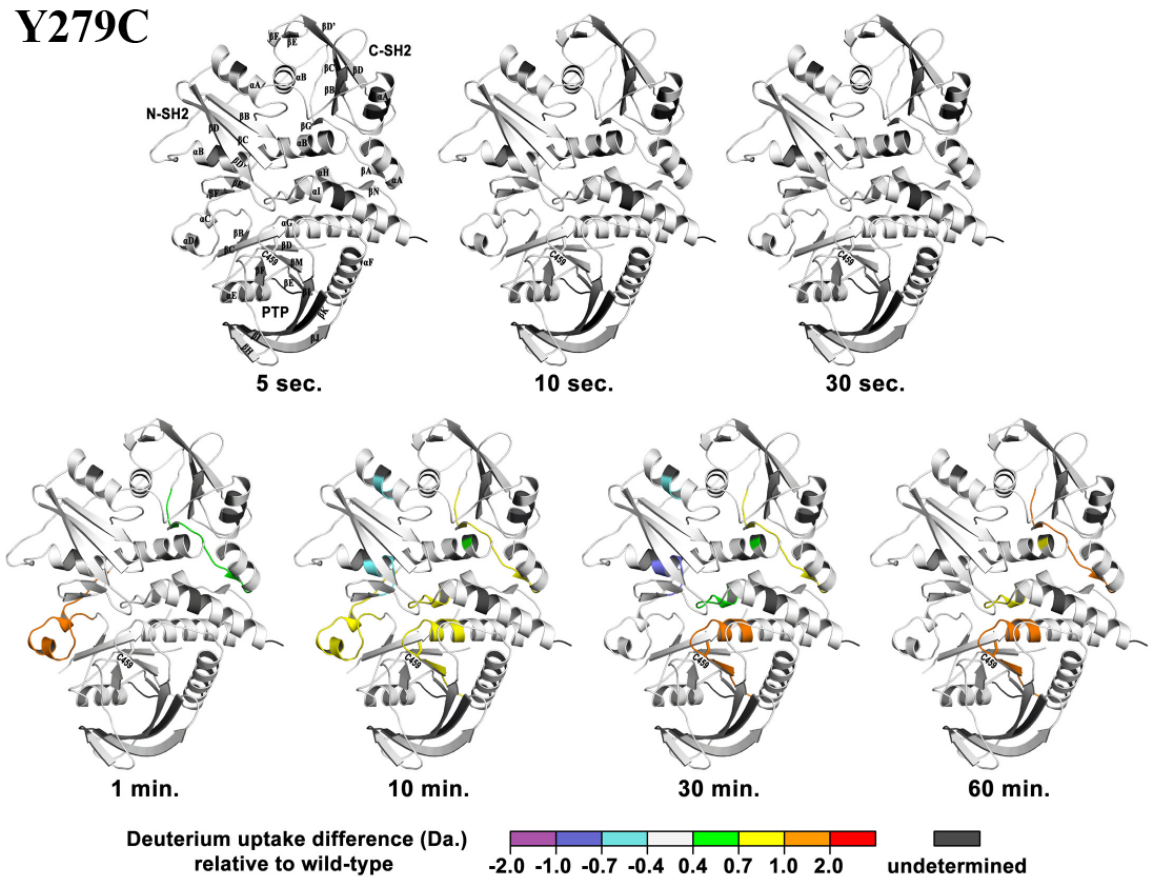

Figure 21: Differential H/DX experienced by the LS-SHP2-Y279C pathogenic mutant. Differential hydrogen exchange experienced by the LS-SHP2-Y279C pathogenic mutant enzyme, relative to the wild-type (WT) enzyme. Differential exchange data is modeled on the WT structure crystal (3OLR). WT as all grey and mutants color coded based upon increased exchange relative to WT as described in the legend. Peptides are colored when they attain exchange significance at two consecutive time points and at least 2σ (st.dev.) relative to WT values. The N-SH2, C-SH2, and PTP domains as well as corresponding 2º-structural elements are labeled in the primary (5s) time point. The catalytic cysteine (Cys459) is labeled for active site orientation.

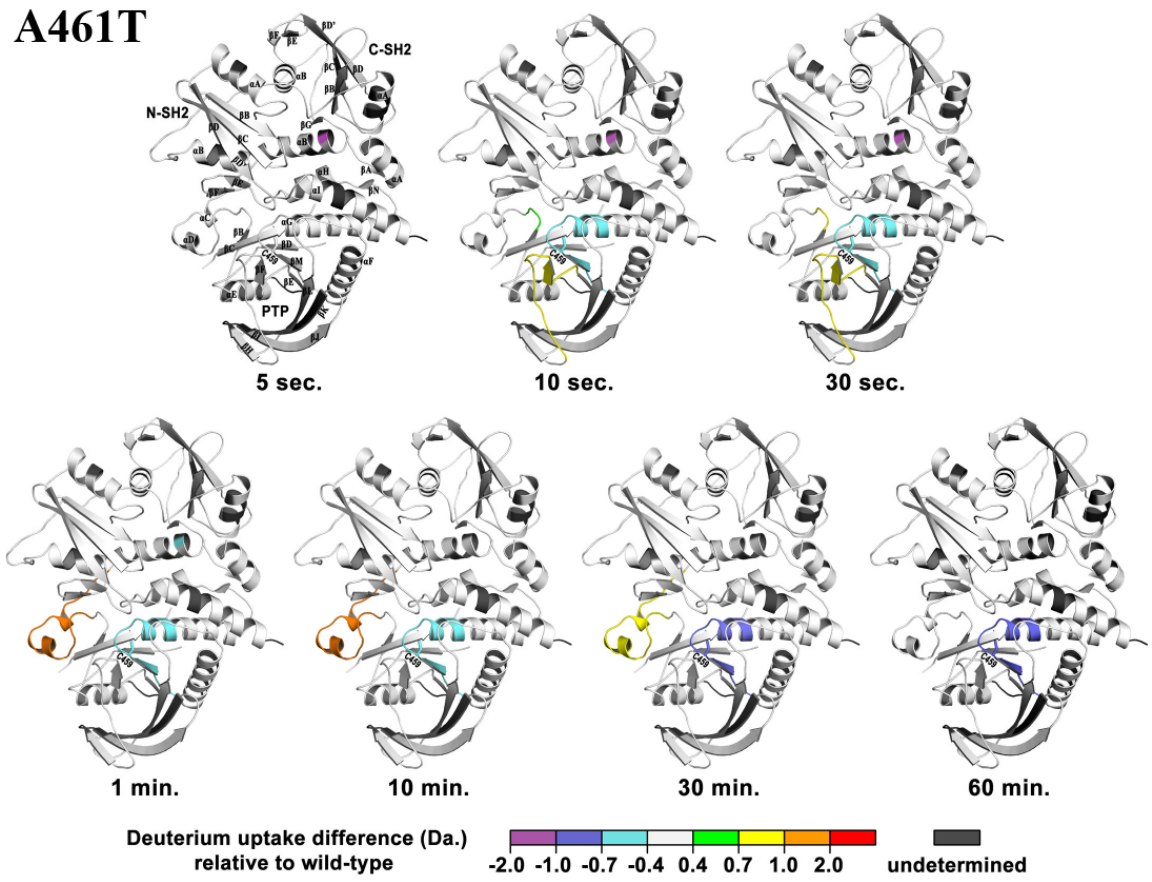

Figure 22: Differential H/DX experienced by the LS-SHP2-A461T pathogenic mutant. Differential hydrogen exchange experienced by the LS-SHP2-A461T pathogenic mutant enzyme, relative to the wild-type (WT) enzyme. Differential exchange data is modeled on the WT structure crystal (3OLR). WT as all grey and mutants color coded based upon increased exchange relative to WT as described in the legend. Peptides are colored when they attain exchange significance at two consecutive time points and at least 2σ (st.dev.) relative to WT values. The N-SH2, C-SH2, and PTP domains as well as corresponding 2º-structural elements are labeled in the primary (5s) time point. The catalytic cysteine (Cys459) is labeled for active site orientation.

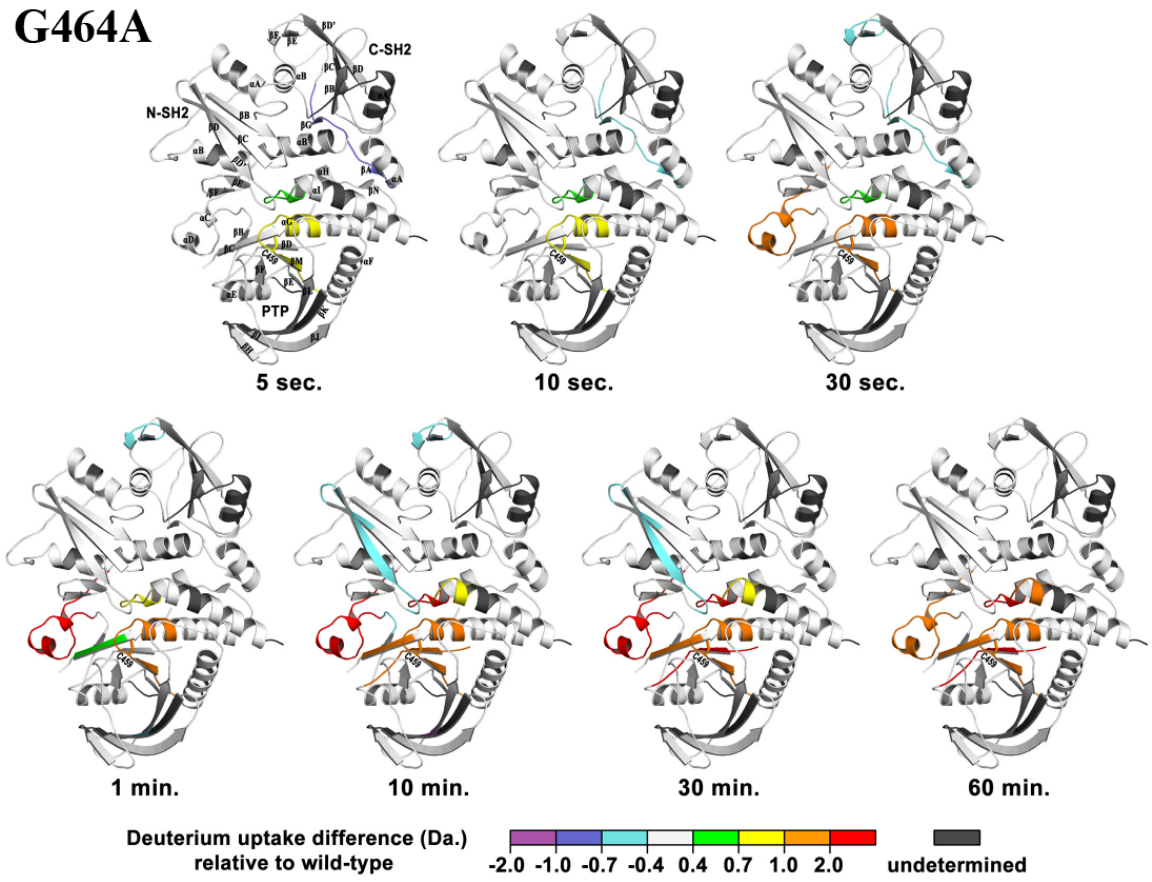

Figure 23: Differential H/DX experienced by the LS-SHP2-G464A pathogenic mutant. Differential hydrogen exchange experienced by the LS-SHP2-G464A pathogenic mutant enzyme, relative to the wild-type (WT) enzyme. Differential exchange data is modeled on the WT structure crystal (3OLR). WT as all grey and mutants color coded based upon increased exchange relative to WT as described in the legend. Peptides are colored when they attain exchange significance at two consecutive time points and at least 2σ (st.dev.) relative to WT values. The N-SH2, C-SH2, and PTP domains as well as corresponding 2º-structural elements are labeled in the primary (5s) time point. The catalytic cysteine (Cys459) is labeled for active site orientation.

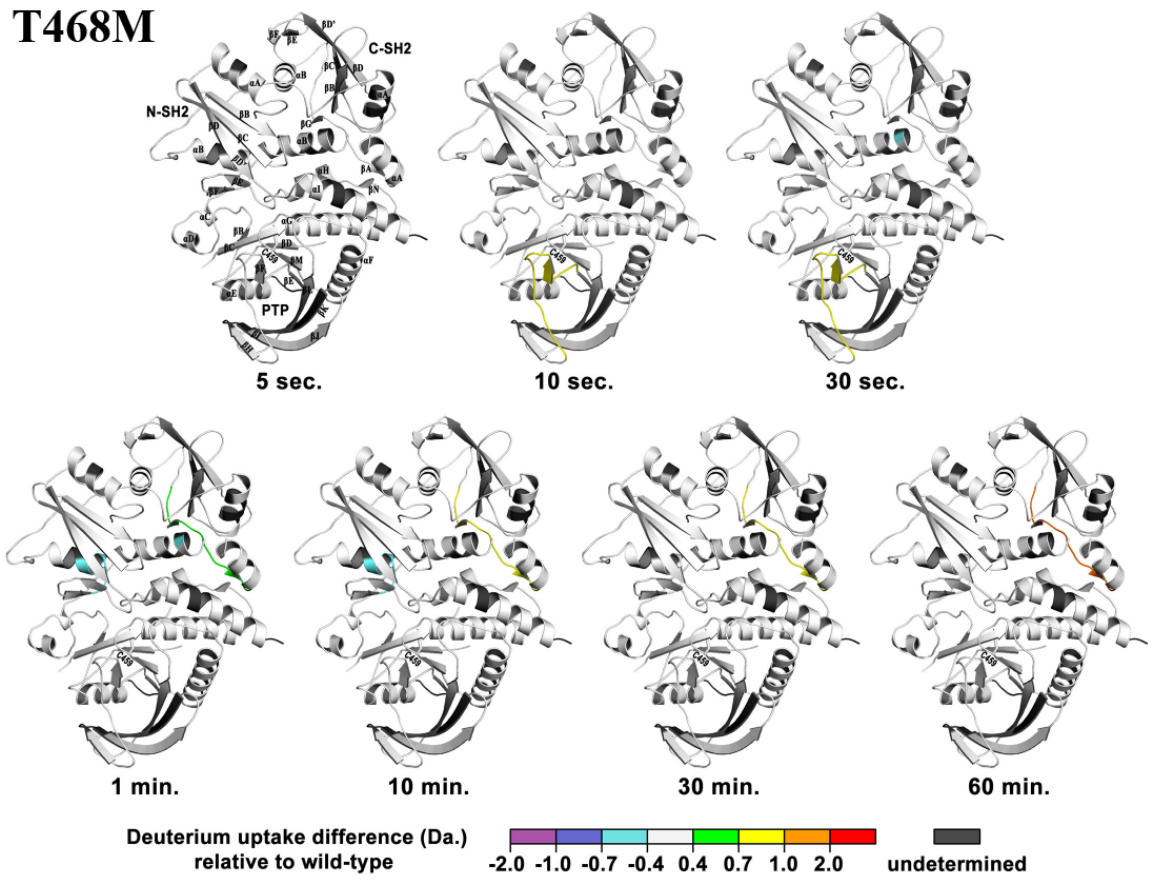

Figure 24: Differential H/DX experienced by the LS-SHP2-T468M pathogenic mutant. Differential hydrogen exchange experienced by the LS-SHP2-T468M pathogenic mutant enzyme, relative to the wild-type (WT) enzyme. Differential exchange data is modeled on the WT structure crystal (3OLR). WT as all grey and mutants color coded based upon increased exchange relative to WT as described in the legend. Peptides are colored when they attain exchange significance at two consecutive time points and at least 2σ (st.dev.) relative to WT values. The N-SH2, C-SH2, and PTP domains as well as corresponding 2º-structural elements are labeled in the primary (5s) time point. The catalytic cysteine (Cys459) is labeled for active site orientation.

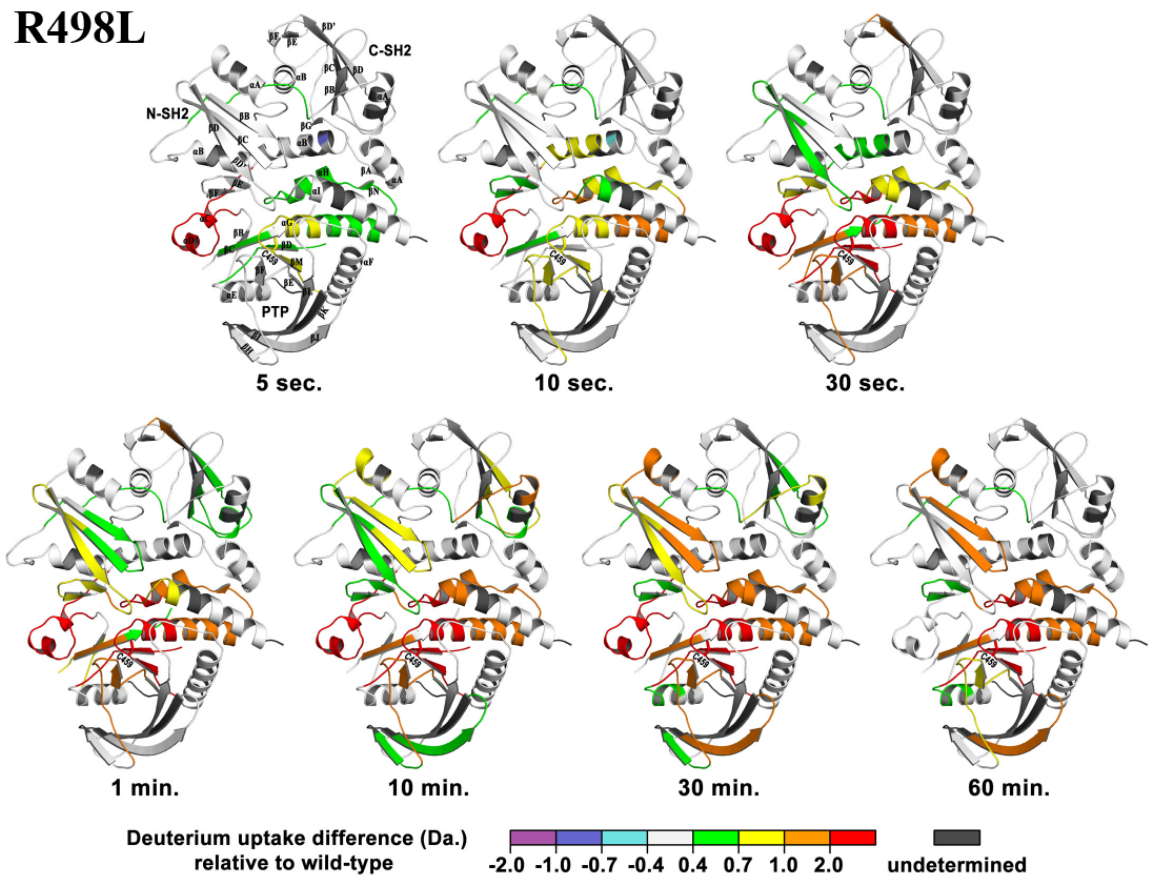

Figure 25: Differential H/DX experienced by the LS-SHP2-R498L pathogenic mutant. Differential hydrogen exchange experienced by the LS-SHP2-R498L pathogenic mutant enzyme, relative to the wild-type (WT) enzyme. Differential exchange data is modeled on the WT structure crystal (3OLR). WT as all grey and mutants color coded based upon increased exchange relative to WT as described in the legend. Peptides are colored when they attain exchange significance at two consecutive time points and at least 2σ (st.dev.) relative to WT values. The N-SH2, C-SH2, and PTP domains as well as corresponding 2º-structural elements are labeled in the primary (5s) time point. The catalytic cysteine (Cys459) is labeled for active site orientation.

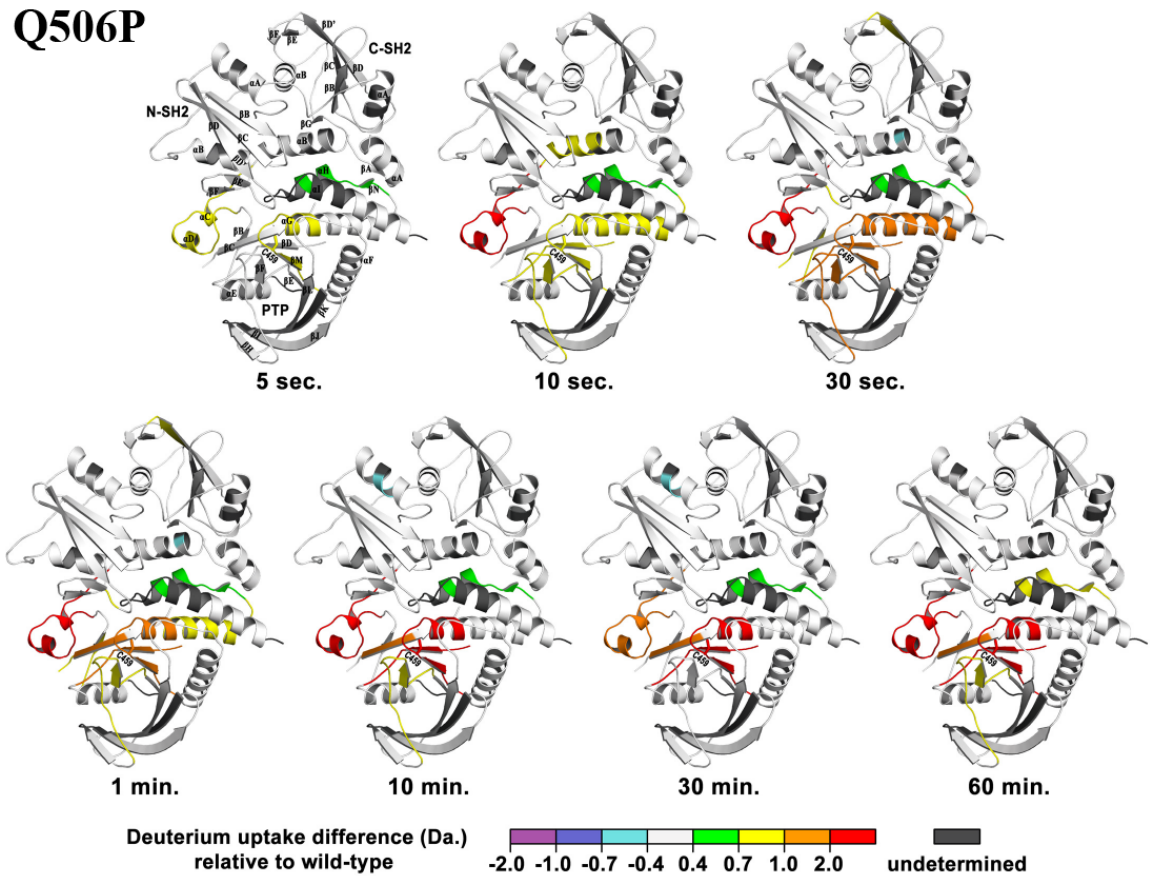

Figure 26: Differential H/DX experienced by the LS-SHP2-Q506P pathogenic mutant. Differential hydrogen exchange experienced by the LS-SHP2-Q506P pathogenic mutant enzyme, relative to the wild-type (WT) enzyme. Differential exchange data is modeled on the WT structure crystal (3OLR). WT as all grey and mutants color coded based upon increased exchange relative to WT as described in the legend. Peptides are colored when they attain exchange significance at two consecutive time points and at least 2σ (st.dev.) relative to WT values. The N-SH2, C-SH2, and PTP domains as well as corresponding 2º-structural elements are labeled in the primary (5s) time point. The catalytic cysteine (Cys459) is labeled for active site orientation.

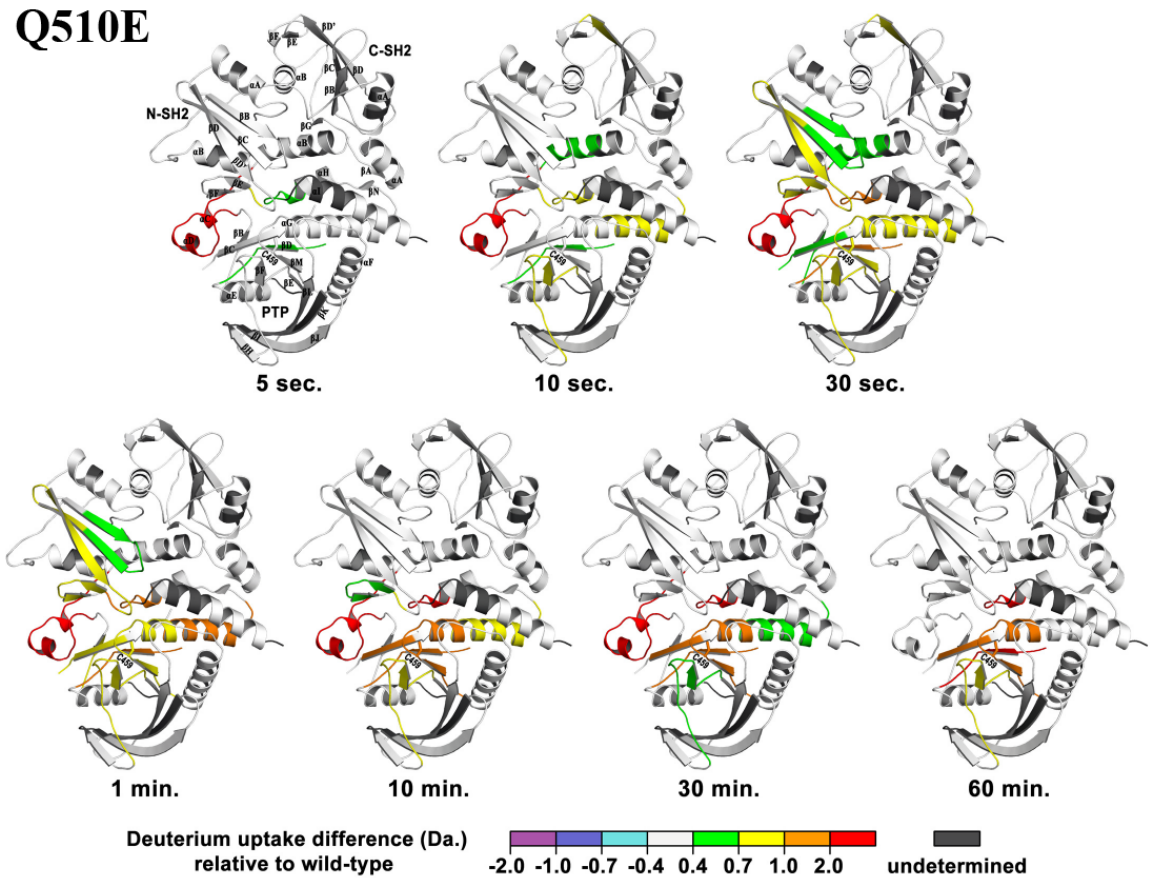

Figure 27: Differential H/DX experienced by the LS-SHP2-Q510E pathogenic mutant. Differential hydrogen exchange experienced by the LS-SHP2-Q510E pathogenic mutant enzyme, relative to the wild-type (WT) enzyme. Differential exchange data is modeled on the WT structure crystal (3OLR). WT as all grey and mutants color coded based upon increased exchange relative to WT as described in the legend. Peptides are colored when they attain exchange significance at two consecutive time points and at least 2σ (st.dev.) relative to WT values. The N-SH2, C-SH2, and PTP domains as well as corresponding 2º-structural elements are labeled in the primary (5s) time point. The catalytic cysteine (Cys459) is labeled for active site orientation.

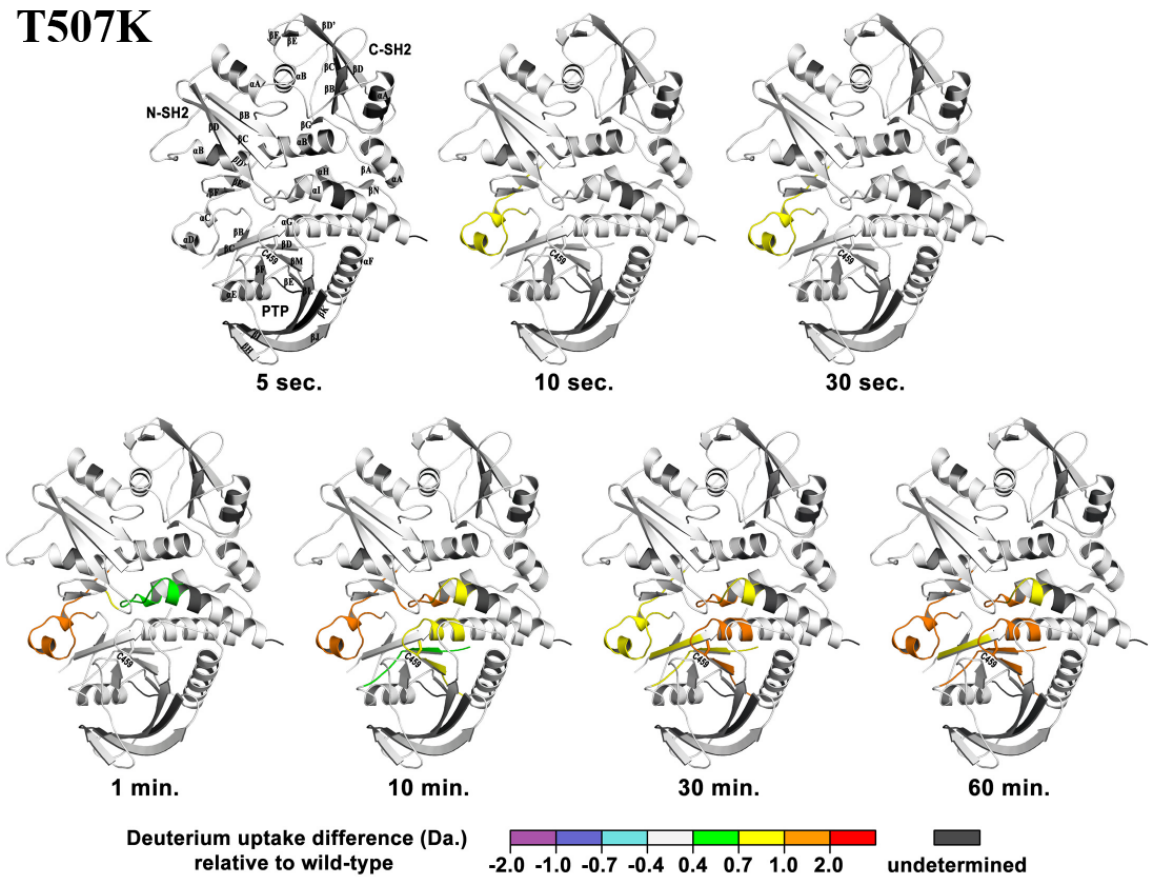

Figure 28: Differential H/DX experienced by the solid tumor-associated SHP2-T507K pathogenic mutant. Differential hydrogen exchange experienced by the solid tumor-associated SHP2-T507K pathogenic mutant enzyme, relative to the wild-type (WT) enzyme. Differential exchange data is modeled on the WT structure crystal (3OLR). WT as all grey and mutants color coded based upon increased exchange relative to WT as described in the legend. Peptides are colored when they attain exchange significance at two consecutive time points and at least 2σ (st.dev.) relative to WT values. The N-SH2, C-SH2, and PTP domains as well as corresponding 2º-structural elements are labeled in the primary (5s) time point. The catalytic cysteine (Cys459) is labeled for active site orientation.

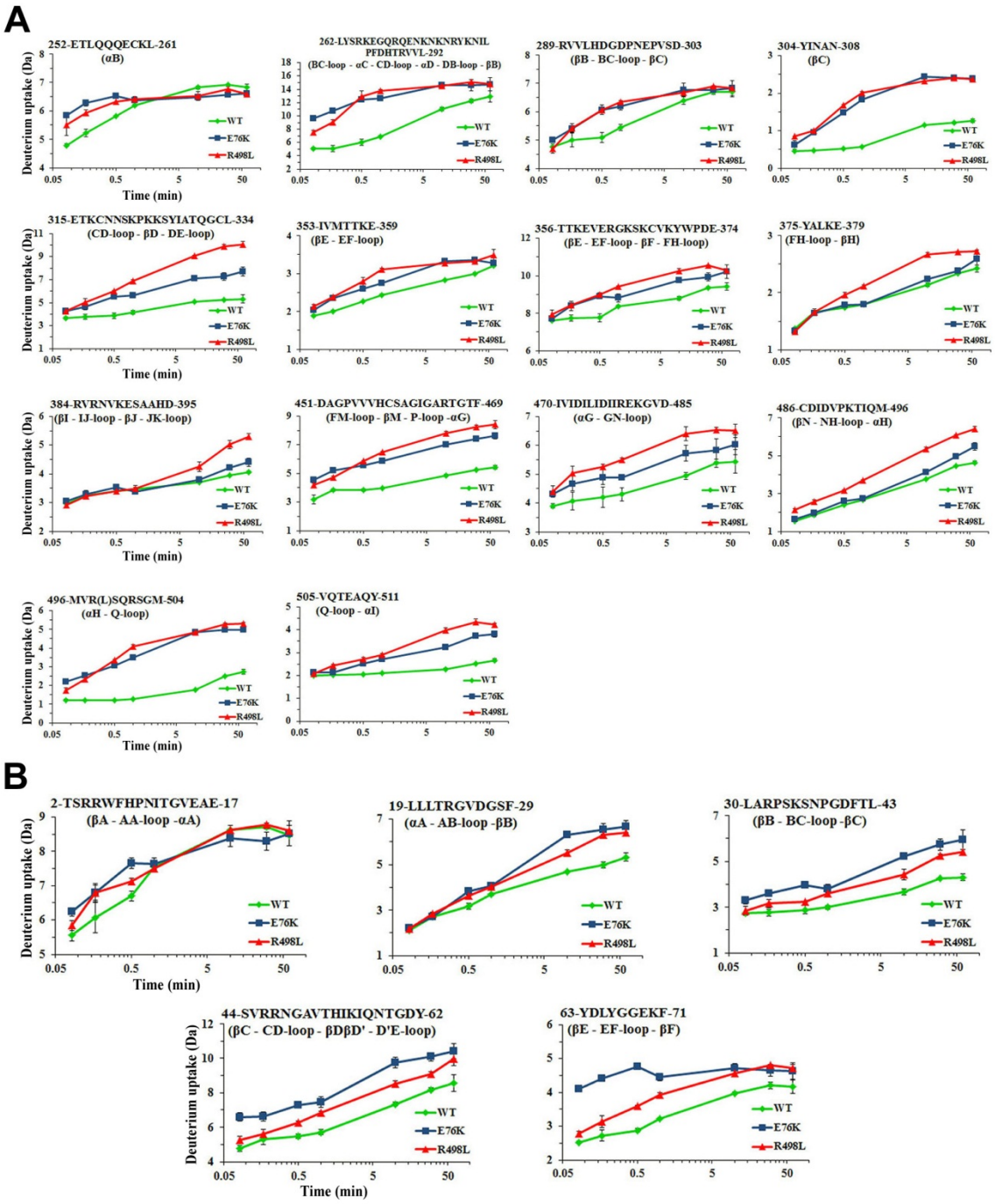

Figure 29 (A and B): Comparative analysis of hydrogen exchange experienced by the GOF Leukemia/NS-SHP2 E76K and the LS-SHP2 R498L pathogenic mutants. SHP2 mutants E76K and R498L show increased conformational dynamic flexibility in solution within the N-SH2/PTP interdomain region, relative to the wild-type (WT) enzyme as assessed by (H/DX-MS). **(A)** Representative comparative hydrogen exchange plots for peptides within the PTP domain portion of the E76K and R498L N-SH2/PTP domain interface regions that attain significant exchange relative to WT. 2º-structure elements are documented so that they can be located in (C). **(B)** Representative comparative hydrogen exchange plots for peptides within the N-SH2 domain portion of the E76K and R498L N-SH2/PTP domain interface regions that attain significant exchange relative to WT.

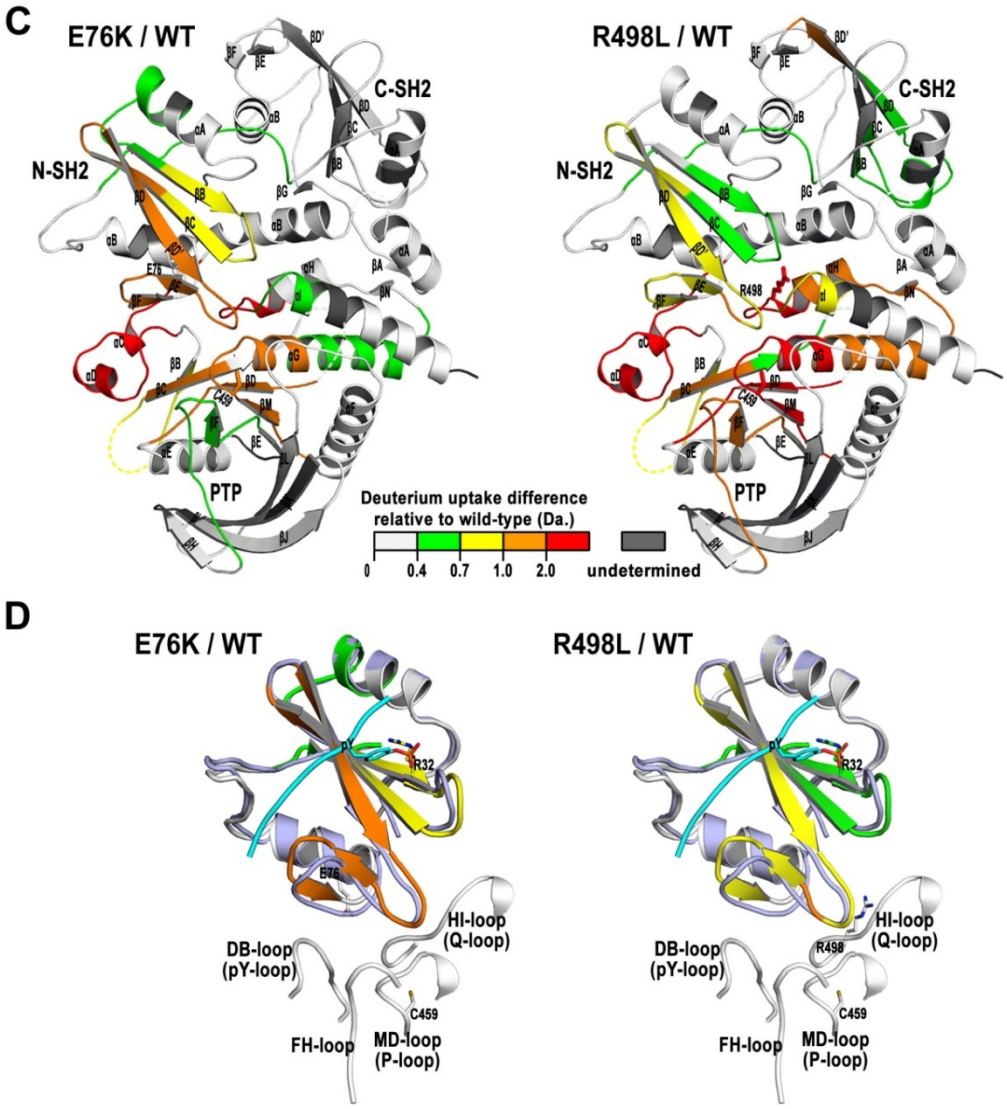

Figure 29 (C and D): Comparative analysis of hydrogen exchange experienced by the GOF Leukemia/NS-SHP2 E76K and the LS-SHP2 R498L pathogenic mutants. SHP2 mutants E76K and R498L show increased conformational dynamic flexibility in solution within the N-SH2/PTP interdomain region, relative to the wild-type (WT) enzyme as assessed by (H/DX-MS). **(C)** 'Heat map' showing significantly increased hydrogen exchange for both the E76K and R498L mutants relative to the WT enzyme at the 1 min time point of deuterium labeling modeled on the WT structure crystal (3OLR). WT as all grey and mutants color coded based upon increased exchange relative to WT as described in the legend. Peptides are colored when they attain exchange significance at two consecutive time points and at least 2σ (st.dev.) relative to WT values. Arg498 is labeled for R498L mutation orientation. The catalytic cysteine (Cys459) is labeled for active site orientation. **(D)** 'Heat map' of the E76K and R498L N-SH2 domains at the 1 min time point modeled on the (A-state) phosphotyrosyl-peptide-bound N-SH2 domain as documented by (Lee et al., 1994; PDB: 1AYA). The A-state (1AYA) structure (colored) is superimposed on the I-state (3OLR) WT structure (grey) (residues 3-103) using Phenix·superimpose to show significant conformational differences within the N-SH2 domain upon phosphopeptide-binding. Phosphopeptide represented in 'blue' with corresponding pTyr-residue in association with Arg32 of the βB-strand.

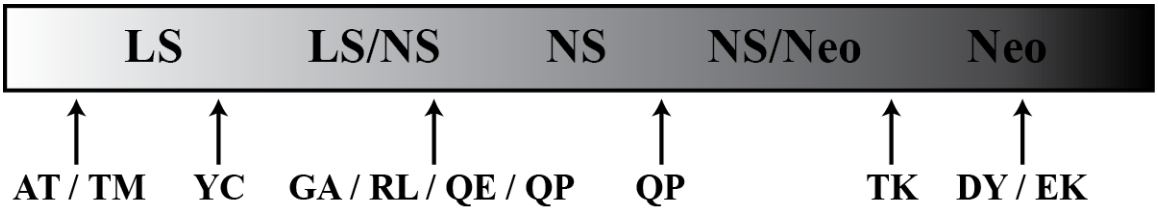

Enzyme	k_{cat} (s^{-1})	K_m (mM)	k_{cat}/K_m (s^{-1}/mM)
D61Y	6	2.7	2.22222
E76K	6.8	3.4	2.00000
T507K	0.23	1.66	0.13855
Q506P	0.046	2.49	0.01847
G464A	0.0184	2.57	0.00716
R498L	0.039	5.95	0.00655
Q510E	0.017	2.8	0.00607
Y279C	0.0275	7.28	0.00378
T468M	0.00359	3.17	0.00113
A461T	0.0023	2.2	0.00105
WT	0.136	3.63	0.03747

Figure 30: Hypothetical disease spectrum associated with SHP2 pathogenic mutants. A hypothetical disease spectrum associated with SHP2 pathogenic mutants was constructed based upon k_{cat}/K_m (s^{-1}/mM) measurements (using *p*NPP as a substrate) and H/DX-MS observations. k_{cat}/K_m (s^{-1}/mM) is used to sort the SHP2 pathogenic mutants as it is a measure of catalytic efficiency and, important to SHP2 function, it encompasses both catalytic competency as well as the ability of the N-SH2 domain to uphold intramolecular autoinhibition. The disease spectrum encompasses LEOPARD syndrome (LS), Noonan syndrome (NS), and Neoplasia (Neo) (encompassing the various hematological malignancies and solid tumors that are potentiated by SHP2 pathogenic mutants). Q506P represents a SHP2 pathogenic mutant documented in both LS and NS/Neoplasia cases and provides evidence that catalytically impaired mutants are capable of giving rise to GOF phenotypes, based upon the extent by which they are catalytically impaired and experience perturbed N-SH2 domain-mediated intramolecular autoinhibition. NS and LS are therefore 'spectrum' diseases potentiated by GOF SHP2 mutants that differ with respect to their inherent catalytic competencies, but are similar with respect to the compromised ability of the N-SH2 domain to uphold intramolecular autoinhibition.

REFERENCES

1. Eckhart, W., Hutchinson, M.A., and Hunter, T. (1979) An activity phosphorylating tyrosine in polyoma T antigen immunoprecipitates. *Cell* 18, 925-933.
2. Hunter, T., and Sefton, B.M. (1980) Transforming gene product of Rous sarcoma virus phosphorylates tyrosine. *Proc Natl Acad Sci USA* 77, 1311-1315.
3. Hunter, T., and Eckhart, W. (2004) The discovery of tyrosine phosphorylation: it's all in the buffer! *Cell* 116, S35-39.
4. Witte, O.N., Dasgupta, A., and Baltimore, D. (1980) Abelson murine leukaemia virus protein is phosphorylated in vitro to form phosphotyrosine. *Nature* 283, 826-831.
5. Ushiro, H., and Cohen, S. (1980) Identification of phosphotyrosine as a product of epidermal growth factor-activated protein kinase in A-431 cell membranes. *J Biol Chem* 255, 8363-8365.
6. Courtneidge, S.A., and Smith, A.E. (1983) Polyoma virus transforming protein associates with the product of the c-src cellular gene. *Nature* 303, 435-439.
7. Blume-Jensen, P., and Hunter, T. (2001) Oncogenic kinase signaling. *Nature* 411, 355-365.
8. Tonks, N.K., Diltz, C.D., and Fischer, E.H. (1988a) Purification of the major protein-tyrosine-phosphatases of human placenta. *J. Biol. Chem* 263, 6722-6730.
9. Tonks, N.K., Diltz, C.D., and Fischer, E.H. (1988b) Characterization of the major protein-tyrosine-phosphatases of human placenta. *J. Biol. Chem* 263, 6731-6737.
10. Charbonneau, H., Tonks, N.K., Kuman, S., Diltz, C.D., Harrylock, M., Cool, D.E., Krebs, E.G., Fischer, E.H., and Walsh, K.A. (1989) Human placenta protein-tyrosine-phosphatase: Amino acid sequence and relationship to a family of receptor-like proteins. *Proc. Natl. Acad. Sci. USA* 86, 5252-5256.
11. Guan, K., Huan, R.S., Watson, S.J., Geahlen, R.L., and Dixon, J.E. (1990) Cloning and expression of a protein-tyrosine-phosphatase. *Proc. Natl. Acad. Sci. USA* 87, 1501-1505.
12. Charbonneau, H., Tonks, N.K., Walsh, K.A., and Fischer, E.H. (1988) The leukocyte common antigen (CD45): A putative receptor-linked protein tyrosine phosphatase. *Proc. Natl. Acad. Sci. USA* 85, 7182-7186.
13. Fischer, E.H., Charbonneau, H., and Tonks, N.K. (1991) Protein tyrosine phosphatases: A diverse family of intracellular and transmembrane enzymes. *Science* 253, 401-406.
14. Walton, K.M., and Dixon, J.E. (1993) Protein tyrosine phosphatases. *Annu. Rev. Biochem* 62, 101-120.
15. Tonks, N.K., and Neel, B.G., (1996) From form to function: Signaling by protein tyrosine phosphatases. *Cell* 87, 365-368.
16. Mustelin, T., Abraham, R.T., Rudd, C.E., Alonso, A., and Merlo, J.J. (2002a) Protein tyrosine phosphorylation in T cell signaling. *Front. Biosci* 7, 918-969.
17. Mustelin, T., Feng, G.-S., Bottini, N., Alonso, A., Kholod, N., Birle, D., Merlo, J., and Huynh, H. (2002b) Protein tyrosine phosphatases. *Frot. Biosci* 7, 85-142.
18. Mustelin, T., and Taskén, K. (2003) Positive and negative regulation of T cell activation through kinases and phosphatases. *Biochem. J* 371, 15-27.

19. Alonso, A., Sasin, J., Bottini, N., Friedberg, I., Osterman, A., Godzik, A., Hunter, T., Dixon, J., and Mustelin, T. (2004) Protein tyrosine phosphatases in the human genome. *Cell* 117, 699-711.
20. Stone, J.C., Atkinson, T., Smith, M.E., and Pawson, T. (1984) Identification of functional regions in the transforming protein of Fujinami sarcoma virus by in-phase insertion mutagenesis. *Cell* 37, 559-568.
21. Sadowski, I., Stone, J.C., and Pawson, T. (1986) A non-catalytic domain conserved among cytoplasmic protein-tyrosine kinases modifies the kinase function and transforming activity of Fujinami sarcoma virus $P130^{gag\text{-}fps}$. *Mol. Cell Biol* 6, 4396-4408.
22. DeClue, J.E., Sadowski, I., Martin, G.S., and Pawson, T. (1987) A conserved domain regulates interactions of the *v-fps* protein-tyrosine with the host cell. *Proc. Natl. Acad. Sci. USA* 84, 9064-9068.
23. Pawson, T. (1988) Non-catalytic domains of cytoplasmic protein tyrosine kinases: regulatory elements in signal transduction. *Oncogene* 3, 491-495.
24. Koch, A., Moran, M., Sadowski, I., and Pawson, T. (1989) The common src homology region 2 domain of cytoplasmic signaling proteins is a positive effector of v-fps tyrosine kinase function. *Mol. Cell. Biol* 9, 4131-4140.
25. Anderson, D., Koch, C.A., Grey, L., Ellis, C., Moran, M.F., and Pawson, T. (1990) Binding of SH2 domains of phospholipase Cγ1, GAP, and Src to activated growth factor receptors. *Science* 250, 979-982.
26. Moran, M.F., Koch, C.A., Anderson, D., Ellis, C., England, L., Martin, G.S., and Pawson, T. (1990) Src homology region 2 domains direct protein-protein interactions in signal transduction. *Proc. Natl. Acad. Sci. USA* 87, 8622-8626.
27. Margolis, B., Li, N., Koch, A., Mohammadi, M., Hurwitz, D.R., Zilberstein, A., Ullrich, A., Pawson, T., and Schlessinger, J. (1990) The tyrosine phosphorylated carboxyterminus of the EGF receptor is a binding site for GAP and PLC-γ. *EMBO J* 9, 4375-4380.
28. Mayer, B.J., Jackson, P.K., and Baltimore, D. (1991) The noncatalytic *src* homology region 2 segment of *abl* tyrosine kinase binds to tyrosine-phosphorylated cellular proteins with high affinity. *Proc. Natl. Acad. Sci. USA* 88, 627-631.
29. Escobedo, J.A., Navankasattusas, S., Kavanaugh, W.M., Milfay, D., Fried, V.A, and Willimas, L.T. (1991) cDNA cloning of a novel 85 kd protein that has SH2 domains and regulates binding of PI 3'-kinase to the PDGF β-receptor. *Cell* 65, 75-82.
30. Koch, C.A., Moran, M.F., Anderson, D., Liu, X., Mbamalu, G., and Pawson, T. (1992) Multiple SH2-mediated interactions in v-*src*-transformed cells. *Mol. Cell. Biol* 12, 1366-1374.
31. Margolis, B., Rhee, S.G., Felder, S., Mervic, M., Lyall, R., Levitzki, A., Ullrich, A., Zilbestein, A., and Schlessinger, J. (1989) EGF induces tyrosine phosphorylation of phospholipase C-II: a potential mechanism for EGF signaling. *Cell* 57, 1101-1107.
32. Meisenhelder, J., Suh, P.-G., Rhee, S.G., and Hunter, T. (1989) Phospholipase C-γ is a substrate for the PDGF and EGF receptor protein-tyrosine kinases in vivo and in vitro. *Cell* 57, 1109-1122.

33. Wahl, M.I., Nishibe, S., Suh, P.-G., Rhee, S.G., and Carpenter, G. (1989) Epidermal growth factor stimulates tyrosine phosphorylation of phospholipase C (II) independently of receptor internalization and extracellular calcium. *Proc. Natl. Acad. Sci. USA* 86, 1568-1572.
34. Molloy, C.,J., Bottaro, D.P., Fleming, T.P., Marshall, M.S., Gibbs, J.B., and Aaronson, S.A. (1989) PDGF induction of tyrosine phosphorylation of GTPase activating protein. *Nature* 342, 711-714.
35. Ellis, C., Moran, M., McCormick, F., and Pawson, T. (1990) Phosphorylation of GAP and GAP-associated proteins by transforming and mitogenic tyrosine kinases. *Nature* 343, 377-381.
36. Manning, G., Whyte, D.B., Martinez, R., Hunter, T., and Sudarsanam, S. (2002) The protein kinase complement of the human genome. *Science* 298, 1912-1934.
37. Ek, B., Westermark, B., Wasteson, A., and Heldin, C.H. (1982) Stimulation of tyrosine-specific phosphorylation by platelet-derived growth factor. *Nature* 295, 419-420.
38. Petruzzeli, L.M., Ganguly, S., Smith, C.J., Cobb, M.H., Rubin, C.S., and Rosen, O.M. (1982) Insulin activates a tyrosine-specific protein kinase in extracts of 3T3-L1 adipocytes and human placenta. *Proc. Natl. Acad. Sci. USA* 79, 6792-6796.
39. Downward, J., Yarden, Y., Mayes, E., Scrace, G., Totty, N., Stockwell, P., Ullrich, A., Schlessinger, J., and Waterfield, M.D. (1984) Close similarity of epidermal growth factor receptor and v-erb-B oncogene protein sequences. *Nature* 307, 521-527.
40. Hunter, T., and Cooper, J.A. (1981) Epidermal growth factor induces rapid tyrosine phosphorylation of proteins in A431 human tumor cells. *Cell* 24, 741-752.
41. Waterfield, M.D., Scrace, G.T., Whittle, N., Stroobant, P., Johnsson, A., Wasteson, A., Westermark, B., Heldin, C.H., Huang, J.S., and Deuel, T.F. (1983) Platelet-derived growth factor is structurally related to the putative transforming protein p28sis of simian sarcoma virus. *Nature* 304, 35-39.
42. Doolittle, R.F., Hunkapiller, M.W., Hood, L.E., Devare, S.G., Robbins, K.C., Aaronson, S.A., and Antoniades, H.N. (1983) Simian sarcoma virus onc gene, v-sis, is derived from the gene (or genes) encoding a platelet-derived growth factor. *Science* 221, 275-277.
43. Rosen, O.M., Herrera, R., Olowe, Y., Petruzzelli, L.M., and Cobb, M.H. (1983) Phosphorylation activates the insulin receptor tyrosine kinase. *Proc. Natl. Acad. Sci. USA* 80, 3237-3240.
44. Weinmaster, G., Zoller, M.J., Smith, M., Hinze, E., and Pawson, T. (1984) Mutagenesis of Fujinami sarcoma virus: evidence that tyrosine phosphorylation of P130gag-fps modulates its biological activity. *Cell* 37, 559-568.
45. Schreiber, A.B., Libermann, T.A., Lax, I., Yarden, Y., and Schlessinger, J. (1983) Biological role of epidermal growth factor-receptor clustering. Investigation with monoclonal anti-receptor antibodies. *J. Biol. Chem* 258, 846-853.
46. Ullrich, A., and Schlessinger, J. (1990) Signal transduction by receptors with tyrosine kinase activity. *Cell* 61, 203-212.
47. Favelyukis, S., Till, J.H., Hubbard, S.R., and Miller, W.T. (2001) Structure and autoregulation of the insulin-like growth factor 1 receptor kinase. *Nat. Struct. Mol. Biol* 8, 1058-1063.

48. Huse, M., and Kuriyan, J. (2002) The conformational plasticity of protein kinases. *Cell* 109, 275-282.
49. Nolen, B., Taylor, S., and Ghosh, G. (2004) Regulation of protein kinases; controlling activity through activation segment conformation. *Mol. Cell* 15, 661-675.
50. Pawson, T. (2004) Specificity in signal transduction: from phosphotyrosine-SH2 domain interactions to complex cellular systems. *Cell* 116, 191-203.
51. Schlessinger, J. (2000) Cell signaling by receptor tyrosine kinases. *Cell* 103, 211-225.
52. Schlessinger, J.,and Lemmon, M.A. (2003) SH2 and PTB domains in tyrosine kinase signaling. *Sci. STKE* 191, RE12.
53. Pawson, T. (2007) Dynamic control of signaling by modular adaptor proteins. *Curr. Opin. Cell Biol* 19, 112-116.
54. Lemmon, M., and Schlessinger J. (2010) Cell Signaling by Receptor Tyrosine Kinases. *Cell* 141, 1117-1134.
55. Temin, H.M. (1966) Genetic and possible biochemical mechanisms in viral carcinogenesis. *Cancer Res.* 26, 212-216.
56. Libermann, T.A., Nusbaum, H.R., Raxon, N., Kris, R., Lax, I., Soreq, H., Whittle, N., Waterfield, M.D., Ullrich, A., and Schlessinger, J. (1985) Amplification, enhanced expression and possible rearrangement of EGF receptor gene in primary human brain tumors of glial origin. *Nature* 313, 144-147.
57. Andersen, J.N., Jansen, P.G., Echwald, S.M., Mortensen, O.H., Fukuda, T., Del Vecchio, R., Tonks, N.K., and Møller, N.P.H. (2004) A genomic perspective on protein tyrosine phosphatases: gene structure, pseudogenes, and genetic disease linkage. *FASEB J* 18, 8-13.
58. Zhang, Z.-Y., and Dixon, J.E. (1994a) Protein Tyrosine Phosphatases: Mechanism of Catalysis and Substrate Specificity. *Advances in Enzymology* 68, 1-36.
59. Zhang, Z.-Y., Wang, Y., and Dixon, J.E. (1994b) Dissecting the Catalytic Mechanism of Protein Tyrosine Phosphatases. *Proc. Natl. Acad. Sci. USA* 91, 1624-1627.
60. Felberg, J., and Johnson, P. (1998) Characterization of recombinant CD45 cytoplasmic domain proteins. Evidence for intramolecular and intermolecular interactions. *J. Biol. Chem* 273, 17839-17845.
61. Streuli, M., Krueger, N.X., Thai, T., Tang, M., and Saito, H. (1990) Distinct functional roles of the two intracellular phosphatase like domains of the receptor-linked protein tyrosine phosphatases LCA and LAR. *EMBO J* 9, 2399-2407.
62. Hof, P., Pluskey, S., Dhe-Paganon, S., Eck, M.J., and Shoelson, S.E. (1998) Crystal structure of the Tyrosine Phosphatase SHP-2. *Cell* 92, 441-450.
63. Neel, B.G., Gu, H., and Pao, L. (2003) The 'Shp'ing news: SH2 domain-containing tyrosine phosphatases in cell singaling. *Trends Biochem. Sci* 28, 284-293.
64. Garton, A.J., Burnham, M.R., Bouton, A.H., and Tonks, N.K. (1997) Association of PTP-PEST with the SH3 domain of p130cas; a novel mechanism of protein tyrosine phosphatase substrate recognition. *Oncogene* 15, 877-885.

65. Pulido, R., Zúñiga, A., and Ullrich, A. (1998) PTP-SL and STEP protein tyrosine phosphatases regulate the activation of the extracellular signal-regulted kinases ERK1 and ERK2 by association through a kinase interaction motif. *EMBO J* 17, 7337-7350.
66. Sun, H., Charles, C.H., Lau, L.F., and Tonks, N.K. (1993) MKP-1 (3CH134), an immediate early gene product, is a dual specificity phosphatase that dephosphorylates MAP kinase in vivo. *Cell* 75, 487-493.
67. Liu, Y., Gorospe, M., Yang, C., Holbrook, N.J. (1995) Role of mitogen-activated protein kinase phosphatase during the cellular response to genotoxic stress. Inhibition of c-Jun N-terminal kinase activity and AP-1-dependent gene activation. *J. Biol. Chem* 270, 8377-8380.
68. Raingeaud, J., Gupta, S., Rogers, J.S., Dickens, M., Han, J., Ulevitch, R.J., and Davis, R.J. (1995) Pro-inflammatory cytokines and environmental stress cause p38 mitogen-activated protein kinase activation by dual phosphorylation on tyrosine and threonine. *J. Biol. Chem* 270, 7420-7426.
69. Camps, M., Nichols, A., Gillieron, C., Antonsson, B., Muda, M., Chabert, C., Boschert, U., and Arkinstall, S. (1998) Catalytic activation of the phosphatase MKP-3 by ERK2 mitogen-activated protein kinase. *Science* 280, 1262-1265.
70. Chu, Y., Solski, P.A., Khosravi-Far, R., Der, C.J., and Kelly, K. (1996) The mitogen-activated protein kinase phosphatase PAC1, MKP-1, and MKP-2 have unique substrate specificities and reduced activity in vivo toward the ERK2 sevenmaker mutation. *J. Biol. Chem* 271, 6497-6501.
71. Hutter, D., Chen, P., Barnes, J., and Liu, Y. (2000) Catalytic activation of mitogen-activated protein (MAP) kinase phosphatase-1 by binding to p38 MAP kinase: critical role of the p38 C-terminal domain in its negative regulation. *Biochem. J* 352, 155-163.
72. Nichols, A., Camps, M., Gillieron, C., Chabert, C., Brunet, A., Wilsbacher, J., Cobb, M., Pouyssegur, J., Shaw, J.P., and Arkinstall, S. (2000) Substrate recognition domains within extracellular signal-regulated kinase mediate binding and catalytic activation of mitogen-activated protein kinase phosphatase-3. *J. Biol. Chem* 275, 24613-24621.
73. Tanoue, T., Adachi, M., Moriguchi, T., and Nishida, E. (2000) A conserved docking motif in MAP kinases common to substrates, activators and regulators. *Nat. Cell Biol* 2, 110-116.
74. Keyse, S.M. (2000) Protein phosphatases and the regulation of mitogen-activated protein kinase signaling. *Curr. Opin. Cell Biol* 12, 186-192.
75. Maehama, T., and Dixon, J.E. (1998) The tumor suppressor, PTEN/MMAC1, dephosphorylates the lipid seconds messenger, phosphatidylinositol 3,4,5-triphosphate. *J. Biol. Chem* 273, 13375-13378.
76. Wu, X., Hepner, K., Castelino-Prabhu, S., Do, D., Kaye, M.B., Yuan, X.J., Wood, J., Ross, C., Sawyers, C.L., and Whang, Y.E. (2000a) Evidence for regulation of the PTEN tumor suppressor by a membrane-localized multi-PDZ domain containing scaffold protein MAGI-2. *Proc. Natl. Acad. Sci USA* 97, 4233-4238.

77. Wu, Y., Dowbenko, D., Spencer, S., Laura, R., Lee, J., Gu, Q., and Lasky, L.A. (2000b) Interaction of the tumor suppressor PTEN/MMAC with a PDZ domain of MAGI3, a novel membrane-associated guanylate kinase. *J. Biol. Chem* 275, 21477-21485.
78. Simpson, L., and Parsons, R. (2001) PTEN: life as a tumor suppressor. *Exp. Cell Res* 264, 29-41.
79. Bessette, D.C., Qiu, D., and Pallen, C.J. (2008) PRL PTPs: mediators and markers of cancer progression. *Cancer Metastasis Rev* 27, 231-252.
80. Gentry, M.S., Dowen, R.H. 3rd, Worby, C.A., Mattoo, S., Ecker, J.R., and Dixon, J.E. (2007) The phosphatase laforin crosses evolutionary boundries and links carbohydrate metabolism to neuronal disease. *J. Cell Biol* 178, 477-488.
81. Roach, P.J. (2011) Are there errors in glycogen biosynthesis and is laforin a repair enzyme? *FEBS Lett* 585, 3216-3218.
82. Tonks, N.K. (2006) Protein tyrosine phosphatases: from genes, to function, to disease. *Nat. Rev. Mol. Cell Biol* 7, 833-846.
83. Digilio, M.C., Conti, E., Sarkozy, A., Mingarelli, R., Dottorini, T., Marino, B., Pizzuti, A., and Dallapiccola, B. (2002) Grouping of Multiple-Lentigines/LEOPARD and Noonan Syndromes on the *PTPN11* Gene. *Am. J. Hum. Genet* 71, 389-394.
84. Tartaglia, M., and Gelb, B.D. (2005) Noonan syndrome and related disorders: Genetics and pathogenesis. *Annu. Rev. Genomics Hum. Genet* 6, 45-68.
85. Bentires-Alj, M., Kontaridis, M.I., and Neel, B.G. (2006) Stops along the RAS pathway in human genetic disease. *Nature Medicine* 12, 283-285.
86. Tartaglia, M., Niemeyer, C.M., Fragale, A., Song, X., Buechner, J., Jung, A., Hählen, K., Hasle, H., Licht, J.D., and Gelb, B.D. (2003) Somatic mutations in PTPN11 in juvenile myelomonocytic leukemia, myelodysplastic syndromes and acute myeloid leukemia. Nat. Genet 34, 148-150.
87. Bentires-Alj, M., Paez, J.G., David, F.S., Keilhack, H., Halmos, B., Naoki, K., Maris, J.M., Richardson, A., Bardelli, A., Sugarbaker, D.J., Richards, W.G., Du, J., Girard, L., Minna, J.D., Loh, M.L., Fisher, D.E., Velculescu, V.E., Vogelstein, B., Meyerson, M., Sellers, W.R., and Neel, B.G. (2004) Activating mutations of the noonan syndrome-associated SHP2/PTPN11 gene in human solid tumors and adult acute myelogenous leukemia. *Cancer Res* 64, 8816-8820.
88. Cully, M., You, H., Levine, A.J., and Mak, T.W. (2006) Beyond PTEN mutations: the PI3K pathway as an integrator of multiple inputs during tumorigenesis. *Nature Rev. Cancer* 6, 184-192.
89. Song, M.S., Salmena, L., and Pandolfi, P.P. (2012) The functions and regulation of the PTEN tumour suppressor. *Nat. Rev. Mol. Cell Biol* 13, 283-296.
90. Bottini, N., Musumeci, L., Alonso, A., Rahmouni, S., Nika, K., Rostamkhani, M., MacMurray, J., Meloni, G.F., Lucarelli, P., Pellecchia, M., Eisenbarth, G.S., Comings, D., and Mustelin, T. (2004) A functional variant of lymphoid tyrosine phosphatase is associated with type I diabetes. *Nat. Genet* 36, 337-338.

91. Smith, D., Cooper, J.D., Collins, J.E., Heward, J.M., Franklyn, J.A., Howson, J.M., Vella, A., Nutland, S., Rance, H.E., Maier, L., Barratt, B.J., Guja, C., Ionescu-Tirgoviste, C., Savage, D.A., Dunger, D.B., Widmer, B., Strachan, D.P., Ring, S.M., Walker, N., Clayton, D.G., Twells, R.C., Gough, S.C., and Todd, J.A. (2004) Replication of an association between the lymphoid tyrosine phosphatase locus *(LYP/PTPN22)* with type I diabetes, and evidence for its role in general autoimmunity locus. *Diabetes* 53, 3020-3023.
92. Begovich, A.B., Carlton, V.E., Honigberg, L.A., Schrodi, S.J., Chokkalingam, A.P., Alexander, H.C., Ardlie, K.G., Huang, Q., Smith, A.M., Spoerke, J.M., Conn, M.T., Chang, M., Chang, S.Y., Saiki, R.K., Catanese, J.J., Leong, D.U., Garcia, V.E., McAllister, L.B., Jeffery, D.A., Lee, A.T., Batliwalla, F., Remmers, E., Criswell, L.A., Seldin, M.F., Kastner, D.L., Amos, C.I.,Sninsky, J.J., and Gregersen, P.K. (2004) A missense single-nucleotide polymorphism in a gene encoding a protein tyrosine phosphatase *(PTPN22)* is associated with rheumatoid arthritis. *Am. J. Hum. Genet* 75, 330-337.
93. Carlton, V.E., Hu, X., Chokkalingam, A.P., Schrodi, S.J., Brandon, R., Alexander, H.C., Chang, M., Catanese, J.J., Leong, D.U., Ardlie, K.G., Kastner, D.L., Seldin, M.F., Criswell, L.A.,Gregersen, P.K., Beasley, E., Thomson, G., Amos, C.I., and Begovich, A.B. (2005) *PTPN22* genetic variation: evidence for multiple variants associated with rheumatoid arthritis. *Am. J. Hum. Genet* 77, 567-581.
94. Kyogoku, C., Tsuchiya, N., Wu, H., Tsao, B.P., and Tokunaga, K. (2004) Association of Fcgamma receptor IIA, but not IIB and IIIA, polymorphisms with systemic lupus erythematosus: A family-based association in Caucasians. *Arthritis Rheum* 50, 671-673.
95. Vang, T., Congia, M., Macis, M.D., Musumeci, L., Orrú, V., Zavattari, P., Nika, K., Tautz, L., Taskén, K., Cucca, F., Mustelin, T., and Bottini, N. (2005) Autoimmune-associated lymphoid tyrosine phosphatase is a gain-of-function variant. *Nat. Genet* 37, 1317-1319.
96. Tagliabracci, V.S., Heiss, C., Karthik, C., Contreras, C.J., Glushka, J., Ishihara, M., Azadi, P., Hurley, T.D., DePaoli-Roach, A.A., Roach, P.J. (2011) Phosphate incorporation during glycogen synthesis and Lafora disease. Cell Metab 13, 274-282.
97. Minassian, B.A., Lee, J.R., Herbrick, J.A., Huizenga, J., Soder, S., Mungall, A.J., Dunham, I., Gardner, R., Fong, C.Y., Carpenter, S., Jardim, L., Satishchandra, P., Andermann, E., Snead, O.C. 3rd, Lopes-Cendes, I., Tsui, L.C., Delgado-Escueta, A.V., Rouleau, G.A., Scherer, S.W. (1998) Mutations in a gene encoding a novel protein tyrosine phosphatase cause progressive myoclonus epilepsy. *Nat. Genet* 20, 171-174.
98. Serratosa, J.M., Gómez-Garre, P., Gallardo, M.E., Anta, B., de Bernabé, D.B., Lindhout, D., Augustijn, P.B., Tassinari, C.A., Malafosse, R.M., Topcu, M., Grid, D., Dravet, C., Berkovic, S.F., de Córdoba, S.R. (1999) A novel protein tyrosine phosphatase gene is mutated in progressive myoclonus epilepsy of the Lafora type (EPM2). *Hum. Mol. Genet* 8, 345-352.

99. Mohn, K.L., Laz, T.M., Hsu, J.C., Melby, A.E., Bravo, R., and Taub, R. (1991) The immediate-early growth response in regenerating liver and insulin-stimulated H-35 cells: comparison with serum-stimulated 3T3 cells and identification of 41 novel immediate-early genes. *Mol. Cell Biol* 11, 381-390.
100. Diamond, R.H., Cressman, D.E., Laz, T.M., Abrams, C.S., and Taub, R. (1994) PRL-1, a unique nuclear protein tyrosine phosphatase, affects cell growth. *Mol. Cell Biol* 14, 3752-3762.
101. Saha, S., Bardelli, A., Buckhaults, P., Velculescu, V.E., Rago, C., St. Croix B., Romans, K.E., Choti, M.A., Lengauer, C., Kinzler, K.W., and Vogelstein, B. (2001) A Phosphatase Associated with Metastasis of Colorectal Cancer. *Science* 294, 1343-1346.
102. Fiordalisi, J.J., Keller, P.J., and Cox, A.D. (2006) PRL tyrosine phosphatases regulate rho family GTPases to promote invasion and motility. *Cancer Res* 66, 3153-3161.
103. Wang, H., Quah, S.Y., Dong, J.M., Manser, E., Tang, J.P., and Zeng, Q. (2007) PRL-3 Down-regulates PTEN Expression and Signals through PI3K to Promote Epithelial-Mesenchymal Transition. *Cancer Res* 67, 2922-2926.
104. Peng, L., Jin, G., Wang, L., Guo, J., Meng, L., and Shou, C. (2006) Identification of integrin alpha1 as an interacting protein of protein tyrosine phosphatase PRL-3. *Biochem. Biophy. Res. Commun* 342, 179-183.
105. Peng, L., Xing, X., Li, W., Qu, L., Meng, L., Lian, S., Jiang, B., Wu, J., and Shou, C. (2009) PRL-3 promotes the motility, invasion, and metastasis of LoVo colon cancer cells through PRL-3-integrin β1-ERK1/2 and -MMP2 signaling. *Mol. Cancer* 8, 110-122.
106. Liang, F., Liang, J., Wang, W.Q., Sun, J.P., Udho, E., and Zhang, Z.-Y. (2007) PRL3 promotes cell invasion and proliferation by down-regulation of Csk leading to Src activation. *J. Biol. Chem* 282, 5413-5419.
107. Liang, F., Luo, Y., Dong, Y., Walls, C.D., Liang, J., Jiang, H.-Y., Sanford, J.R., Wek, R.C., and Zhang, Z.-Y. (2008) Translational Control of C-terminal Src Kinase (Csk) Expression by PRL3 Phosphatase. *J. Biol. Chem* 283, 10339-10346.
108. Iliuk, A.B., Martin, V.A., Alicie, B.M., Geahlen, R.L., and Tao, W.A. (2010) In-depth Analysis of Kinase-dependent Tyrosine Phosphoproteomes Based on Metal Ion-functionalized Soluble Nanopolymers. *Mol. Cell Proteomics* 9, 2162-2172.
109. Fragale, A., Tartaglia, M., Wu, J., and Gelb, B.D. (2004) Noonan syndrome-associated SHP2/PTPN11 mutants cause EGF-dependent prolonged GAB1 binding and sustained ERK2/MAPK1 activation. *Hum. Mutat* 23, 267-277.
110. Keilhack, H., David, F.S., McGregor, M., Cantley, L.C., and Neel, B.G. (2005) Diverse biochemical properties of Shp2 mutants: implication for diseases phenotypes. *J. Biol. Chem* 280, 30984-30993.
111. Martinelli, S., Torreri, P., Tinti, M., Stella, L., Bocchinfuso, G., Flex, E., Grottesi, A., Ceccarini, M., Palleschi, A., Cesareni, G., Castagnoli, L., Petrucci, T. C., Gelb, B. D., and Tartaglia, M. (2008) Diverse driving forces underlie the invariant occurrence of the T42A, E139D, I282V and T468M SHP2 amino acid substitutions causing Noonan and LEOPARD syndromes. *Hum. Mol. Genet* 17, 2018-2029.

112. Oishi, K., Gaengel, K., Krishnamoorthy, S., Kamiya, K., Kim, I.K., Ying, H., Weber, U., Perkins, L.A., Tartagli, M., Mlodzik, M., Pick, L., and Gelb, B.D. (2006) Transgenic Drosophila models of Noonan syndrome causing PTPN11 gain-of-function mutations. *Hum. Mol. Genet* 15, 543-553.
113. Tartaglia, M., Martinelli, S., Stella, L., Bocchinfuso, G., Flex, E., Cordeddu, V., Zampino, G., Burgt, I., Palleschi, A., Petrucci, T.C., Sorcini, M., Schoch, C., Foa, R., Emanuel, P.D., and Gelb, B.D. (2006) Diversity and functional consequences of germline and somatic PTPN11 mutations in human disease. *Am. J. Hum. Genet* 78, 279-290.
114. Hanna, N., Montagner, A., Lee, W.H., Miteva, M., Vidal, M., Vidaud, M., Parfait, B., and Raynal, P. (2006) Reduced phosphatase activity of SHP-2 in LEOPARD syndrome: consequences for PI3K binding on Gab1. *FEBS Lett* 580, 2477-2482.
115. Kontaridis, M.I., Swanson, K.D., David, F.S., Barford, D., and Neel, B.G. (2006) PTPN11 (Shp2) mutations in LEOPARD syndrome have dominant negative, not activating, effects. *J. Biol. Chem* 281, 6785-6792.
116. Wells, C.D., Fawcett, J.P., Traweger, A., Yamanaka, Y., Goudreault, M., Elder, K., Kulkami, S., Gish, G., Virag, C., Lim, C., Colwill, K., Starostine, A., Metalnikov, P., and Pawson, T. (2006) A Rich1/Amot Complex Regulates the Cdc42 GTPase and Apical-Polarity Proteins in Epithelial Cells. *Cell* 125, 535-548.
117. Fitzpatrick, D.P.G., You, J.-S., Bemis, K.G., Wery, J.-P., Ludwig, J.R., and Wang, M. (2007) Searching for potential biomarkers of cisplatin resistance in human ovarian cancer using a label-free LC/MS-based protein quantification method. *Proteomics Clin. Appl* 1, 246-263.
118. Hale, J.E., Butler, J.P., Gelfanova, V., You, J.S., and Knierman, M.D. (2004) A simplified procedure for the reduction and alkylation of cysteine residues in proteins prior to proteolytic digestion and mass spectral analysis. *Anal. Biochem* 333, 174-181.
119. Higgs, R.E., Knierman, M.D., Gelfanova, V., Butler, J.P., and Hale, J.E. (2005) Comprehensive label-free method for the relative quantification of proteins from biological samples. *J. Proteome Res* 4, 1442-1450.
120. Ficarro, S.B., Zhang, Y., Lu, Y., Moghimi, A.R., Askenazi, M., Hyatt, E., Smith, E.D., Boyer, L., Schlaeger, T.M., Luckey, C.J., and Marto, J.A. (2009) Improved electrospray ionization efficiencies compensates for diminished chromatographic resolution and enables proteomics analysis of tyrosine signaling in embryonic stem cells. *Anal. Chem* 81, 3440-3447.
121. Winkler, R. (2010) ESIprot: A universal tool for charge state determination and molecular weight calculation of proteins from electrospray ionization mass spectrometry data. *Rapid Commun. Mass Spectrom* 24, 285-294.
122. Weiss, D.D., Engen, J.R., and Kass, I.J. (2006) Semi-automated data processing of hydrogen exchange mass spectra using HX-Express. *J. Am. Soc. Mass Spectrom* 17, 1700-1703.
123. Wales, T.E., and Engen, J.R. (2006) Hydrogen exchange mass spectrometry for the analysis of protein dynamics. *Mass Spectrom. Rev* 25, 158-170.
124. Zhang, Z.-Y. (2001) Protein tyrosine phosphatases: prospects for therapeutics. *Curr. Opin. Chem. Biol* 5, 416-423.

125. Arena, S., Benvenuti, S., and Bardelli, A. (2005) Genetic analysis of the kinome and phosphatome in cancer. *Cell Mol. Life Sci* 62, 2092-2099.
126. Cates, C.A., Michael, R.L., Stayrook, K.R., Harvey, K.A., Burke, Y.D., Randall, S.K., Crowell, P.L., and Crowell, D.N. (1996) Prenylation of oncogenic human PTP(CAAX) protein tyrosine phosphatases. *Cancer Lett* 110, 49-55.
127. Zeng, Q., Hong, W., and Tan, Y.H. (1998) Mouse PRL-2 and PRL-3, two potentially prenylated protein tyrosine phosphatases homologous to PRL-1. *Biochem. Biophys. Res. Commun* 244, 421-427.
128. Bardelli, A., Saha, S., Sager, J.A., Romans, K.E., Xin, B., Markowitz, S.D., Lengauer, C., Velculescu, V.E., Kinzler, K.W., and Vogelstein, B. (2003) PRL-3 expression in metastatic cancers. *Clin. Cancer Res* 9, 5607-5615.
129. Kato, H., Semba, S., Miskad, U.A., Seo, Y., Kasuga, M., and Yokozaki, H. (2004) High expression of PRL-3 promotes cancer cell motility and liver metastasis in human colorectal cancer: A predictive molecular marker of metachronous liver and lung metastasis. *Clin. Cancer Res* 10, 7318-7328.
130. Al-Aidaroos, A.Q.O., and Zeng, Q. (2010) PRL-3 Phosphatase and Cancer Metastasis. *J. Cell Biochem* 111, 1087-1098.
131. Guzińska-Ustymowicz, K., and Pryczynicz, A. (2011) PRL-3, an emerging marker of carcinogenesis, is strongly associated with poor prognosis. *Anticancer Agents Med. Chem* 11, 99-108.
132. Zeng, Q., Dong, J.M., Guo, K., Li, J., Tan, H.X., Koh, V., Pallen, C.J., Manser, E., and Hong, W. (2003) PRL-3 and PRL-1 promote cell migration, invasion, and metastasis. *Cancer Res* 63, 2716-2722.
133. Wu, X., Zeng, H., Zhang, X., Zhao, Y., Sha, H., Ge, X., Zhang, M., Gao, X., and Xu, Q. (2004) Phosphatase of regenerating liver-3 promotes motility and metastasis of mouse melanoma cells. *Am. J. Pathol* 164, 2039- 2054.
134. Kato, H., Semba, S., Miskad, U.A., Seo, Y., Kasuga, M., and Yokozaki, H. (2004) High expression of PRL-3 promotes cancer cell motility and liver metastasis in human colorectal cancer: a predictive molecular marker of metachronous liver and lung metastases. *Clin. Cancer Res* 10, 7318-7328.
135. Rouleau, C., Roy, A., St. Martin, T., Dufault, M.R., Boutin, P., Liu, D., Zhang, M., Puorro-Radzwill, K., Rulli, L., Reczek, D., Bagley, R., Byrne, A., Weber, W., Roberts, B., Klinger, K., Brondyk, W., Nacht, M., Madden, S., Burrier, R., Shankara, S., and Teicher, B.A. (2006) Protein tyrosine phosphatase PRL-3 in malignant cells and endothelial cells: expression and function. *Mol. Cancer Ther* 5, 219-229.
136. Qian, F., Li, Y.P., Sheng, X., Zhang, Z.C., Song, R., Dong, W., Cao, S.X., Hua, Z.C., and Xu, Q. (2007) PRL-3 siRNA inhibits the metastasis of B16-BL6 mouse melanoma cells in vitro and in vivo. *Mol. Med* 13, 151-159.
137. Polyak, K., and Weinberg, R.A. (2009) Transitions between epithelial and mesenchymal states: acquisition of malignant and stem cell traits. *Nat. Rev. Cancer* 9, 265-273.
138. Krndija, D., Münzberg, C., Maass, U., Hafner, M., Adler, G., Kestler, H.A., Seufferlein, T., Oswald, F., von Wichert, G. (2012) The phosphatase of regenerating liver 3 (PRL-3) promotes cell migration through Arf-activity-dependent stimulation of integrin α5 recycling. *J. Cell Sci* 125, 3883-3892.

139. Su, J., Muranjan, M., and Sap, J. (1999) Receptor protein tyrosine phosphatase alpha activates Src-family kinases and controls integrin-mediated responses in fibroblasts. *Curr. Biol* 9, 505-511.
140. Ponniah, S., Wang, D.Z.M., Lim, K.L., and Pallen, C.J. (1999) Targeted disruption of the tyrosine phosphatase PTPα leads to constitutive downregulation of the kinases Src and Fyn. *Curr. Biol* 9, 535-538.
141. Chen, M., Chen, S.C., and Pallen, C.J. (2006) Integrin-induced Tyrosine Phosphorylation of Protein-tyrosine Phosphatase-α Is Required for Cytoskeletal Reorganization and Cell Migration. *J. Biol. Chem* 281, 11972-11980.
142. Oneyama, C., Hikita, T., Enya, K., Dobenecker, M.W., Saito, K., Nada, S., Tarakhovsky, A., and Okada, M. (2008) The lipid raft-anchored adapter protein Cbp controls the oncogenic potential of c-Src. *Mol. Cell* 30, 426-436.
143. Resh, M.D. (2008) The ups and downs of SRC regulation: tumor suppression by Cbp. *Cancer Cell* 13, 469-471.
144. Sirvent, A., Bénistant, C., Pannequin, J., Veracini, L., Simon, V., Bourgaux, J.F., Hollande, F., Cruzalequi, F., and Roche, S. (2010) Src family tyrosine kinases-driven colon cancer cell invasion is induced by Csk membrane delocalization. *Oncogene* 29, 1303-1315.
145. Rush, J., Moritz, A., Lee, K.A., Guo, A., Goss, V.L., Spek, E.J., Zhang, H., Zha, M.-X., Polakiewicz, R.D., and Comb, M.J. (2005) Immunoaffinity profiling of tyrosine phosphorylation in cancer cells. *Nat. Biotechnol* 23, 94-101.
146. Luo, W., Slebos, R.J., Hill, S., Li, M., Brábek, J., Ramars, A., Chaerkady, R., Pandey, A., Ham, A.-J.L., and Hanks, S.K. (2008) Global Impact of Oncogenic Src on a Phosphotyrosine Proteome. *J. Proteome Res* 7, 3447-3460.
147. Hanahan, D., and Weinberg, R.A. (2000) The hallmarks of cancer. *Cell* 100, 57-70.
148. Hynes, R.O. (2002) Integrins: Bidirectional, Allosteric Signaling Machines. *Cell* 110, 673-687.
149. Playford, M.P., and Schaller, M.D. (2004) The interplay between Src and integrins in normal and tumor biology. *Oncogene* 23, 7928-7946.
150. Tadokoro, S., Shattil, S.J., Eto, K., Tai, V., Liddington, R.C., de Pereda, J.M., Ginsberg, M.H., and Calderwood, D.A. (2003) Talin binding to integrin beta tails: a final common step in integrin activation. *Science* 302, 103-106.
151. Mitra, S.K., Hanson, D.A., and Schlaepfer, D.D. (2005) Focal adhesion kinase: in command and control of cell motility. *Nat. Rev. Mol. Cell Biol* 6, 56-68.
152. Giancotti, F.G., and Tarone, G. (2003) Positional control of cell fate through joint integrin/receptor protein kinase signaling. *Annu. Rev. Cell Dev. Biol* 19, 173-206.
153. Cabodi, S., and Defilippi, P. (2005) The Essence of Integrin Signal Transduction: Assembly of Dynamic Scaffolds and Cross-Talk with Other Receptors. *Integrins and Development* Chap. 4.
154. Defilippi, P., Di Stefano, P., and Cabodi, S. (2006) p130Cas: a versatile scaffold in signaling networks. *Trends Cell Biol* 16, 257-263.
155. Gustavsson, A., Yuan, M., and Fällman, M. (2004) Temporal dissection of β1-integrin signaling indicates a role for p130Cas-Crk in filapodia formation. *J. Biol. Chem* 279, 22893-22901.

156. Webb, D.J., Donais, K., Whitmore, L.A., Thomas, S.M., Turner, C.E., Parsons, J.T., and Horwitz, A.F. (2004) FAK-Src signaling through paxillin, ERK and MLCK regulates adhesion disassembly. *Nat. Cell Biol* 6, 154-161.
157. Cabodi, S., del Pilar Camacho-Leal, M., Di Stefano, P. and Defilippi, P. (2010) Integrin signaling adaptors: not only figurants in the cancer story. *Nat. Rev. Cancer* 10, 858-870.
158. Holmqvist, K., Cross, M., Riley, D., and Welsh, M. (2003) The Shb adaptor protein causes Src-dependent cell spreading and activation of focal adhesion kinase in murine brain endothelial cells. *Cell Signal* 15, 171-179.
159. Lu, L., Annerén, C., Reedquist, K.A., Bos, J.L., and Welsh, M. (2000) NGF-Dependent neurite outgrowth in PC12 cells overexpressing the Src homology 2-domain protein shb requires activation of the Rap1 pathway. *Exp. Cell Res* 259, 370-377.
160. Tu, Y., Li, F., and Wu, C. (1998) Nck-2, a Novel Src Homology2/3-containing Adaptor Protein That Interacts with the LIM-only Protein PINCH and Components of Growth Factor Receptor Kinase-signaling Pathways. *Mol. Biol. Cell* 9, 3367-3382.
161. Li, W., Fan, J., and Woodley, D.T. (2001) Nck/Dock: an adapter between cell surface receptors and the actin cytoskeleton. *Oncogene* 20, 6403-6417.
162. Meisenhelder, J., and Hunter, T. (1992) The SH2/SH3 domain-containing protein Nck is recognized by certain anti-phospholipase C-gamma 1 monoclonal antibodies, and its phosphorylation on tyrosine is stimulated by platelet-derived growth factor and epidermal growth factor treatment. *Mol. Cell Biol* 12, 5843-5856.
163. Xu, N.-J. and Henkemeyer, M. (2009) Ephrin-B3 reverse signaling through Grb4 and cytoskeletal regulators mediates axon pruning. *Nat. Neurosci* 12, 268-276.
164. Kullander, K., and Klein, R. (2002) Mechanisms and Functions of Eph and Ephrin Signaling. *Nat. Rev. Mol. Cell Biol* 3, 475-486.
165. Fang, W.B., Brantley-Sieders, D.M., Hwang, Y., Ham, A.J., and Chen, J. (2008) Identification and functional analysis of phosphorylated tyrosine residues within EphA2 receptor tyrosine kinase. *J. Biol. Chem* 283, 16017-16026.
166. Zisch, A.H., Kalo, M.S., Chong, L.D., and Pasquale, E.B. (1998) Complex formation between EphB2 and Src requires phosphorylation of tyrosine 611 in the EphB2 juxtamembrane region. *Oncogene* 16, 2657-2670.
167. Palmer, A., Zimmer, M., Erdmann, K.S., Eulenburg, V., Porthin, A., Heumann, R., Deutsch, U., and Klein, R. (2002) EphrinB Phosphorylation and Reverse Signaling: Regulation by Src Kinases and PTP-BL Phosphatase. *Mol. Cell* 9, 725-737.
168. Dolfi, F., Garcia-Guzman, M., Ojaniemi, M., Nakamura, H., Matsuda, M., and Vuori, K. (1998) The adaptor protein Crk connects multiple cellular stimuli to the JNK signaling pathway. *Proc. Natl. Acad. Sci USA* 95, 15394-15399.
169. Oktay, M., Wary, K.K., Dans, M., Birge, R.B., and Giancotti, F.G. (1999) Integrin-mediated activation of focal adhesion kinase is required for signaling to Jun NH2-terminal kinase and progression through the G1 phase of the cell cycle. *J. Cell Biol* 145, 1461-1469.

170. Kirsch, K., Kensinger, M., Hanafusa, H., and August, A. (2002) A p130Cas tyrosine phosphorylated substrate domain decoy disrupts *v-Crk* signaling. *BMC Cell Biol* 3, 18-33.
171. Manser, E., Leung, T., Salihuddin, H., Tan, L., and Lim, L. (1993) A non-receptor tyrosine kinase that inhibits the GTPase activity of p21cdc42. *Nature* 363, 364-367.
172. Galisteo, M.L., Yang, Y., Ureña, J., and Schlessinger, J. (2006) Activation of the nonreceptor protein tyrosine kinase Ack by multiple extracellular stimuli. *Proc. Natl. Acad. Sci. USA* 103, 9796-9801.
173. Chan, W., Sit, S.T., and Manser, E. (2011) The Cdc42-associated kinase ACK1 is not autoinhibited but requires Src for activation. *Biochem. J* 435, 355-364.
174. Symons, M., Derry, JMJ., Karlak, B., Jiang, S., Lemahieu, V., McCormick, F., Francke, U., and Abo, A. (1996) Wiskott-Aldrich syndrome protein, a novel effector for the GTPase CDC42Hs, is implicated in actin polymerization. *Cell* 84, 723-734.
175. Millard, T.H., Sharp, S.J., and Machesky, L.M. (2004) Signalling to actin assembly via the WASP (Wiskott-Aldrich syndrome protein)-family proteins and the Arp2/3 complex. *Biochem. J* 380, 1-17.
176. Nobes, C., and Hall, A. (1994) Regulation and function of the Rho subfamily of small GTPases. *Curr. Opin. Genet. Dev* 4, 77-81.
177. Ridley, A.J., and Hall, A. (1992) The small GTP-binding protein rho regulates the assembly of focal adhesions and actin stress fibers in response to growth factors. *Cell* 70, 389-399.
178. Amano, M., Ito, M., Kimura, K., Fukata, Y., Chihara, K., Nakano, T., Matsuura, Y., and Kaibuchi, K. (1996) Phosphorylation and activation of myosin by Rho-associated kinase (Rho-kinase). *J. Biol. Chem* 271, 20246-20249.
179. Seppä, H., Grotendorst, G., Seppä, S., Schiffmann, E., and Martin, G.R. (1982) Platelet-derived growth factor in chemotactic for fibroblasts. *J. Cell Biol* 92, 584-588.
180. Lynch, S.E., Nixon, J.C., Colvin, R.B., and Antoniades, H.N. (1987) Role of platelet-derived growth factor in wound healing: Synergistic effects with other growth factors. *Proc. Natl. Acad. Sci. USA* 84, 7696-7700.
181. Heldin, C.-H., and Westermark, B. (1999) Mechanism of Action and In Vivo Role of Platelet-Derived Growth Factor. *Physiol. Rev* 79, 1283-1316.
182. Betsholtz, C., Karisson, L., and Lindahl, P. (2001) Developmental roles of platelet-derived growth factors. *Bioessays* 23, 494-507.
183. Board, R., and Jayson, G.C. (2005) Platelet-derived growth factor receptor (PDGFR): A target for anticancer therapeutics. *Drug Resist. Update* 8, 75-83.
184. Zhao, W., Zhao, T., Huang, V., Chen, Y., Ahokas, R.A., and Sun, Y. (2011) Platelet-derived growth factor involvement in myocardial remodeling following infarction. *J Mol. Cell Cardiol* 51, 830-838.
185. Arimura, K., Ago, T., Kamouchi, M., Nakamura, K., Ishitsuka, K., Kuroda, J., Sugimori, H., Ooboshi, H., Sasaki, T., and Kitazono, T. (2012) PDGF receptor β signaling in pericytes following ischemic brain injury. *Curr. Neurovasc. Res* 9, 1-9.
186. Ralston, R., and Bishop, J.M. (1985) The product of the protooncogene c-src is modified during the cellular response to platelet-derived growth factor. *Proc. Natl. Acad. Sci. USA* 82, 7845-7849.

187. Gould, K., and Hunter, T. (1988) Platelet-derived growth factor induces multisite phosphorylation of pp60c-src and increases its protein-tyrosine kinase activity. *Mol. Cell Biol* 8, 3345-3356.
188. Kypta, R.M., Goldberg, Y., Ulug, E.T., and Courtneidge, S.A. (1990) Association between the PDGF receptor and members of the Src family of tyrosine kinases. *Cell* 62, 481-492.
189. Mori, S., Rönnstrand, L., Yokote, K., Engström, A., Courtneidge, S.A., Claesson-Welsh, L., and Heldin, C.-H. (1993) Identification of two juxtamembrane autophosphorylation sites in the PDGF beta-receptor; involvement in the interaction with Src family tyrosine kinases. *EMBO J* 12, 2257-2264.
190. Zhang, S.Q., Yang, W., Kontaridis, M.I., Bivona, T.G., Wen, G., Araki, T., Luo, J., Thompson, J.A., Schraven, B.L., Philips, M.R., and Neel, B.G. (2004) Shp2 regulates SRC family kinase activity and Ras/Erk activation by controlling Csk recruitment. *Mol. Cell* 13, 341-355.
191. Bromann, P.A., Korkaya, H., and Courtneidge, S.A. (2004) The interplay between Src family kinases and receptor tyrosine kinases. *Oncogene* 23, 7957-7968.
192. Hansen, K., Johnell, M., Siegbahn, A., Rorsman, C., Engström, U., Wernstedt, C., Heldin, C.H., and Rönnstrand, L. (1996) Mutation of a Src phosphorylation site in the PDGF beta-receptor leads to increased PDGF-stimulated chemotaxis but decreased mitogenesis. *EMBO J* 15, 5299-5313.
193. Plattner, R., Kadlec, L., DeMali, K.A., Kazlauskas, A., and Pendergast, A.M. (1999) c-Abl is activated by growth factors and Src family kinases and has a role in the cellular response to PDGF. *Genes Dev* 13, 2400-2411.
194. Furstoss, O., Dorey, K., Simon, V., Barilá, D., Superti-Furga, G., and Roche, S. (2002) c-Abl is an effector of Src for growth factor-induced c-myc expression and DNA synthesis. *EMBO J* 21, 514-524.
195. Srinivasan, D., Kaetzel, D.M., and Plattner, R. (2009) Reciprocal regulation of Abl and receptor tyrosine kinases. *Cell Signal* 21, 1143-1150.
196. Bazenet, C.E., Gelderloos, J.A., and Kazlauskas, A. (1996) Phosphorylation of tyrosine 720 in the platelet-derived growth factor alpha receptor is required for binding of Grb2 and SHP-2 but not for activation of Ras or cell proliferation. *Mol. Cell Biol* 16, 6926-6936.
197. Hooshman-Rad, R., Lu, L., Heldin, C.H., Claesson-Welsh, L., and Welsh, M. (2000) Platelet-derived growth factor receptor-mediated signaling through the Shb adaptor protein: effects on cytoskeletal organization. *Exp. Cell Res* 257, 245-254.
198. Ekman, S., Kallin, A., Engström, U., Heldin, C.H., and Rönnstrand, L. (2002) SHP-2 is involved in heterodimer specific loss of phosphorylation of Tyr771 in the PDGF beta-receptor. *Oncogene* 21, 1870-1875.
199. Ikuno, Y., Leong, F.L., and Kazlauskas, A. (2002) PI3K and PLCgamma play a central role in experimental PVR. *Invest. Ophthalmol. Vis. Sci* 43, 483-490.
200. Eriksson, A., Nånberg, E., Rönnstrand, L., Engström, U., Hellman, U., Rupp, E., Carpenter, G., Heldin, C.H., and Claesson-Welsh, L. (1995) Demonstration of functionally different interactions between phospholipase C-gamma and the two types of platelet-derived growth factor receptors. *J. Biol. Chem* 270, 7773-7781.

201. Blake, R.A., Broome, M.A., Liu, X., Wu, J., Gishizky, M., Sun, L., and Courtneidge, S.A. (2000) SU6656, a Selective Src Family Kinase Inhibitor, Used To Probe Growth Factor Signaling. *Mol. Cell Biol* 20, 9018-9027.
202. Guo, K., Li, J., Tang, J.P., Koh, V., Gan, B.Q., and Zeng, Q. (2004) Catalytic domain of PRL-3 plays an essential role in tumor metastasis: formation of PRL-3 tumors inside the blood vessels. *Cancer Biol. Ther* 3, 945-951.
203. Guo, K., Li, J., Wang, H., Osato, M., Tang, J.P., Quah, S.Y., Gan, B.Q., and Zeng, Q. (2006) PRL-3 initiates tumor angiogenesis by recruiting endothelial cells in vitro and in vivo. *Cancer Res* 66, 9625-9635.
204. Zhao, W.B., Li, Y., Liu, X., Zhang, L.Y., and Wang, X. (2008) Evaluation of PRL-3 expression, and its correlation with angiogenesis and invasion in hepatocellular carcinoma. *Int. J. Mol. Med* 22, 187-192.
205. Ming, J., Liu, N., Qiu, X., and Wang, E.H. (2009) PRL-3 facilitates angiogenesis and metastasis by increasing ERK phosphorylation and up-regulating the levels and activities of Rho-A/C in lung cancer. *Pathology* 41, 118-126.
206. Xu, J., Cao, S., Wang, L., Xu, R., Chen, G., and Xu, Q. (2011) VEGF promotes the transcription of the human PRL-3 gene in HUVEC through transcription factor MEF2C. *PLoS One* 6, e27165.
207. Quilliam, L.A., Zhong, S., Raburn, K.M., Carpenter, J.W., South, T.L., Der, C.J., and Campbell-Burk, S. (1995) Biological and structural characterization of a Ras transforming mutation at the phenylalanine-156 residue, which is conserved in all members of the Ras superfamily. *Proc. Natl. Acad. Sci. USA* 92, 1272-1276.
208. Karlsson, T., Songyang, Z., Landgren, E., Lavergne, C., Di Fiore, P.P., Anafai, M., Pawson, T., Cantley, L.C., Claesson-Welsh, L., and Welsh, M. (1995) Molecular interactions of the Src homology 2 domain protein Shb with phosphotyrosine residues, tyrosine kinase receptors and Src homology 3 domain proteins. *Oncogene* 10, 1475-1483.
209. Welsh, M., Songyang, Z., Frantz, J.D., Trüb, T., Reedquist, K.A., Karlsson, T., Miyazaki, M., Cantley, L.C., Band, H., and Shoelson, S.E. (1998) Stimulation through the T cell receptor leads to interactions between SHB and several signaling proteins. *Oncogene* 16, 891-901.
210. Lindholm, C.K., Gylfe, E., Zhang, W., Samelson, L.E., and Welsh, M. (1999) Requirement of the Src homology 2 domain protein Shb for T cell receptor-dependent activation of the interleukin-2 gene nuclear factor for activation of T cells element in Jurkat T cells. *J. Biol. Chem* 274, 28050-28057.
211. Bennett, A.M., Tang, T.L., Sugimoto, S., Walsh, C.T., and Neel, B.G. (1994) Protein-tyrosine-phosphatase SHPTP2 couples platelet-derived growth factor receptor β to Ras. *Proc. Natl. Acad. Sci. USA* 91, 7335-7339.
212. Rhee, S.G. (2001) Regulation of phosphoinositide-specific phospholipase C. *Annu. Rev. Biochem* 70, 281-312.
213. Bunney, T.D., and Katan, M. (2011) PLC regulation: emerging pictures for molecular mechanisms. *Trends Biochem. Sci* 36, 88-96.
214. Berridge, M.J. (1993) Inositol triphosphate and calcium signaling. *Nature* 361, 315-325.
215. Nishizuka, Y. (1995) Protein kinase C and lipid signaling for sustained cellular responses. *FASEB J* 9, 484-496.

216. Koivunen, J., Aaltonen, V., and Pelton, J. (2006) Protein kinase C (PKC) family in cancer progression. *Cancer Lett* 235, 1-10.
217. Sözeri, O., Vollmer, K., Liyanage, M., Frith, D., Kour, G., Mark, G.E. 3rd, and Stabel, S. (1992) Activation of the c-Raf protein kinase by protein kinase C phosphorylation. *Oncogene* 7, 2259-2262.
218. Kolsh, W., Heidecker, G., Kochs, G., Hummel, R., Vahidi, H., Mischak, H., Finkenzeller, G., Marmé, D., and Rapp, U.R. (1993) Protein kinase C alpha activates RAF-1 by direct phosphorylation. *Nature* 364, 249-252.
219. McParland, V., Varsano, G., Li, X., Thornton, J., Baby, J., Aravind, A., Meyer, C., Pavic, K., Rios, P., and Köhn, M. (2011) The metastasis-promoting phosphatase PRL-3 shows activity toward phosphoinositides. *Biochemistry* 50, 7579-7590.
220. Kim, H.K., Kim, J.W., Zilberstein, A., Margolis, B., Kim, C.K., Schlessinger, J., and Rhee, S.G. (1991) Stimulation of inositol phospholipid hydrolysis requires PLC-γ phosphorylation on residues 783 and 1254. *Cell* 65, 435-441.
221. Falasca, M., Logan, S.K., Lehto, V.P., Baccante, G., Lemmon, M.A., and Schlessinger, J. (1998) Activation of phospholipase Cγ by PI 3-kinase-induced PH domain-mediated membrane targeting. *EMBO J* 17, 414-422.
222. Cuevas, B.D., Yiling, L., Mao, M., Zhang, J., LaPushin, R., Siminovitch, K., and Mills, G.B. (2001) Tyrosine Phosphorylation of p85 Relieves Its Inhibitory Activity on Phosphatidylinositol 3-Kinase. *J. Biol. Chem* 276, 27455-27461.
223. Coles, L.C., and Shaw, P.E. (2002) PAK1 primes MEK1 for phosphorylation by Raf-1 kinase during cross-cascade activation of the ERK pathway. *Oncogene* 21, 2236-2244.
224. King, A.J., Wireman, R.S., Hamilton, M., and Marshall, M.S. (2001) Phosphorylation site specificity of the Pak-mediated regulation of Raf-1 and cooperativity with Src. *FEBS Lett* 497, 6-14.
225. Darnell, J.E. Jr., Kerr, I.M., and Startk, G.R. (1994) Jak-STAT pathways and transcriptional activation in response to IFNs and other extracellular signaling proteins. *Science* 264, 1415-1421.
226. Schindler, C., and Darnell, J.E. Jr. (1995) Transcriptional responses to polypeptide ligands: the JAK-STAT pathway. *Annu. Rev. Biochem* 64, 621-651.
227. Wang, Y.Z., Wharton, W., Garcia, R., Kraker, A., Jove, R., and Pledger, W.J. (2000) Activation of Stat3 preassembled with platelet-derived growth factor receptors requires Src kinase activity. *Oncogene* 19, 2075-2085.
228. Bowman, T., Broome, M.A., Sinibaldi, D., Wharton, W., Pledger, W.J., Sedivy, J.M., Irby, R., Yeatman, T., Courtneidge, S.A., and Jove, R. (2001) Stat3-mediated Myc expression is required for Src transformation and PDGF-induced mitogenesis. *Proc. Natl. Acad. Sci. USA* 98, 7319-7324.
229. Simon, A.R., Takahashi, S., Severgnini, M., Fanburg, B.L., and Cochran, B.H. (2002) Role of the JAK-STAT pathway in PDGF-stimulated proliferation of human airway smooth muscle cells. *Am. J. Physiol. Lung Cell Mol. Physiol* 282, L1296-L1304.
230. Yu, C.L., Meyer, D.J., Campbell, G.S., Larner, A.C., Carter-Su, C., Schwartz, J., and Jove, R. (1995) Enhanced DNA-binding activity of a Stat3-related protein in cells transformed by the Src oncoprotein. *Science* 269, 81-83.

231. Cao, X., Tay, A., Guy, G.R., and Tan, Y.H. (1996) Activation and association of Stat3 with Src in v-Src-transformed cell lines. *Mol. Cell Biol* 16, 1595-1603.
232. Darnell, J.E. Jr. (1997) STATs and gene regulation. *Science* 277, 1630-1635.
233. Cirri, P., Chiarugi, P., Marra, F., Raugei, G., Camici, G., Manao, G., and Ramponi, G. (1997) c-Src activates both STAT1 and STAT3 in PDGF-stimulated NIH3T3 cells. *Biochem. Biophys. Res. Commun* 239, 493-497.
234. Cambell, G.S., Yu, C.L., Jove, R., and Carter-Su, C. (1997) Constitutive activation of JAK1 in Src-transformed cells. *J. Biol Chem* 272, 2591-2594.
235. Leonard, W.J., and O'Shea, J.J. (1998) Jaks and STATs: biological implications. *Annu. Rev. Immunol* 16, 293-322.
236. Bromberg, J.F., Horvath, C.M., Besser, D., Lathem, W.W., and Darnell, J.E. Jr. (1998) Stat3 activation is required for cellular transformation by v-src. *Mol. Cell Biol* 18, 2553-2558.
237. Yu, H., Pardoll, D., and Jove, R. (2009) STATs in cancer inflammation and immunity: a leading role for STAT3. *Nat. Rev. Cancer* 9, 798-809.
238. Turkson, J., Bowman, T., Garcia, R., Caldenhoven, E., De Groot, R.P., and Jove, R. (1998) Stat3 activation by Src induces specific gene regulation and is required for cell transformation. *Mol. Cell Biol* 18, 2545-2552.
239. Bowman, T., Garcia, R., Turkson, J., and Jove, R. (2000) STATs in oncogenesis. *Oncogene* 19, 2474-2488.
240. Turkson, J., and Jove, R. (2000) STAT proteins: novel molecular targets for cancer drug discovery. *Oncogene* 19, 6613-6626.
241. Huang, S. (2007) Regulation of metastases by signal transducer and activator of transcription 3 signaling pathway: clinical implications. *Clin. Cancer Res* 13, 1362-1366.
242. Suzuki, K., Oneyama, C., Kimura, H., Tajima, S., and Okada, M. (2011) Down-regulation of the tumor suppressor C-terminal Src kinase (Csk)-binding protein (Cbp)/PAG1 is mediated by epigenetic histone modifications via the mitogen-activated protein kinase (MAPK)/phosphatidylinositol 3-kinase (PI3K) pathway. *J Biol. Chem* 286, 15698-15706.
243. Tartaglia, M., Mehler, E.L., Goldberg, R., Zampino, G., Brunner, H.G., Kremer, H., van der Burgt, I., Crosby, A.H., Ion, A., Jeffery, S., Kalidas, K., Patton, M.A., Kucher-lapati, R.S., and Gelb, B.D. (2001) Mutations in PTPN11, encoding the protein tyrosine phosphatase SHP-2, cause Noonan syndrome. *Nat. Genet*. **29**, 465-468.
244. Tartaglia, M., Martinelli, S., Cazzaniga, G., Cordeddu, V., Iavarone, I., Spinelli, M., Palmi, C., Carta, C., Pession, A., Arico, M., Masera, G., Basso, G., Sorcini, M., Gelb, B.D., and Biondi, A. (2004) Genetic evidence for lineage-related and differentiation stage-related contribution of somatic PTPN11 mutations to leukemogenesis in childhood acute leukemia. *Blood* 104, 307-313.
245. Loh, M.L., Vattikuti, S., Schubbert, S., Reynolds, M.G., Carlson, E., Lieuw, K.H., Cheng, J.W., Lee, C.M., Stokoe, D., Bonifas, J.M., Curtiss, N.P., Gotlib, J., Meschinchi, S., LeBeau, M.M., Emanuel, P.D., and Shannon, K.M. (2004a) Blood 103, 2325-2331.

246. Loh, M. L., Reynolds, M. G., Vattikuti, S., Gerbing, R. B., Alonzo, T. A., Carlson, E., Cheng, J. W., Lee, C. M., Lange, B. J., Meshinchi, S., and Children's Cancer Group. (2004b) "PTPN11 mutations in pediatric patients with acute myeloid leukemia: results from the Children's Cancer Group", *Leukemia* 18, 1831-1834.
247. Kratz, C. P., Niemeyer, C. M., Castleberry, R. P., Cetin, M., Bergsträsser, E., Emanuel, P. D., Hasle, H., Kardos, G., Klein, C., Kojima, S., Stary, J., Trebo, M., Zecca, M., Gelb, B. D., Tartaglia. M., and Loh. M. L. (2005) The mutational spectrum of PTPN11 in juvenile myelomonocytic leukemia and Noonan syndrome/myeloproliferative disease. *Blood* 106, 2183-2185.
248. Miyamoto, D., Miyamoto, M., Takahashi, A., Yomogita, Y., Higashi, H., Kondo, S., and Hatakeyama, M. (2008) Isolation of a distinct class of gain-of-function SHP-2 mutants with oncogenic RAS-like transforming activity from solid tumors. *Oncogene* 27, 3508-3515.
249. Freeman Jr., R.M., Plutzky, J., and Neel, B.G. (1992) Identification of a human src homology 2-containing protein tyrosine-phosphatase: A putative homolog of Drosophila corkscrew. *Proc. Natl. Acad. Sci. USA* 89, 11239-11243.
250. Sugimoto, S., Wandless, T. J., Shoelson, S. E., Neel, B. G. & Walsh, C. T. (1994) Activation of the SH2-containing protein tyrosine phosphatase, SH-PTPs by phosphotyrosine-containing peptides derived from insulin receptor substrate-1. *J. Biol. Chem* 269, 13614-13622.
251. Pluskey, S., Wandless, T.J., Walsh, C.T, and Shoelson, S.E. (1995) Potent stimulation of SH-PTP2 phosphatase activity by IRS-1 binding to both of its SH2 domains. *J. Biol. Chem* 270, 2897-2900.
252. Pei, D., Wang, J., and Walsh, C.T. (1996) Differential functions of the two Src homology 2 domains in protein tyrosine phosphatase SH-PTP1. *Proc. Natl. Acad. Sci. USA* 93, 1141-1145.
253. Lechleider, R.J., Sugimoto, S., Bennett, A.M., Kashishian, A.S., Cooper, J.A., Shoelson, S.E., Walsh, C.T., and Neel, B.G. (1993) Activation of the SH2-containing phosphotyrosine phosphatase SH-PTP2 by it binding site, phosphotyrosine 1009, on the human platelet-derived growth factor receptor β. *J. Biol. Chem* 268, 21478-21481.
254. Jia, Z.C., Barford, D., Flint, A.J., and Tonks, N.K. (1995) Structural basis for phosphotyrosine peptide recognition by protein tyrosine phosphatase 1B. *Science* 268, 1754-1758.
255. Sours, K.M., and Ahn, N.G. (2010) Analysis of MAP Kinases by Hydrogen Exchange Mass Spectrometry. *Methods Mol. Biol* 661, 239-255.
256. Lee, C.-H., Kominos, D., Jaques, S., Margolis, B., Schlessinger, J., Shoelson, S.E., and Kuriyan, J. (1994) Crystal structures of peptide complexes of the N-terminal SH2 domain of the Syp tyrosine phosphatase. *Structure* 2, 423-438.
257. Eck, M.J., Pluskey, S., Trub, T., Harrison, S.C., and Shoelson, S.E. (1996) Spatial constraints on the recognition of phosphoproteins by the tandem SH2 domains of the phosphatase SH-PTP2. *Nature* 379, 277-280.
258. Legius, E., Schrander-Stumpel, C., Schollen, E., Pulles-Heintzberger, C., Gewillig, M., and Fryns, J.-P. (2002) PTPN11 mutations in LEOPARD syndrome. *J. Med. Genet* 39, 571-574.

259. Oishi, K., Zhang, H., Gault, W.J., Wang, C.J., Tan, C.C., Kim, I.-K., Ying, H., Rahman, T., Pica, N., Tartaglia, M., Mlodzik, M., and Gelb, B.D. (2009) Phosphatase-defective LEOPARD syndrome mutations in PTPN11 gene have gain-of-function effects during Drosophila development. *Hum. Mol. Genet* 18, 193-201.
260. Oishi, K., Gaengel, K., Krishnamoorthy, S., Kamiya, K., Kim, I.K., Ying, H., Weber, U., Perkins, L.A., Tartaglia, M., Mlodzik, M., Pick, L., and Gelb, B.D. (2006) Transgenic Drosophila models of Noonan syndrome causing PTPN11 gain-of-function mutations. *Hum. Mol. Genet* 15, 543-553.
261. Carvajal-Vergara, X., Sevilla, A., D'Souza, S.L., Ang, Y.-S., Schaniel, C., Lee, D.-F., Yang, L., Kaplan, A.D., Adler, E.D., Rozov, R., Ge, Y.C., Cohen, N., Edelmann, L.J., Chang, B., Waghray, A., Su, J., Pardo, S., Lichtenbelt, K.D., Tartaglia, M., Gelb, B.D., and Lemischka, I.R. (2010) Patient-specific induced pluripotent stem-cell-derived models of LEOPARD syndrome. *Nature* 465, 808-812.
262. Pandit, B., Sarkozy, A., Pennacchio, L.A., Carta, C., Oishi, K., Martinelli, S., Pogna, E.A., Schackwitz, W., Ustaszewska, A., Landstrom, A., Bos, J.M., Ommen, S.R., Esposito, G., Lepri, F., et al. (2007) Gain-of-function RAF1 mutations cause Noonan and LEOPARD syndromes with hypertrophic cardiomyopathy. *Nature Genet* 39, 1007-1012.
263. Gelb, B.D., and Tartaglia, M. (2006) Noonan syndrome and related disorders: dysregulated RAS-mitogen activated protein kinase signal transduction. *Hum. Mol. Genet* 15, R220-R226.
264. Östman, A., Hellberg, C., and Böhmer, F.D. (2006) Protein-tyrosine phosphatases and cancer. *Nat. Rev. Cancer* 6, 307-320.

CURRICULUM VITAE

Chad Daniel Walls

Education

2005-2012 Ph.D. in Biochemistry and Molecular Biology
Indiana University, Indianapolis, Indiana
Advisor: Zhong-Yin Zhang, Ph.D.
Title: Functional Insights into Oncogenic Protein Tyrosine Phosphatases by Mass Spectrometry

1997-2001 B.S. in Biochemistry
Indiana University, Bloomington, Indiana

Work Experience

2003-2005 Analytical Instrumentation Research Associate: Monarch Life Sciences (Indiana Centers for Applied Protein Sciences (INCAPS))
Indianapolis, Indiana
Supervisor: Dr. Mu Wang, Ph.D.

2002-2003 Data Management Associate (Eli Lilly and Company): MedFocus, Inc.
Indianapolis, Indiana

Publications

1. Walls, C.D., Iliuk, A.B., Tao, W.A., Wang, Mu, and Zhang, Z.-Y. (2012) Phosphatase of Regenerating Liver 3 (PRL3) drives pro-metastatic molecular events through a Src kinase-induced aberrant tyrosine phosphoproteome. *Manuscript submitted.*
2. Walls, C.D., Yu, Z.-H., and Zhang, Z.-Y. (2012) LEOPARD syndrome (LS)-associated SHP2 mutants exist in an 'open' conformational state and promote gain-of-function effects in signal transduction. *In Progress*.
3. Yu, Z.-H., Xu, J., Walls, C., Chen, L., Zhang, S., Wu, L., Wang, L., Liu, S. and Zhang, Z.-Y. (2012) Mechanistic Insights into LEOPARD Syndrome-Associated SHP2 Mutations. *Manuscript Submitted*.
4. Dumaual, C.M., Steere, B.A., Walls, C.D., Zhang, Z.-Y., and Randall, S.K. (2012) Novel insights to PRL-1 signaling gained through integrated analysis of mRNA and protein expression data. *Manuscript Submitted*.
5. Bai, Y., Luo, Y., Liu, S., Zhang, L., Shen, K., Dong, Y., Walls, C.D., Quilliam, L.A., Wells, C.D., Cao, Y. and Zhang, Z.-Y. (2011) PRL-1 protein promotes ERK1/2 and RhoA protein activation through a non-canonical interaction with the Src homology 3 domain of p115 Rho GTPase-activating protein. *J Biol Chem* 286, 42316-42324.
6. Walls, C., Zhou, B. and Zhang, Z.-Y. (2009) Activity-based protein profiling of protein tyrosine phosphatases. *Methods Mol Biol* 519, 417-429.

7. Liang, F., Luo, Y., Dong, Y., Walls, C.D., Liang, J., Jiang, H.Y., Sanford, J.R., Wek, R.C., Zhang, Z.Y. (2008) Translational control of C-terminal Src kinase (Csk) expression by PRL3 phosphatase. *J Biol Chem* 283, 10339-10346.
8. Abdo, M., Liu, S., Zhou, B., Walls, C.D., Wu, L., Knapp, S. and Zhang, Z.-Y. (2008) Seleninate in place of phosphate: irreversible inhibition of protein tyrosine phosphatases. *J Am Chem Soc* 130, 13196-13197.
9. Hurley, T.D., Walls, C., Bennett, J.R., Roach, P.J., Wang, M. (2006) Direct detection of glycogenin reaction products during glycogen initiation. *Biochem Biophys Res Commun* 348, 374-378.
10. Gokmen-Polar, Y., Escuin, D., Walls, C.D., Soule, S.E., Wang, Y., Sanders, K.L., Lavallee, T.M., Wang, M., Guenther, B.D., Giannakakou, P., Sledge, G.W. Jr. (2005) beta-Tubulin mutations are associated with resistance to 2-methoxyestradiol in MDA-MB-435 cancer cells. *Cancer Res* 65, 9406-9414.
11. Zhang, Y., Vander Fits, L., Voerman, J.S., Melief, M.J., Laman, J.D., Wang, M., Wang, H., Wang, M., Li, X., Walls, C.D., Gupta, D., Dziarski, R. (2005) Identification of serum N-acetylmuramoyl-l-alanine amidase as liver peptidoglycan recognition protein 2. *Biochim Biophys Acta* 1752, 34-46.